Queen Mary
University of London

School of Biological and Chemical Sciences

Toward the Control of Partial Covalent Modification of Glassy Carbon Surfaces

Jessica Groppi

Submitted in partial fulfilment of the requirements of the Degree of Doctor of Philosophy

August, 2015

Statement of originality

I, Jessica Groppi, confirm that the research included within this thesis is my own work or that where it has been carried out in collaboration with, or supported by others, that this is duly acknowledged below and my contribution indicated. Previously published material is also acknowledged below.

I attest that I have exercised reasonable care to ensure that the work is original, and does not to the best of my knowledge break any UK law, infringe any third party's copyright or other Intellectual Property Right, or contain any confidential material.

I accept that the College has the right to use plagiarism detection software to check the electronic version of the thesis.

I confirm that this thesis has not been previously submitted for the award of a degree by this or any other university.

The copyright of this thesis rests with the author and no quotation from it or information derived from it may be published without the prior written consent of the author.

Signature: 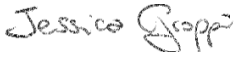

Date: 21/08/2015

Abstract

The patterning of surfaces with control over the relative ratios of different components represents one of the goals in the creation of devices for biosensing and energy storage, since it could improve the stability and sensitivity of the response. Considering this, a general methodology for the creation of controlled mixed monolayers on glassy carbon (GC) surfaces was developed, using osmium bipyridyl complexes and anthraquinone as model redox probes, but potentially applicable to more complex systems.

The work consisted in the electrochemical grafting on GC of a mixture of diamine linkers in different ratios and characterised by protecting groups which allowed orthogonal deprotection. After optimisation of the deprotection conditions, it was possible to selectively remove one of the protecting groups, couple a suitable osmium complex and cap the residual free amines. The removal of the second protecting group allowed the coupling of anthraquinone. The characterisation of the surfaces by cyclic voltammetry showed the variation of the surface coverage of the two redox centres in relation to the initial ratio of the linking amine in solution. It was then possible to build patterned surfaces where the osmium complex acted as mediator for Glucose dehydrogenase (GDH), covalently bonded to GC through an exposed cysteine residue to a maleimide moiety.

Acknowledgements

I would like to thank Prof. Jeremy Kilburn and Prof. Phil Bartlett for the supervision during the PhD and the ongoing help in becoming a researcher.

I would also like to thank all the past and present group members both at Queen Mary and Southampton University for sharing research projects, knowledge and free time. Thank you to everyone I had the chance to work and interact with at QMUL either students, technicians or academics.

A big thank you to all the friends, those that I've known for years and those that I've met during this great PhD experience. Thank you for all the time spent together even if we are far apart for most of the year and we meet just for the holidays; thank you for all the travels, the nights out in front of a pint or just at home in front of the TV, the lunches, brunches and barbeques. Thank you having fun with me, sharing your ideas and experiences and helping me.

A huge thank you to my parents and my sister for always being present and supporting me even from 1000 miles away, always welcoming me home and taking time to travel and visit me as often as possible. A little thank you also to Leo for being the best bunny rabbit ever.

Finally thanks to you, Reader, who maybe don't fit in any of the previous groups but still took some time to check my account of the last four years of (hard) work, though probably you're just forced to.

Cheers,

Jessica

CONTENTS

Table of figures

List of schemes

List of abbreviations

1-BA	1-butylamine
1-PA	1-propylamine
ADOA	8-amino-3,6-dioxaoctanoic acid
Ag/AgCl	Silver/silverchloride reference electrode
AQ	Anthraquinone
BDD	Boron doped diamond
bpy	Bipyridyl
Boc	tert-butylcarbonate
CME	Chemically modified electrode
CV	Cyclic voltammogramm
DCM	Dichloromethane
DET	Direct electron transfer
DFT	Density functional theory
DMAP	Dimethylaminopyridine
DMF	Dimethylformamide
DMSO	Dimethylsulfoxide
DPV	Differential pulse voltammetry
EDA-Boc	N-Boc-ethylenediamine
EDA-tfa	N-tfa-ethylenediamine
EDC	N-(3-Dimethylaminopropyl)-N′-ethylcarbodiimide
EDC.HCl	N-(3-Dimethylaminopropyl)-N′-ethylcarbodiimide hydrochloride
Fmoc	fluorenylmethyloxycarbonate
GC	Glassy carbon
GcGDH	Glucose dehydrogenase from glomerella cingulata
HMPB	4-(4-Hydroxymethyl-3-methoxyphenoxy)butyryl
HBTU	N,N,N′,N′-Tetramethyl-O-(1H-benzotriazol-1-yl)uronium hexafluorophosphate, O-(Benzotriazol-1-yl)-N,N,N′,N′-tetramethyluronium hexafluorophosphate
HDA-Boc	N-Boc-hexamethylenediamine
HDA-tfa	N-tfa-hexamethylenediamine
HOPG	Highly oriented pyrolytic graphite
HR-MS	High resolution mass spectrometry
Im	Imidazole
IR	Infra-red spectroscopy
ISE	Ion-selective electrode
LR-MS	Low resolution mass spectrometry
m-CPBA	3-Chloroperoxybenzoic acid
MET	Mediated electron transfer
MLCT	Metal-ligand charge transfer
MW	Molecular wire
MWCNT	Multi walled carbon nanotubes
n-BuLi	n-butyllithium
NHS	N-Hydroxysuccinimide
NMR	Nuclear magnetic resonance spectroscopy
PBS	Phosphate buffer solution

PDB	Protein data bank
RDE	Rotating disk electrode
SAM	Self-assembled monolayer
SCE	Saturated calomel electrode
smFRET	Single molecule fluorescence resonance energy transfer
Sn2	Nucleophilic substitution of second order
SPPS	Solid phase peptide synthesis
SWCNT	Single walled carbon nanotubes
TBATFB	Tetrabutylammonium tetrafluoroborate salt
TBS	Tert-butyldimethylsilil protecting group
TEATFB	Tetraethylammonium tetrafluoroborate salt
TFA	Trifluoroacetic acid
tfa	trifluoroacetate
TLC	Thin layer chromatography
UV	Ultra-violet spectroscopy
XPS	X-ray photoelectron spectroscopy
XRD	X-Ray diffraction

1. Introduction

1.1. Biosensors: definitions and applications

In general a sensor is defined as a self-contained integrated device able to convert a chemical process into an electrical signal carrying qualitative and quantitative information about an analyte. The main components of a sensor are the receptor, representing the chemical recognition system, and the physicochemical transducer, whose role is translating the information from the chemical domain to the electrical domain.[1]

Biosensors are a class of sensor that involves the use of biological macromolecules as receptor, conferring higher selectivity and sensitivity to the device thus making them ideal for the analysis of complex matrices.[2] The biological elements commonly used as receptors in biosensors are enzymes,[3] antigen/antibody systems,[4] DNA,[5] oligonucleotides,[6] and whole cells,[7] while the transducing devices can employ electrochemical, colorimetric,[8] piezoelectric[9] and optical techniques.[10] The first example of a biosensor was developed in 1962 by Clark *et al.* with the creation of a first generation glucose oxidase sensor for continuous monitoring in surgeries.[11] Since then biosensors have constantly developed, finding application in many areas including food industry,[12] clinical[13] and environmental[14] analysis.

Although work in the field of biosensing has led to the creation of better and better devices, research is always focusing on improving the stability and reliability of the systems while reducing the costs and dimensions of the final products.

1.1.1. Electrochemical biosensors

Biosensors are classified according to the detection techniques used and, amongst the different typologies available, the electrochemical ones are the most widespread. These are classified in three groups based on the transducing component: potentiometric, amperometric and impedimetric. The potentiometric sensors measure the generation of an electrochemical potential using ion-selective electrodes (ISE) and glass electrodes as transducers for the detection of small ions and inorganic molecules, while the impedimetric sensors often rely on interdigitated metal electrodes for the detection of urea and oligonucleotides. Amperometric biosensors are the most interesting type in terms of sophistication and applications, in this case the transducing component is represented by Chemically Modified Electrodes (CME).[15,16] The performance of an amperometric device can be tuned by changing

the electrode material (noble metals, carbon), the chemical nature of the modifications introduced at the surface and the interactions between the electrode material and the modifying layer.[17] The biological recognition element is usually represented by an enzyme but whole cells and organic tissue have also been used.[16]

The general process occurring in an amperometric biosensor can be described as follows: an enzyme reacts with a substrate through a redox process, generating a catalytic current which is transferred to the electrode surface for the measurement.[18] Three main generations of amperometric biosensors can be distinguished (Figure **1**): the first generation were sensors where either a substrate (e.g. oxygen) or a product generated by the enzymatic reaction (e.g. hydrogen peroxide) were directly detected at the transducer. These required the application of high overpotentials for the reaction to occur and were frequently subject to interfence by secondary analytes. In order to overcome these drawbacks, alternative solutions were developed: in the second generation a redox mediator able to react with the enzyme was added to the system, to enhance the electron transfer between enzyme and electrode surface, this process is called Mediated Electron Transfer (MET).[17] The third generation biosensors achieve communication between the enzyme and the electrode surface by Direct Electron Transfer (DET): electrons tunnel between the enzyme active site and the electrode, this process is significantly affected by the enzyme orientation and distance of the active site from the electrode surface.[19]

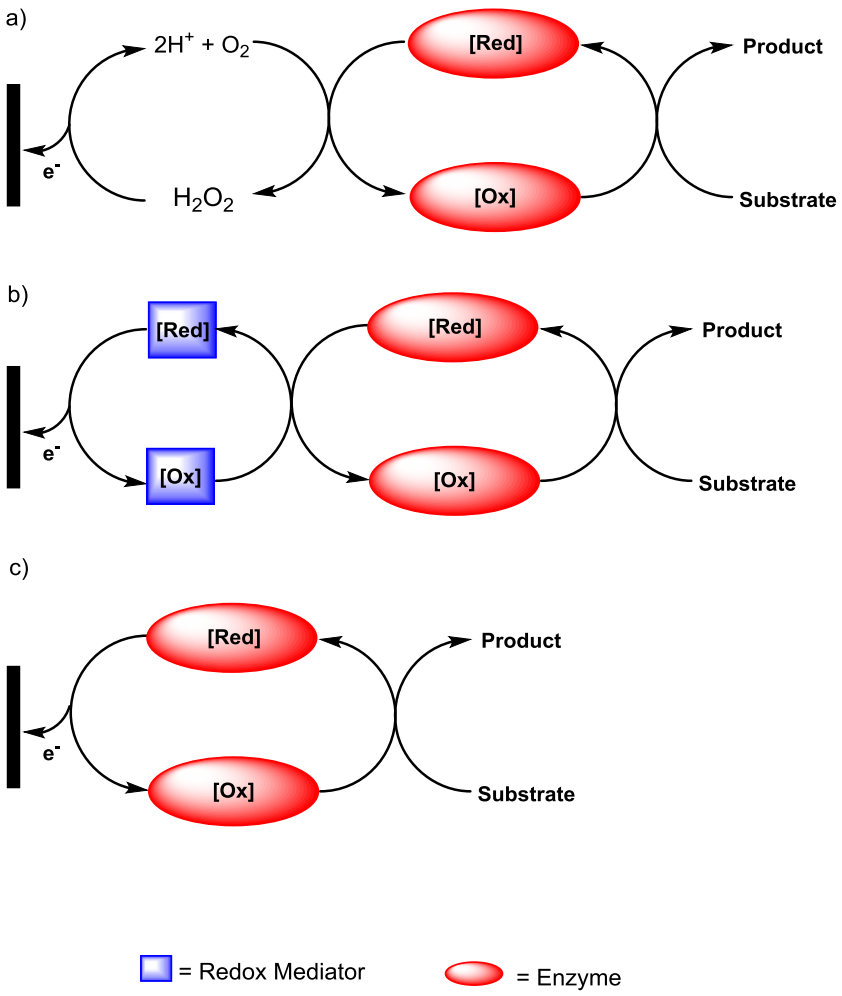

Figure 1. *Biosensors generations: a) First generation, b) Second generation, c) Third generation.*

Several approaches for the immobilisation of enzymes on electrodes are available:[20,21] from simple adsorption to carbon electrodes,[22] to embedding the enzyme in conducting polymeric matrices,[23,24] to the use of rigid conjugated molecular wires that reach inside the active site cavity[25] and covalent binding of the enzyme to the surface.[26,27] Nonetheless the majority of enzymes present active centres buried too deeply in the proteic structure to establish efficient DET,[20] for this reason MET is currently the most applied approach in commercially available biosensing devices.

1.1.2. Redox mediators

Redox mediators are small redox molecules whose role is to improve the electron transfer between the electrode surface and the enzyme, by undergoing a redox process themselves. Molecules able to act as electron carriers are commonly present even in the simplest biological systems and have the function of lowering the energy required for metabolic processes. Similar properties could be used in artificial systems.[28]

In a general MET process the enzyme reacts with the substrate and is converted back to its original oxidation state by reacting with the mediator, which, in turn, is regenerated at the electrode surface. In order for a redox molecule to be an effective redox mediator, some conditions have to be respected:

- It should react rapidly with the enzyme and at the electrode;
- The redox process should occur at low potentials, this to ensure their redox potential is lower than the redox potential of the interferences, and be reversible;
- It should be stable under working conditions both in the oxidised and reduced form and should not perform side reactions with interferents or oxygen.

An important aspect to consider in the choice of the mediator/enzyme system is that oxidative enzymes require mediators with a more positive redox potential, while reductive enzymes need mediators whose redox potential is more negative.[29]

The viability of a mediated process is directly related to the concentration of the mediator: in order to enhance the performance it is necessary to keep a constant amount of mediator relative to the enzyme; methods that have been used to achieve this have included either the covalent modification of the enzyme with the mediator[30] or, more frequently, the anchorage of the mediator to CME.

Organic dyes, quinones and metal complexes have commonly been used as redox mediators.[29]

1.1.3. Enzymes and enzyme engineering

Enzymes are proteins which act as catalysts in biological processes; they are characterised by a main protein structure but that includes non-proteic groups (metal centres, cofactors) which determine the catalytic activity of the enzyme. Enzymes are organised in categories according to the type of reactions they promote and in the field of biosensors, oxidoreductase enzymes are of particular interest, since they catalyse redox reactions monitorable by amperometric techniques. Oxidases and dehydrogenases are oxidoreductase enzymes that catalyse the transfer of hydrogen from a substrate either to oxygen or a cofactor such as NAD^+ or FAD^{2+}.[31]

First and second generation biosensors have relied mainly on oxidases: laccase,[32] peroxidase[33] and glucose oxidase[34] were and still are the most applied enzymes in commercially available devices.

Recently the focus has shifted to dehydrogenase enzymes, since these present some advantages: the hydrogen transfer to cofactors instead of oxygen prevents the formation of H_2O_2, which can cause electrode fouling. Moreover the group of dehydrogenases has many more members than the oxidases with a wider range of substrates.[35]

The enzyme represents both the strength and the limitation of biosensors: the dependence of their stability on pH and temperature added to problems with leakage and restricted access to the active site, often limit the devices to single use. For this reasons enzyme engineering has become a new tool in the field.

Through enzyme engineering scientists aim to design and tailor enzymes according to the properties required for each specific biosensing system, which could mean to increase the affinity for the substrate or introduce groups for the immobilisation to the electrode, while retaining the functionality.[36]

1.2. Electrode materials

The electrode material can significantly affect the signal to noise ratio and the reproducibility of the response. The choice of the proper material has, first of all, to consider the type of species that are going to interact with the electrode surface and the stability of the material within the operating potential window of the final device. Electrical conductivity, mechanical properties, biocompatibility and cost are features to take into account.[37]

1.2.1. Carbon electrodes

Carbon materials are available in three allotropes: graphite, diamond and fullerene. Diamond itself has low conductivity and can be used as electrode material only by addition of a doping element such as boron (BDD) and nitrogen. The relative inertness of BDD means greater stability, reduced need for pretreatment of the surfaces upon utilisation, low adsorption of organic species. Although it is possible to chemically modify a diamond electrode, the elevated cost and difficult production of diamond limit its use.[38]

Fullerenes have been increasingly applied in the form of carbon nanotubes (CNT). Carbon nanotubes are defined single walled (SWCNT), when constituted by only one sheet of graphene rolled in a cylindrical shape, or multi walled (MWCNT), when multiple sheets of graphene organise in concentric cylinders. According to the direction of the graphene sheets folding, CNT can be either semiconductors or metallic (Figure **2**).

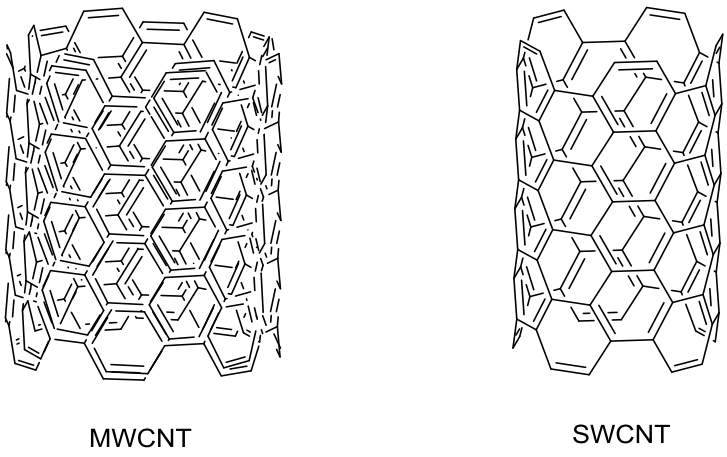

Figure 2. *Examples of the possible structures of carbon nanotubes*

The advantages of carbon nanotubes derive from the generation of high surface area electrodes, providing an increase in the amount of biocatalyst at the surface with a consequent increase in the current generated, coupled with good conductivity; for this reasons carbon nanotubes find application in many fields especially in energy storage systems.[39]

Graphite is the most employed form of carbon in biosensors: the treatment of hydrocarbons or carbon polymers in different conditions of temperature, pressure and presence of inert gases, allows the generation of graphitic sheets that organise to form three-dimensional materials such as highly oriented pyrolytic graphite (HOPG), carbon fibres and glassy carbon (GC).[38] GC has been widely studied and applied because of its stability in a wide potential window both in aqueous and organic solvents, the number of possible functionalities that can be introduced at the surface and the relatively convenient costs. GC is obtained by heating polyacrylonitrile at 1000-3000°C in an inert atmosphere: the graphite sheets generated by such a technique organise in randomly distributed ribbons, characterised by edge planes and basal planes (Figure **3**).[38]

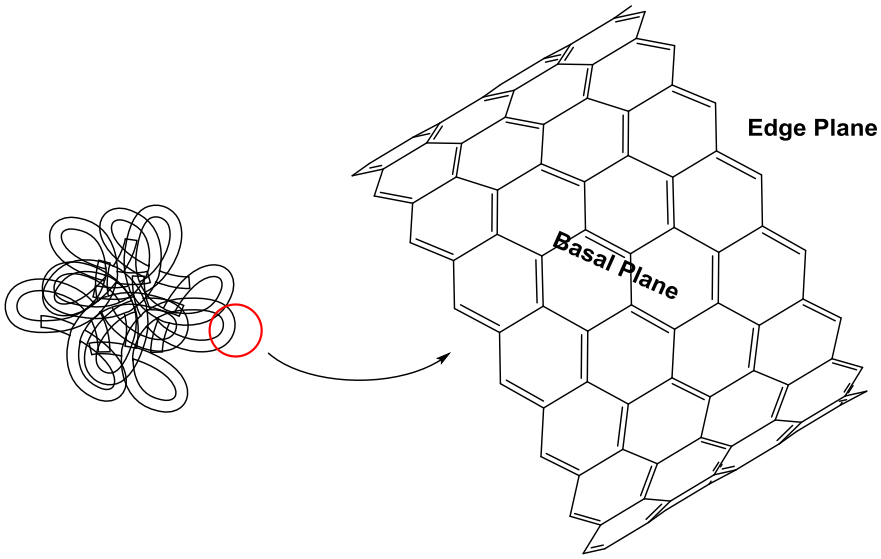

Figure 3. *Representation of the organization of graphene sheets in GC and distinction between basal and edge planes.*

The high reactivity of GC and the poor organisation of the graphene planes, mean that the electrodes requires a careful pre-treatment before use in order to obtain highly smooth surfaces with reproducible behaviour. The main methods applied for

the GC surface preparation are mechanical polishing, thermal pre-treatment and electrochemical pretreatment.[40]

1.2.2. Metal electrodes

Within the metals available, only a few have suitable characteristics for application as working electrodes in electrochemical systems.

Noble metals, specifically platinum and gold, are the most frequently used materials. Platinum and gold present good electron-transfer kinetics and, contrary to most metals, stability in a wide potential window depending on the nature of the media in which they operate.[37] Platinum is mainly applied in sensors for the detection of small organic molecules, in the presence of adsorbed reactants, yet its high cost limits its use.[41]

Gold is used in its polycrystalline form, consisting of a combination of crystallites ordered in a relatively organised manner. The advantages of gold as an electrode material are the ease with which thin layers and colloids can be created and can be patterned using etching and lithography techniques. Furthermore gold is inert compared to other metals and does not react with oxygen.[42] The behaviour of gold surfaces is comparable to glassy carbon in terms of chemical modification and dependence of the reproducibility of the results on the polishing technique.[43]

Although not part of the noble metals, copper presents high conductivity. It finds applications in electroanalytical systems for the detection of small molecules, carbohydrates and amino acids combined with separation techniques such as liquid chromatography and electrophoresis. The advantage of using copper is represented by the low adsorption of the generated species at the surface, which causes the fouling of the electrode when gold and platinum are used in continuous mode.[44]

1.3. Chemical modification of electrode surfaces

The chemical modification of electrode surfaces has been one of the central aspects in the development of biosensors for the last forty years, since it represents a powerful tool for improving the stability of such devices and creating complex systems at the surface.[45]

Chemical modification consists of the formation of thin layers of a compound, either monolayers or multilayers, in order to transfer to the electrode surface the same chemical and physical properties of the modifying film. The chemical modification of surfaces can be achieved with different techniques which involve the formation of surface/modifying layer interactions with different levels of strength.[46]

1.3.1. Chemisorption

Chemisorption is an ideally irreversible adsorption process in which a chemical layer interacts with the electrode surface through valence forces comparable with the forces occurring in the formation of covalent bonds.[46]

A well-known example of chemisorption process are self-assembled monolayers (SAMs) of thiols on gold: thin organic films that spontaneously grow either from solution or from the gas phase onto the solid surface in an organised way (Figure **4**). The energy associated with a S-Au bond is 126 kJ/mol, lower compared to the common energy range associated with a covalent interaction between sulphur and other atoms (220 – 350 kJ/mol), but still more significant than secondary interactions. The stability and behaviour of such films is not only affected by the bond between sulphur and gold, but by the nature of the R groups, since they are able to establish weaker interactions with each other within the film. [47]

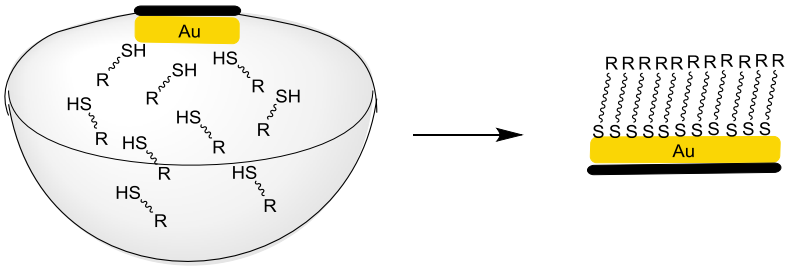

Figure 4. *Formation of thiol SAMs on gold by self-assembly from solution.*

The ease of preparation and versatility of SAMs meant their application in many different fields. The mild conditions required for their growth and the easy

procedures for the introduction of thiol functionalities on biomolecules made them one of the main techniques for the development of biosensors.[48] SAMs have been used as tools for model studies of the behaviour of monolayers and of complex architectures on surfaces at the interface between solid and liquid phase.[49]

The main drawbacks of SAMs are the defects that can occur to the monolayer due to the polishing of the gold surface, desorption and mobility of the thiols on the surface, which prevent the organisation of modifications on the surface in a stable manner, and their tendency to oxidise over time.[42]

1.3.2. Covalent bonding

Through covalent bonding a modifying film is irreversibly attached to the electrode surface.[46] The covalent modification can be achieved by electrografting, oxidation of carbon materials to generate hydroxy and carboxylic acid functionalities at the surface, spontaneous attachment of compounds and reactions induced by the application of heat, UV light and the use of reducing agents. Extensive reviews have been written describing in detail mechanisms, conditions and applications of all these techniques.[50] Here, focus will be given to the main electrografting techniques and the oxidation of carbon surfaces.

1.3.2.1. Oxidation of carbon surfaces

As discussed in paragraph 1.2.1., basal planes and edge planes can be identified on graphitic ribbons of carbon materials. The edge planes present defects with such reactivity to be able to react with atmospheric oxygen and moisture to generate different oxygen functionalities like hydroxy groups, quinones and carboxylic acids (Figure **5**).[38]

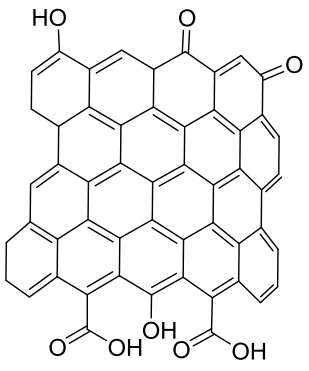

Figure 5. *Oxygen functionalities spontaneously generated at the edge plane of graphene.*

This has been exploited to develop methodologies for chemically inducing the formation of activated carbon surfaces characterised by carboxylic acid groups available for further modification. The techniques reported for the oxidation of carbon surfaces involve the heating of graphite in the presence of air[51] and the treatment of surfaces with radiofrequency oxygen plasma.[52] Once the –COOH groups were introduced at the surface, they were converted to acyl chlorides by reaction with $SOCl_2$ for them to react readily with amines or alcohols (Scheme **1**).

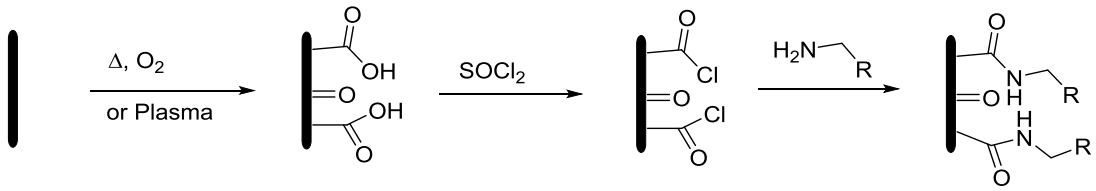

Scheme 1. *Steps for the modification of carbon electrodes through oxidation.*

The oxidation of carbon surfaces, although being one of the first methods for the creation of CME, did not find widespread use, due to the lack of control over the level of oxidation of the species introduced at the surface and consequently the impossibility of obtaining uniform monolayers in a reproducible way.[52]

1.3.2.2. Electrografting – Reduction of diazonium salts

The reduction of diazonium salts is the most applied technique for the covalent modification of surfaces, since it can be used for the creation of organic films on carbon, metals and other semiconductor surfaces.[53]

The diazonium salts for the modification of surfaces are derivatives of *para* substituted anilines and can either be isolated as stable tetrafluoroborate salts by treatment of the amino group with $NaNO_2$ and HBF_4 or generated *in situ* with the use of $NaNO_2$ and HCl, the chloride salts present lower stability compared to the tetrafluoroborate ones. The application of a potential, which can vary according to the electronic properties of the *para* substituent, causes the formation of an aryl radical by reduction of the diazonium and production of N_2 (Scheme **2**).[54, 55]

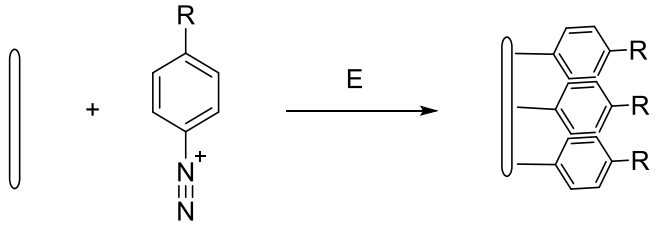

Scheme 2. *Electrografting of diazonium salts on electrodes.*

The nature of the *para* group determines the final properties of the modified surface and the possibility for further modification.[56]

The main drawback of diazonium salts is the difficulty in stopping the modification process at the monolayer level: the delocalization of the charge in the aromatic ring allows new aryl radicals forming in solution to react with the carbons in the *meta* position in a polymerisation reaction with the generation of irregular multilayers (Scheme **3**).[57]

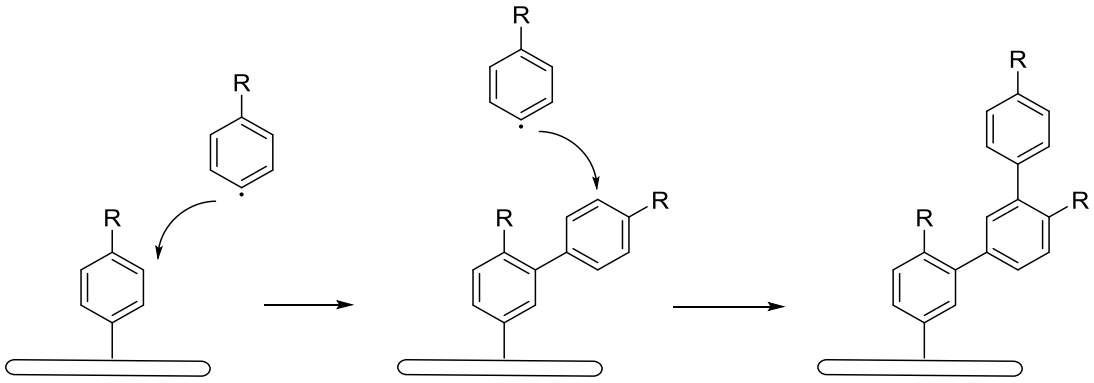

Scheme 3. *Formation of multilayers during the electrografting of diazonium salts.*

A possible solution to this problem is the introduction of bulky protecting groups at the *para* position, in order to hinder the approach of the aryl radicals.[58]

1.3.2.3. Electrografting – Oxidation of primary amines

Although less applied than the reduction of diazonium salts, the oxidation of primary amines is a reliable tool to form very stable monolayers on carbon electrodes. The limitation of this method to carbon materials is due to the high potentials required to achieve the oxidation of the amino group, which would not be compatible with the stability of other materials.[59]

The mechanism of electrografting consists in the generation of a radical cation by loss of an electron, followed by deprotonation of the nitrogen and attachment of a neutral aminyl radical to the carbon surface (Scheme **4**).[60]

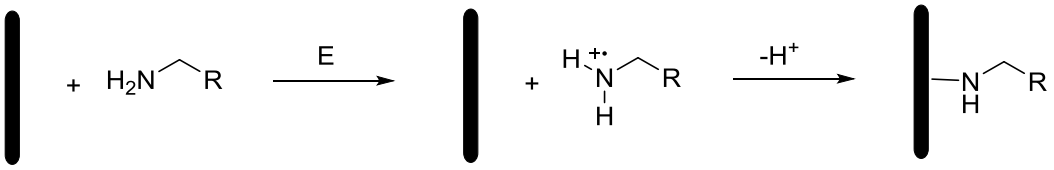

Scheme 4. *Mechanism of modification of GC by oxidation of primary amines.*

The energy needed for the generation of the radical increases from tertiary to primary amines, but the steric hindrance on tertiary and secondary amines is such that only primary amines are able to attach to surfaces effectively.[50]

Particular interest was focused on the study of the creation of monolayers with ω-diamines, since they can represent an anchoring platform for other layers.[61] The early problems, caused by polymerisation and attachment of both amino groups to the electrode surface, were solved by mono-protecting the diamines with easily removable groups once the monolayer was generated at the surface.[58]

1.3.3. Polymer film coating

Electrode surfaces are coated with a layer of polymeric material, either organic, organometallic or inorganic. The polymeric coating is deposited on the surface using different techniques which determine the strength of their interaction, but in general polymers stick to electrodes through adsorption and low solubility in the operating solution. The most common deposition techniques are dip-coating, solvent evaporation and electrochemical polymerisation. Dip-coating consists in dipping the electrode in a solution containing monomers and initiator, until part of the generated polymer adsorbs at the surface; by solvent evaporation, the polymer, dissolved in a suitable solvent, is cast on the electrode surface and the solvent removed by evaporation leaving only the adsorbed polymer. Electrochemical polymerisation allows the formation of the polymer directly at the surface either by activation of the monomer through direct oxidation/reduction at the electrode or by electrochemical generation of the radical initiator. In the first case, the thickness of the polymer layer is limited to the passivation of the electrode surface, unless electroactive species are

included in the polymerisation process. Instead, the generation of the initiator allows the polymerisation to continue until the radical process stops.[46]

Polymer coating has been frequently applied in the creation of biosensors since redox mediators and biomolecules can be either copolymerised or entrapped in the growing polymer, with control over the loading. The disadvantages of using this technique for the modification of electrodes are the impossibility of stopping the polymerisation process at the monolayer level, lack of control over the orientation of the species embedded in the polymer, especially in the case of enzymes, and leakage of the species from the film over time.[62]

1.4. Solid phase peptide synthesis

Solid phase synthesis consists in the use of solid supports to achieve the synthesis of compounds, from small organic molecules to peptides and DNA strands. The advantages of using solid phase methods are several: the reactions present high yields, the work-up required to isolate products is minimal, chemoselectivity can be controlled and a large number of experimental conditions can be tested quickly, using small amounts of reagents.[63]

Solid phase peptide synthesis (SPPS) was developed by Merrifield in 1963: an amino acid was anchored to a solid polymeric resin, insoluble in the reaction solvent and characterised by a suitable functional group for the attachment. By a step-wise procedure, different amino acids were sequentially added to the first to generate the final peptide, which was then cleaved from the solid support.[64]

In general, amino acids are attached to the resin on the C-terminus, while the N-terminus presents a protecting group: the removal of the protecting group allows the coupling of the following protected amino acid using the appropriate coupling agents (Scheme **5**).

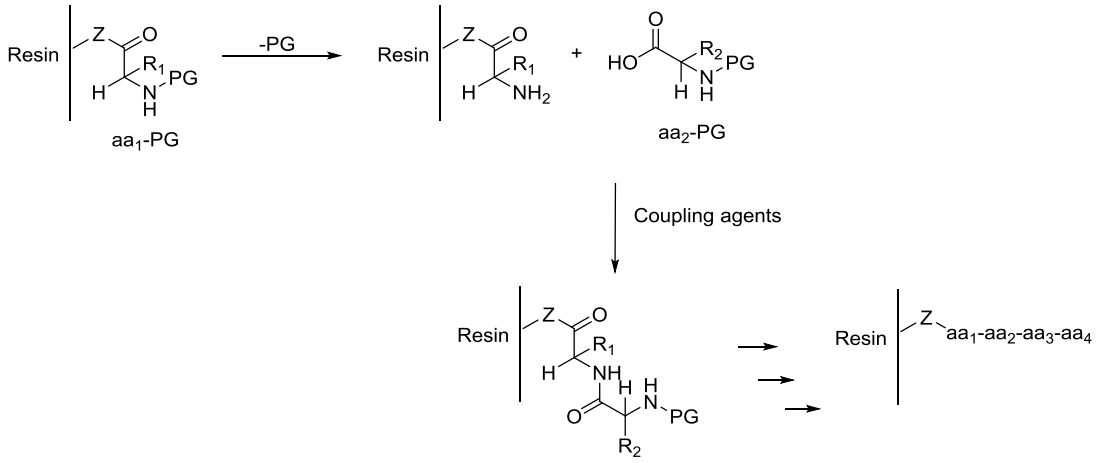

Scheme 5. *General steps for the solid phase synthesis of peptides.*

The choice of the protecting group on the N-terminus depends on the stability of the protecting groups on the side chains of the peptidic backbone: ideally the groups should be orthogonal, which means that the conditions to remove the first one on the N-terminus should not affect any other group. There are two main approaches to SPPS: the Boc strategy and the Fmoc strategy. The Boc strategy involves the use of t-butylcarbonate (Boc) as the protecting group for the N-terminus, the removal is achieved in acidic conditions. The alternative is the use of fluorenylmethyloxycarbonate (Fmoc), which requires milder basic conditions for the removal. In order to generate the amide bond between solid phase bound peptide and the next amino acid, it is necessary to activate the carboxylic acid in solution using coupling agents, with the generation of highly reactive esters.[63]

Several coupling agents classes have been reviewed: the choice of the optimal coupling system depends on the stability of the reaction components and problems with racemisation of amino acids. The most used coupling agents belong to the class of carbodiimides, uronium reagents and phosphonium and aminium salts.[65]

The concepts described for SPPS can be easily transferred to the modification of electrode surfaces to create complex architectures and to study monolayers in terms of electrochemical and physical properties.[58, 61, 66]

1.5. Mixed monolayers: advantages and examples

The general methodology for the creation of elaborate monolayer systems at electrode surfaces for the development of biosensors, involves the sequential introduction of a linker (A) followed by a spacer (B) and finally either a redox mediator or a functional group for the covalent binding of the receptor biomolecule (C) (Figure **6**).

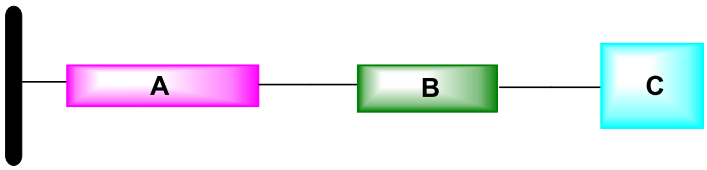

Figure 6. *General representation of a chemically modified electrode.*

The attachment of such modification on the surface can be achieved in conditions of full coverage, with the formation of a uniform monolayer, or in conditions of partial coverage, obtaining mixed monolayers where different species alternate on the surface (Figure **7**).

Figure 7. *Possible modification of electrode surfaces with monolayers. a) Full monolayer composed by: linker (Pink), spacer (Green) and redox species (Light blue); b) Mixed monolayer composed by: two different linkers (Light/Dark pink), spacers of variable length (Green/Brown) and two different redox species(Dark/Light blue).*

The development of methodologies for the creation of mixed monolayers has been the focus of research in various fields, from the creation of semiconductors to organic electronics and sensors.[67] The appeal of mixed monolayers resides in the possibility of assembling multiple components in a bottom-up approach, with control over their organisation to the molecular level.[68] Currently most of the studies focus on mixed SAMs on gold followed by the electrografting of aryl diazonium salts.

The production of mixed SAMs has been achieved through several techniques: electrochemical oxidation of thiols followed by replacement reaction,[69] selective reduction of adsorbed thiols[70] and electrochemical control,[71] but commonly binary monolayers of thiols are obtained by co-adsorption.[72] Usually, the purpose

of mixed SAMs is the creation of surfaces where a linker is surrounded by a diluting compound. Gooding *et al.* published a series of papers where mixed SAMs of ferrocene or anthraquinone derived norbornylogous bridges and alkyl chains of different length as diluents, were used to study the behaviour of redox probes within the electrical double layer.[49, 73] Lee *et al.* recently reported the modification of gold surfaces with mixed SAMs of 1-undecanethiol and 2-bromoisobutylate terminated undecanethiol, as initiator platforms for the polymerisation of pOEGMA brushes modified with biotin for the binding of proteins.[74]

The use of diazonium salts extended the possibility of applying mixed monolayers to a wide range of materials, including carbon. Gooding *et al.* reported first the electrografting of mixtures of diazonium salts on gold in 2005,[75] since then they studied the mechanism of grafting and the properties of the mixed layers both on gold and glassy carbon.[55] They applied this technique for the creation of surfaces modified with oligo(phenylethynylene) molecular wires (MW) diluted with poly(ethylene-glycol), the role of the MW was to provide a rigid anchoring group for the covalent attachment of horseradish peroxidase, with good electron transfer kinetics.[25] Following work involved the use of mixtures of MW/aryl carboxylic acid groups alternated, whose role was both to anchor and stabilise the glucose oxidase enzyme and orient the active site toward the electrode at the electrode surface.[76] In both cases the direct electron transfer between enzyme and electrode was investigated. Most recently the combination MW/poly(ethyleneglycol) was applied to the creation of an electrochemical immuno-biosensor.[77]

Downard et al. reported the formation of mixed monolayers by sequential electrografting of diazonium salts: the use of a bulky protecting group on the first modifier allowed enough space for the second group to attach to the surface.[78]

Our group reported a different approach to the creation of mixed monolayers: the creation of a monolayer of N-Boc-ethylenediamine by oxidation of the free primary amine and removal of the protecting group, the surface was sequentially modified with three redox probes by dipping the electrode in three different coupling solutions each containing a single component.[79] Alternatively, mixed monolayers of diamines have been obtained by electrografting of two amines in solution in variable relative ratios.[80]

The use of mixed monolayers presents many advantages in the development of biosensors: enzymes can be anchored to the surface and surrounded by redox mediators to improve the mediated electron transfer and their orientation, density and distance to the surface could be regulated, in order to achieve an optimal response from the system (Figure **8**). Moreover they could be used to create models that mimic the environment of the active site of enzymes by surrounding redox mediators with peptides that could affect their physical and electrochemical properties.

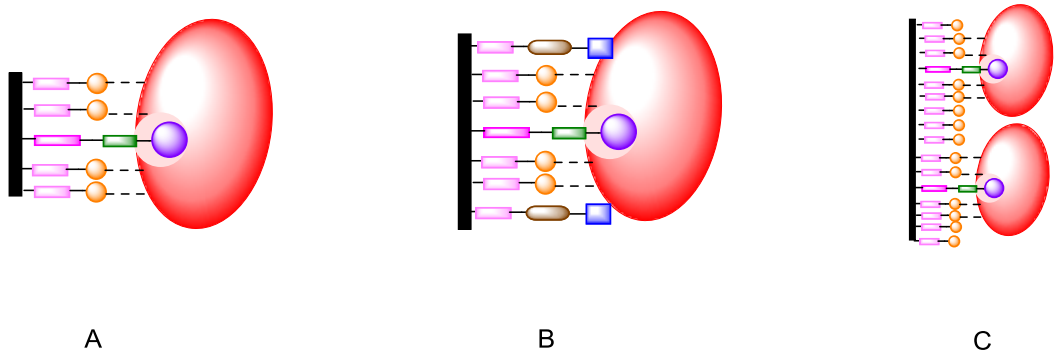

Figure 8. *Application of mixed monolayers in biosensors. Enzymes (Red) could be covalently bound to a surface using dedicated anchoring groups (Purple) attached to linkers (Light/Dark Pink) and spacers (Green/Brown) of optimised length, in order to: A) stabilise the enzyme by secondary interactions through suitable functional groups (Orange); B) alternate enzyme and redox mediator (Blue) on the surface; C) control density, orientation and distance of the enzyme from the surface.*

1.6. Aims of the project

The aim of the project is the development of a methodology to create mixed monolayers at glassy carbon surfaces in a reliable and reproducible way, using the oxidation of primary amines and solid phase peptide synthesis as the main tools.

The initial objective is the synthesis of redox molecules, specifically osmium bipyridyl complexes, suitable for the attachment to the surface and potentially able to act as redox mediator for an enzyme.

The methodology for the creation of mixed monolayers is optimised using an osmium complex and anthraquinone as redox probes. As explained previously, the use of mixed monolayers presents several advantages: the control over the amount of species at the surface, the possibility to covalently bind biomolecules in an organised way choosing orientation and distance from the surface.

Here, we aim to develop a glucose biosensor where the osmium complex alternates on the surface to an engineered glucose dehydrogenase (GDH): ideally the distribution of the components and their relative orientation should be such to obtain a stable response from the device.

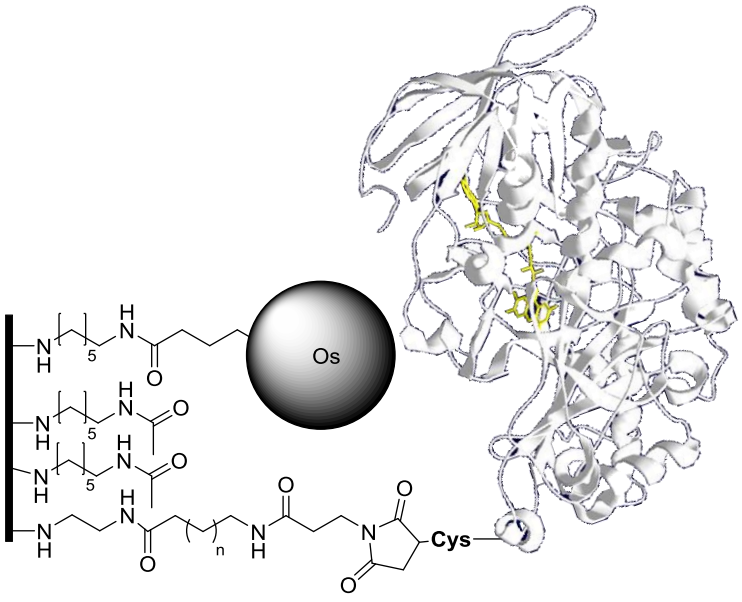

Figure 9. *Representation of the final enzyme/redox mediator modified surface.*

1.7. References

[1] Thévenot, D.R.; Toth, K.; Durst, R.A.; Wilson, G.S. *Pure Appl. Chem.* **1999,** *71,* 2333-2348.

[2] Domìnguez-Renedo, O.; Alonso-Lomillo, M.A.; Arcos-Martinez, M.J. *Current Research, Technology and Education Topics in Applied Microbiology and Microbial Biotechnology*, vol. 2, Mendez-Vilà, A., Ed., Formatex: Badajoz (Spain), 2010.

[3] a) Kotanen, C.N.; Moussy, F.G.; Carrara, S.; Guiseppi-Elie, A. *Biosens. Bioelectron.* **2012,** *35,* 14-26. b) Zhao, Z.; Jiang, H., *Biosensors*, Serra, P.A., Ed., InTech: Rijeka (Croatia), 2010.

[4] a) Ghindilis, A.L.; Atanasov, P.; Wilkins, M.; Wilkins, E. *Biosens. Bioelectron*. **1998,** *13,* 113-131. b) Luppa, P.B.; Sokoll, L.J.; Chan, D.W. *Clin. Chim. Acta,* **2001,** *314,* 1-26. c) Ricci, F.; Adornetto, G.; Palleschi, G. *Electrochim. Acta*, **2012,** *84,* 74-83.

[5] a) Dai, N.; Kool, E.T. *Chem. Soc. Rev.* **2011,** *40,* 5756-5770; b) Junhui, Z.; Hong, C.; Ruifu, Y. *Biotechnol. Adv*. **1997,** *15,* 43-58.

[6] a) Han, K.; Liang, Z.; Zhou, N. *Sensors* **2010,** *10,* 4541-4557. b) Navani, N.K.; Li, Y. *Curr. Opin. Chem. Biol*. **2006,** *10,* 272-281.

[7] a) D'Souza, S.F. *Biosens. Bioelectron.* **2001,** *16,* 337-353; b) Pancrazio, J.J.; Whelan, J.P.; Borkholder, D.A.; Ma, W.; Stenger, D.A. *Ann. Biomed. Eng.* **1999,** *27,* 697-711.

[8] Liu, J.; Lu, Y. *J. Fluoresc.* **2004,** *14,* 343-354.

[9] Pramanik, S.; Pingguan-Murphy, B.; Azuan Abu Osman, N. *Int. J. Electrochem. Sci.* **2013,** *8,* 8863-8892.

[10] Long, F.; Zhu, A.; Shi, H. *Sensors* **2013,** *13,* 13928-13948.

[11] Clark, L.C.; Lyons, C. *Ann. N. Y. Acad. Sci.* **1962,** *102,* 29-45.

[12] Prodromidis, M.I.; Karayannis, M.I. *Electroanalysis* **2002,** *14,* 241-261.

[13] a) Heller, A.; Feldman, B. *Chem. Rev*. **2008,** *108,* 2482-2505. b) Koncki, R. *Anal. Chim. Acta* **2007,** *509,* 7-15.

[14] a) Dennison, M.J.; Turner, A.P.F. *Biotechnol. Adv.* **1995,** *13,* 1-12; b) Shah, J.; Wilkins, E. *Electroanalysis* **2003,** *15,* 157-166. c) Trojanowicz, M. *Electroanalysis* **2002,** *14,* 19-20.

[15] Grieshaber, D.; MacKenzie, R.; Voros, J.; Reimhult, E. *Sensors* **2008,** *8,* 1400-1458.

[16] Pohanka, M.; Skladal, P. *J. Appl. Biomed.* **2008,** *6,* 57-64.

[17] Mehrvar, M.; Abdi, M. *Anal. Sci.* **2004,** *20,* 1113-1126.

[18] Ronkainen, N.J.; Halsall, H. B.; Heineman, W.R. *Chem. Soc. Rev.* **2010,** *39,* 1747-1763.

[19] Karyakin, A.A. *Bioelectrochemistry* **2012,** *88,* 70-75.

[20] Noll, T.; Noll, G. *Chem. Soc. Rev* **2011,** *40,* 3564-3576.

[21] Putzbach, W.; Ronkainen, N.J. *Sensors* **2013,** *13,* 4811-4840.

[22] Tasca, F.; Gorton, L.; Harreither, W.; Haitrich, D.; Ludwig, R.; Noll, G. *Anal. Chem.* **2009,** *81,* 2791-2798.

[23] Bartlett, P.N.; Birkin, P.R.; Wang, J.H.; Palmisano, F.; De Benedetto, G. *Anal. Chem.* **1998,** *70,* 3685-3694.

[24] Hiller, M.; Kranz, C.; Huber, J.; Bauerle, P.; Schuhmann, W. *Adv. Mater.* **1996,** *8,* 219-222.

[25] Liu, G.; Gooding, J. J. *Langmuir* **2006,** *22,* 7421-7430.

[26] Polsky, R.; Harper, J.C.; Dirk, S.M.; Arango, D.C.; Wheeler, D.R.; Brozik, S.M. *Langmuir* **2007,** *23,* 364-366.

[27] Ran, Q.; Peng, R.; Liang, C.; Ye, S.; Xian, Y.; Zhang, W.; Jin, L. *Anal. Chim. Acta* **2011,** *697,* 27-31.

[28] Watanabe, K.; Manefield, M.; Lee, M.; Kouzuma, A. *Curr. Opin. Biotechnol.* **2009,** *20,* 633–641.

[29] Chaubey, A.; Malhotra, B.D. *Biosens. Bioelectron.* **2002,** *17,* 441-456.

[30] Battaglini, F.; Bartlett, P.N.; Wang, J.H. *Anal. Chem.* **2000,** *72,* 502-509.

[31] Buchholz, K.; Kasche, V.; Bornscheuer, U.T. *Biocatalysts and Enzyme Technology* (2nd Edition), Wiley – Blackwell, 2012,

[32] a) Fernandez-Fernandez, M.; Angeles Sanroman, M.; Moldes, D. *Biotechnol. Adv.* **2013,** *31,* 1808–1825. b) Mayer, A.M.; Staples, R.C. *Phytochem.* **2002,** *60,* 551–565.

[33] a) Ruzgas, T.; Csoregi, E.; Emnéus, J.; Gorton, L.; Marko-Varga, G. *Anal. Chim. Acta* **1996,** *330,* 123–138. b) Veitch, N.C. *Phytochem.* **2004,** *65,* 249–259.

[34] a) Bankar, S.B.; Bule, M.V.; Singhal, R.S.; Ananthanarayan, L. *Biotechnol. Adv.* **2009,** *27,* 489–500. b) Gregg, B.A.; Heller, A. *Anal. Chem.* **1990,** *62,* 258–253.

[35] Lobo, M.J.; Miranda, A.J.; Tunon, P. *Electroanalysis* **1997,** *9,* 191–202.

[36] Campas, M.; Prieto-Simon, B.; Marty, J.L. *Sem. Cell. Dev. Biol.* **2009,** *20,* 3-9.

[37] Wang, J. *Analytical Electrochemistry* (2nd Edition), Wiley-VCH, 2000.

[38] a) McCreery, R.L. *Chem. Rev.* **2008,** *108,* 2646-2667. b) Wildgoose, G.G.; P. Abiman, Compton, R.G. *J. Mater. Chem.* **2009,** *19,* 4875-4886.

[39] Baughman, R.G.; Zakhidov, A.A.; De Heer, W.A. *Science* **2002,** *297,* 787-792.

[40] a) Gonon, F.G.; Navarre, F.; Buda, M.J. *Anal. Chem.* **1984,** *56,* 575-578. b) Kamau, G.N.; Willis, W.S.; Rusling, J.F. *Anal. Chem.* **1985,** *57,* 545-551. c) Kazee, B.; Weisshaar, D.E.; Kuwana, T. *Anal. Chem.* **1985,** *57,* 2739-2740. d) S. Ranganathan, S.; Kuo, T.-C.; McCreery, R.L. *Anal. Chem.* **1999,** *71,* 3574-3580.

[41] a) Marinovic, V.; Marinovic, S.; Jovanovic, M.; Jovanovic, J.; Nesic, G.; Stojanovic, M. *Int. J. Electrochem. Sci.* **2013,** *8,* 1986-1998. b) Wurdarska, E.; Chrzescijanska, E.; Kusmierek, E.; Rynkowski, J. *Electrochim. Acta* **2013,** *93,* 189-194.

[42] Love, J.C.; Estroff, L.A.; Kriebel, J.K.; Nuzzo, R.G.; Whitesides, G.M. *Chem. Rev.* **2005,** *105,* 1103-1169.

[43] Carvalhal, R.F.; Freire, R.S.; Kubota, L.T. *Electroanalysis* **2005,** *17,* 1251-1259.

[44] a) Luo, M.Z.; Baldwin, R.P. *J. Electroanal. Chem.* **1995,** *387,* 87-94. b) Paixao, T.R.L.C.; Corbo, D.; Bertotti, M. *Anal. Chim. Acta* **2002,** *472,* 123-131.

[45] a) *Advances in Electrochemical Science and Engineering: Chemically Modified Electrodes*, Volume 11, Alkire, R.C.; Kolb, D.M.; Lipkowsky, J.; Ross, P.N., Eds. Wiley-VCH, 2009. b) Murray, R.W. *Acc. Chem. Res.* **1980,** *13,* 135-141.

[46] Durst, R.A.; Baumner, A.J.; Murray, R.W.; Buck, R.P.; Andrieux, C.P. *Pure Appl. Chem.* **1997,** *69,* 1317-1323.

[47] Schreiber, F. *Prog. Surf. Sci.* **2000,** *65,* 151-256.

[48] a) Islam, N.; Gugel, P.V.; Rojas, O.J.; Carbonell, R.G. *J. Phys. Chem. C* **2014,** *118,* 5361-5373. b) Mukherjee, S.; Sengupta, K.; Das, M.R.; Jana, S.S.; Dey, A. *J. Biol. Inor.*

Chem. **2012,** *17,* 1009-1023. c) Wong, E.L.S.; Erokhin, P.; Gooding, J.J. *Electrochem. Comm.* **2004,** *6,* 648-654.

[49] a) Darwish, N.; Eggers, P.K.; Ciampi, S.; Tong, Y.; Ye, S.; Paddon-Row, M.N.; Gooding, J.J. *J. Am. Chem. Soc.* **2012,** *134,* 18401-18409. b) Hong, H.-G.; Park, W. *Langmuir* **2001,** *17,* 2485-2492.

[50] a) Barriere, F.; Downard, A.J. *J. Solid State Electrochem.* **2008,** *12,* 1231-1244. b) Belanger, D.; Pinson, J. *Chem. Soc. Rev.* **2011,** *40,* 3995-4048.

[51] Ireland, P.S.; Olson, L.W.; Brown, T.L. *J. Am. Chem. Soc.* **1975,** *97,* 3549-3550.

[52] Evans, J.F.; Kuwana,V. *Anal. Chem.* **1977,** *49,* 1632-1635.

[53] Gooding, J.J. *Electroanalysis* **2008,** *20,* 573-582.

[54] Pinson, J.; Podvorica, F. *Chem. Soc. Rev.* **2005,** *34,* 429-439.

[55] Liu, G.; Chockalingham, M.; Khor, S.M.; Gui, A.L.; Gooding, J.J. *Electroanalysis* **2010,** *22,* 918-926.

[56] a) Allongue, P.; Delamar, M.; Desbat, B.; Fagebaume, O.; Hitmi, R.; Pinson, J.; Saveant, J.-M. *J. Am. Chem. Soc.* **1997,** *119,* 201-207. b) Mahouche, S.; Mekni, N.; Abbassi, L.; Lang, P.; Perruchot, C.; Jouini, M.; Mammeri, F.; Turmine, M.; Romdhane, H.B.; Chehimi, M.M. *Surf. Sci.* **2009,** *603,* 3205-3211. c) Saby, C.; Ortiz, B.; Champagne, G.Y.; Belanger, D. *Langmuir* **1997,** *13,* 6805-6813.

[57] Kariuki, J.K.; McDermott, M.T. *Langmuir* **2001,** *17,* 5947-5951.

[58] a) Chretien, J.-M.; Ghanem, M.A.; Bartlett, P.N.; Kilburn, J.D. *Chem. Eur. J.* **2008,** *14,* 2548-2556; b) Leroux, Y.R.; Fei, H.; Noel, J.-M.; Roux, C.; Hapiot, P. *J. Am. Chem. Soc.* **2010,** *132,* 14039-14041.

[59] Cruickshank, A.C.; Tan, E.S.Q.; Brooksby, P.A; Downard, A.J. *Electrochem. Comm.* **2007,** *9,* 1456-1462.

[60] Barnes, K.K.; Mann, C.K. *J. Org. Chem.* **1967,** *32,* 1474-1479.

[61] a) Barbier, B.; Pinson, J.; Desarmot, G.; Sanchez, M. *J. Electrochem. Soc.* **1990,** *137,* 1757-1764. b) Ghanem, M.A.; Chretien, J.-M.; Pinczewska, A.; Kilburn, J.D.; Bartlett, P.N. *J. Mater. Chem.* **2008,** *18,* 4917-4927.

[62] Cosnier, S. *Biosens. Bioelectron.* **1999,** *14,* 443-456.

[63] Dorwald, F. Z *Organic Synthesis on Solid Phase* (2nd Edition.), Wiley-VCH, **2002**.

[64] Merrifield, R.B. *J. Am. Chem. Soc.* **1963,** *85*, 2149-2154.

[65] Prasad. K.; Bharathi, K.; Haseena Banu, B. *Int. J. Pharm. Sci. Rev. Res.* **2011,** *8*, 108-119.

[66] Sosna, M.; Chretien, J.-M.; Kilburn, J.D.; Bartlett, P.N. *Phys. Chem. Chem. Phys.* **2010,** *12*, 10018-10026.

[67] a) Downard, A.J.; D.J. Garrett, E.S.Q. Tan, *Langmuir* **2006,** *22*, 10739-10746. b) Hasobe, T.; Imahori, H.; Kamat, P.V.; Ahn, T.K.; Kim, S.K.; Kim, D.; Fujimoto, A.; Hirakawa, T.; Fukuzumi, S. *J. Am. Chem. Soc.* **2005,** *127*, 1216-1228. c) Santos, L.; Mattiuzzi, A.; Jabin, I.; Vandencasteele, N.; Reniers, F.; Reinaud, O.; Hapiot, P.; Lhenry, S.; Leroux, Y.; Lagrost, C. *J. Phys. Chem. C* **2014,** *118*, 15919-15928.

[68] Unruh, D.A.; Mauldin, C.; Pastine, S.J.; Rolandi, M.; Frechet, J.M.J. *J. Am. Chem. Soc.* **2010,** *132*, 6890-6891.

[69] Chen, Y.; Yang, C.; Wang, F.-B. *Electrochim. Acta* **2010,** *55*, 3951-3956.

[70] Imabayashi, S.; Hobara, D.; Kakiuchi, T. *Langmuir* **1997,** *13*, 4502-4504.

[71] González-Granados, Z.; Sánchez-Obrero, G.; Madueño, R.; Sevilla, J.M.; Blázquez, M.; Pineda, T. *J. Phys. Chem. C* **2013,** *117*, 24307-24316.

[72] a) Bain, C.D.; Evall, J.; Whitesides, G.M. *J. Am. Chem. Soc.* **1989,** *111*, 7155-7164. b) Bain, C.D.; Evall, J.; Whitesides, G.M. *J. Am. Chem. Soc.* **1989,** *111*, 7164-7175.

[73] a) Darwish, N.; Eggers, P.K.; Da Silva, P.; Zhang, Y.; Tong, Y.; Ye, S.; Gooding, J.J.; Paddon-Row, M.N. *Chem. Eur. J.* **2012,** *18*, 283-292. b) Darwish, N.; Paddon-Row, M.N.; Gooding, J.J. *Acc. Chem. Res.* **2014,** *47*, 385-395. c) Eggers, P.K.; Darwish, N.; Paddon-Row, M.N.; Gooding, J.J. *J. Am. Chem. Soc.* **2012,** *134*, 7539-7544.

[74] Jeong, S.P.; Lee, B.S.; Kang, S.M.; Ko, S.; Choi, I.S.; Lee, J.K. *Chem. Comm.* **2014,** *50*, 5291-5293.

[75] Liu, G.; Liu, J.; Bocking, T.; Eggers, P.K.; Gooding, J.J. *Chem. Phys.* **2005,** *319*, 136-146.

[76] Liu, G.; Paddon-Row, M.N.; Gooding, J.J. *Electrochem. Comm.* **2007,** *9*, 2218-2223.

[77] Liu, G.; Paddon-Row, M.N.; Gooding, J.J. *Chem. Comm.* **2008,** *33*, 3870-3872.

[78] Lee, L.; Brooksby, P.A.; Leroux, Y.R.; Hapiot, P.; Downard, A.J. *Langmuir* **2013,** *29,* 3133-3139.

[79] Chretien, J.-M.; Ghanem, M.A.; Bartlett, P.N.; Kilburn, J.D. *Chem. Eur. J.* **2009,** *15,* 11928-11936.

[80] Wright, E.J.; Sosna, M.; Bloodworth, S.; Kilburn, J.D.; Bartlett, P.N. *Chem. Eur. J.* **2014,** *20,* 5550-5554.

2. The redox mediator: synthesis, properties and characterisation of osmium bipyridyl complexes.

2.1. Applications of osmium bipyridyl complexes as redox mediators

Transition metal complexes have found application as catalysts in electro-oxidation reactions[1] and in the development of devices for energy storage and biosensing since they present advantages in terms of redox and luminescence properties and stability.[2] Osmium, with iron and ruthenium, belongs to group VII and their complexes are amongst the most exploited as redox mediators.[3] In particular, osmium bipyridyl complexes present favourable aspects which make them ideal redox mediators: the couple $Os^{2+/3+}$ has well defined values of redox potential that can be varied by changing the number and structure of the ligands and both oxidation states are stable.[4] Moreover the steric bulk of the metal complex appears to prevent its adsorption on graphite surfaces, a process unavoidable with other redox mediators such as organic dyes and quinones.[5]

Several studies describe the behaviour of osmium bipyridyl complexes at metal surfaces either as SAMs on gold or chemisorbed to platinum through a pendant pyridine nitrogen: their stability in both reduced and oxidised states makes them optimal probes for the study of electron transfer processes and monolayer organisation, moreover, in conjunction with their spectroscopic properties, they have been tested for potential application in transistors, diodes and molecular switches.[6]

Most of the literature concerning the use of osmium complexes as redox mediators involves their embedding in polymeric matrices or hydrogels, where one of the ligands is cross-linked in the polymeric backbone in order to avoid leakage of the species. In these systems, osmium complexes have proven suitable mediators for various enzymes including laccase, glucose oxidase and glucose dehydrogenase.[7]

The covalent attachment of the metal centre on the electrode surface allows the creation of stable monolayers and it can be performed by three main methods (Scheme **6**):

a) attachment of a ligand on a layer of linkers on the surface followed by the formation of the complex;[8]
b) synthesis in solution of the desired complex with ligands presenting moieties suitable for the attachment to a linker on the surface;[9]
c) direct electrochemical attachment of the complex bearing primary amines or diazonium salt functionalities; [8,10]

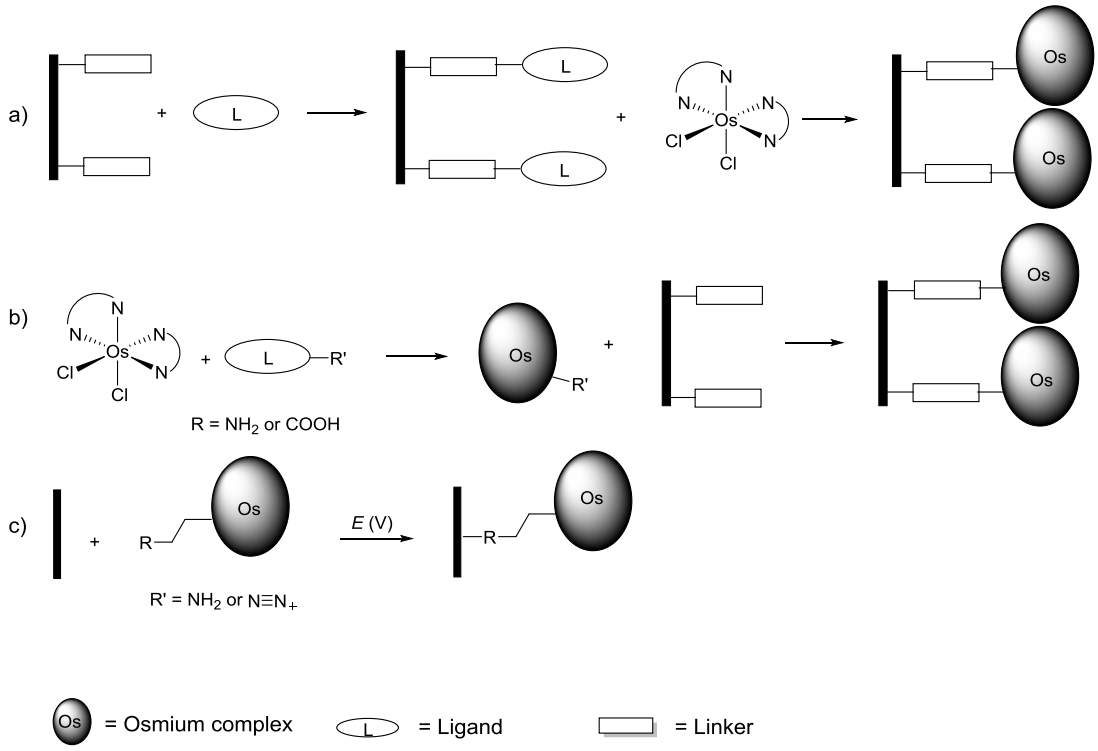

Scheme 6. *Possible approaches to the covalent attachment of an osmium bipyridyl complex to the electrode surface.*

Here the aim was the creation of mixed monolayers using the oxidation of mono-protected primary diamines as the main tool, with the use of redox molecules as probes to test the behaviour of the underlying layer by coupling them to the free amines through solid phase synthesis procedures, the approach described in figure **6b**. The usual procedure for the coupling of osmium complexes to surfaces consists in the creation of a monolayer of carboxylic acid functionalities to which an osmium bipyridyl complex presenting a 4-aminomethylpyridine ligand is coupled.[9] In this project, the opposite system is used, similar to the classical solid phase peptide synthesis setup, and the synthesis of osmium bipyridyl complexes presenting carboxylic acid functional groups suitable for the coupling to the amine modified surface was required. Having the free amines at the electrode surface could represent an advantage: if the carboxylic acid linkers are close packed in a monolayer, the yield of the formation of the activated ester reaction could be lowered by the hindering, while if the activation occurs in solution, with the carboxylic acid function on the redox molecule, then ideally the highest amount of mediator is able to react with the linker monolayer.

2.2. Synthesis and characterisation of osmium bipyridyl complexes

Most of the recent literature reporting osmium complexes with 2,2'-bipyridyl ligands focuses on the study of the electrochemical behaviour of the $Os^{2+/3+}$ redox couple. However references reporting a full characterisation are limited, leaving unclear results concerning the organisation of the osmium complexes at the GC surface. In order to have control over the creation of mixed monolayers and remove any variability resulting from the purity of the synthesised complexes upon coupling to the electrode surface, a complete characterisation of the complexes was required.

2.2.1. Synthesis of cis-bis-(2,2'-bipyridyl) osmium(II) chloride

The precursor used for the syntheses of the complexes of the type $[Os(bpy)_2LCl]^+$, was the complex *cis*-bis-(2,2'-bipyridyl) osmium(II) chloride (cis-$Os(bpy)_2Cl_2$) **1**, obtained following a method described by Kober *et al.*[11] (Scheme **7**). The procedure consisted of refluxing $(NH_4)_2OsCl_6$ with 2 equivalents of 2,2'-bipyridyl (bpy) followed by the addition of a solution of an excess of sodium dithionite, to reduce the Os (III) to Os (II). The product was a black-purple solid, routinely isolated in yields over 80% (*Lit*: [11] 85%).

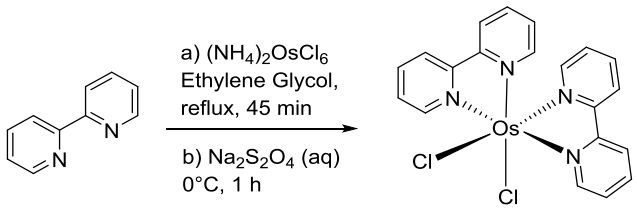

1

Scheme 7. *Steps for the synthesis of complex* ***1*****.**

In general, osmium(II) is paramagnetic, but in bipyrydyl complexes, the two bpy molecules coordinated to the metal centre generate a strong ligand field, forming octahedral complexes with a low-spin d^6 electronic configuration, making them diamagnetic, hence suitable for characterisation by NMR spectroscopy.[14] The analysis of the compound by ^1H NMR (Appendix II) confirmed the formation of the cis-complex **1** presenting 8 different peaks integrating for 2 protons, which suggested that the two bipyridyl ligands lay in orthogonal planes and their protons were subjected to the same environment.

Definitive confirmation of the structure of **1** was provided by X-ray diffraction of the crystals of the compound obtained by slow evaporation of dichloromethane (DCM) (Figure **10**). The crystal contains one molecule of *cis*-$Os(bpy)_2Cl_2$ and one DCM molecule of crystallisation per cell; the chloride ligands are arranged cis relative to each other and the two bpy ligands lay in perpendicular planes.

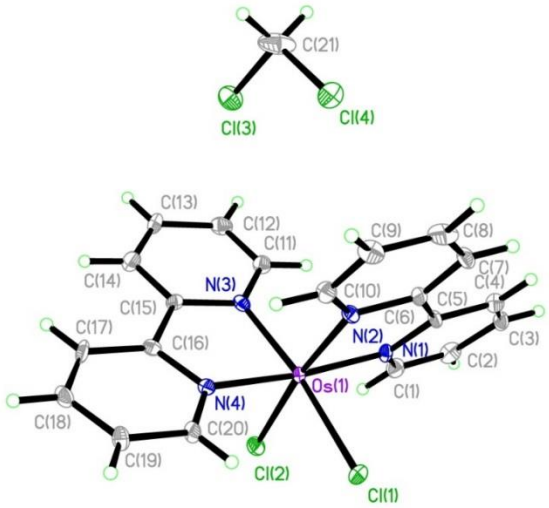

Figure 10. *Crystal structure of complex* ***1.***

The CV (Figure **11**) recorded for a 5 mM solution of **1** in CH_3CN with 0.1 M tetrabutylammonium tetrafluoroborate (TBATFB) as supporting electrolyte showed a reversible redox peak at E_{mp} = 0.111 V vs. Ag/AgCl, corresponding to a one electron process.

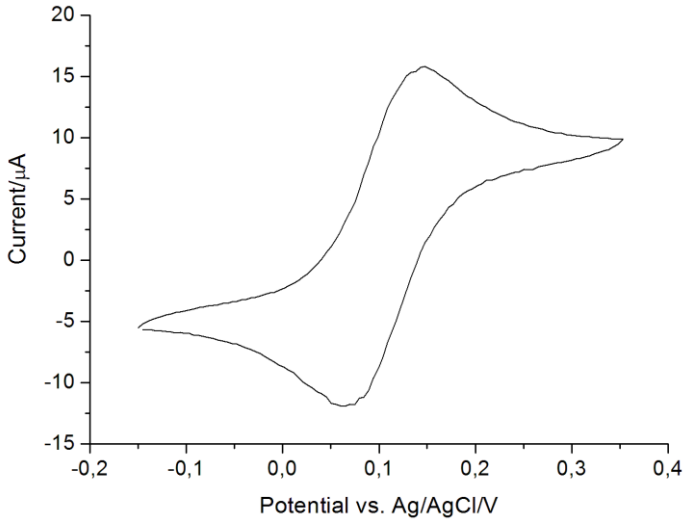

Figure 11. *CV of a 5 mM solution of complex* ***1*** *in CH_3CN with 0.1 M TBATFB recorded at 50 mV s^{-1}, electrode area 0.071 cm^2.*

2.2.2. Synthesis of the ligands

It was decided to test two new ligands: a monodentate pyridine ligand **3** and a bidentate pyridine imidazole ligand **5** (Figure **12**).

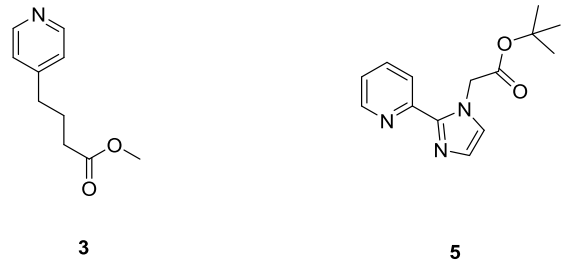

Figure 12. *Structures of the synthesised ligands.*

The synthesis of the monodentate ligand is presented in Scheme **8**: diethyl malonate was deprotonated using sodium hydride and the nucleophile generated was reacted with 4-vinylpyridine by refluxing in ethanol; the intermediate obtained was directly hydrolysed to 4-(4-pyridyl)butyric acid **2** by evaporating the solvent from the previous step and refluxing in 20% HCl solution, the product was isolated by precipitation from ethyl acetate in 60% yield (*Lit*:[12] 64 %). **2** was then converted to the methylester derivative **3** in 47% yield by reaction with methanol using sulphuric acid as catalyst, in order to avoid the chelation of osmium by the carboxylate group upon formation of the complex.

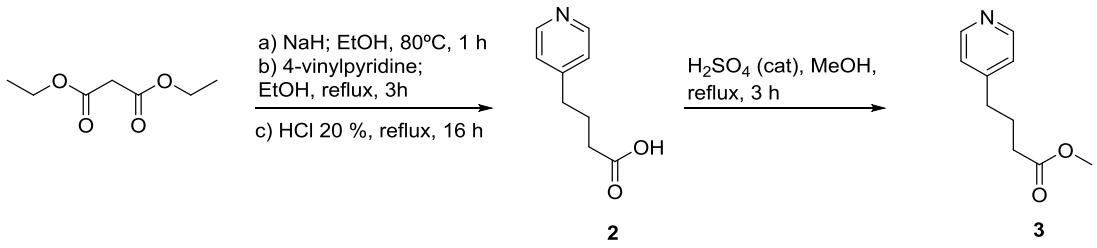

Scheme 8. *Synthetic steps for monodentate ligand **3**.*

Scheme **9** shows the synthetic steps for the formation of the bidentate ligand. The first step was the formation of the imidazole ring by the Radziszewsky reaction, where glyoxal reacts with ammonia to form a diimine, followed by the reaction with pyridine-2-carboxaldehyde to give compound **4** in 21% yield (*Lit*:[13] 33%). The formation of **5** occurred by reacting **4** with *tert*-butyl bromoacetate in the presence of *n*-butyllithium (*n*-BuLi). *n*-BuLi acted as a base, deprotonating the imidazole nitrogen and creating the highly nucleophilic anion, which reacted with the bromo

ester according to Sn_2 mechanism. Given the high reactivity of *n*-BuLi, the first step of the reaction required dry conditions and low temperature (-78 °C). The formation of the nucleophilic anion occurred over 3 hours, after which *tert*-butyl bromoacetate was added to the reaction mixture. Product **5** was obtained in 75% yield.

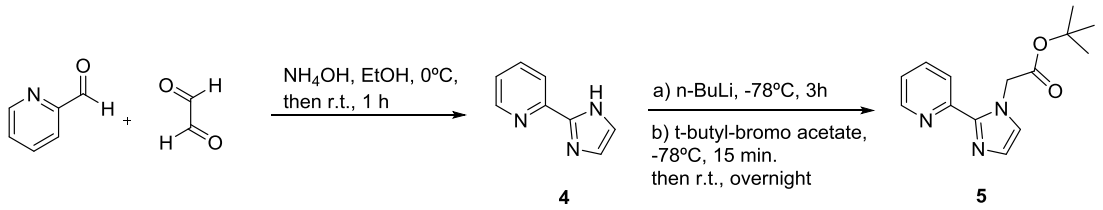

Scheme 9. *Synthetic steps for bidentate ligand* ***5.***

As for ligand **3**, the *tert*-butyl ester acted as a protecting group for the carboxylic acid moiety, to avoid the possible chelation of the osmium by the carboxylate anion instead of the pyridine-imidazole nitrogens, and it could be removed under mild acidic conditions after the formation of the complex.

2.2.3. Synthesis of the complexes

The commonly reported procedure for the formation of $[Os(bpy)_2LCl]^+$ and $[Os(bpy)_2L^{'}\text{-}L']^{2+}$ consists in refluxing the precursor **1** in ethylene glycol in the presence of an excess of the ligand for 4 hours under nitrogen atmosphere. The complexes are then isolated as hexafluorophosphate (PF_6^-) salts by addition of a aqueous solution of an excess of ammonium hexafluorophosphate: PF_6^- exchanges the Cl^- counter ion of the complexes, forming a tight ion pair insoluble in water, which can be easily isolated by filtration (Scheme **10**).[11, 14]

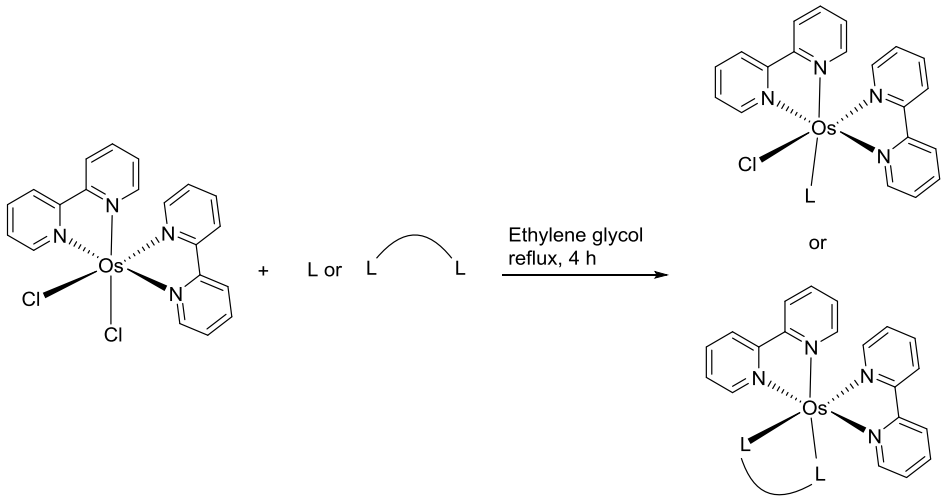

Scheme 10. *General procedure for the substitution of one or two chloride ligands with a monodentate or bidentate ligand in an osmium bipyridyl complex.*

When the procedure was applied to generate complexes **6** and **8**, two problems occurred: compound **6** was formed mixed with the di-substituted complex and the *tert*-butyl group on **5** was removed, causing secondary reactions to occur that made the characterisation of the complex difficult. Figure **13** shows the cyclic voltammogram recorded for the solid isolated upon synthesis of complex **6**: it presents two peaks, the first at E_{mp} = 0.49 V vs. Ag/AgCl can be associated with the desired mono-substituted product, while the peak at E_{mp} = 0.83 V vs. Ag/AgCl corresponds to the di-substituted product, obtained in a ratio mono/di-substituted 4:1.

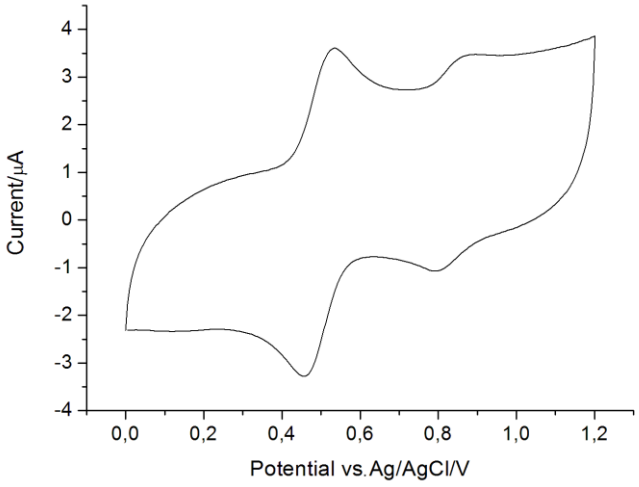

Figure 13. *CV of a 2 mM solution of the product of reaction of complex **1** with ligand **3** (according to conditions reported in scheme **10**) in CH_3CN with 0.1 M TBATFB recorded at 50 mV s^{-1}, electrode area 0.071 cm^2.*

After the optimisation of the reaction conditions by testing different temperatures, reaction times and solvents, a final procedure was developed: **1** was dissolved with

ethylene glycol and 1.01 equivalents of the chosen ligand were added, the mixture was heated at 100 °C for 2 hours, followed by precipitation of the PF_6^- salts. Complex **6** was obtained in 80% yield while complex **7** was obtained in 68% yield (Scheme **11**).

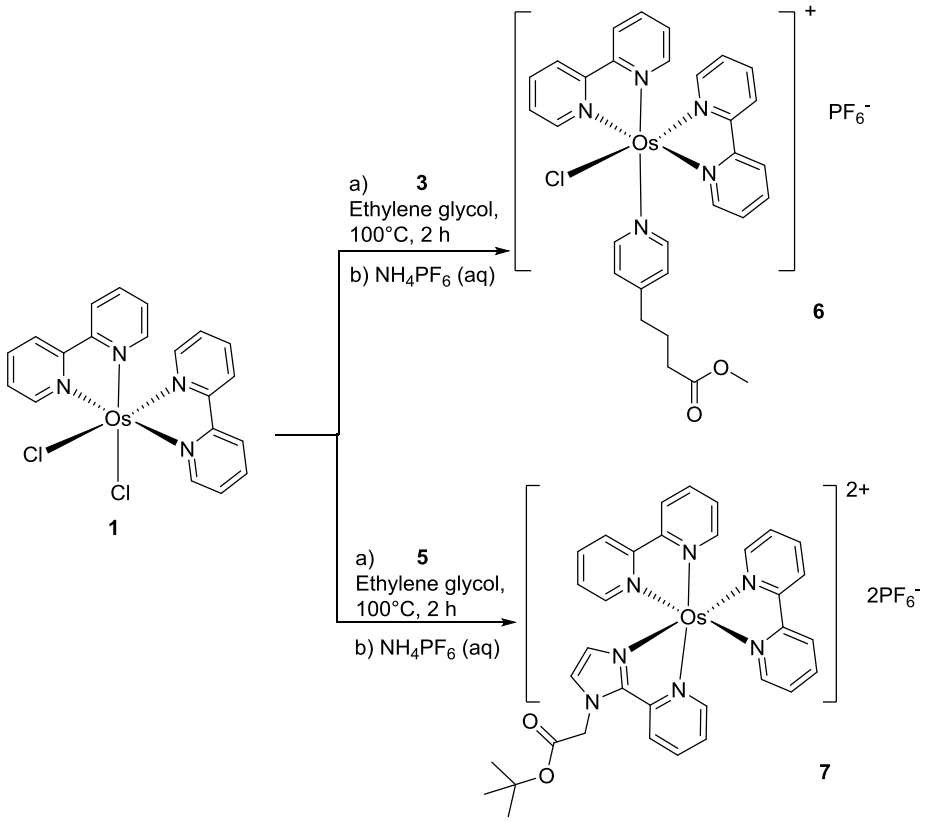

Scheme 11. *Synthetic steps for the formation of complexes **6** and **7**.*

The treatment of **6** with 2 M potassium hydroxide in methanol/water gave complex **8** in 83% yield as a red-brown solid, while the treatment of **7** with trifluoroacetic acid in DCM caused the removal of the tert-butyl group to obtain **9** in 95% yield as a green solid, both suitable for the coupling to an amine modified surface (Scheme **12**). The products were characterised by NMR spectroscopy, UV-vis, IR, mass spectroscopy and CV.

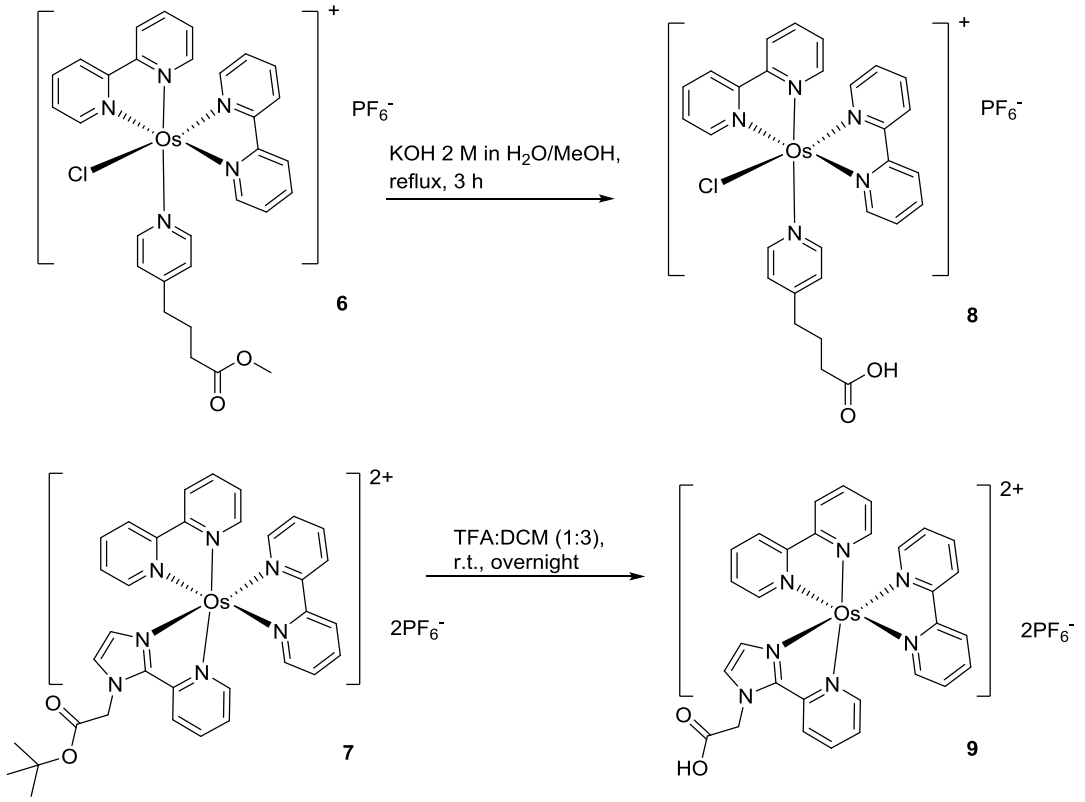

Scheme 12. *Synthetic steps for the generation of complexes* ***8*** *and* ***9.***

It is known from the literature that the substitution of the remaining chloride ligands on the osmium centre in **1** with nitrogen heterocyclic compounds, induces a shift of the E_{mp} of the $Os^{2+/3+}$ couple to more positive potential, by a value tuneable by choosing the structure of the new ligand.[11] Figure **14** shows the comparison of the CVs for complexes **8**, **9** and precursor **1**. The substitution of a chloride with a monodentate ligand induces a shift in the potential values of the redox peaks by 0.39 V compared to complex **1**: complex **8** presents a reversible redox peak associated with a one electron process at E_{mp} = 0.492 V vs Ag/AgCl. The addition of the bidentate ligand induces a further shift by 0.38 V, the CV of complex **9** is characterised by a reversible peak associated to a one electron process at E_{mp} = 0.871 V vs Ag/AgCl.

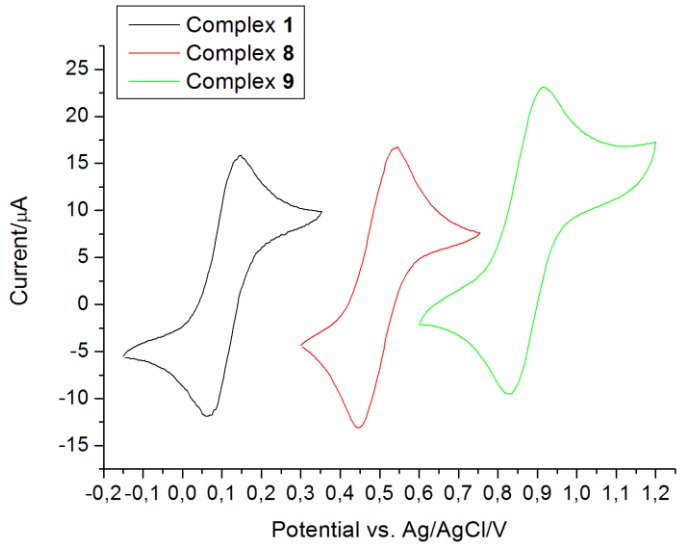

Figure 14. *CV of a 5 mM solution of complexes **1**, **8** and **9** in CH_3CN with 0.1 M TBATFB recorded at 50 mV s^{-1}, electrode area 0.071 cm^2.*

A similar effect could be detected in the UV spectra of the compounds (Figure **15**): the absorption spectra of all the complexes present three bands which can be assigned to the Os (dπ) → bpy (π*) metal-ligand charge transfer (MLCT) transitions: the bands move to higher energy as the redox potential of the $Os^{2+/3+}$ couple is shifted to higher values.[11] In this case the shift of the absorption bands is in good agreement with the data reported by Buckingham and Kober.[11, 14]

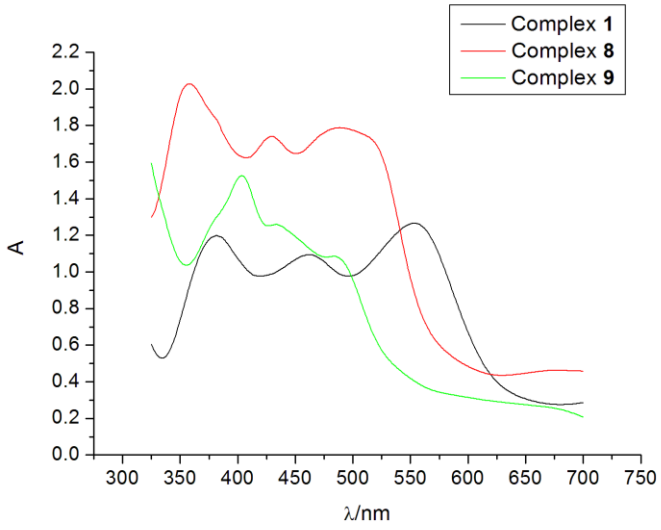

Figure 15. *Electronic spectra in the visible region recorded for 10^{-4}M solutions of complexes **1**, **8** and **9** in CH_3CN.*

The NMR spectra of the compounds were recorded in d^6-DMSO at 300 MHz: given the complexity of the structure, with all the symmetry removed from the structures of the ligands by anisotropic effect of the neighbouring groups, the spectra presented several signals, often overlapping with each other, which made the assignments of the protons difficult. Nonetheless, with the help of the {^{1}H-^{1}H} COSY spectra it was possible to assign all the signals. The crystals of complex **8** were obtained by dissolving in DCM/MeOH (8:2), then slowly evaporating the solvent (Figure **16**).

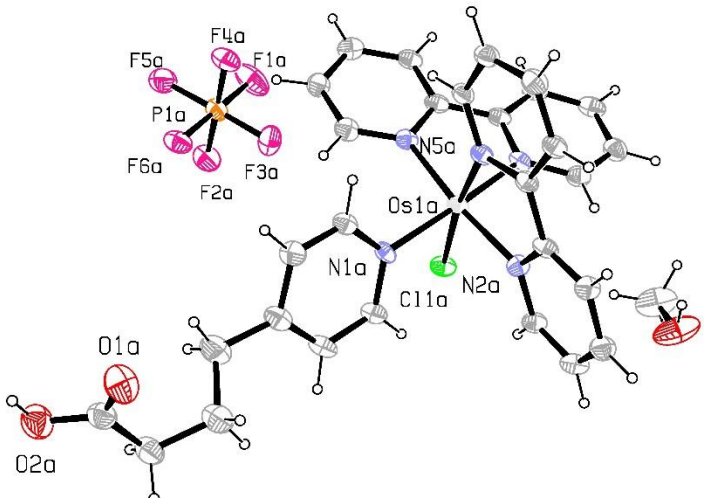

Figure 16. *Crystal structure of complex* ***8.***

2.3. Coupling of the synthesised complexes to amine modified GC surfaces

A series of sets of GC electrodes were modified with N-Boc-ethylenediamine (EDA-Boc), creating a monolayer through the electroxidation of the free primary amine. The mechanism associated with the process has been described in Section 1.3.2.3; experimentally the formation of the monolayer was achieved by dipping the GC working electrodes in a 20 mM solution of EDA-Boc in CH_3CN, with 0.1 M TBATFB as supporting electrolyte, and cycling the potential 4 times between 0.5 V and 2 V vs. Ag/AgCl at 50 mV s^{-1} scan rate. Figure **17** shows the voltammograms recorded for the grafting process: the first cycle is characterised by an irreversible oxidation peak at E = 1.8 V vs. Ag/AgCl associated with the generation of the amine radical in solution. The attachment of the radicals to GC in the following cycles causes the complete passivation of the surface as confirmed by the lack of redox peaks on the last cycle.[15]

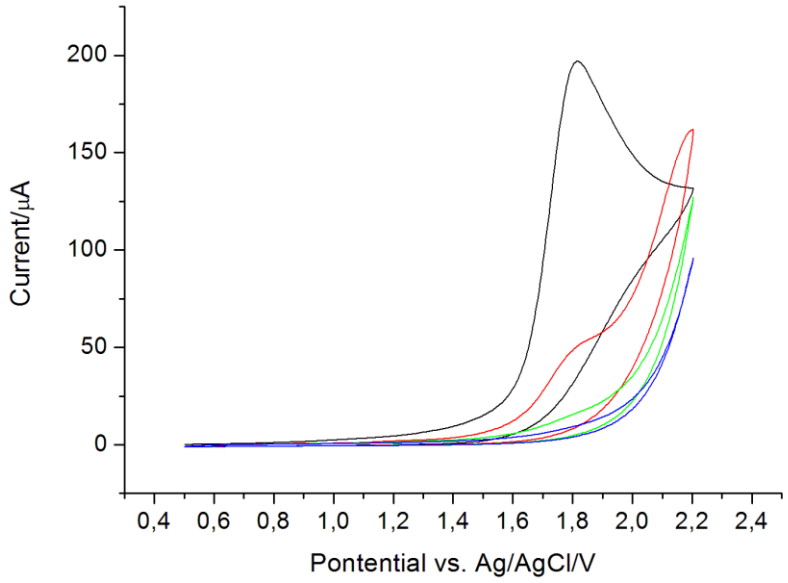

Figure 17. *CV recorded in a 20 mM solution of EDA-Boc in CH_3CN with 0.1 M TBATFB at a scan rate of 50 mV s^{-1}, GC electrode area 0.071 cm^2.*

The removal of the Boc group gave the free amines for coupling to the complexes (Scheme **13**).

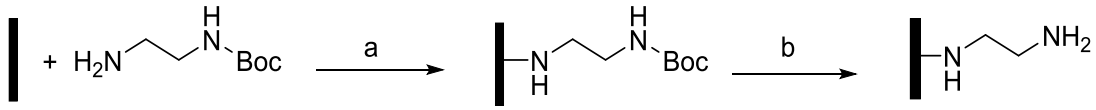

Scheme 13. *Synthetic steps for the creation of EDA-Boc monolayers. Conditions: a) 20 mM solutions in CH_3CN with 0.1 M TBATFB, CV 0.5-2 V; b) 4 M HCl in dioxane, r.t., 1 h.*

The approach optimised by our group for the coupling of carboxylic acid functionalised compounds to the amine monolayer consisted in the use of the combination of HBTU and DIEA in DMF as coupling agents.[15] The commonly applied protocol for the coupling of osmium bipyridyl complexes presenting a free pendant amine to a carboxylic acid monolayer at electrode surface involves the use of EDC and NHS as coupling agents in phosphate buffer pH 6.[9, 16] It was decided to test both procedures: the use of buffers was discarded since the compounds synthesised were poorly soluble in aqueous solvents and DMF was chosen as the reaction solvent (Scheme **14**).

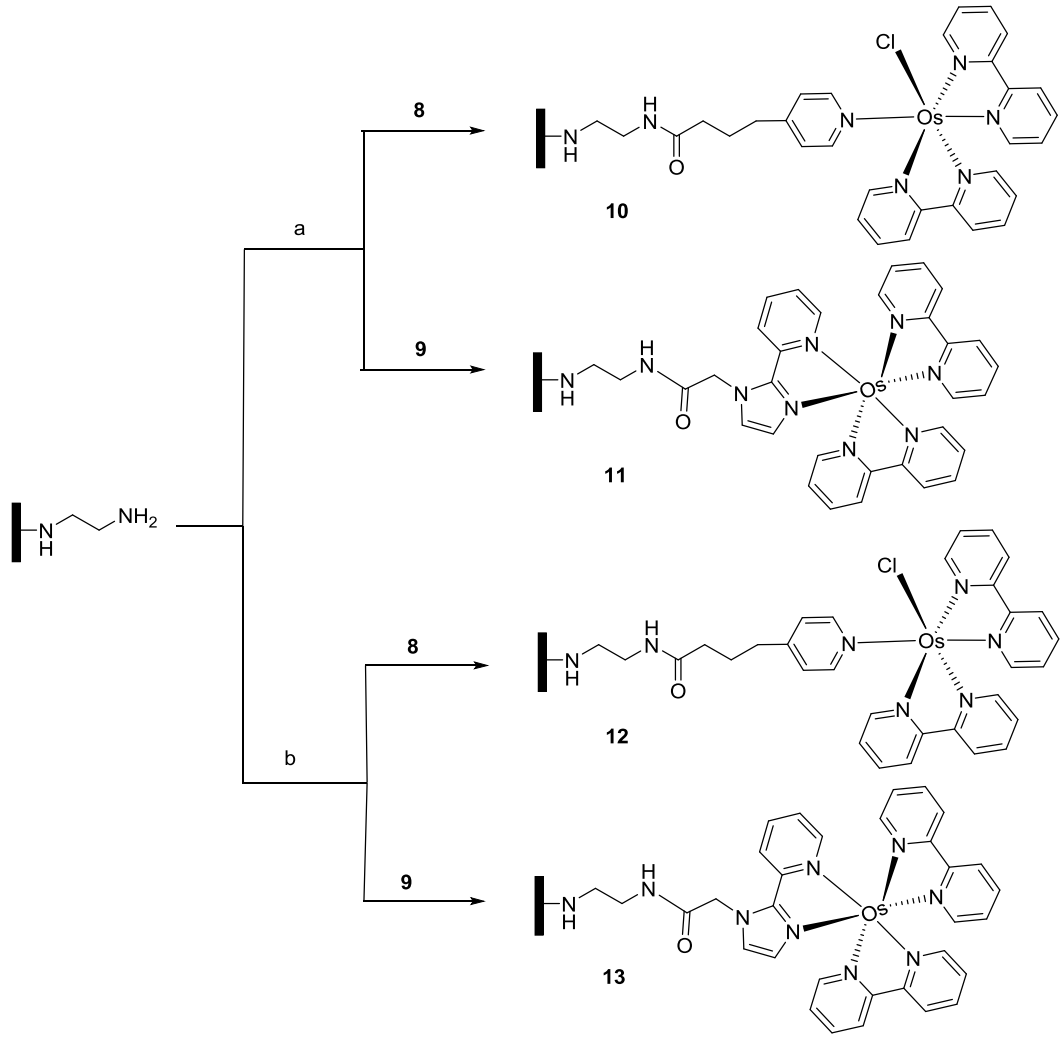

Scheme 14. *Synthetic steps for the coupling of complexes **8** and **9** to the amine monolayer. Conditions: a) 10 mM complex **8** or **9**, 60 mM HBTU, 0.2 M DIEA in DMF, r.t., 16 h; b) 10 mM complex **8** or **9**, 0.1 M EDC, 60 mM NHS in DMF, r.t., 16 h.*

In order to compare the efficiency of the attachment of complex **8** and **9** at the GC, surface coverages (Γ) were calculated using Faraday's law (**1**) where *Q* is the charge associated with the redox process, *F* is the Faraday constant, *n* is number of electrons transferred which is 1 in the case of the $Os^{2+/3+}$ couple, *A* is the geometric area of the electrode (0.071 cm^2) and ρ is the surface roughness of the GC electrode.

$$\Gamma = \frac{Q}{nFA\rho} \qquad (\mathbf{1})$$

A definitive methodology for the calculation of the real area of carbon electrodes is not available yet. Jaegfelt *et al.* mapped the surface of graphite electrodes, polished with emery paper grade 600, by scanning electrode microscope, estimating a real area 2 to 5 times greater than the geometrical area.[17] Here, the GC electrodes were

polished on dry silicon carbide coated abrasive paper grade P1200 and the roughness factor was assumed to be 4 as reported in past publications for the same polishing procedure.[18]

The value of charge associated with the redox process was calculated by analysing the recorded CVs with the software Origin 7.0. The area included within the CV is directly proportional to the current generated at the working electrode according to (**2**) where *v* is the scan rate at which the CV is recorded:

$$Q = \frac{CVArea}{v} \qquad (\mathbf{2})$$

The process is characterised by two components of the current: the charging current, which represents the background, and the faradaic current generated by the oxidation and reduction of the redox molecule, the value needed to calculate the surface coverage of the species. To separate the two current components and extract only the faradaic one, the background has to be reconstructed by creating the baselines to the redox peaks, through the non-linear curve fit function in the software. Once the area of the background is determined by integration, it can be subtracted from the total CV area, giving the area associated with the faradaic process, which divided by 2, can be used in equation (**2**) to calculate the charge (Figure **18**).

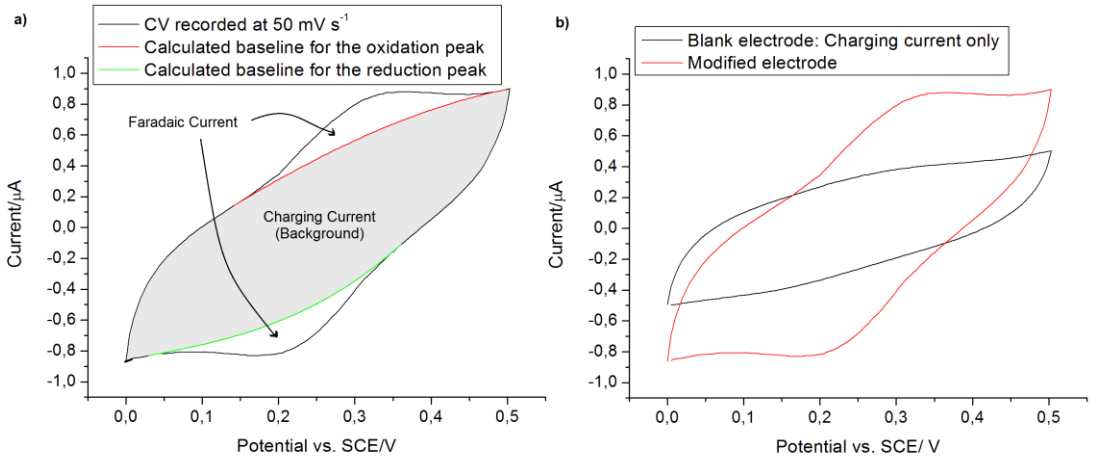

Figure 18. *CVs recorded in 0.1 M PBS solution pH 7 vs. SCE, electrode area 0.071 cm^2, at 50 mV s^{-1}scan rate for complex* ***8****: a) elaborated with Origin 7.0 to show the simulated peak baselines and the current components, b) comparison between modified and blank electrode.*

Figure **19a** shows the CVs recorded in phosphate buffer solution (PBS) pH 7 for the electrodes modified with complex **8**: a reversible redox peak is present at E_{mp} = 0.265 V vs. SCE. The coupling agents combination of EDC and NHS in DMF gave

the highest value of surface coverage, Γ = 18.6 pmol cm^{-2} (Figure **19b**), and was chosen for the following experiments. It needs to be noted that the controls, obtained by dipping the amine modified electrodes in a 10 mM solution of **8** with no coupling agents presented unexpectedly a significant surface coverage. Figure **19c** shows the CVs recorded for complex **9**: the expected reversible redox peak at E ~ 0.7 V vs. SCE was not detected. This could suggest that the coupling reaction did not work, probably due to the short chain on the pyridine-imidazole ligand, which did not allow the carboxylic acid group to react with the coupling agents. Although, since no redox peak of the complex was detected on the controls, it could indicate that the shape of the CV, caused by the unavoidable oxidation of the GC surface in aqueous solutions, obscured the peak associated with the small amount of complex present at the surface.

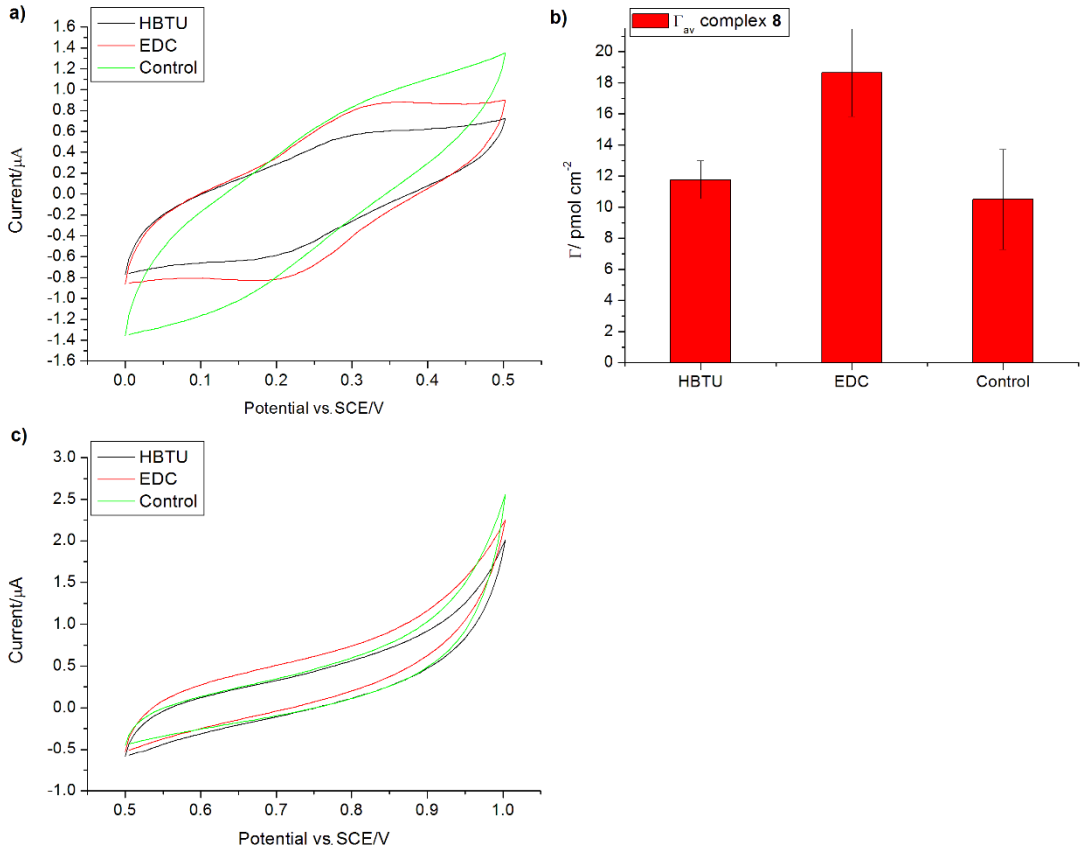

Figure 19. *a) Comparison of the CVs recorded in 0.1 M PBS solution pH 7 vs. SCE, electrode area 0.071 cm^2, at 50 mV s^{-1}scan rate for complex **8**. b) Barplot for the variation of Γ of complex **8** according to the coupling agent used, calculated by averaging the values obtained for two replicates; the control was obtained by dipping amine modified electrodes in a neat 10 mM solution of complex **8** in DMF; c) Comparison of the CVs recorded in 0.1 M PBS solution pH 7 vs. SCE, electrode area 0.071 cm^2, at 50 mV s^{-1}scan rate for complex **9**.*

Literature data showed that, between the two compounds synthesised, complex **8** presented the most suitable redox potential to be used as a redox mediator for the GDH enzyme to be used in the following experiments; for this reason the following optimisation focused on complex **8**.[19]

2.3.1. Control reactions for the coupling of complex 8 to the amine monolayer

In order to determine what caused the presence of **8** at the surface when no coupling agents were present a series of test reactions were performed. First, to verify that the amount of material detected on the control electrodes did not come from the spontaneous reaction of the carboxylic acid group with the free amines at the surface, a set of electrodes was modified with a monolayer of 1-propylamine (1-PA) and then dipped in a 10 mM solution of complex **8** in DMF for 16 hours. Moreover the adsorption of **8** at the bare electrode was tested (Scheme **15**).

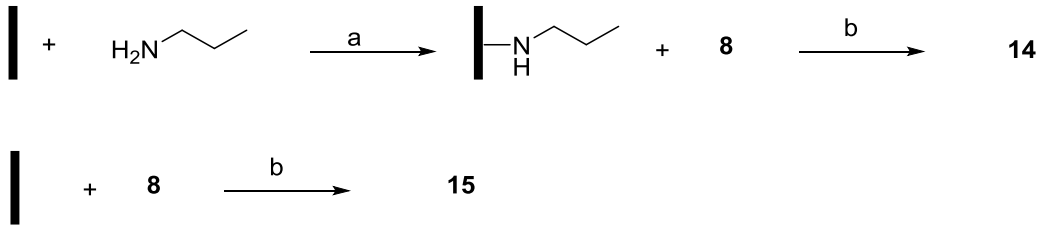

Scheme 15. S*teps for the modification of the controls. Conditions: a) 20 mM solutions of 1-PA in CH_3CN with 0.1 M TBATFB, CV 0.5-2 V; b) 10 mM complex **8** in DMF, r.t., 16 h.*

At the end of the 16 hours, all the electrodes presented a significant amount of complex, it was then decided to try and wash the electrodes in CH_3CN for 24 hours to try and remove the adsorbed material. After stirring in CH_3CN, the electrodes still presented adsorbed material, but it was not possible to remove any more of it by washing further (Figure **20**).

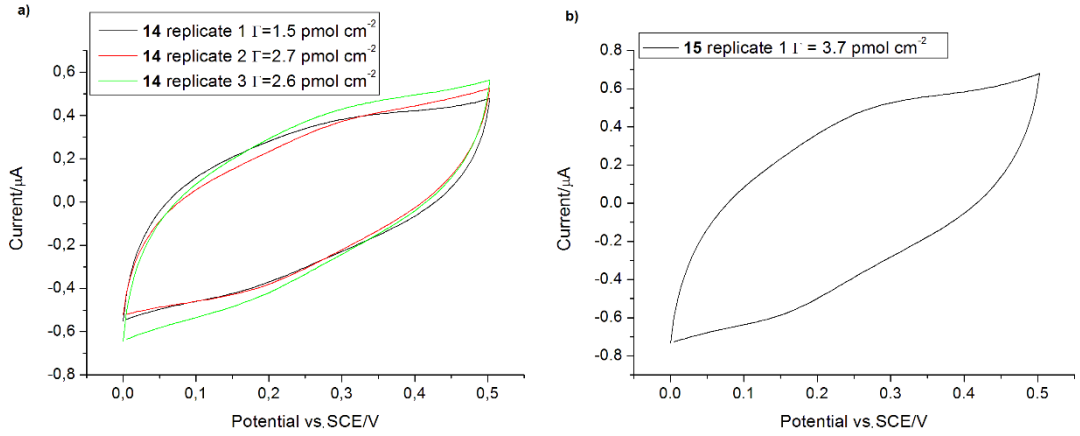

Figure 20. *Comparison of the CVs recorded in 0.1 M PBS solution pH 7 vs. SCE, electrode area 0.071 cm^2, at 50 mV s^{-1}scan rate for electrodes* ***14*** *(a) and* ***15*** *(b).*

Since complex **8** was detected on electrodes where the amine functionality had not been introduced, it was concluded that its presence in the controls did not depend on the spontaneous reaction between free amines at the surface and COOH group on the complex, but on adsorption processes. The experiment demonstrated that through washing the electrodes with CH_3CN, the amount of material adsorbed at the surface could be reduced to 20% of the initial value. To determine if the adsorption was affected by the presence of the 4 carbon chain on complex **8**, complex **16** was synthesised, following the procedure described in section **2.2.3** (Scheme **16**). The product was a red-brow solid obtained in 43% yield.

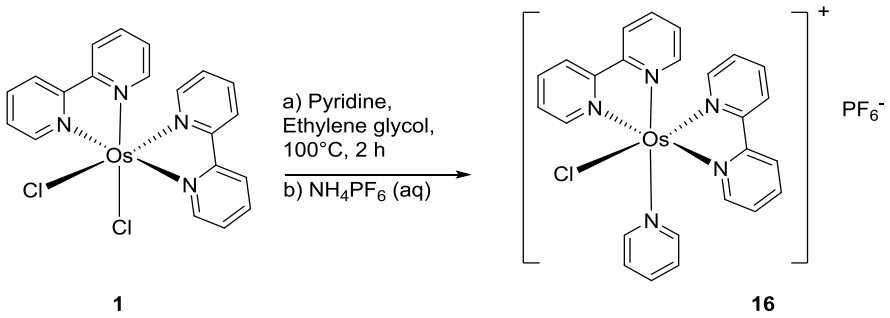

Scheme 16. *Synthetic steps for the formation of complex* ***16.***

Three sets of electrodes were modified as presented in Scheme **17**.

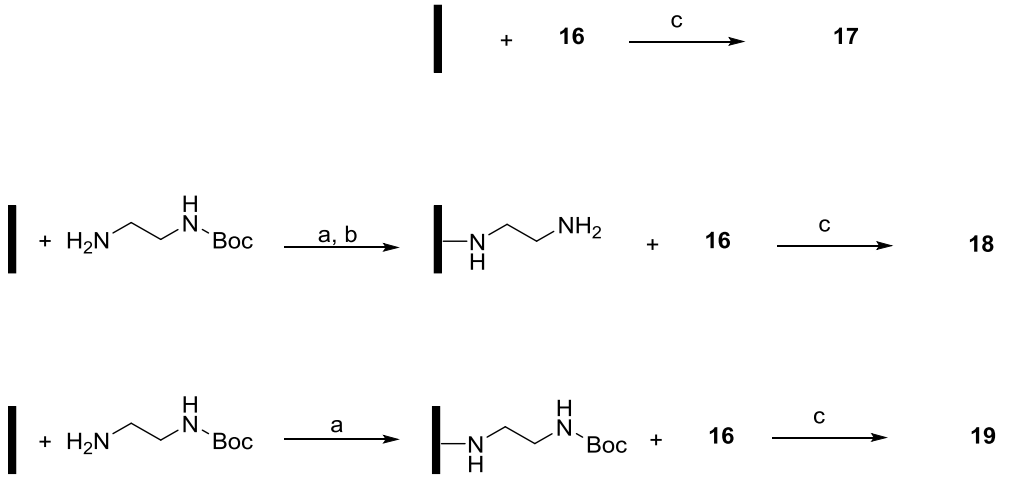

Scheme 17. S*teps for the modification of the controls. Conditions: a) 20 mM solution of EDA-Boc in CH_3CN with 0.1 M TBATFB, CV 0.5-2 V; b) 4 M HCl in dioxane, r.t., 1 h; c) 10 mM complex* **16** *in DMF, r.t., 16 h.*

After stirring for 24 hours in CH_3CN, some of the electrodes still had adsorbed material, but it was not possible to remove any more material by washing further as seen previously (Figure **21**).

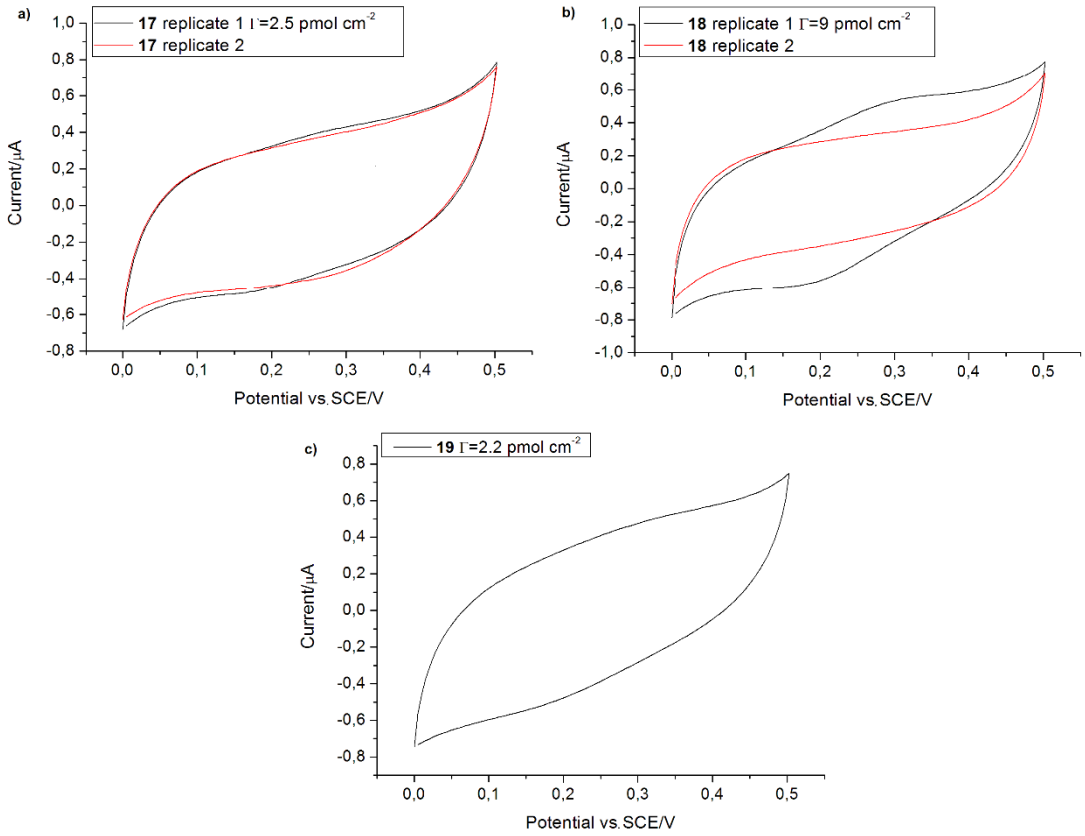

Figure 21. *Comparison of the CVs recorded in 0.1 M PBS solution pH 7 vs. SCE, electrode area 0.071 cm^2, at 50 mV s^{-1}scan rate for electrodes* ***17*** *(a),* ***18*** *(b) and* ***19*** *(c).*

The result obtained shows that the presence of complex **8** at the surface of control electrodes in the previous experiment is not dependent on the presence of the side chain. Finally the coupling of complex **8** to an EDA monolayer was repeated using EDC and NHS in DMF as coupling agents and adding the washing step after the modification (Scheme **18**).

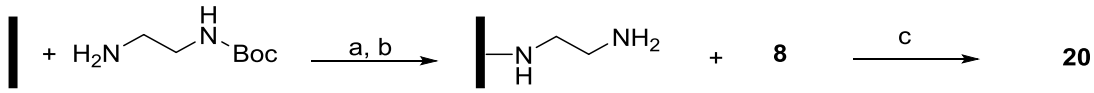

Scheme 18. *Synthetic steps for the electrode surface modification. Conditions: a) 20 mM solution of EDA-Boc in CH_3CN with 0.1 M TBATFB, CV 0.5-2 V; b) 4 M HCl in dioxane, r.t., 1 h; c) 10 mM complex **8**, 0.1 M EDC, 60 mM NHS in DMF, r.t., 16 h.*

From this point on the polishing method for the GC electrodes followed the procedure described in the experimental chapter: after polishing with carbide abrasive paper, the surfaces were treated with 0.3 μm alumina slurry to a "shiny mirror" finish. Such treatment determines a significant decrease of the roughness of the surface and for this reason the roughness factor was assumed to be $\rho = 1$.

The barplot in figure **22** shows the average surface coverage calculated for the covalently modified electrodes and the controls: the washing process does not affect the surface coverage of the electrodes where complex **8** is covalently bound to the amine monolayer and the values calculated are consistent with the results obtained in the previous experiment (**12**).

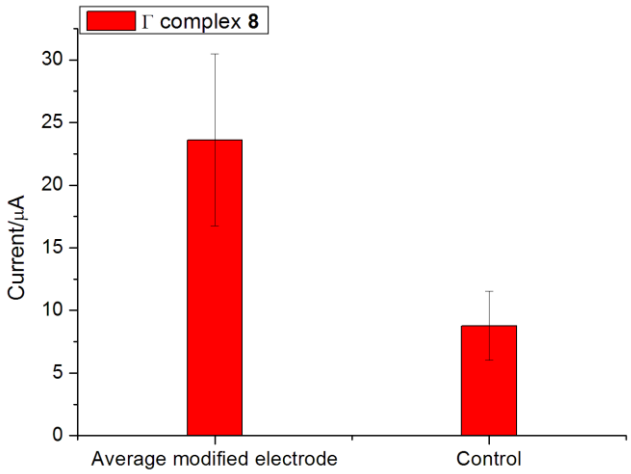

Figure 22. *Barplot for Γ of complex **8** calculated by averaging the values obtained for two replicates; the control was obtained by dipping amine modified electrodes in a neat 10 mM solution of complex **8** in DMF.*

These control experiments allowed to gain a better understanding of the processes occurring at the surface for the system created. Although it was initially assumed that osmium bipyridyl complexes would not adsorb to the GC surface given their structure, the experiments proved that, in the time required for the coupling step, adsorption processes occurred to some extent. Washing the modified electrodes in acetonitrile for 24 hours helped reduce the non-covalently attached material. Moreover the presence of complex **8** at the surface on the controls did not depend on secondary reactions due to its specific structure, since complex **16** displayed the same behaviour.

2.4. *Determination of the kinetic parameters for complex 8 under homogeneous and heterogeneous conditions*

The variation of the scan rate values in a cyclic voltammetry experiment allows the determination of useful kinetic parameters associated with the diffusion of redox species in solution and the rate of the electron transfer through a linker when the redox molecule is covalently bound in a monolayer at the electrode surface. First, in order to characterise the electrochemical behaviour of complex **8** in solution, a series of CVs were recorded at different scan rate for a 1.2 mM solution of **8** in 50 mM citrate buffer pH 5.5 (Figure **23**).

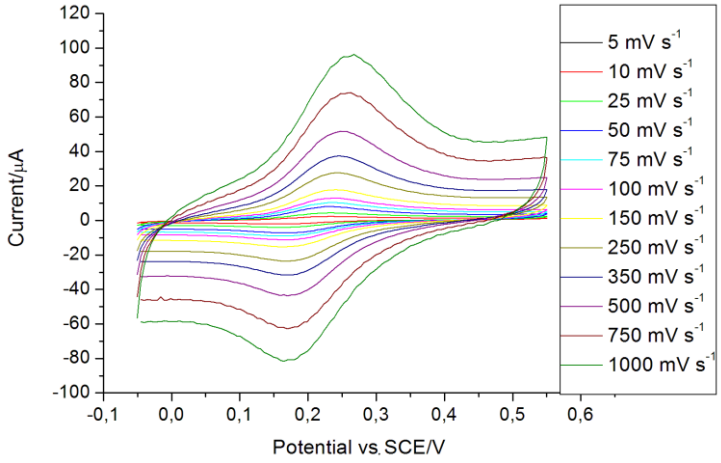

Figure 23. *Comparison of the CVs recorded in a 1.2 mM solution of complex **8** in 50 mM citrate buffer pH 5.5 at different scan rates, electrode area 0.071 cm^{-2}.*

The dependence of the peak current *i* on the scan rate values *v* is described by the Randles-Sevčik equation (**3**):[20]

$$i = 2.69 \times 10^5 n^{\frac{3}{2}} A[Os] D^{\frac{1}{2}} v^{\frac{1}{2}} \quad \textbf{(3)}$$

where *n* is the number of electrons transferred in the redox process, 1 for the $Os^{2+/3+}$ redox couple, *A* is the electrode area, which corresponds to 0.071 cm^2, and D is the diffusion coefficient in cm^2 s^{-1} of the redox molecule from the bulk solution to the electrode surface. Plotting the experimental values of current, obtained considering the estimated baseline, *i* vs $v^{1/2}$ for both oxidation and reduction peaks showed a linear relationship (**4**) between the two variables (Figure **24**).

$$y = A + Bx \quad \textbf{(4)}$$

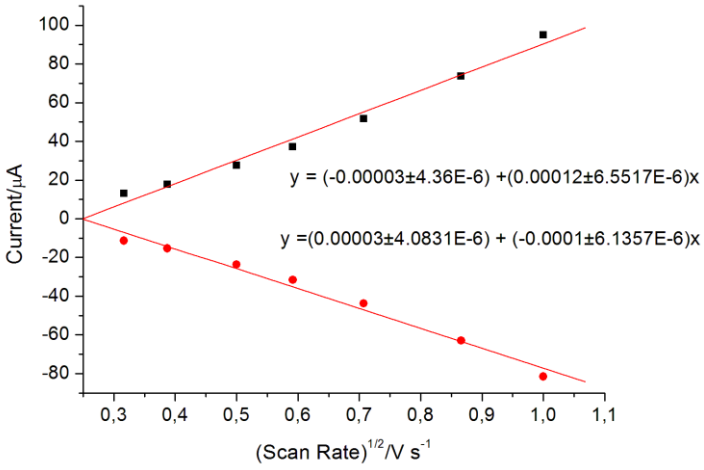

Figure 24. *Plot of i vs* $v^{1/2}$ *for oxidation peak (squares) and reduction peak (dots) and corresponding linear regression lines with equations.*

Through the values of the linear regression coefficients, specifically the slope value B, it was possible to calculate the diffusion coefficient of complex **8** using equation (**5**). The result obtained was D = 2.74x10^{-5} cm^2 s^{-1}, one order of magnitude greater than the reported value for similar compounds.[21]

$$D = \left[\frac{B}{2.69\times10^{5} n^{\frac{3}{2}} A[\mathrm{Os}]}\right]^2 \qquad (5)$$

Once the redox molecule is covalently bound to the electrode surface through a linker, the diffusion of the molecule becomes irrelevant, since the electrons are supposed to travel from the redox centre to the electrode through the linker. Analysing the effect of the variation of scan rate on the potential values of the redox peaks would allow to determine the apparent rate constant k_{app} and the transfer coefficient α of the linker/redox molecule system through the Laviron model.[22] A set of electrodes was modified as presented in scheme **19** and the kinetic parameters were calculated.

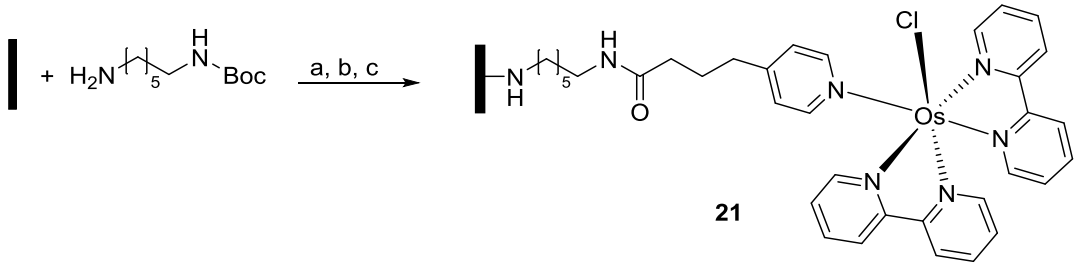

Scheme 19. *Synthetic steps for the electrode surface modification. Conditions: a) 20 mM solution of N-Boc-hexamethylenediamine (HDA-Boc) in CH_3CN with 0.1 M TBATFB, CV 0.5-2 V; b) 4 M HCl in dioxane, r.t., 1 h; c) 10 mM complex **8**, 0.1 M EDC, 60 mM NHS in DMF, r.t., 16 h.*

The electrodes were characterised by cyclic voltammetry at different scan rates and the difference E_{peak}-E_{mp} was plotted vs Log(v) to obtain the Laviron plot (Figure **25**). According to Laviron's theory for irreversibly adsorbed redox species, the curves associated to anodic and cathodic peak should meet at low scan rates, but, as can be seen in figure **25b**, the two present a constant separation for $v < 40$ mV s^{-1}. Although this behaviour is common for monolayers of redox molecules at surfaces, no clear explanation has ever been given.

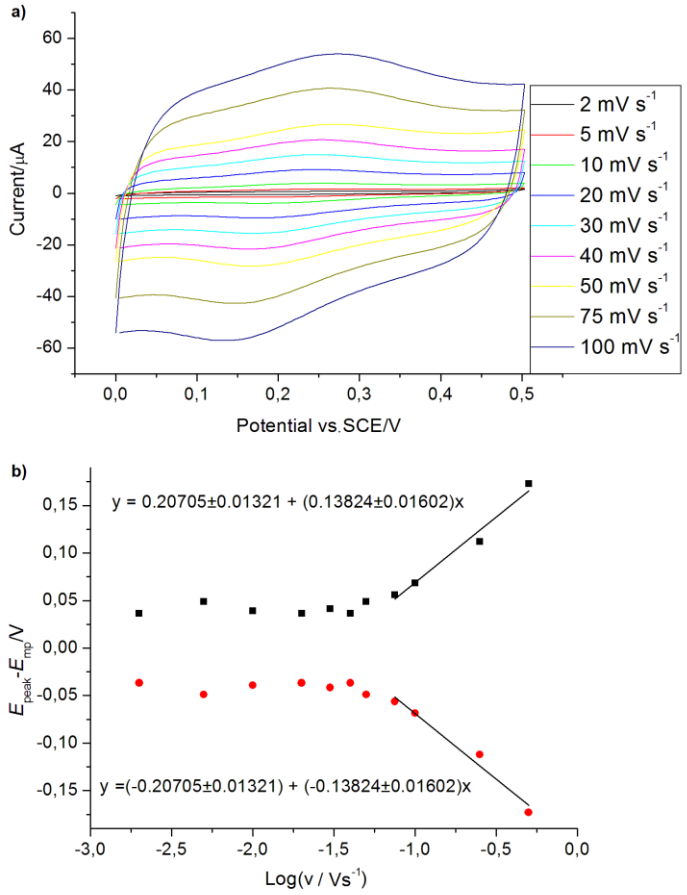

Figure 25. *a) Comparison of the CVs recorded for* ***21*** *0.1 M phosphate buffer pH 7 at different scan rates, electrode area 0.071 cm^{-2}, b) Laviron plot of* E_{peak}-E_{mp} *vs Log(*v*) for* ***21*** *with linear regression equations.*

At high scan rates the slope B_c and B_a respectively for the cathodic and anodic peaks of the linear regression curves (**4**) correspond to the value:[22, 23]

$$B_c = \frac{-2.3RT}{\alpha nF} \quad \textbf{(6a)}$$

$$B_a = \frac{2.3RT}{(1-\alpha)nF} \quad \textbf{(6b)}$$

where R = 8.3144 J mol^{-1} K^{-1} is the gas constant and T = 298 K is the temperature. The transfer coefficients were calculated to be α_a = 0.57 and α_c = 0.43, the values of α calculated are within the values expected for similar systems.[24] In order to determine the apparent electron transfer rate k_{app}, equation (**7**) was applied, assuming v = 0.0318 V s^{-1}, calculated as the x-intercept of the linear regression equation in figure **25**.[23]

$$k_{app} = \frac{\alpha n F v}{RT} \quad (7)$$

The apparent electron transfer constant was calculated to be k_{app} = 0.71 s^{-1}. Such value falls within the range of electron transfer constant values of $k_{app.c}$ = 0.4 s^{-1} and $k_{app.a}$ = 1.2 s^{-1} determined by Ghanem *et al.* for an anthraquinone reporting redox molecule attached to the same HDA linker.[25] The k_{app} calculated appear to be lower compared to values determined in the past for SAMs on gold where the linkers used for the osmium complex were long alkyl chains.[24] A possible explanation for such result could be the presence on an ohmic drop in the electrochemical cell: the uncompensated resistance generated causes an incorrect reading of the peak potential which usually bring to the determination of low rate constants.[26]

2.5. Conclusions

A new osmium bipyridyl complex suitable for the coupling to an amine monolayer modified electrode was synthesised and fully characterised. First, monodentate ligand **3** was synthesised then the conditions for the formation of osmium complexes reported by Kober *et al*. were optimised. The coupling conditions to an EDA monolayer at GC electrodes were optimised: EDC and NHS in DMF proved to be the most suitable coupling agents and reproducible surfaces coverages of 19 pmol cm^{-1} were achieved. Control reactions to clarify the adsorption processes of the complexes at the surface were performed and it was determined that a washing step of the electrodes in CH_3CN was necessary to obtain reproducible results. The diffusion coefficient of the synthesised complex in 50 mM citrate buffer pH 5.5 was calculated to be $D = 2.74 \times 10^{-5}$ cm^2 s^{-1}, this will be useful for the study of the mediated electrocatalytic oxidation of glucose by GDH. The kinetic parameters for the synthesised complex coupled to an HDA monolayer were determined through the Laviron model to be $\alpha_a = 0.57$ and $\alpha_c = 0.43$ and $k_{app} = 0.71$ s^{-1}, in line with previous results reported for similar systems.

2.6. References

[1] Cheung, K.-C.; Wong, W.-L.; Ma, D.-L.; Lai, T.-S., Wong, K.-Y. *Coord. Chem. Rev.* **2007,** *251*, 2367-2385.

[2] a) Hoertz, P.G.; Staniszewski, A.; Marton, A., Higgins, G.T.; Incarvito, C.D.; Rheingold, A.L.; Meyer, G.J. *J.Am. Chem.Soc.* **2006,** *128,* 8234-8245. b) Mardanya, S.; Karmakar, S.; Maity, D.; Baitalik, S. *Inorg. Chem.* **2015,** 54, 513-526.

[3] a) Chaubey, A.; Malhotra, B.D. *Biosens. Bioelectron.* **2002,** *17*, 441-456. b) Liu, J.; Sun, S.; Liu, C., Wei, S. *Measurement* **2011,** *44*, 1878-1883.

[4] Buckingam, D.A.; Dwyer, F. P.; Sargeson, A.M. *Inorg, Chem.* **1966,** *7*, 1243-1249.

[5] Shi, K.; Shiu, K.-K. *J. Electroanal. Chem.* **2004,** *574*, 63-70.

[6] a) Albrecht, T.; Guckian, A.; Ulstrup, J.; Vos, J.G. *Nano Lett.* **2005,** *7*, 1451-1455. b) Forster. R.; Vos, J.G.; Keyes, T.E. *Analyst* **1998,** *123,* 1905-1911.

[7] a) Ackermann, Y.; Guschin, D.A.; Eckhard, K.; Shleev, S.; Schuhmann, W. *Electrochem. Comm.* **2010,** *12*, 640-643. b) Heller, A. *Curr. Opin. Chem. Biol.* **2006,** *10,* 664-672.

[8] Aramata, A.; Takahashi, S.; Yin, G.; Gao, Y.; Inose, Y.; Mihara, H.; Tadjeddine, A.; Zheng, W.Q.; Pluchery, O.; Bittner, A.; Yamagishi,A., *Thin Solid Films* **2003,** *424*, 239-246.

[9] a) Boland, S.; Foster, K.; Leech, D. *Electrochem. Acta* **2009,** *54*, 1986-1991. b) Ricci, A.M.; Tagliazucchi, M.; Calvo, E.J. *Phys. Chem. Chem. Phys.* **2012,** *14*, 9988-9995.

[10] a) Garrett, D.J.; Jenkins, P.; Polson, M.I.J.; Leech, D.; Baronian, K.H.R.; Downard, A.J. *Electrochim. Acta* **2011,** *56,* 2213-2220. b) Kumar, R.; Leech, D. *Electrochim. Acta,* **2014,** *140*, 209-216.

[11] Kober, E.M.; Caspar, J.V.; Sullivan, B.P.; Meyer, T.J. *Inorg. Chem.* 1988, 25, 4587-4598.

[12] Menghin, S.; Pertz, H.H.; Kramer, K.; Seifert, R.; Schunack, W.; Elz, S. *J. Med. Chem.*, **2003,** *46*, 5458-5464.

[13] a) Yue, S.-M.; Xu, H.-B.; Ma, J.-F.; Su, Z.-M.; Kan, Y.-H.; Zhang, H.-J. *Polyhedron* **2006**, *25*, 635–644. b) Saha, D.; Das, S.; Maity, D.; Baitalik, S.; *Indian J. Chem.* **2011**, *50A*, 1418-1428.

[14] Buckingam, D.A.; Dwyer, F.P.; Goodwin, H.A.; Sagerson, A.M. *Aust. J. Chem.* **1964,** *17,* 325-326.

[15] Chrétien, J.-M.; Ghanem, M.A.; Bartlett, P.N.; Kilburn, J.D. *Chem. Eur. J.* **2008**, *14*, 2548-2556.

[16] Boland, S.; Barriére, F.; Leech, D. *Langmuir* **2008**, *24*, 6351-6358.

[17] Jaegfeldt, H.; Kuwana, T.; Johansson, G. J. *Am. Chem. Soc.* **1983,** *105,* 1805-1814.

[18] a) Chrétien, J.-M.; Ghanem, M.A.; Bartlett, P.N.; Kilburn, J.D. *Chem. Eur. J.* **2009**, *15*, 11928-11936. b) Ghanem, M.A.; Chrétien, J.-M.; Kilburn, J.D.; Bartlett, P.N. *Bioelectrochemistry* **2009**, *76*, 115-125.

[19] Zafar, M.N.; Wang, X.; Sygmund, C.; Ludwig, R.; Leech, D.; Gorton, L. *Anal. Chem.* **2012,** *84,* 334-341.

[20] Bard, A.J.; Faulkner, L.R. *Electrochemical Methods: Fundamentals and Applications* **1980,** John Wiley and Sons: New York.

[21] Flexer, V.; Ielmini, M.V.; Calvo, E.J.; Bartlett, P.N. *Bioelectrochemistry* **2008**, *74*, 201-209.

[22] Laviron, E. *J. Electroanal. Chem.* **1979,** *101,* 19-28.

[23] Eckermann, A.L.; Feld, D.J.; Shaw, J.A.; Meade, T.J. *Coord Chem. Rev.* **2010,** *254,* 1769-1802.

[24] Ricci, A.; Rolli, C.; Rothacher, S.; Baraldo, L.; Bonazzola, C.; Calvo, E.J.; Tognalli, N.; Fainstein, A. *J. Solid State Electrochem.* **2007,** *11,* 1511-1520.

[25] Ghanem, M.A.; Chrétien, J.-M.; Pinczewska, A.; Kilburn, J.D.; Bartlett, P.N. *J. Mater. Chem.* **2008**, *18*, 4917-4927.

[26] a) Myland, J.C.; Oldham, K.B. *Anal. Chem.* **2000,** *17,* 3972-3980. b) Roullier, L.; Laviron, E. *J. Electroanal. Chem.* **1983,** *157,* 193-203.

3. Control over the creation of mixed monolayers

3.1. Chronoamperomentry as a technique for creating mixed monolayers

The optimisation of the conditions for the coupling of osmium complexes to an amine linker monolayer allowed an investigation of the possibility of controlling the surface coverage of the redox centre in a precise way, creating mixed monolayers. Previous results showed that complex **8** (Figure **26**) was the most suitable derivative for coupling to the surface and its characteristic redox potential makes it an ideal mediator for the GDH enzyme that was ultimately to be used to develop a biosensing device.[1] In order to have clear information about the behaviour of the mixed monolayers with multiple components, anthraquinone-2-carboxylic acid (**AQ**) was chosen as the second redox probe: its redox potential (E_{mp} ~ -0.45V vs SCE) is far enough from the $Os^{2+/3+}$ couple potential (E_{mp} ~ 0.25V vs SCE) to avoid overlap of the CV peaks and, compared to other quinone compounds, it is very stable.[2]

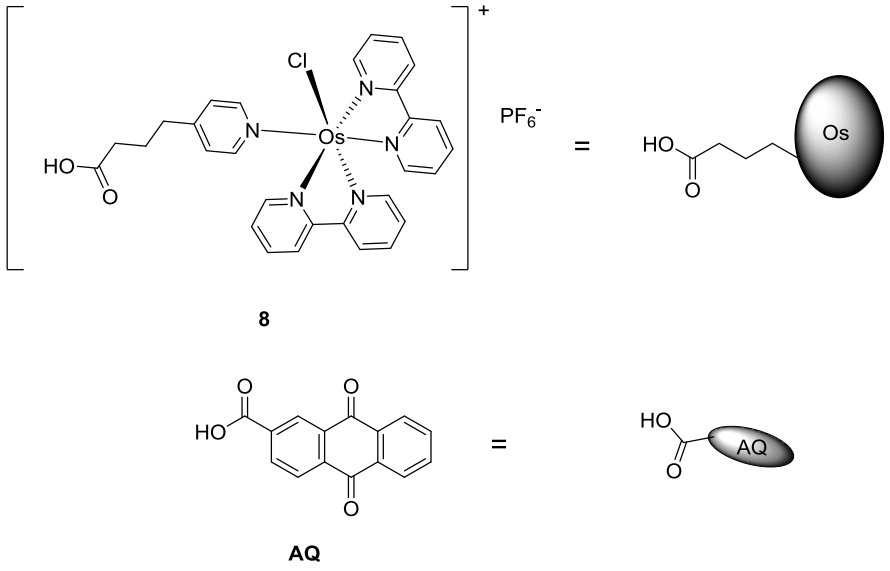

Figure 26. *Structures of the osmium complex and anthraquinone-2-carboxylic acid (**AQ**) used for the studies of the mixed monolayers and their schematic representation.*

The approach chosen for the creation of mixed monolayers consisted of the attachment of mixtures of primary amines, whose relative ratio were varied in the grafting solution.

The use of cyclic voltammetry to create one component monolayers of amines showed that each amine is characterised by a different oxidation potential E_{ox} vs Ag/AgCl, as reported in figure **27**. The values of E_{ox} can be influenced by the length of the alkyl chain, the presence of bulky groups that could hinder the access of solvent to the amine nitrogen and, for mono-protected diamines, by the possible formation of intramolecular hydrogen bond in aprotic solvents.[3]

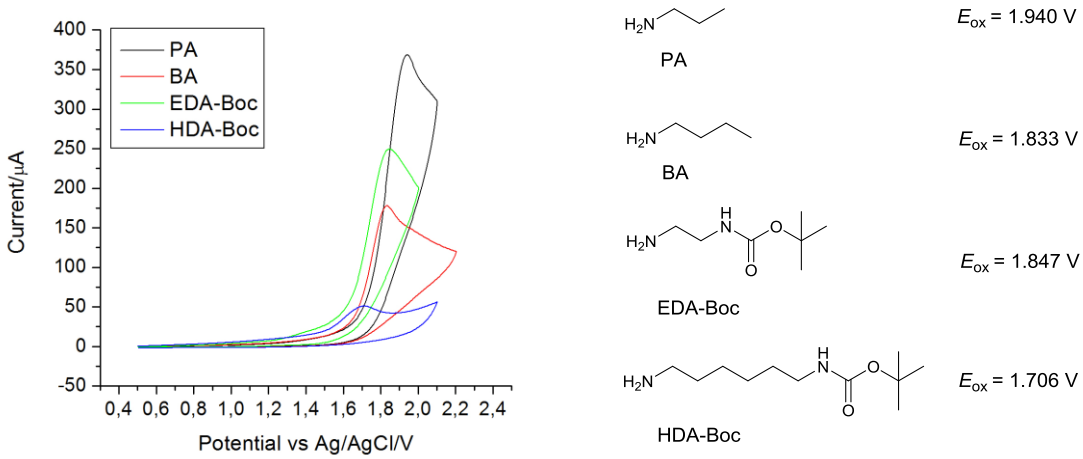

Figure 27. *Cyclic voltammograms recorded in 20 mM solutions of each amine in CH_3CN with 0.1 M TBATFB at a scan rate of 50 mV s^{-1} and E_{ox} vs Ag/AgCl values for each amine.*

Studies on the creation of mixed monolayers of diazonium salts demonstrated that, given a solution containing two components in definite % ratio and characterised by different reduction potentials, the grafting by cyclic voltammetry provided an excess at the surface of the component with a more positive reduction potential.[4]

In order to minimise the possible effects of differences in the oxidation potentials of the primary amines, the grafting process was performed by chronoamperometry. In a chronoamperometry experiment, a constant potential is applied to the working electrode for a definite interval of time and the variation of current due to the processes occurring in solution is recorded. Figure **28** shows the variation of current during the grafting of a monolayer of EDA-Boc: the potential was held at 2 V, applying to the system a potential high enough to generate the amine radical cation, and the current decreased with the progressive passivation of the GC surface by formation of the layer.

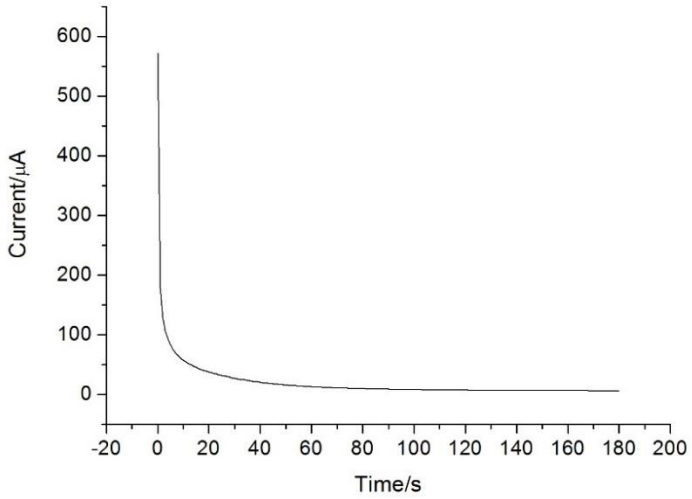

Figure 28. *Chronoamperogram recorded in a 20 mM solution of EDA-Boc in CH_3CN with 0.1 TBATFB at a constant potential of 2 V vs Ag/AgCl, GC electrode area 0.071 cm^2.*

3.2. Mixed monolayers: diamine linker/monoamine

The first experiment designed consisted of the creation of mixed monolayers containing a Boc-mono-protected diamine as linker for complex **8** and a short chain alkyl amine as diluting agent for the linkers on the surface. Scheme **20** shows the initial amine combination tested: solutions in CH_3CN, with 0.1 M TBATFB as supporting electrolyte, were prepared, containing EDA-Boc and PA in different ratios and total concentration 20 mM, starting from 100% EDA-Boc and gradually increasing the fraction of PA up to 99.9%. The removal of the Boc group in acidic conditions yielded free NH_2 groups on the surface, available for coupling with complex **1**, under solid phase synthesis conditions.

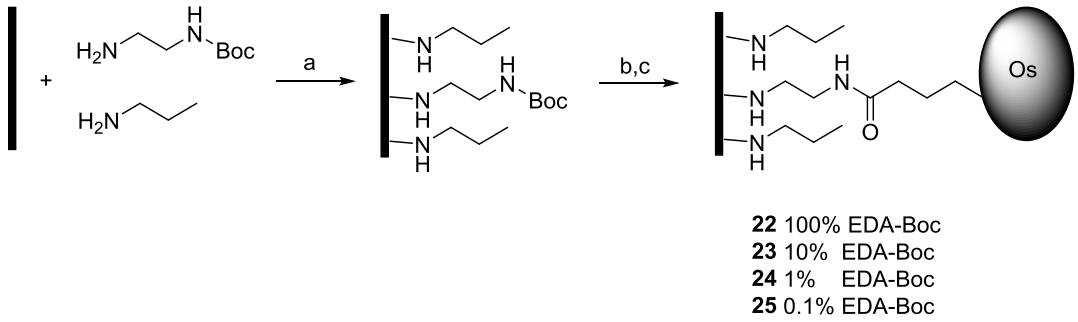

Scheme 20. *Synthetic steps for the creation of EDA-Boc/PA mixed monolayers and coupling of complex **8**. Conditions: a) 20 mM solutions in CH_3CN with 0.1 M TBATFB, chronoamperometry 2 V, 18 0s; b) 4 M HCl in dioxane, r.t., 1 h; c) 10 mM complex **8**, 0.1 M EDC, 60 mM NHS in DMF, r.t., 16 h.*

Figure **29a** shows the results obtained: the CVs show the redox peaks for the $Os^{2+/3+}$ covalently bound to the surface at ~ 0.22 V vs. SCE. Significantly the calculated surface coverages (Fig. **29c**) did not reflect the variation of concentration of linker in solution, moreover the control electrode for 0.1% EDA-Boc presented an unexpected amount of osmium complex (Γ = 18.2 pmolcm^{-2}) which could not be removed even after stirring in acetonitrile for several hours, indicating that it was not present due to non-covalent adsorption.

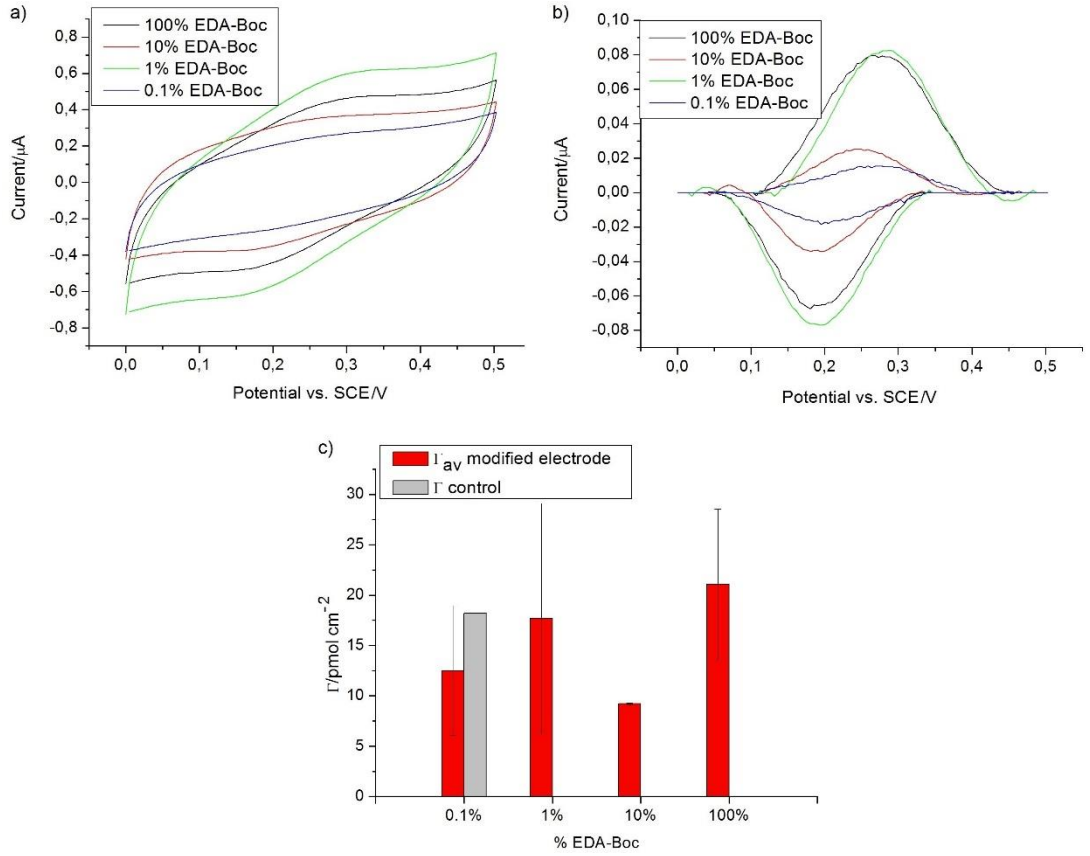

Figure 29. *a) Comparison of the CVs recorded in 0.1 M PBS solution pH 7 vs. SCE, electrode area 0.071 cm^2, at 50 mV s^{-1}scan rate for different EDA-Boc linker solution ratios. b) Background-subtracted CVs obtained by analysing the data with Origin 7.0. c) Barplot for the variation of Γ of complex* ***8*** *according to the ratio of EDA-Boc linker in solution, calculated by averaging the values obtained for two replicates; the control was obtained by dipping amine modified electrodes in a neat 10 mM solution of complex* ***8*** *in DMF.*

A possible cause of the observed result could have been the volatility of PA resulting in the concentration of this amine being lower than expected during the amine reduction experiment, leading to an excess of EDA-Boc being coupled on the electrode surface.

For this reason a different combination of amines was tested: a mixed monolayer of HDA-Boc and the less volatile BA was created following the same procedure described previously (Scheme **21**)

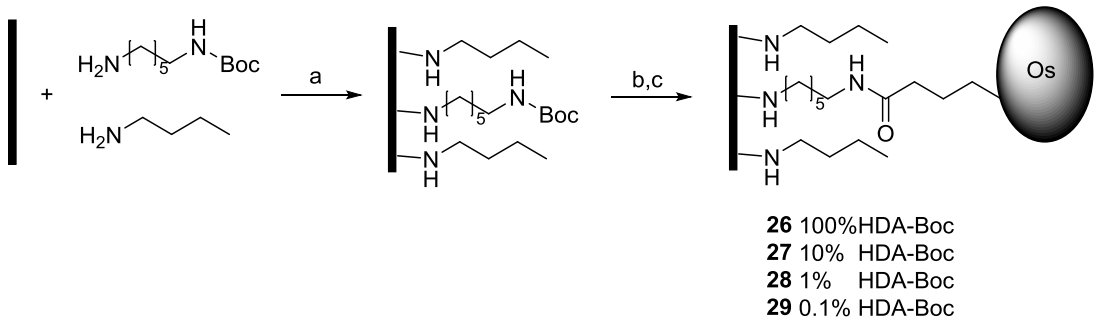

Scheme 21. *Synthetic steps for the creation of HDA-Boc/BA mixed monolayers and coupling of complex* ***8****. Conditions: a) 20 mM solutions in CH_3CN with 0.1 M TBATFB, chronoamperometry 2 V, 180 s; b) 4 M HCl in dioxane, r.t., 1 h; c) 10 mM complex* ***8****, 0.1 M EDC, 60 mM NHS in DMF, r.t., 16 h.*

The results are presented in figure **30**: in this case the CVs showed a clear trend of the variation of surface coverage depending on the amount of linker in solution, which was more evident once the background current was subtracted from the CVs. However the comparison of Γ values shows that the relative concentration of the two amines in solution is not directly reflected on the relative surface. This can depend on two factors: the kinetics of attachment of the primary amines radicals to the GC surface and the dimensions of the osmium complex. The use of chronoamperometry did not solve the problem with the excess at the surface of the easier to oxidise amine, here HDA-Boc, with an excess of linker at the surface. Moreover the bulkiness of complex **8** could have prevented it from reaching high surface coverages in conditions of full monolayer, explaining the small range of Γ values detectable upon creation of the mixed monolayer, to confirm this theoretical calculations of surface coverage were run. Nonetheless the promising result was an incentive to increase the level of complexity of the system.

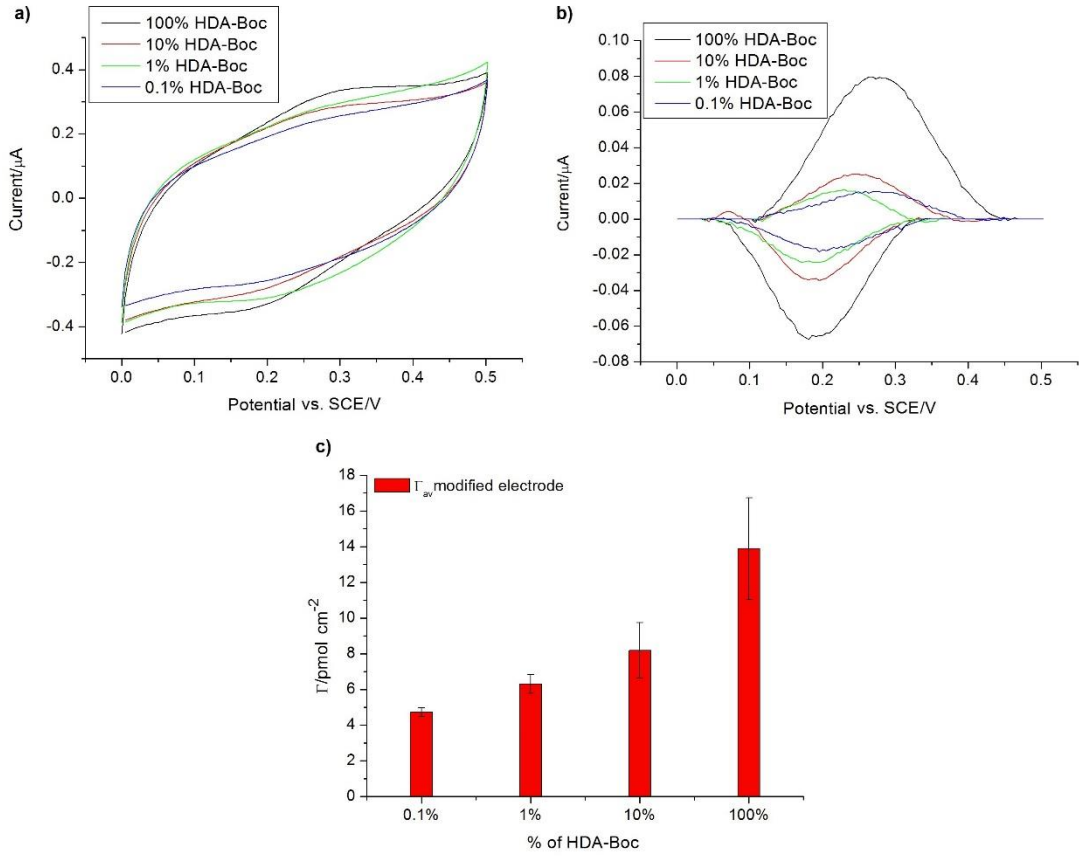

Figure 30. *a) Comparison of the CVs recorded in 0.1M PBS solution pH 7 vs. SCE, electrode area 0.071 cm^2, at 50 mV s^{-1}scan rate for different HDA-Boc linker solution ratios. b) Background-subtracted CVs obtained by analysing the data with Origin 7.0. c) Barplot for the variation of Γ of complex* ***8*** *according to the ratio of HDA-Boc linker in solution, calculated by averaging the values obtained for two replicates; the control was obtained by dipping amine modified electrodes in a neat 10 mM solution of complex* ***8*** *in DMF.*

3.3. Theoretical calculations of the surface coverage of complex 8

The results obtained in paragraph **3.2** suggested that the dimensions of complex **8** have a relevant effect on the range of surface coverage values detectable on the GC electrodes surface and this could be confirmed by calculating the theoretical surface coverage of complex **8**. The surface coverages usually reported in literature as reference values for osmium complexes similar to complex **8** vary, according to the type of electrode used, between 40 – 100 pmolcm^{-2} and they generally refer to a monolayer of complexes adsorbed to the electrode surface. In general these reference values were obtained experimentally by integration of the redox peaks of the species, but no actual theoretical values calculations are available for osmium bipyridyl complexes.[5] Having access to the crystal structure of complex **8**, allowed to transfer the coordinates of the atoms to the software Gaussian. Gaussian analysed the crystallographic coordinates, using the DFT hybrid method B3LYP with the standard 6-31G basis set for the organic components of the complex while the basis set given for osmium was LanL2DZ, to create a computational model of the complex (Figure **31**), where its dimensions could be measured.[6]

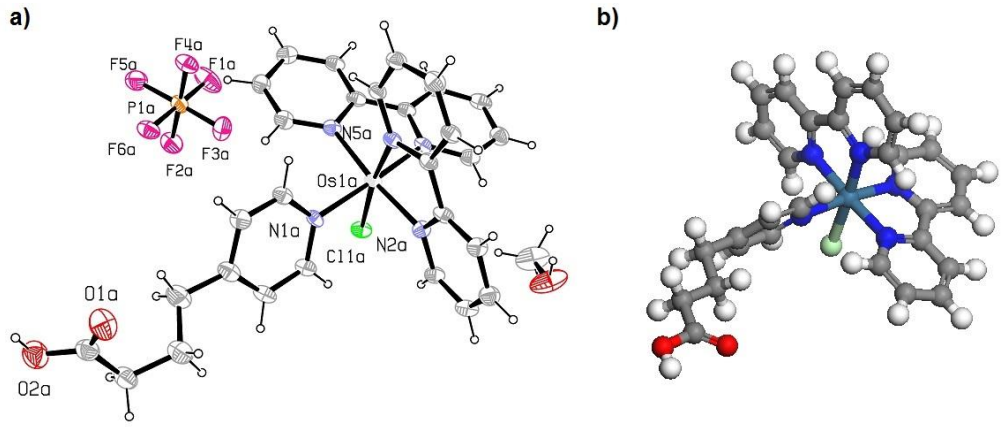

Figure 31. *a) Crystal structure of complex **8**. b) Computational model of complex **8** obtained from the atom coordinates of the crystal structure.*

The structure of the complex could be described as a “mushroom shape”, with a height of 16.5 Å and a diameter of 11.9 Å (Figure **32**).

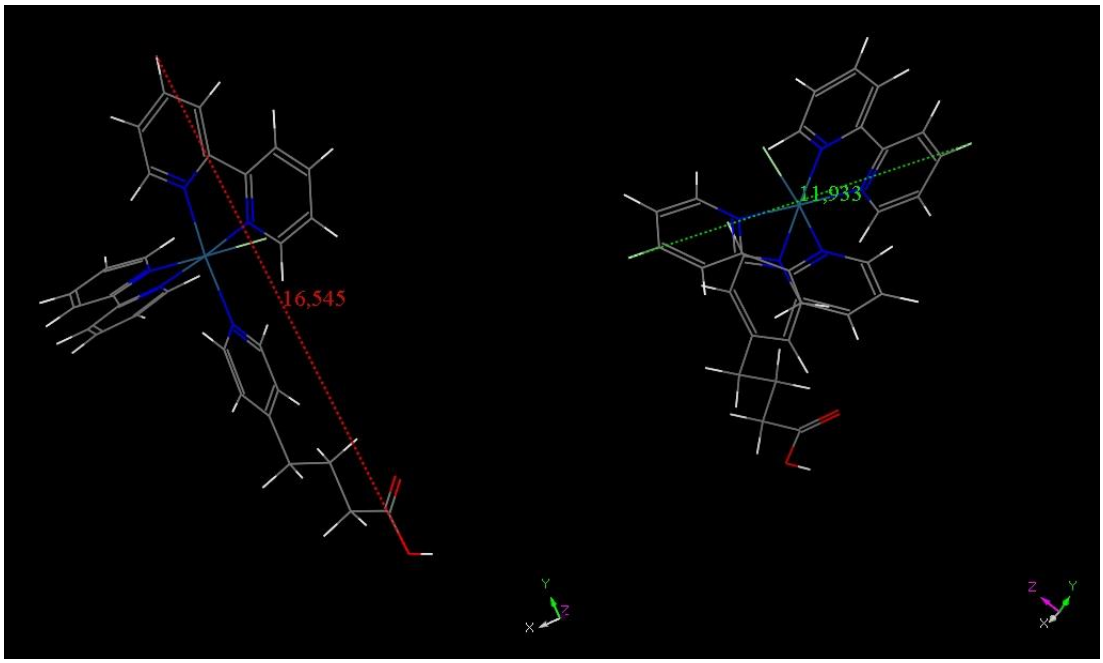

Figure 32. *Dimensions of complex **8** measured on the computational model with Gaussian.*

In order to calculate the maximum surface coverage of a monolayer of complex **8**, three assumptions were made: the diamine linkers monolayer on the GC surface is tightly packed, the amines have no mobility and no repulsion occurs between positively charged osmium complexes. Figure **33** represents two extreme situations that could occur at the electrode surface: a) the molecules are standing perpendicular to the surface and can be approximated to circles with radius r_1 = 5.96 Å organised in a hexagonal close-packed disposition; b) since complex **8** is attached to the amine linker through a 4 carbon chain, the molecules can lean on the electrode surface in different directions in time, occupying on average an area corresponding to a circle with radius r_2 = 16.5 Å, assumed to be hexagonally close-packed.

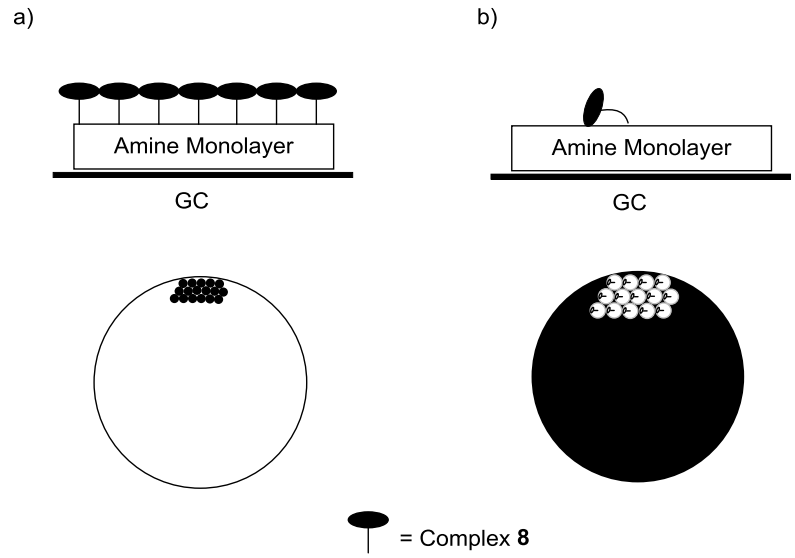

Figure 33. *Possible organisation at the surface of complex **8**. a) Tightly packed monolayer; b) the molecules lean on the surface occupying a greater area.*

The hexagonal close-packing represents the densest form of organisation of molecules in a monolayer.[7] According to this model the area occupied by each molecule can be calculated using the formula:

$$A = 2\sqrt{3}r^2 \qquad (\mathbf{8})$$

The surface coverage for a monolayer of complex **8** was calculated knowing the GC rod area (0.071 cm^2) and the area occupied by each molecule; given the two possible situations presented in figure **35** the final surface coverage could vary between 134 – 17 pmol cm^{-2}.

The surface coverage measured by integration of the CV redox peaks after the coupling of complex **8** to a monolayer of HDA fell within the values range determined by theoretical calculation. The average experimental value Γ = 18 – 20 pmol cm^{-2}, suggested that, in the system developed, the behaviour of the molecules at the electrode surface was better described by the model in figure 8b: the complexes that coupled initially to the free amines hindered the attachment of similar molecules. Moreover, this explained why in the creation of the mixed monolayers a significant amount of complex **8** could be detected for 0.1% linker in solution. The coverage for a monolayer of HDA, determined by XPS, is reported to be Γ = 1 nmol cm^{-2},[8] a value 50 times bigger than the surface coverage of a monolayer

of complex **8**, which meant that at 10% HDA on the surface, if uniformly distributed, a full monolayer of complex **8** was still achievable.

3.4. Mixed monolayer: diamine linker/diamine linker

The modification of the GC surface with two redox components requires a step-wise approach: two linkers must be attached to the surface and selectively reacted with the molecules of interest. It is known from peptide synthesis that the use of orthogonal protecting groups allows the control of the site of elongation of, for example, a peptidic chain, by carefully choosing the conditions, basic or acidic, for the selective removal of one or the other of the protecting groups (Section **1.4**).

Up to this point, the linkers used were diamines presenting the protecting group Boc, removable in acidic conditions, therefore the second linker needed a protecting group easily removed in mild basic conditions. Several base labile protecting groups are reported in literature; here the group chosen was trifluoroacetyl (tfa): slightly less bulky than Boc and not presenting an aromatic structure that could cause non-covalent adsorption on the GC surface, as might be the case with, for example, the Fmoc protecting group. Tfa is also reported to be labile to acidic conditions,[9] hence it had to be the first protecting group to be removed during the synthesis steps at the surface; this protecting group is often cleaved by treatment with 10% K_2CO_3 in methanol/water solution.[10] In order to test the consistency of the surface coverages with the linkers presenting the new protecting group, a monolayer of N-ethylenediamine-2,2,2-trifluoroacetamide (EDA-tfa) was grafted to the electrode surface and complex **8** was coupled to the free EDA after deprotection, the values obtained were compared to those obtained after the coupling to a monolayer of EDA-Boc (Scheme **22**).

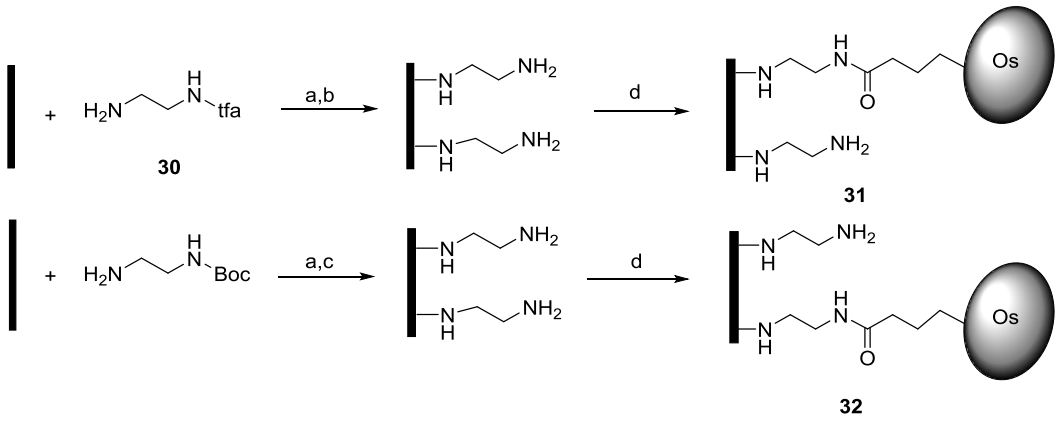

Scheme 22. *Synthetic steps to test the cleavage conditions of the tfa group. Conditions: a) 20 mM solutions in CH_3CN with 0.1 M TBATFB, chronoamperometry 2 V, 180 s; b) 10% K_2CO_3 in MeOH/H_2O (7:3), r.t., 6 h; c) 4 M HCl in dioxane, r.t., 1 h; d) 10 mM complex **8**, 0.1 M EDC, 60 mM NHS in DMF, r.t., 16 h.*

Figure **34** shows the surface coverages obtained: the results with the EDA-tfa monolayer present less variability and the surface coverage values are consistent with the results obtained in previous experiments with Boc protected amine.

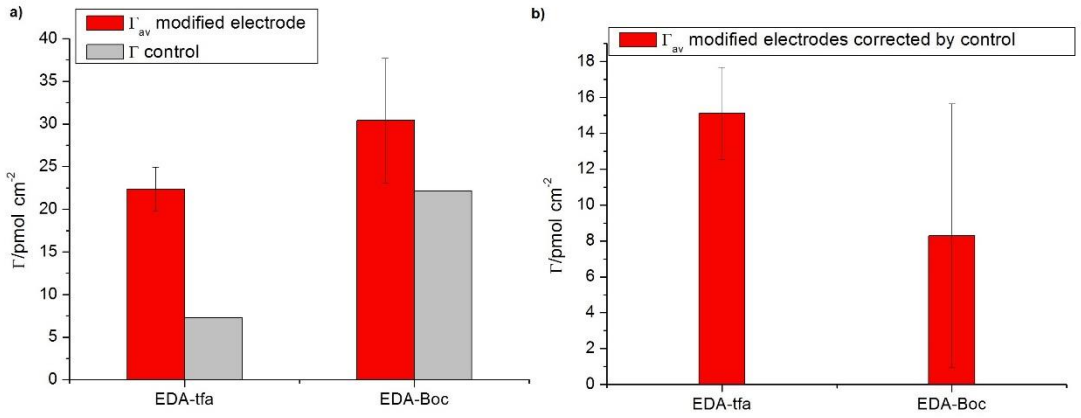

Figure 34. *a) Comparison of Γ of complex **8** obtained by coupling of a monolayer of EDA-tfa and EDA-Boc after deprotection, calculated by averaging the values obtained for three replicates; the control was obtained by dipping amine modified electrodes in a neat 10 mM solution of complex **8** in DMF. b) Barplot for the variation of Γ of complex **8** corrected by the corresponding controls Γ.*

The experiments with mixed monolayers of diamine linker/monoamine showed that the use of a longer linker for complex **8** gave better control over the coverages; considering this, N-(6-aminohexyl)-2,2,2-trifluoroacetamide (HDA-tfa) was chosen as the linker for the osmium complex, while EDA-Boc served as a linker for **AQ**. The synthetic procedure followed for the surface modification is given in scheme **23**.

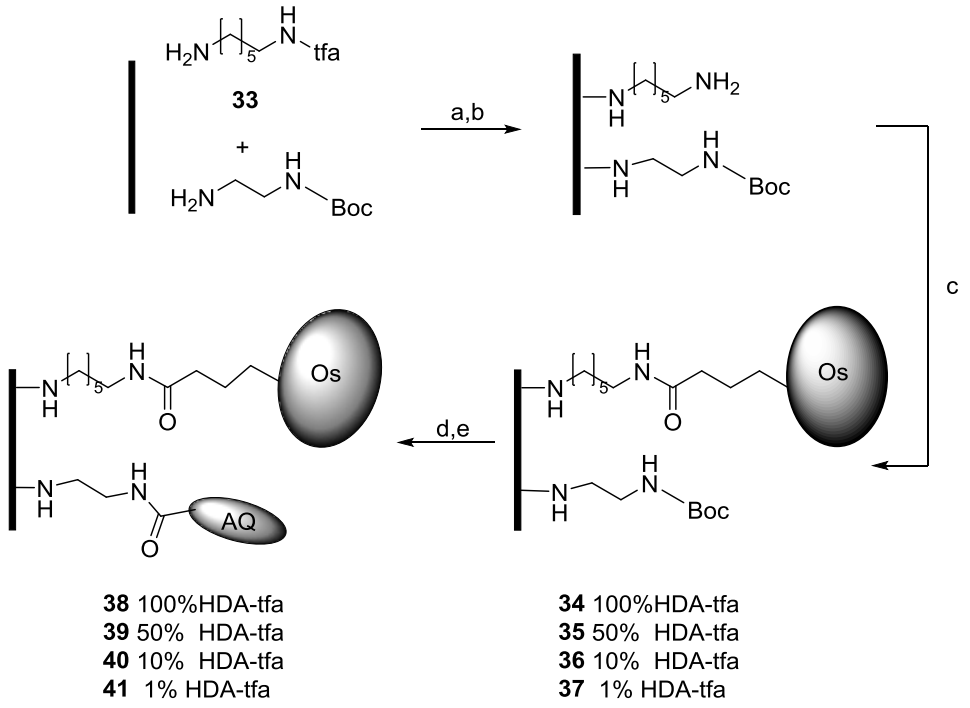

Scheme 23. *Synthetic steps for the creation of HDA-tfa/EDA-Boc mixed monolayers and coupling of complex* ***8*** *and anthraquinone. Conditions: a) 20 mM solutions in CH_3CN with 0.1 M TBATFB, chronoamperometry 2 V, 180 s; b) 10% K_2CO_3 in MeOH/H_2O (7:3), r.t., 6 h; c) 10 mM complex* ***8****, 0.1 M EDC, 60 mM NHS in DMF, r.t., 16 h; d) 4 M HCl in dioxane, r.t., 1 h; e) 50 mM* ***AQ****, 0.5 M EDC, 0.3 M NHS in DMF, r.t., 16 h;*

After the coupling of complex **8** to the free HDA, the electrodes were left stirring in acetonitrile for 24 h, in order to remove as much adsorbed material as possible, then checked by cyclic voltammetry (Figure **35**). The surface coverage of complex **8** decreased according to the decrease of HDA linker in solution, although this was not directly correlated with the relative ratios of the two amines in solution, as previously observed. In addition, the control electrodes exhibited a significant amount of residual osmium and anthraquinone that could not be washed off.

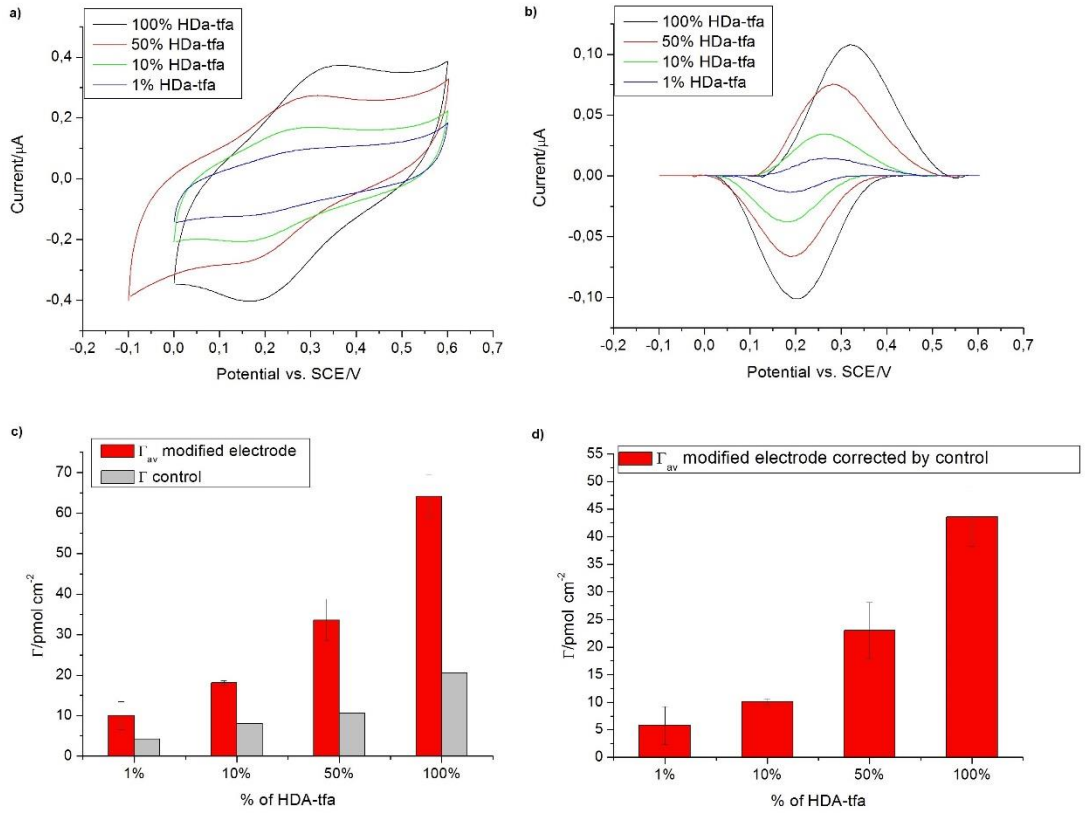

Figure 35. *a) Comparison of the CVs recorded in 0.1 M PBS solution pH 7 vs. SCE, electrode area 0.071 cm^2, at 50 mVs^{-1}scan rate for different HDA-tfa linker solution ratios. b) Background-subtracted CVs obtained by analysing the data with Origin 7.0. c) Barplot for the variation of Γ of complex* ***8*** *according to the ratio of HDA-tfa linker in solution, calculated by averaging the values obtained for two replicates; the control was obtained by dipping amine modified electrodes in a neat 10 mM solution of complex* ***8*** *in DMF. d) Barplot for the variation of Γ of complex* ***8*** *according to the ratio of HDA-tfa linker in solution corrected by the corresponding controls Γ.*

The removal of the Boc group allowed the coupling of **AQ** and the results obtained after stirring for 2 days in acetonitrile are presented in figure **36**. The surface coverage of **AQ** varies as the ratio of HDA-tfa is decreased in the grafting solution. In these experiments the control electrodes were significantly contaminated with non-covalently adsorbed material which could not be removed, as would be expected for **AQ**, whose flat aromatic structure makes the non-covalent stacking on the surface easier.

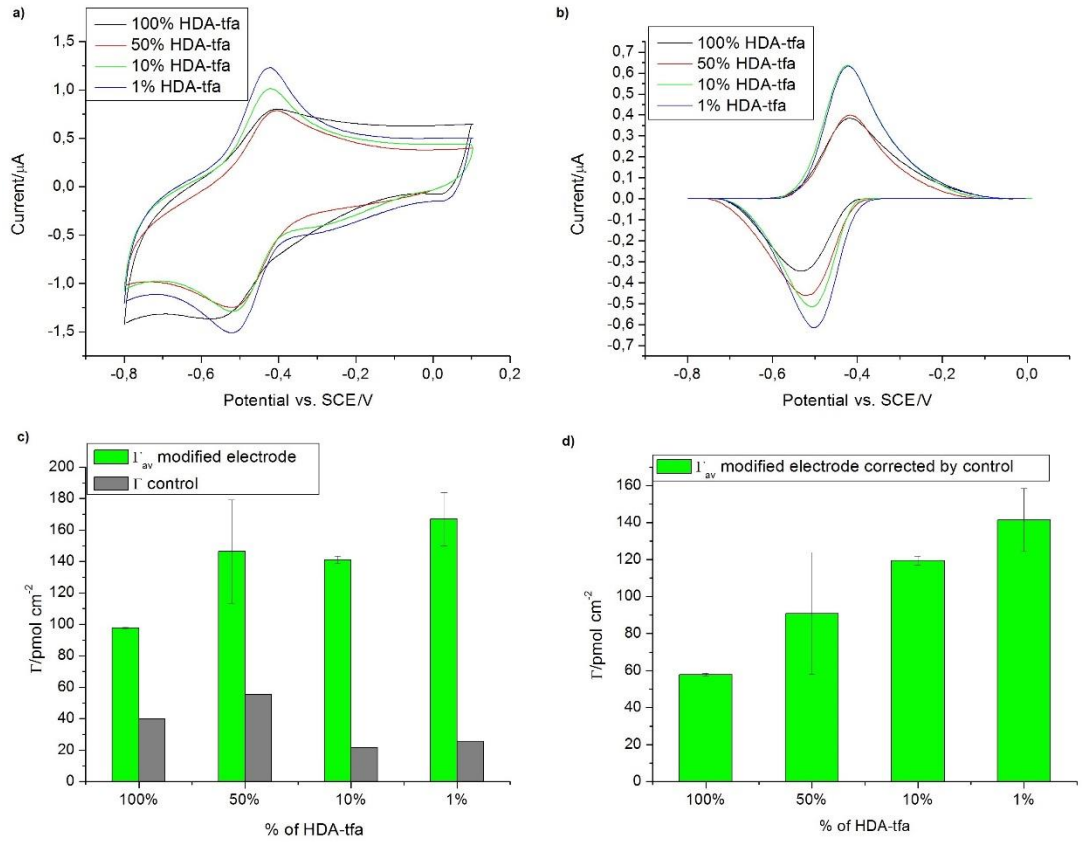

Figure 36. *a) Comparison of the CVs recorded in 0.1 M PBS solution pH 7 vs. SCE, electrode area 0.071 cm^2, at 50 mV s^{-1}scan rate for different HDA-tfa linker solution ratios. b) Background-subtracted CVs obtained by analysing the data with Origin 7.0. c) Barplot for the variation of Γ of* ***AQ*** *according to the ratio of HDA-tfa linker in solution, calculated by averaging the values obtained for two replicates; the control was obtained by dipping amine modified electrodes in a neat 50 mM solution of* ***AQ*** *in DMF. d) Barplot for the variation of Γ of* ***AQ*** *according to the ratio of HDA-tfa linker in solution corrected by the corresponding controls Γ.*

The background subtracted CVs suggested a shift of the redox potential of the species depending on the amount of linkers present at the surface. The calculation of the middle-peak potential (E_{mp}) showed a clear shift for complex **8** to lower potentials with the decrease of the amount of HDA-tfa linker with ΔE_{mp} = 42 mV, while the effect for anthraquinone was more contained with ΔE_{mp} = 12 mV to lower potentials with a decrease of the linker for **AQ** (Figure **37**).

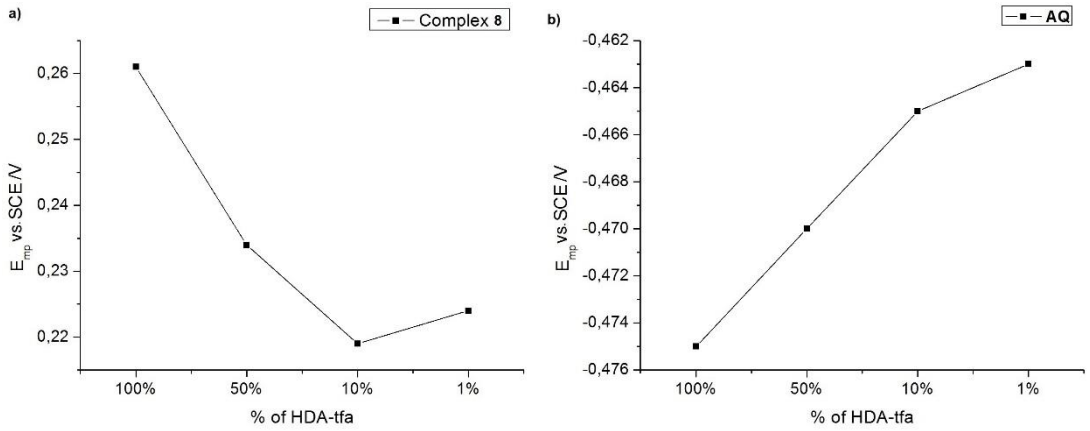

Figure 37. *Graphs showing the shift of E_{mp} according to the ratio of HDA-tfa linker in the grafting solution for the two redox molecules: a) complex **8**, b) **AQ**.*

Since this project focused on the development of a methodology for the control of the creation of mixed monolayers, no further investigation was dedicated to the study of the factors affecting the potential of the redox probes. In the literature, several factors that can influence the redox potential of molecules are reported, such as pH of the buffer, environment at the surface and interactions between the molecules themselves.[11] The redox potential of osmium complexes with similar structure to complex **8** are not affected by changes in the pH of the buffer solution, hence the effect measured could have been due either to the distance of the redox centre from the underlying amine monolayer, by the protonation state of the amines surrounding it or by the interaction between osmium complexes, whose intensity decreases when the molecules are diluted at the surface. None of these hypotheses could be discarded without more experiments.

Figure **38** summarises the results obtained: the CV (Figure **38a**) shows the redox peaks for the two species present at the same time on the surface. The peak associated with **AQ** is present at -0.48 V vs SCE, while the peak for $Os^{2+/3+}$ falls at 0.25 V vs SCE as seen in the CVs of the single redox centres. The barplot (Figure **38b**) shows the variation of surface coverage of both species plotted against the fraction of HDA-tfa in the starting solutions. It is worth noting the result for 100% HDA-tfa: here, although only complex **8** should have been present, a significant amount of **AQ** was detected. This result could be explained considering the dimensions and shape of the two redox molecules: during the coupling step, the osmium complexes already present at the surface hinder the approach of other similar molecules, leaving free NH_2 groups available for coupling later with **AQ**, able to fill the gaps. This said, it is important to underline that the total surface coverage stays reasonably constant for all the different concentrations, suggesting that the methodology developed is working.

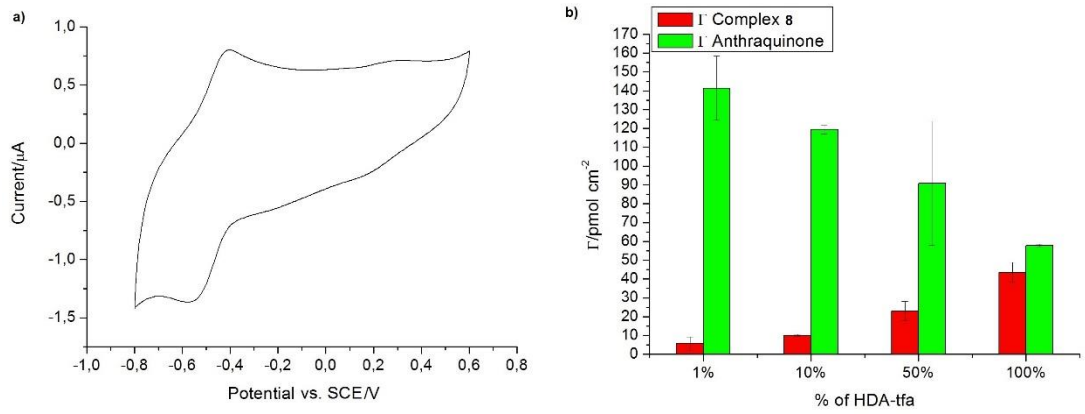

Figure 38. *a) CV recorded in 0.1 M PBS solution pH 7 vs. SCE, electrode area 0.071 cm^2, at 50 mV s^{-1}scan rate for 100% HDA-tfa linker showing both redox centres present on the surface. b) Barplot comparing the variation of Γ of complex **8** and anthraquinone according to the ratio of HDA-tfa linker in solution corrected by the corresponding controls Γ.*

The amount of complex **8** at the control electrodes represented an unexpected problem: tests for the adsorption/desorption of the complex showed that even after several days of washing the material could not be removed. Moreover the cleaning of the electrodes proved difficult, requiring the oxidation of the surface in phosphate buffer at high potentials and various rounds of polishing on abrasive paper. Even after these rigorous treatments non-covalent adsorption of anthraquinone remained a problem the more the experiments were performed on the same electrode, suggesting

that the problem could depend on the presence of material on the sides of the GC rod. Figure **39a** shows the setup of the working electrode that had been adopted until this point in the electrochemical experiments: the GC rod was encased in a glass holder tube by thermally shrinking the glass around the rod. In these conditions, it was assumed that only the exposed surface at the bottom was able to interact with the buffer solution. Supposing that the sides of the GC rod could also in part contribute to the signal detected on the CVs and that part of the material was trapped between the glass holder and the carbon, due to leakages caused by the different thermal expansion coefficients of glass and GC, a different setup was tested (Figure **39b**). In the meniscus configuration the end of the GC rod is exposed and not encased by the glass holder and only the bottom surface is allowed to be in contact with the buffer solution through the meniscus, setup usually applied with rotating disk electrodes (RDE).[12] This avoided any contribution to the detected signals from the sides of the rod.

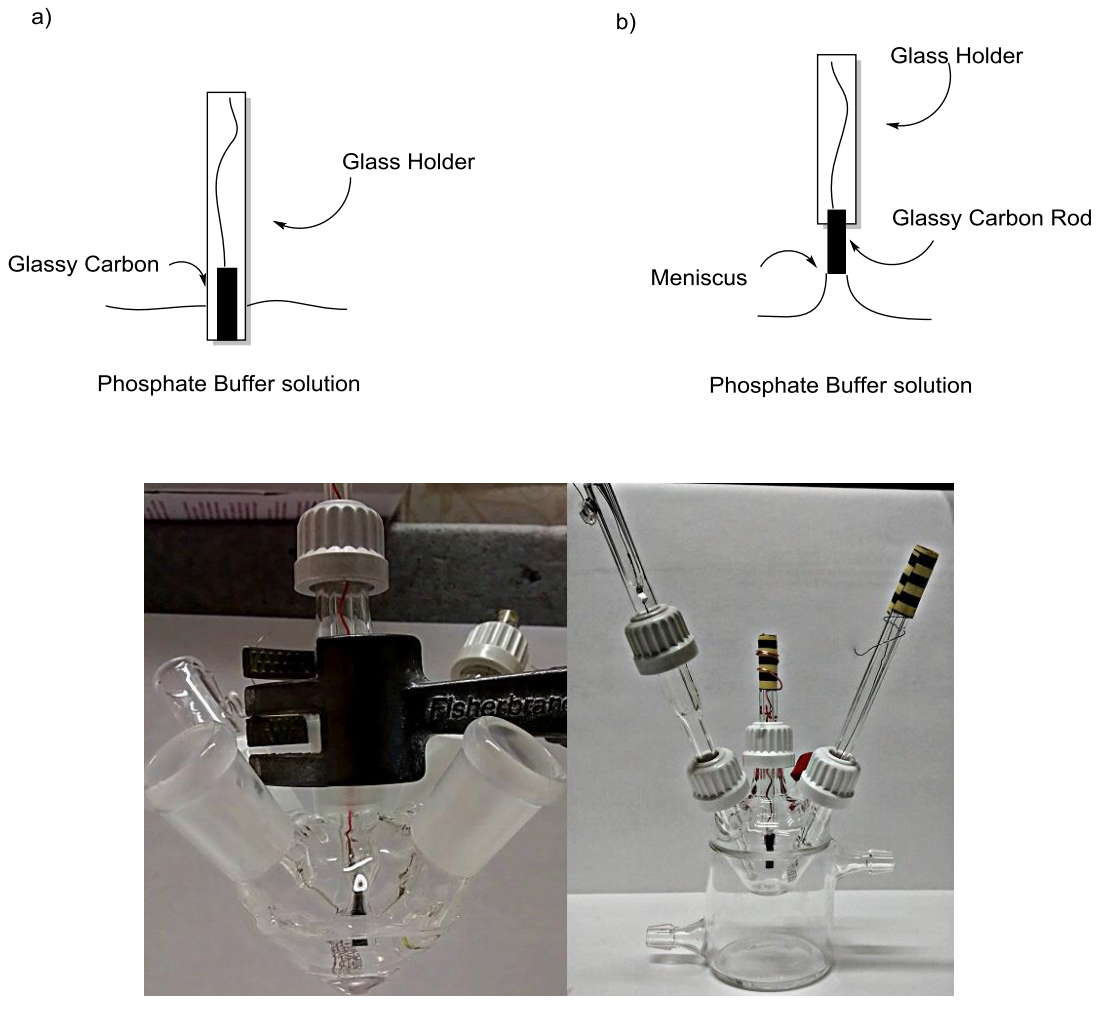

Figure 39. *Working electrode and cell setup for the electrochemical experiments.*

After a re-design of the electrochemical glassware to adapt to the new setup and to be able to work in controlled atmosphere, the mixed monolayer experiment was repeated to check the validity of the methodology (Scheme **24**).

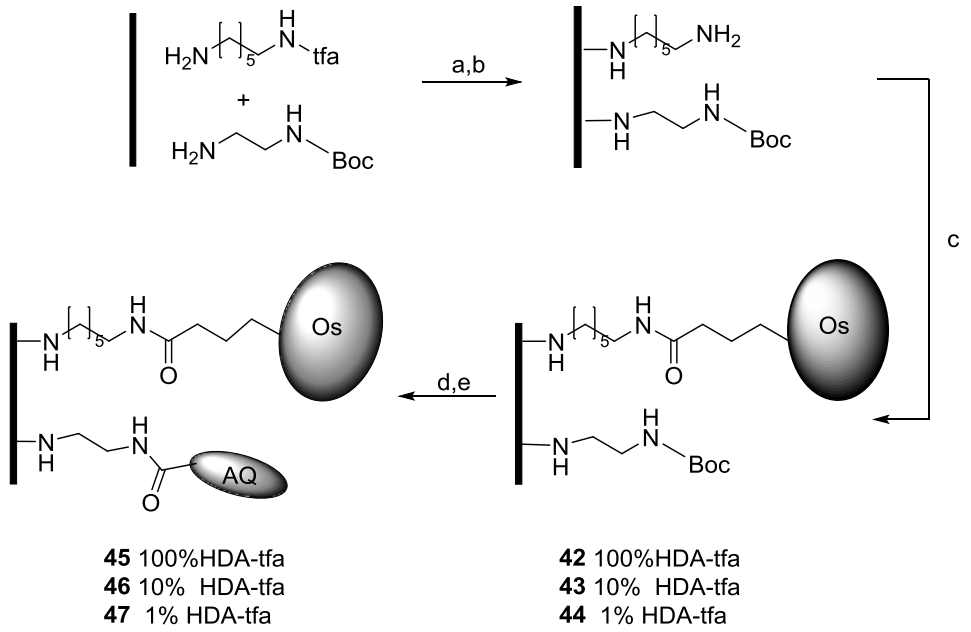

Scheme 24. *Synthetic steps for the creation of HDA-tfa/EDA-Boc mixed monolayers and coupling of complex* ***8*** *and anthraquinone. Conditions: a) 20 mM solutions in CH_3CN with 0.1 M TBATFB, chronoamperometry 2 V, 180 s; b) 10% K_2CO_3 in MeOH/H_2O (7:3), r.t., 6 h; c) 10 mM complex* ***8****, 0.1 M EDC, 60 mM NHS in DMF, r.t., 16 h; d) 4 M HCl in dioxane, r.t., 1 h; e) 50 mM* ***AQ****, 0.5 M EDC, 0.3 M NHS in DMF, r.t., 16 h.*

Figure **40** shows the results obtained with the new setup: the variation of surface coverages for the two species is consistent with the previous results, although the values, especially for **AQ**, were lower, suggesting that there was a significant contribution from adsorbed material with the old setup. The control electrodes for complex **8**, presented no adsorbed material after 20 h washing in acetonitrile, while the **AQ** electrodes required longer washing time in acetonitrile, 48 h, to achieve a stable signal where no desorption was detected, but still some material remained.

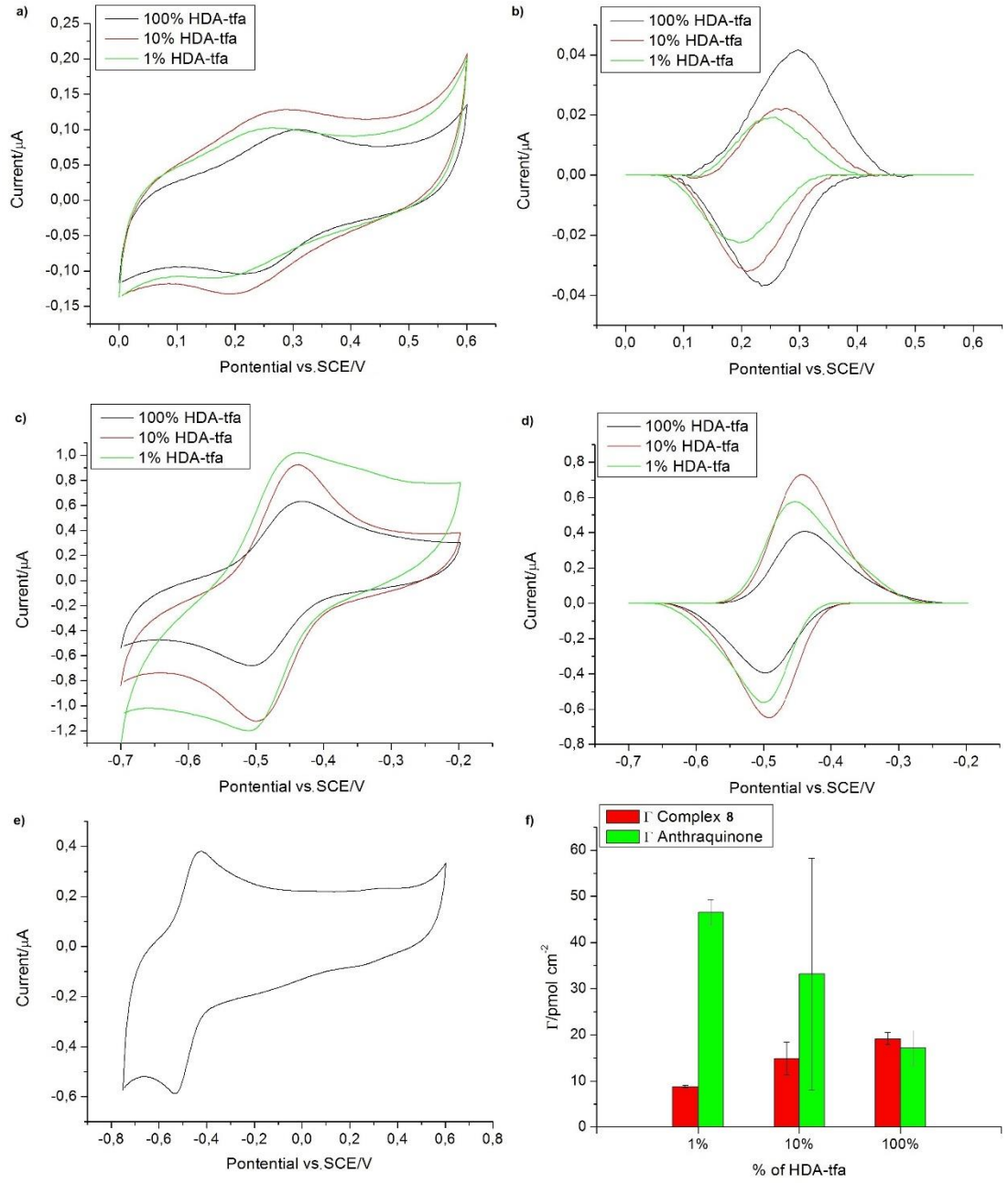

Figure 40. *a) Comparison of the CVs recorded for complex **8** in 0.1 M PBS solution pH 7 vs. SCE, electrode area 0.071 cm^2, at 50 mV s^{-1}scan rate for different HDA-tfa linker solution ratios. b) Background-subtracted CVs for complex **8** obtained by analysing the data with Origin 7.0. c) Comparison of the CVs recorded for **AQ** in 0.1 M PBS solution pH 7 vs. SCE, electrode area 0.071 cm^2, at 50 mV s^{-1}scan rate for different HDA-tfa linker solution ratios. d) Background-subtracted CVs for **AQ** obtained by analysing the data with Origin 7.0. e) CV recorded in 0.1 M PBS solution pH 7 vs. SCE, electrode area 0.071 cm^2, at 50 mV s^{-1} scan rate for 100% HDA-tfa linker showing both redox centres present on the surface. f) Barplot comparing the variation of Γ of complex **8** and **AQ** according to the ratio of HDA-tfa linker in solution corrected by the corresponding controls Γ.*

The comparison of the CVs of the blank electrodes recorded with the two different setups showed a decrease in the background current (Figure **41**).

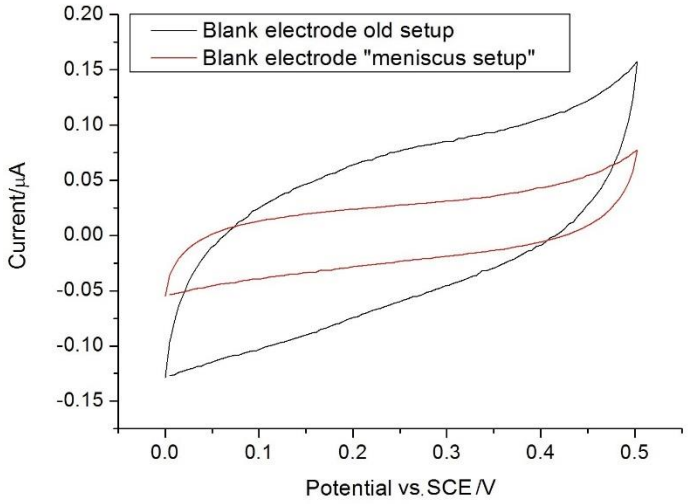

Figure 41. *Comparison of the CVs recorded in 0.1 M PBS solution pH 7 vs. SCE, electrode area 0.071 cm^2, at 50 mV s^1 scan rate for the blank electrodes in the old and new setup.*

Hoping to detect complex **8** at the surface for lower amounts of HDA linker, a set of electrodes were modified with amine grafting solutions containing 0.1% and 0.01% HDA-tfa and complex **8** was coupled to the surface after removal of the tfa protecting group (Scheme **25**).

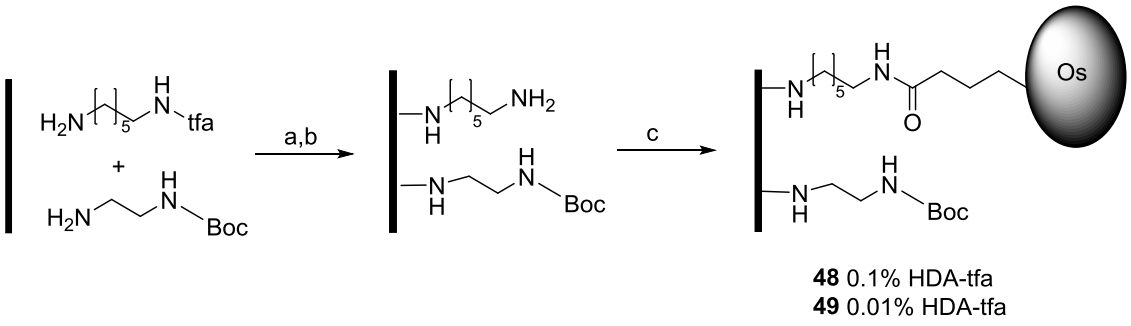

Scheme 25 *Synthetic steps for the modification of the surface with lower HDA-tfa linker concentrations. Conditions: a) 20 mM solutions in CH_3CN with 0.1 M TBATFB, chronoamperometry 2 V, 180 s; b) 10% K_2CO_3 in MeOH/H_2O (7:3), r.t., 6 h; c) 10 mM complex **8**, 0.1 M EDC, 60 mM NHS in DMF, r.t., 16 h.*

The CVs recorded (figure **42**) showed presence of complex **8** and the surface coverages calculated gave the same value for different amounts of linker, suggesting that probably a small amount of EDA-Boc was deprotected during step (b) of the synthesis at the surface.

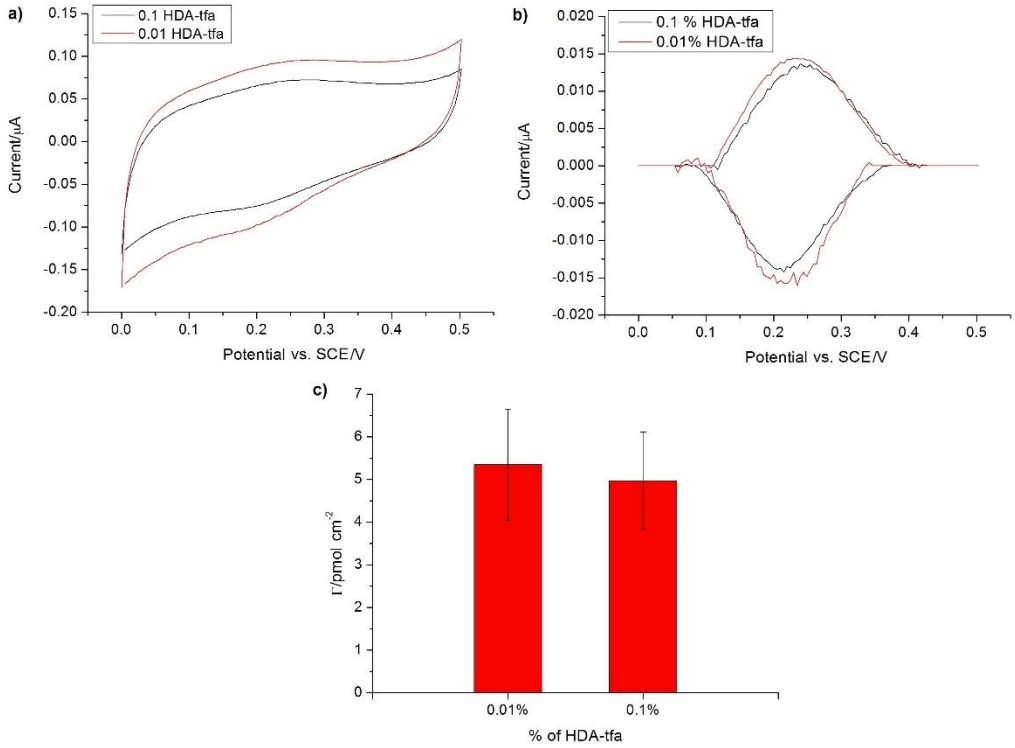

Figure 42. *a) Comparison of the CVs recorded in 0.1 M PBS solution pH 7 vs. SCE, electrode area 0.071 cm^2, at 50 mV s^{-1}scan rate for different HDA-tfa linker solution ratios. b) Background-subtracted CVs obtained by analysing the data with Origin 7.0. c) Barplot for the variation of Γ of complex **8** according to the ratio of HDA-tfa linker in solution, calculated by averaging the values obtained for two replicates.*

An experiment was run to test this hypothesis: a set of electrodes modified with a monolayer of EDA-Boc was exposed to the removal conditions for tfa and then dipped in a coupling solution of complex **8** (Scheme **26**).

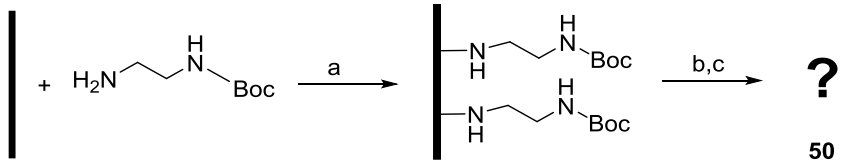

Scheme 26. *Test experiment for the stability of the Boc protecting group. Conditions: a) 20 mM solution in CH_3CN with 0.1 M TBATFB, chronoamperometry 2 V, 180 s; b) 10% K_2CO_3 in MeOH/H_2O (7:3), r.t., 6 h; c) 10 mM complex **8**, 0.1 M EDC, 60 mM NHS in DMF, r.t., 16 h.*

The results obtained confirmed the partial removal of Boc (Figure **43**).

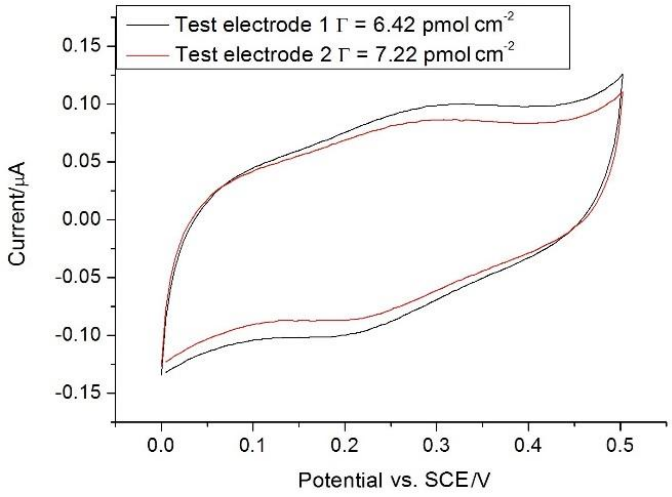

Figure 43. *Comparison of the CVs recorded in 0.1 M PBS solution pH 7 vs. SCE, electrode area 0.071 cm^2, at 50 mV s^{-1} scan rate for two replicates of* ***50****.*

Assuming that the 6 h reaction time was too long and a shorter reaction time was required, a screening of deprotection times was run on a set of electrodes modified with a monolayer of HDA-tfa, followed by coupling of complex **8** (Scheme **27**).

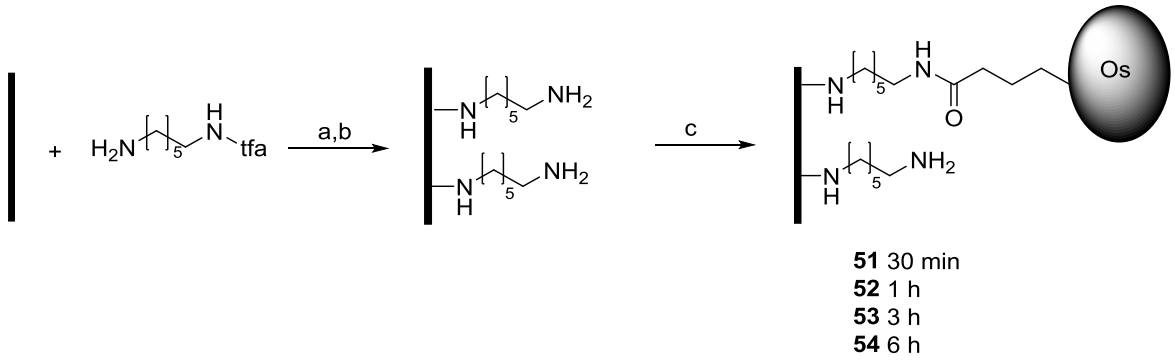

Scheme 27. *Test experiment for the reaction time of tfa removal. Conditions: a) 20 mM solution in CH_3CN with 0.1 M TBATFB, chronoamperometry 2 V, 180 s; b) 10% K_2CO_3 in MeOH/H_2O (7:3), r.t.,* ***different reaction time****; c) 10 mM complex* ***8****, 0.1 M EDC, 60 mM NHS in DMF, r.t., 16h.*

The surface coverages calculated (Figure **44**) showed that a deprotection time of 1 h was enough to obtain values consistent with 6 h reaction time previously used.

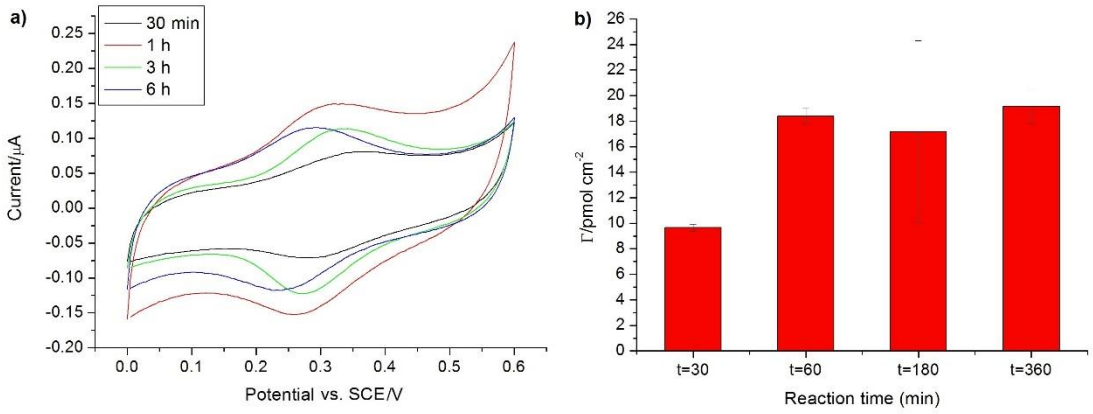

Figure 44. *a) Comparison of the CVs recorded in 0.1 M PBS solution pH 7 vs. SCE, electrode area 0.071 cm^2, at 50 mV s^{-1}scan rate for different deprotection times. b) Barplot for the variation of Γ of complex* ***8*** *according to the deprotection time, calculated by averaging the values obtained for two replicates.*

To verify that the new reaction time did not affect the Boc group, the test presented in scheme **26** was repeated, exposing the amine modified electrodes to a 10 % K_2CO_3 solution just for 1 h. Figure **45** shows that, after the required washing, the signal of complex **8** was not detected on such electrodes.

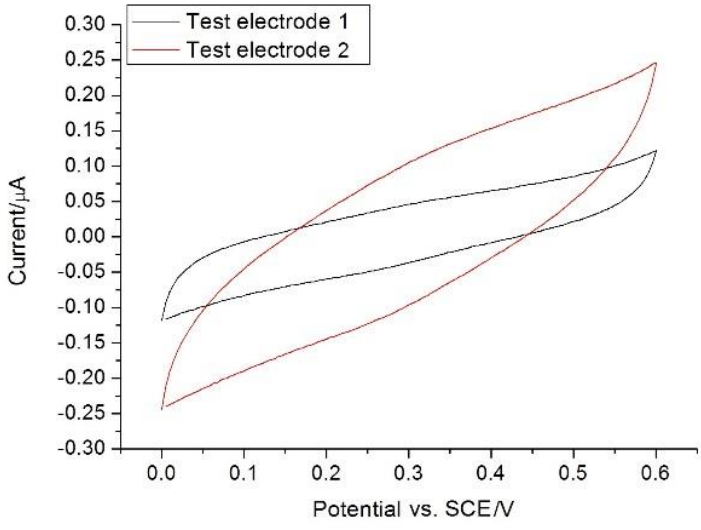

Figure 45. *Comparison of the CVs recorded in 0.1 M PBS solution pH 7 vs. SCE, electrode area 0.071 cm^2, at 50 mV s^{-1} scan rate for two replicates.*

The final problem was the free HDA linkers left after the coupling of complex **8**, this could be easily solved by adding an acylation step in the synthetic procedure at the surface. In order to find the best acylating agent a test reaction was run (Scheme **28**). Two acylating agents were tested: acyl chloride (AcCl) and acetic anhydride (Ac_2O).

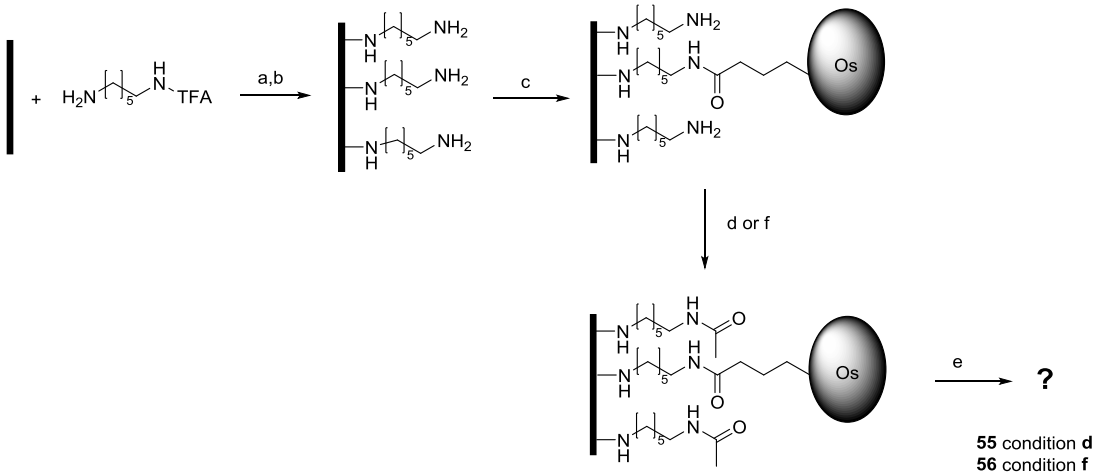

Scheme 28. *Test reaction for the acylation conditions. Conditions: a) 20 mM solution in CH_3CN with 0.1 M TBATFB, chronoamperometry 2 V, 180 s; b) 10% K_2CO_3 in MeOH/H_2O (7:3), r.t., 1 h; c) 10 mM complex **8**, 0.1 M EDC, 60 mM NHS in DMF, r.t., 16 h; d) 10 mM Ac_2O, DCM (dry), Et_3N, DMAP (cat.), r.t., overnight; f) 10 mM AcCl, DCM (dry), Et_3N, DMAP(cat.), r.t., overnight; e) 50 mM **AQ**, 0.5 M EDC, 0.3 M NHS in DMF, r.t., 16 h.*

Overall the acylation step led to a significant reduction of AQ at the surface (Figure **46**), both on modified and control electrodes, this could have meant that the non-covalent attachment of anthraquinone at the surface depended not only on adsorption processes but also on interactions with the residual free amines, such as hydrogen bonding. Acyl chloride gave the lowest values of surface coverage for **AQ**, so it was chosen as acylating agent.

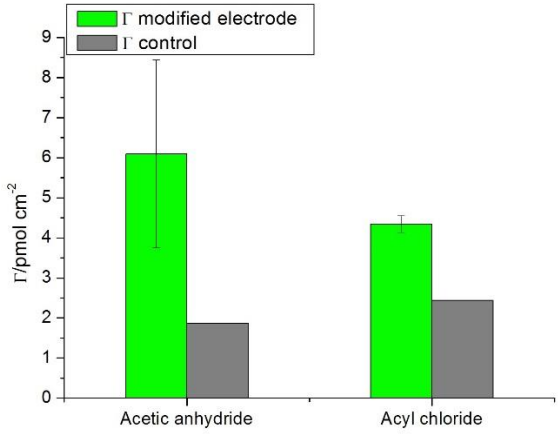

Figure 46. *Barplot for the variation of Γ of* ***AQ*** *according to the acylating agent, calculated by averaging the values obtained for two replicates.*

Once the optimisation of the synthetic steps with the "meniscus setup" was completed, the whole procedure for the creation of the mixed monolayers was repeated.

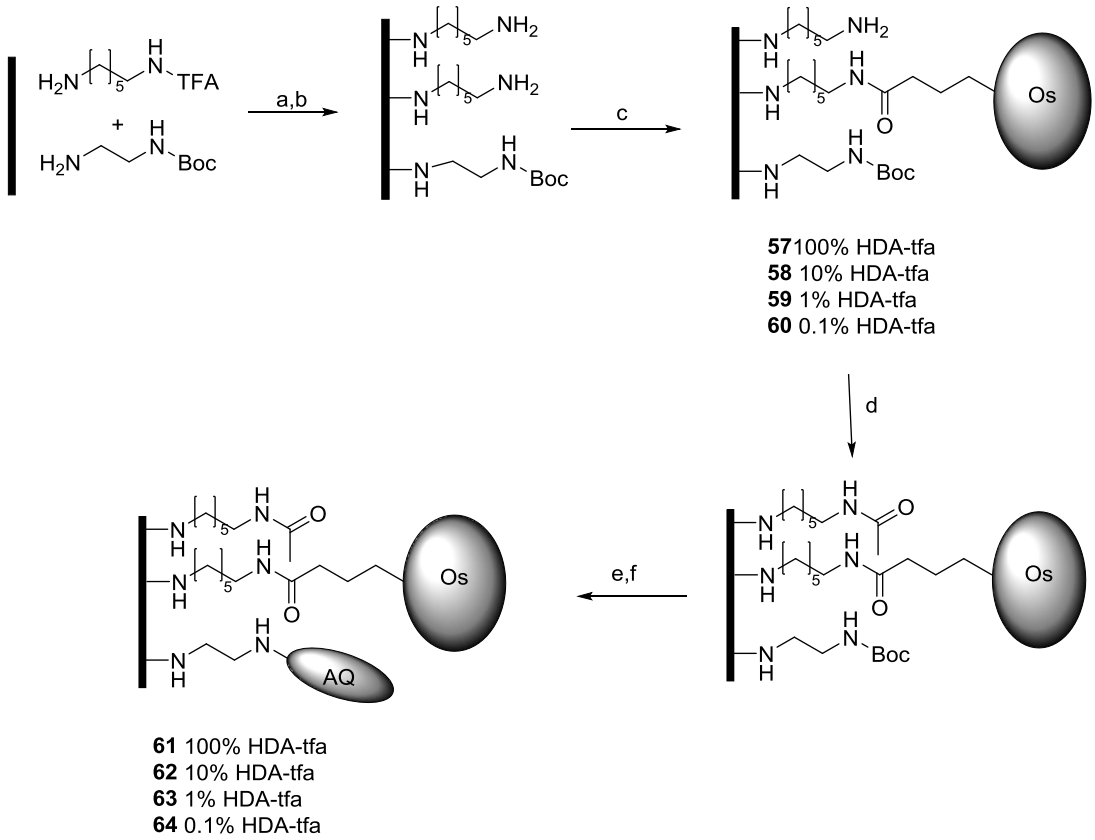

Scheme 29. *Synthetic steps for the creation of HDA-tfa/EDA-Boc mixed monolayers and coupling of complex* ***8*** *and anthraquinone with the "meniscus setup". Conditions: a) 20 mM solutions in CH_3CN with 0.1 M TBATFB, chronoamperometry 2 V, 180 s; b) 10% K_2CO_3 in MeOH/H_2O (7:3), r.t., 1 h; c) 10 mM complex* ***8****, 0.1 M EDC,*

60 mM NHS in DMF, r.t., 16 h; d) 10 mM AcCl, DCM (dry), Et_3N, DMAP(cat.), r.t., overnight; e) 4M HCl in dioxane, r.t., 1 h; f) 50 mM ***AQ****, 0.5 M EDC, 0.3 M NHS in DMF, r.t., 16 h.*

Figure **47** summarises the results obtained: the new conditions gave a better control over the variation of surface coverage of the redox species, and the non-covalent attachment of material to the electrode surface was limited to a large degree. The values of surface coverage reflected what was expected from previous considerations: at lower concentrations of HDA linker attachment of complex **8** still presents a significant surface coverage. This was due to two factors: HDA-tfa oxidises more easily than EDA-Boc, so its concentration at the surface will always be higher than that in solution. Moreover the bulkiness of complex **1** limits the range of Γ values achievable as explained in section **3.3**. **AQ** shows a much more evident variation, suggesting that the acylation step was necessary.

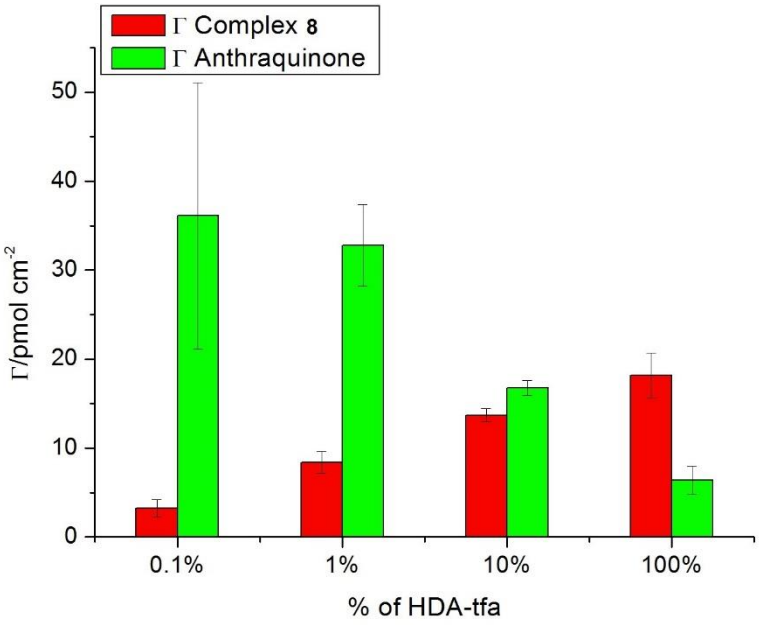

Figure 47. *Barplot comparing the variation of Γ of complex* ***8*** *and* ***AQ*** *according to the ratio of HDA-tfa linker in solution corrected by the corresponding controls Γ.*

3.5. Conclusions

A methodology for the creation of mixed monolayers on GC with a sequential approach, using the electrochemical oxidation of amines and solid phase synthesis techniques was developed. It was possible to control the relative amount of two redox probes at the surface by varying the relative amount of the respective amine linkers in solution. The optimisation of the method revealed that many factors have to be considered in order to obtain reproducible and reliable results. The structure of the redox probes has a great impact on the surface coverage values since they can hinder the attachment of similar molecules (complex **8**) or determine non-covalent adsorption (**AQ**). The setup of the working electrode is an important factor to consider: since the material can adsorb on the sides of the GC rod giving an overestimation of the surface coverage, using the meniscus configuration allowed us to characterise only the desired modified surface. The solid phase synthesis approach applied had to be adapted to the system developed: instead of the classical Boc/F-moc orthogonal protecting groups, the combination Boc/tfa was adopted, in order to avoid interferences by the possible non covalent adsorption at the GC surface of the F-moc group, characterised by a flat aromatic structure. The deprotection conditions were optimised and through the addition of an acylation step, residual free amines left after the first coupling step were capped, procedure routinely applied in solid phase peptide synthesis.

3.6. References

[1] Zafar, M.N.; Wang, X.; Sygmund, C.; Ludwig, R.; Leech, D.; Gorton, L. *Anal. Chem.* **2012,** *84,* 334-341.

[2] Rosso, K.M.; Smith, D.M.A.; Wang, Z.; Ainsworth, C.C.; Fredrickson, J.K. *J. Phys Chem. A* **2004,** *108,* 3292-3303.

[3] a) Bourdelande, J.L.; Gallardo, I.; Guirado, G. *J. Am. Chem. Soc.,* **2007,** *129,* 2817–2821. b) Steffel, L.R.; Cashman, T.J.; Reutershan, M.H.; Linton, B.R. *J. Am. Chem. Soc.,* **2007,** *129,* 12956–12957.

[4] Louault, C.; D'Amours, M.; Belanger, D. *Chem. Phys. Chem.,* **2008,** *9,* 1164–1170.

[5] a) Acevedo, D.; Abruna, H.D. *J. Phys. Chem.,* **1991,** *95,* 9590-9594. b) Forster, R.J.; Faulkner, L.R. *J. Am. Chem. Soc.,* **1994,** *116,* 5444-5452.

[6] Wang, H.; De Yonker, N.J; Gao, H.; Tan, C.; Zhang, X.; Ji, L.; Zhao, C.; Mao, Z.-W. *RSC Adv.* **2012,** *2,* 436-446.

[7] Vos, J.G.; Forster, R.J.; Keyes, T.E. *Interfacial Supramolecular Assemblies*, John Wiley & Sons, LTD, **2003.**

[8] Ghanem, M.A.; Chretien, J.-M.; Pinczewska, A.; Kilburn, J.D.; Bartlett, P.N. *J. Mater. Chem.* **2008,** *18,* 4917-4927.

[9] Wuts, P.G.M.; Greene, T.W. *Protective Groups in Organic Synthesis* (4th Edition), Wiley-Interscience, **2007.**

[10] Boger, D.L.; Yohannes, D. *J. Org. Chem.,* **1989,** *54,* 2498.

[11] a) Eggers, P.K.; Darwish, N.; Paddon-Row, M.N.; Gooding, J.J. *J. Am. Chem. Soc.* **2012,** *134,* 7539-7544. b) Ricci, A.M.; Tagliazucchi, M.; Calvo, E.J. *Phys. Chem. Chem. Phys.,* **2012,** *14,* 9988-9995.

[12] Villullas, H.M.; Teijelo, M.L. *J. Electroanal. Chem.* **1995,** *384,* 25-30.

4. Construction of a biosensor for D-(+)-Glucose

4.1. Engineered GDH as enzyme for the detection of glucose

The previous chapter showed how it was possible, through an accurate modification of the electrode surface, to create a system where the surface coverage of two redox species can be controlled. The methodology developed could potentially be used to build more stable and reliable devices, by covalent attachment of both a redox mediator and an enzyme to an electrode surface. The covalent attachment of native enzymes to surfaces is usually achieved through exposed amino acid residues on the surface of the enzyme. The main drawback of this approach resides in the limited control over the organisation of the biomolecules at the surface: each enzyme may present multiple residues able to react with the chemically modified electrode, causing a random orientation of the active site and reducing the response of the device. Moreover the conditions for the attachment could cause the partial inactivation of the enzyme.[1] Enzyme engineering allows the introduction of specific mutations on selected residues of the peptidic backbone, allowing control of the attachment of the enzyme according to the requirements of the system.[2]

The enzyme adopted in this project is a mutated GDH presenting a free cysteine residue in position T343C (Figure **48**), provided by the University of Natural Resources and Life Sciences, BOKU (Vienna).[i]

[i] The creation and production of engineered GcGDH for this project was carried out by Prof. Roland Ludwig group at BOKU University, within the Collaborative EU FP7 funded project "Three-dimensional nanobiostructure-based self-contained devices for biomedical application"

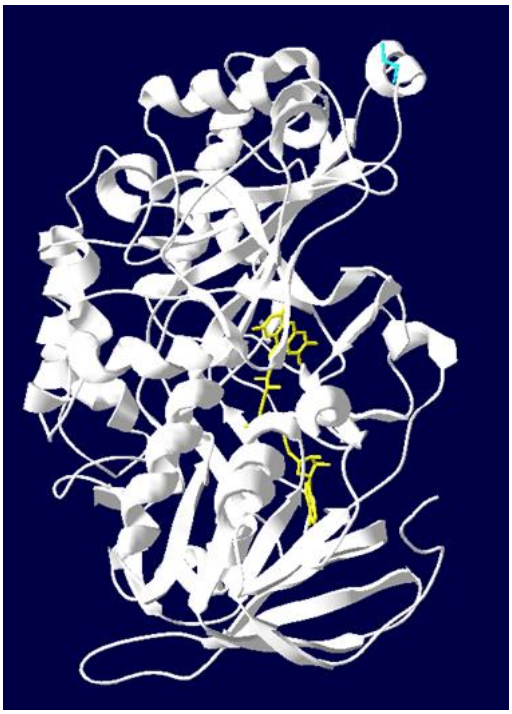

Figure 48. *Ribbon structure of the GDH mutant T343C, showing the cysteine residue introduced in cyan*.

GDH is an FAD dependent enzyme that can be found in various organisms, the variant presented above was discovered in the fungus *Glomerella cingulata* (GcGDH). It presents substrate specificity for β-D-Glucose and D-Xylose, is characterised by high turnover rates, good stability and is unaffected by oxygen; publications reporting the characterisation and catalytic properties of native GcGDH are available in literature.[3] BOKU provided the PDB file of the enzyme structure, which allowed the calculation of its maximum theoretical surface coverage applying the same method presented in section **3.3** for complex **8**. Figure **49** shows the structure of GcGDH analysed with the software PyMol.

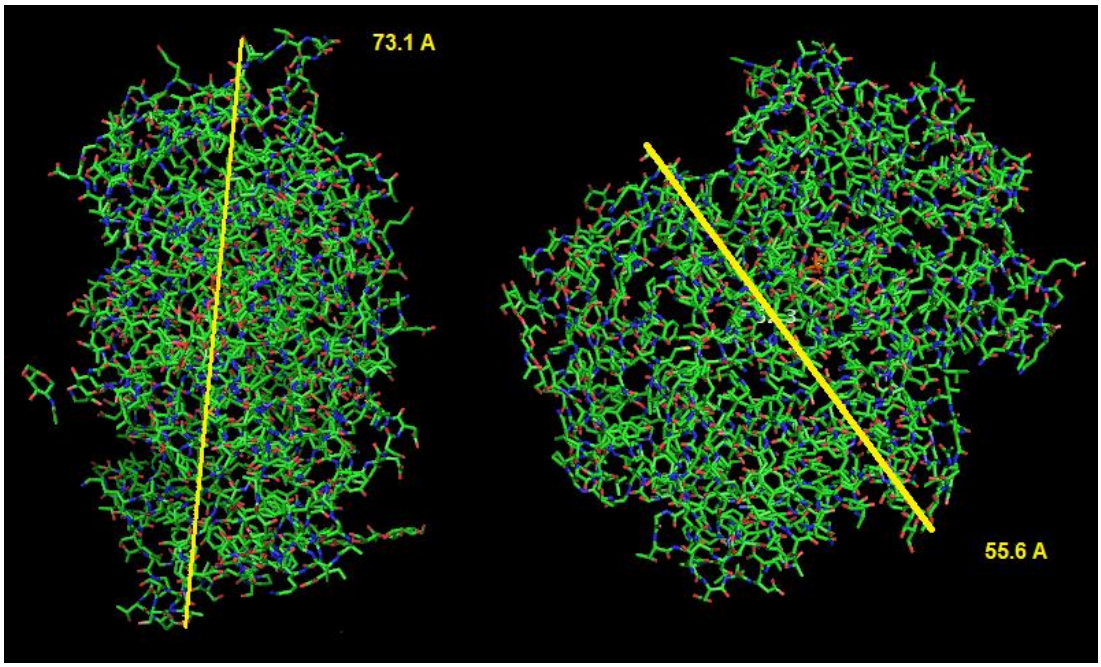

Figure 49. *Measurement of the dimensions of GcGDH obtained analysing the PDB file in PyMol.*

In order to apply the hexagonal-close packing model to determine the maximum surface coverage, the shape of the enzyme needed to be approximated to a sphere: the radius of this sphere was assumed to be r = 36.5 Å, considering the longest diameter measured. The surface coverage calculated in these conditions was $\Gamma = 3.5$ pmol cm^{-2}.

4.1.1. Determination of the kinetic parameters for homogeneous GcGDH reaction with D-(+)-glucose mediated by osmium complex 8

The analysis of experimental data obtained from the study of homogeneous mediator/enzyme systems is the main tool for determining the suitability of a redox mediator to be employed in the creation of a biosensor. The theoretical calculations for the determination of kinetic parameters in homogenous mediated enzymatic processes at the electrode surface have been described thoroughly in literature.[4] In general the process can be represented as in Figure **50**: the enzyme (E_{Ox}) oxidises the substrate (S) generating the product (P); the reduced form of the enzyme (E_{Red}) thus obtained reacts with the oxidised form of the mediator (M_{Ox}) and the reduced mediator (M_{Red}) is re-oxidised at the electrode surface.

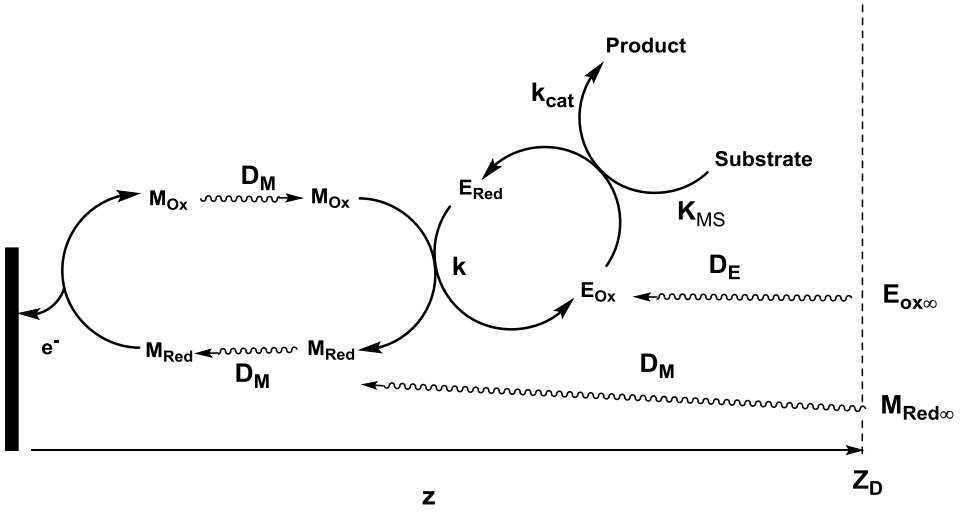

Figure 50. *General representation of the mediated enzyme process occurring in proximity of the electrode surface.*

The reactions can be represented as follows:

$$M_{Red} \longrightarrow M_{Ox} + e^- \qquad (\mathbf{9})$$

$$M_{Ox} + E_{Red} \xrightarrow{k} M_{Red} + E_{Ox} \qquad (\mathbf{10})$$

$$E_{Ox} + S \underset{}{\overset{K_M}{\rightleftharpoons}} ES \xrightarrow{k_{cat}} E_{Red} + P \qquad (\mathbf{11})$$

The catalytic processes (**9**) and (**10**) occur in solution while the regeneration of the mediator (**11**) occurs at the electrode surface. Two approximations are made:

- The diffusion coefficient for the enzyme D_E is the same for both reduced and oxidised form, which means that the total enzyme concentration is constant e_Σ;
- The diffusion coefficient for the mediator D_M is the same for both reduced and oxidised form, which means that the total mediator concentration is constant m_Σ;

The kinetics and diffusion of the species within the diffusion layer Z_D are described by four differential equations which, assuming the condition of steady state, present multiple analytical solutions. According to the boundary conditions chosen, four cases with approximate solutions have been described. In the system here analysed, the processes occurring are:

$$Os^{2+} \longrightarrow Os^{3+} + e^- \quad (\mathbf{12})$$

$$2Os^{3+} + GcGDH_{Red} \xrightarrow{k} 2Os^{2+} + GcGDH_{Ox} \quad (\mathbf{13})$$

$$GcGDH_{Ox} + Glucose \overset{K_M}{\rightleftharpoons} GcGDH/Glu \xrightarrow{k_{cat}} GcGDH_{Red} + Gluconolactone \quad (\mathbf{14})$$

The kinetics of the overall process could be affected by the rate of each of these reactions. Reaction (**12**) corresponds to the redox process of complex **8** at the electrode surface: this is a fast process, it follows the Randles-Sevičk equation, which allows the determination of the diffusion coefficient, $D_M = 2.74x10^{-5}$ cm^2 s^{-1}, in 50 mM citrate buffer solution pH 5.5 (Section **2.4**). Reaction (**13**) describes the mediator/enzyme interaction: the rate of the reaction depends on the concentration of both species and since two molecules of complex **8** are required to regenerate the enzyme the process can be broken down to two sequential steps:

$$Os^{3+} + GcGDH_{Red} \longrightarrow Os^{2+} + (GcGDH)' \quad (\mathbf{13a})$$

$$Os^{3+} + (GcGDH)' \longrightarrow Os^{2+} + GcGDH_{Ox} \quad (\mathbf{13b})$$

and the rate constant is of second order. Reaction (**3**) is the enzymatic oxidation of glucose: the process is described by the Michaelis-Menten model where:

$$v = \frac{V_{max}[Glu]}{K_M + [Glu]} \quad (\mathbf{14})$$

For [Glu] ≪ K_M the kinetics of the process are of first order in glucose concentration, while for [Glu] ≫ K_M the process is independent of glucose concentration. In order to calculate the kinetic parameters for the mediator/enzyme used in this project, a set of CVs was recorded at 5 mV s^{-1} in a 50 mM citrate buffer solution pH 5.5 solution containing GcGDH, e_Σ = 1.94 μM, and complex **8**, m_Σ = 1.2 mM with 0.1 M TEATFB as supporting electrolyte (Figure **51)**. The oxidation current increased upon addition of aliquots of a 100 mM solution of D-(+)-glucose, until reaching the saturation of the enzyme at high glucose concentration.

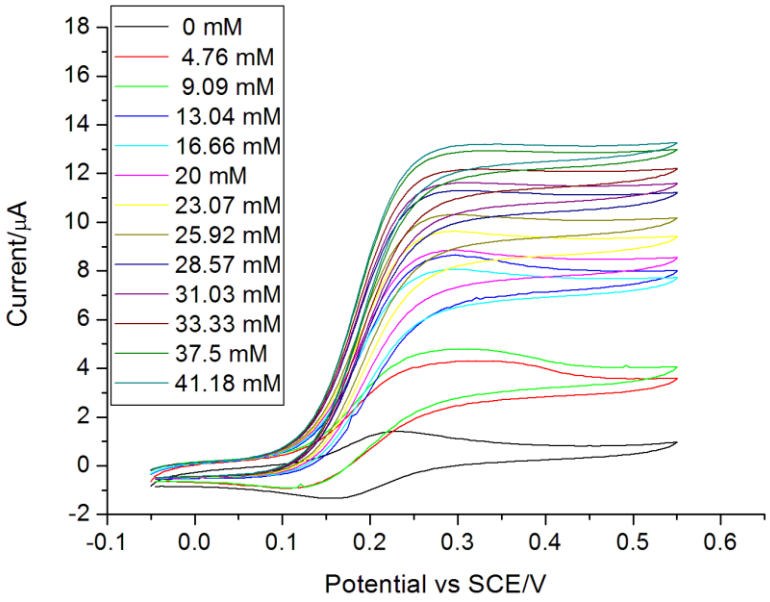

Figure 51. *CVs recorded in 50 mM citrate buffer solution pH 5.5 vs SCE containing [GcGDH]= 1.94 μM, [complex **8**] = 1.2 mM with 0.1 M TEATFB at 5 mV s^{-1}, electrode area 0.071 cm^2.*

The plot in Figure **52** shows the variation of oxidation current with increasing glucose concentration.

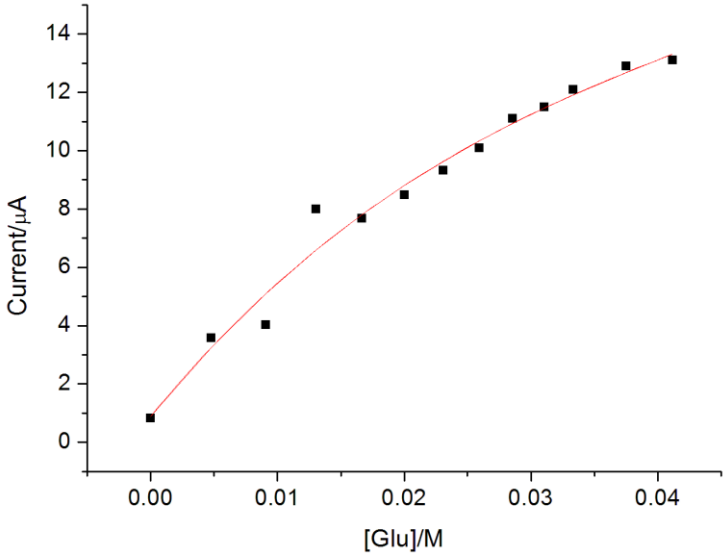

Figure 52. *Plot of the variation of oxidation current in function of the glucose concentration.*

Within the glucose concentration range where the current increases, the kinetics are limited by the reaction of the enzyme consuming the substrate and the current is determined by the Michaelis-Menten equation for non-saturated systems:

$$i_3 = nFA\left(\frac{2D_{\mathrm{M}}k_{cat}e_{\Sigma}m_{\Sigma}[\mathrm{Glu}]}{K_{\mathrm{M}}}\right)^{\frac{1}{2}} \quad \textbf{(15)}$$

When the current stops increasing and reaches the plateau value, the process could either be limited by high substrate concentration enzyme kinetics ([Glu] ≫ K_{M}) **(14)**, described by the Michaelis-Menten equation for the saturated system:

$$i_4 = nFA(2D_{\mathrm{M}}k_{\mathrm{cat}}e_{\Sigma}m_{\Sigma})^{\frac{1}{2}} \quad \textbf{(16)}$$

and the variation of current for the overall process is given by:

$$i_{3\to4} = nFA(2D_{\mathrm{M}}k_{\mathrm{cat}}e_{\Sigma}m_{\Sigma})^{\frac{1}{2}}\left(\frac{[\mathrm{Glu}]}{[\mathrm{Glu}]+K_{\mathrm{M}}}\right)^{\frac{1}{2}} \quad \textbf{(17)}$$

Or it could be limited by the reaction of regeneration of the enzyme by the mediator (**13**), which is not fast enough to match the rate of the enzymatic glucose oxidation and the plateau current is reached at lower values for the same glucose concentration. In this case:

$$i_2 = nFAm_{\Sigma}(2D_{\mathrm{M}}ke_{\Sigma})^{\frac{1}{2}} \quad (\mathbf{18})$$

And the variation of current for the overall process is given by:

$$i_{3\to2} = nFA(2D_{\mathrm{M}}e_{\Sigma}m_{\Sigma})^{\frac{1}{2}}(k_{\mathrm{cat}}m_{\Sigma})^{\frac{1}{2}}\left(\frac{[\mathrm{Glu}]}{[\mathrm{Glu}]+\left(\frac{K_{\mathrm{M}}km_{\Sigma}}{k_{\mathrm{cat}}}\right)}\right)^{\frac{1}{2}} \quad (\mathbf{19})$$

Both equations (**17**) and (**19**) can be converted to the general formula:

$$i = V''_{\mathrm{Max}}\left(\frac{[\mathrm{Glu}]}{[\mathrm{Glu}]+K''_{\mathrm{M}}}\right)^{\frac{1}{2}} \quad (\mathbf{20})$$

Equation (**20**) was fitted to the experimental values of current and glucose concentration to determine the apparent constants V'_{Max} and K''_{M}, using the non-linear least squares regression. The values obtained were V'_{Max} = 1.10 x 10^{-5} A and K''_{M} = 6.02 mM, value previously reported for the electrocatalytic oxidation of glucose by GcGDH mediated by osmium polymers. Once the apparent constants were calculated, k_{cat}/K_M = 3.79 x 10^3 M^{-1} s^{-1} was determined using equation (**22**), the value obtained is in the same order of magnitude as the ones reported for other redox mediators.[3]

$$\frac{V''_{\mathrm{Max}}}{(K''_{\mathrm{M}})^{\frac{1}{2}}} = \frac{V_{\mathrm{Max}}}{(K_{\mathrm{M}})^{\frac{1}{2}}} = nFA\left(2D_{\mathrm{M}}\frac{k_{\mathrm{cat}}}{K_{\mathrm{M}}}e_{\Sigma}m_{\Sigma}\right)^{\frac{1}{2}} \quad (\mathbf{21})$$

$$\left(\frac{k_{\mathrm{cat}}}{K_{\mathrm{M}}}\right)^{\frac{1}{2}} = \frac{V''_{\mathrm{Max}}}{(K''_{\mathrm{M}})^{\frac{1}{2}}}\frac{1}{nFA(2D_{\mathrm{M}}e_{\Sigma}m_{\Sigma})^{\frac{1}{2}}} \quad (\mathbf{22})$$

4.2. Maleimide as Michael acceptor: synthesis and optimisation of the attachment to the surface

The attachment of biomolecules presenting free thiol groups to surfaces can be easily achieved by functionalising such surfaces with Michael acceptor groups. A Michael acceptor compound is characterised by an alkene functional group with at least one electron withdrawing substituent that increases the electrophilicity of the double bond. These compounds react readily with good nucleophiles, such as thiols. Maleimide is the most common Michael acceptor adopted for the anchoring of biomolecules, since the presence of two carbonyl substituents on the double bond increases the reactivity, allowing the Michael addition of a thiol to occur spontaneously under controlled pH conditions.[5] Albeit being reported to be reversible in strong acidic conditions, the maleimide/thiol adduct is stable under biological conditions.[6] Wright *et al.* optimised some aspects of the maleimide/enzyme chemistry using a cytochrome c characterised by a cysteine residue at the surface.[7]

The general synthetic procedure for obtaining a maleimide suitable for the coupling to a free amine monolayer on the surface is available in literature and is presented in Scheme **30**.[8]

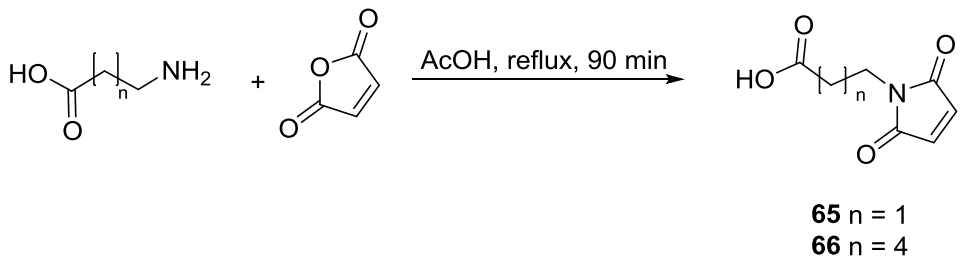

65 n = 1
66 n = 4

Scheme 30. *Synthesis of 3-maleimidopropionic acid (**65**) and 6-maleimidocaproic acid (**66**).*

Compounds **65** and **66** could be coupled to an electrode surface using classic solid phase synthesis conditions. Given the high reactivity of the maleimido group, side reactions could occur during the coupling that rendered the group unavailable for the enzyme attachment. For this reason a test reaction was run in solution where **65** was reacted with excess EDA-Boc under the coupling conditions applied at the surface (Scheme **31**).

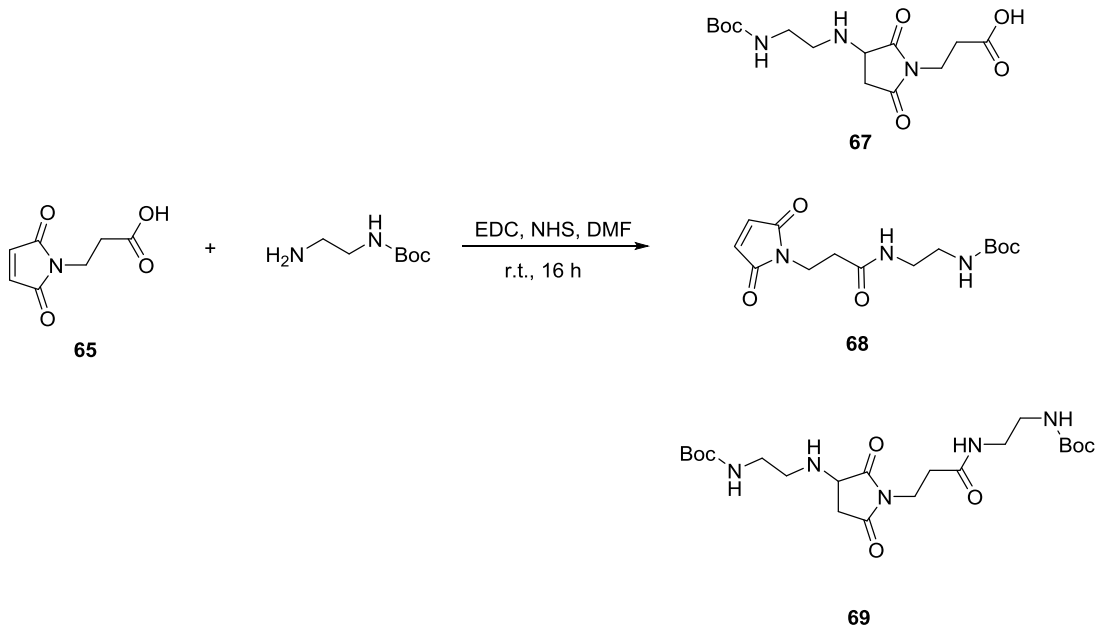

Scheme 31. *Test reaction for the coupling of* ***65*** *to an amine and possible products obtainable.*

After the required reaction time had passed, the crude product obtained after the aqueous work-up was characterised by H-NMR (Figure **53**): no peaks assignable to compounds **67** and **69** were present.

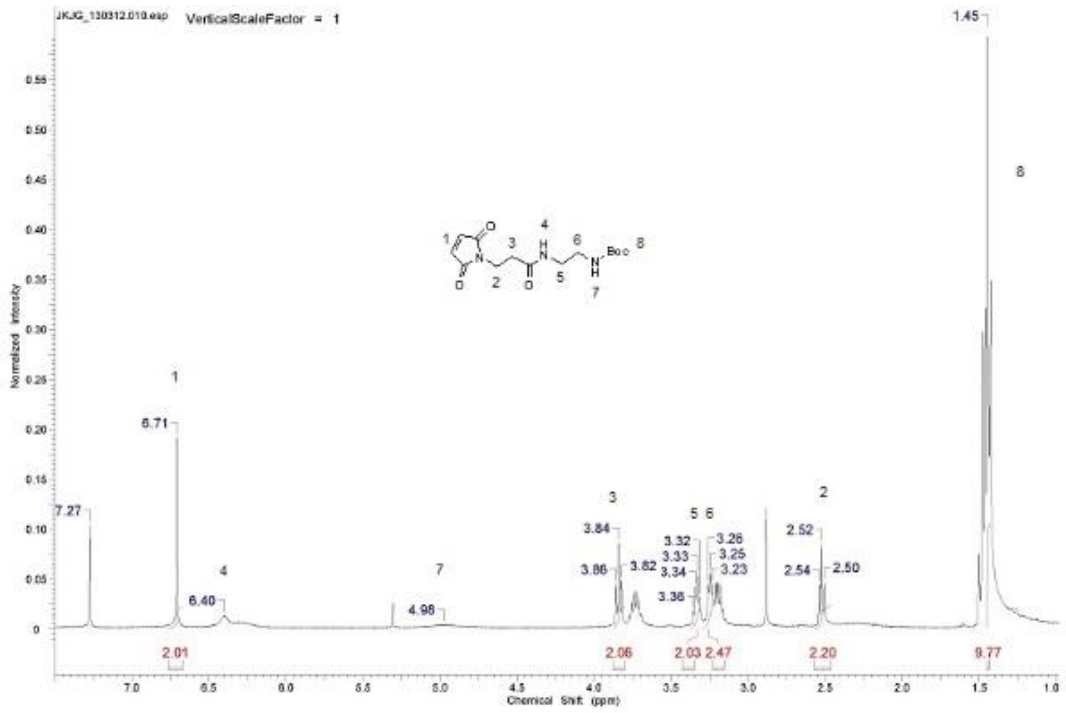

Figure 53. *H-NMR spectrum for the reaction crude for reaction in Scheme* ***31****, recorded at 300 MHz in* $CDCl_3$.

Although side reactions did not occur in solution, the reaction performed at the surface could still be affected by the very large excess of reactants. Avoiding unwanted reactions on the Michael acceptor can be achieved by protecting the double bond with an easily removable group: the protecting group previously reported is phenylselenyl, labile after oxidation with m-CPBA.[9] The phenylselenyl protected derivative of **65** was synthesised (Scheme **32**) following a literature procedure.

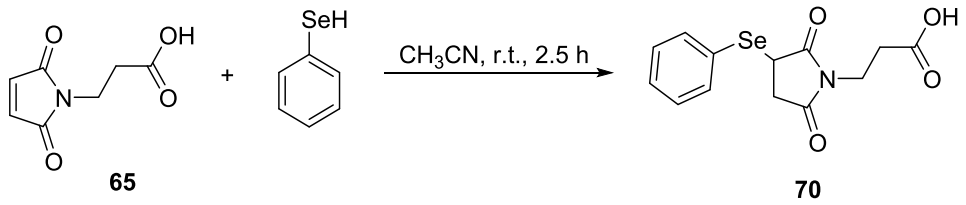

65 **70**

Scheme 32. *Synthesis of phenylselenyl protected maleimide.*

A control reaction was performed at the electrode surface to compare the yield of the maleimide/thiol reaction on the electrode surface with or without protecting group. The reaction is presented in Scheme **33**: two sets of electrodes were modified with HDA-Boc, after removal of the Boc group, one set was modified with compound **65** while a set was modified with compound **70** followed by treatment with a solution containing m-CPBA.

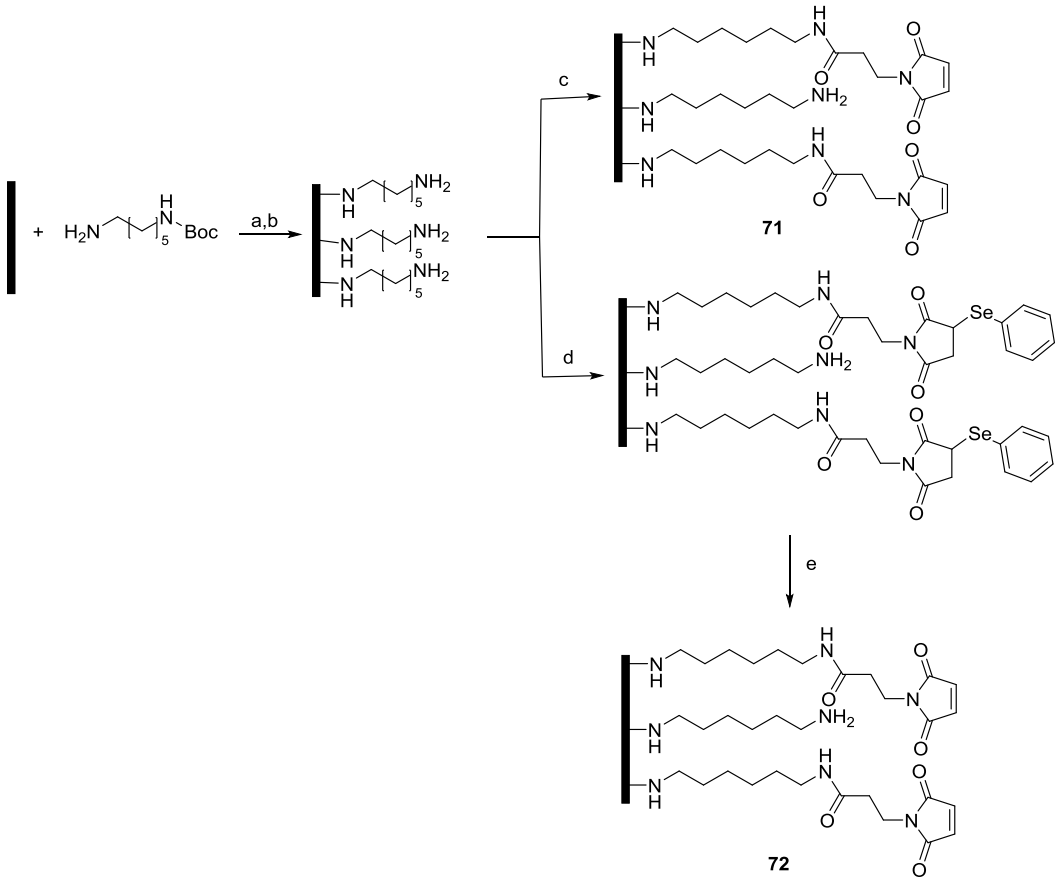

Scheme 33. *Synthetic steps for the modification of the electrode surface with* ***65*** *or* ***70****: a) 20 mM solution of HDA-Boc in* CH_3CN *with 0.1 M TBATFB, chronoamperometry 2 V, 180 s; b) 4 M HCl in dioxane, r.t., 1 h; c)10 mM solution of* ***65****, 0.1 M EDC, 60 mM NHS in DMF, r.t., 16 h.; d) 10 mM solution of* ***70****, 0.1 M EDC, 60 mM NHS in DMF, r.t., 16 h.; e) 10 mM m-CPBA in* CH_3CN*, 0°C then r.t., 2 h.*

In order to characterise the maleimide monolayer, an osmium bipyridyl complex presenting a free thiol was synthesised (Scheme **34**): the first step involved the protection of 3-mercaptopropionic acid with the acyl group in order to avoid the oxidation of the thiol moiety during the following steps. The coupling of **73** to 4-aminomethylpyridine generated the monodentate ligand **74**, which was reacted with the osmium bipyridyl dichloride precursor to form complex **75** isolated as the hexafluorophosphate salt. The removal of the acyl group in basic conditions, yielded complex **76**, suitable for the attachment to maleimide.

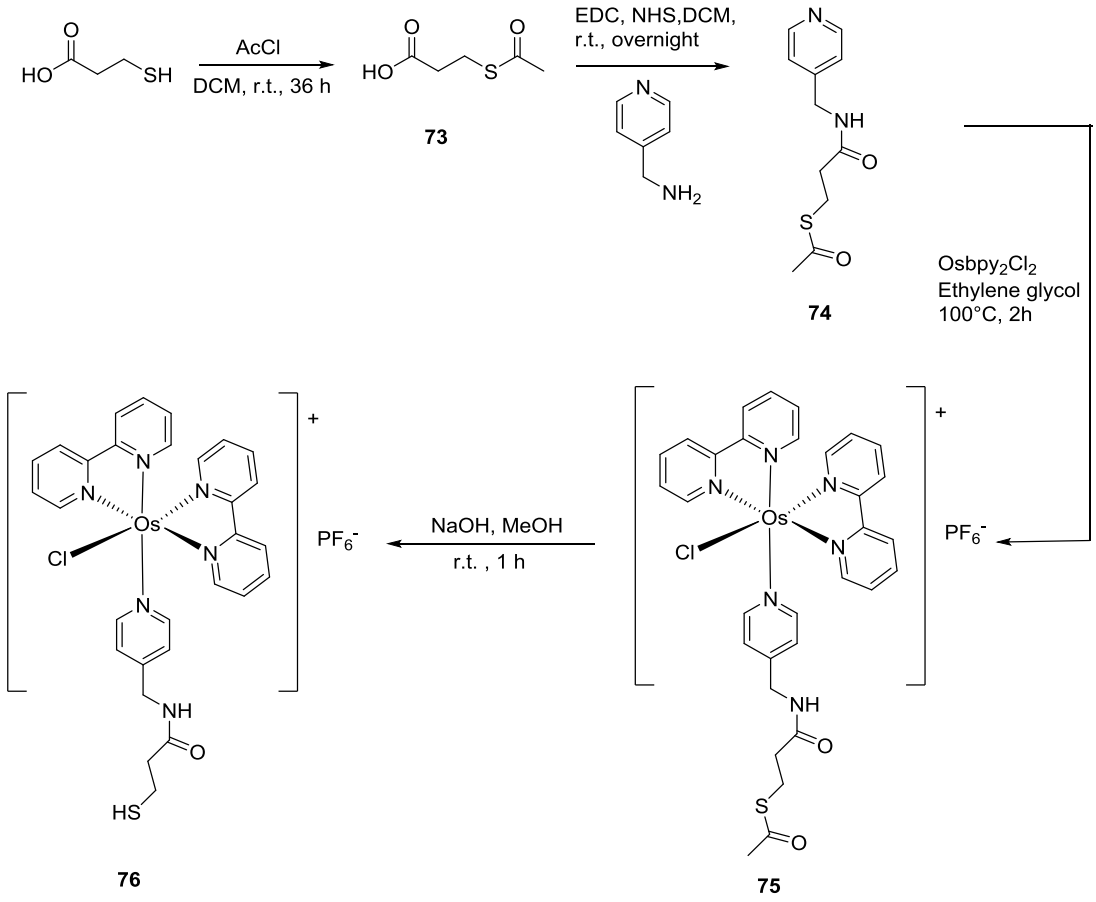

Scheme 34. *Steps for the synthesis of complex* ***76*** *presenting a free thiol group suitable for the attachment to the maleimide group.*

The two sets of electrodes **71** and **72** were dipped in a 10 mM solution of complex **76** in presence of a base and left stirring overnight.

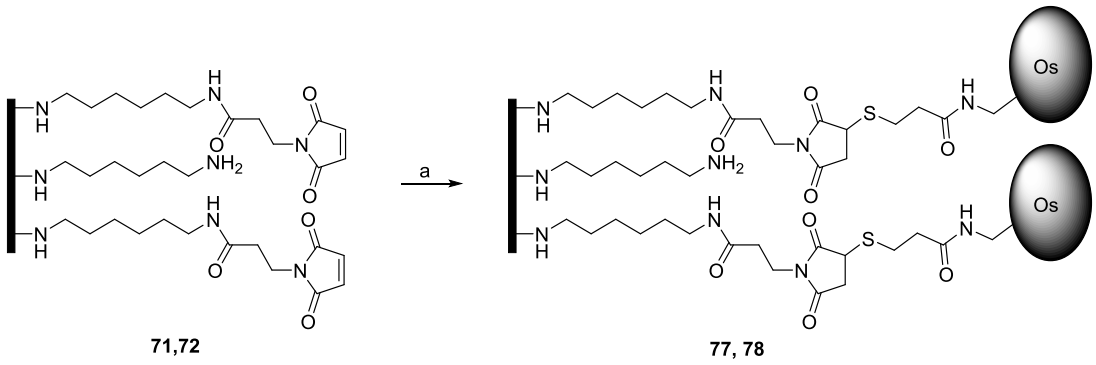

Scheme 35. *Attachment of complex **76** to the maleimide modified electrode surface: a) 10 mM **12** in MeOH, Et_3N, r.t., overnight.*

The results obtained are shown in Figure **54**: the two methodologies gave very similar surface coverages and the values obtained were consistent with the results previously seen for a monolayer of osmium bipyridyl complex. The use of the protecting group was discarded since it also required fewer synthetic steps at the surface.

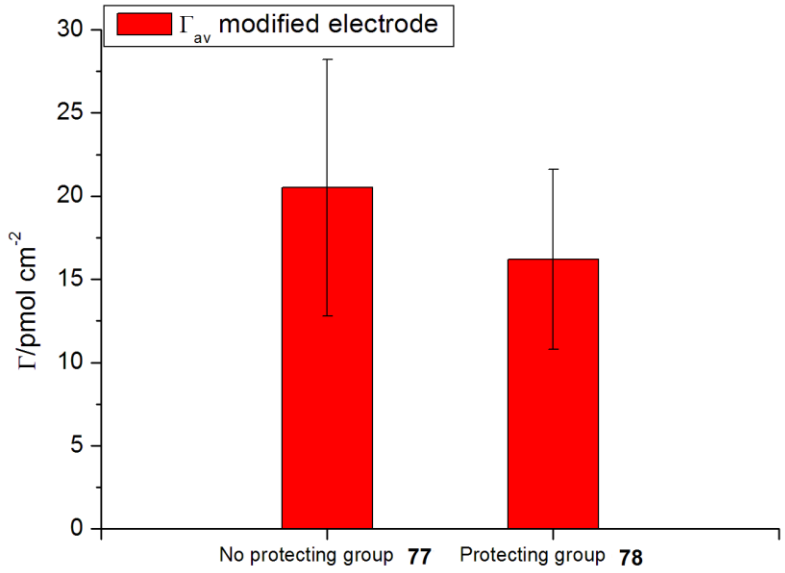

Figure 54. *Barplot for the variation of Γ of complex **76** calculated by averaging the values obtained for two replicates.*

4.3. Design of a mixed monolayer for the attachment of complex 8 and GcGDH

The construction of a surface, where both redox mediator and enzyme are covalently bound to a mixed monolayer of linkers, requires a careful design: the relative ratios of the two linkers should be such as to avoid one component hindering the approach of the other and the components should be oriented to allow efficient electron flow during the electrocatalytic process. It is clear from literature, as described in section **1.5**, that the use of a "diluting agent" able to spread the linkers on the surface is the most viable method to solve the first problem, while the precise relative orientation of the two components is difficult, since it would require a control at the molecular level that has been impossible to achieve up until now.[10]

The methodology optimised in Chapter **3** for the creation of mixed monolayers of two amines was tested for a system containing three amines: HDA as linker for complex **8**, EDA as the linker for **AQ** and 1-BA was added as a diluting agent. The relative ratios of the three amines were chosen giving consideration to the optimal surface for the enzyme: Wright *et al.* determined that 10% linker for maleimide in the grafting solution was the optimal amount to achieve the best interaction between enzyme and surface.[7] With this in mind, the ratio of EDA-Boc was kept constant at 10% and the ratio of HDA-tfa and 1-BA was varied (Scheme **36**). The synthetic steps performed at the surface followed the methodology optimised in chapter **3**: mixtures of the three amines in varying ratios were grafted to the GC electrode. Following the selective removal of the tfa group in basic conditions, complex **8** was coupled to the surface. The residual free HDA groups remaining after the coupling step were acylated and the Boc group was removed from EDA in acidic conditions, allowing the coupling of anthraquinone.

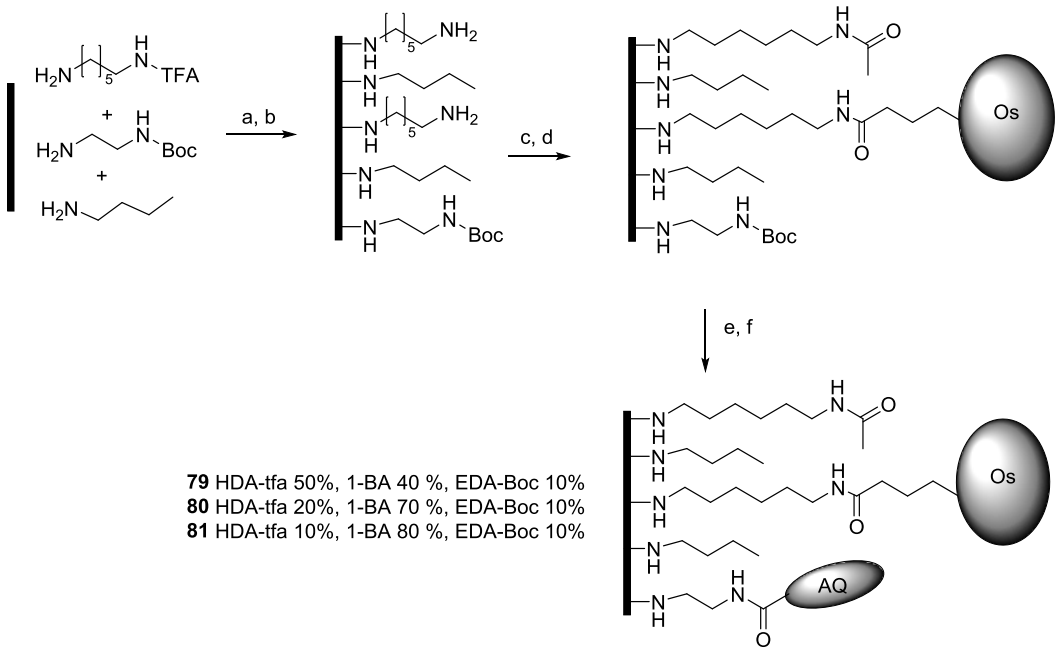

Scheme 36. *Synthetic steps for the creation of HDA-tfa/1-BA/EDA-Boc mixed monolayers and coupling of complex* ***8*** *and anthraquinone. Conditions: a) 20 mM solutions in CH_3CN with 0.1 M TBATFB, chronoamperometry 2 V, 180 s; b) 10% K_2CO_3 in MeOH/H_2O (7:3), r.t., 1 h; c) 10 mM complex* ***8****, 0.1 M EDC, 60 mM NHS in DMF, r.t., 16 h; d) 10 mM AcCl, DCM (dry), Et_3N, DMAP(cat.), r.t., overnight; e) 4M HCl in dioxane, r.t., 1 h; f) 50 mM* ***AQ****, 0.5 M EDC, 0.3 M NHS in DMF, r.t., 16 h.*

Figure **51** shows the results: the values for the surface coverage of complex **8** decreased with the decrease of HDA-tfa in solution, with values consistent with the previous results. The surface coverage values for AQ, on the electrodes where the EDA linker was present in 10% ratio in solution, were constant considering the error bars obtained.

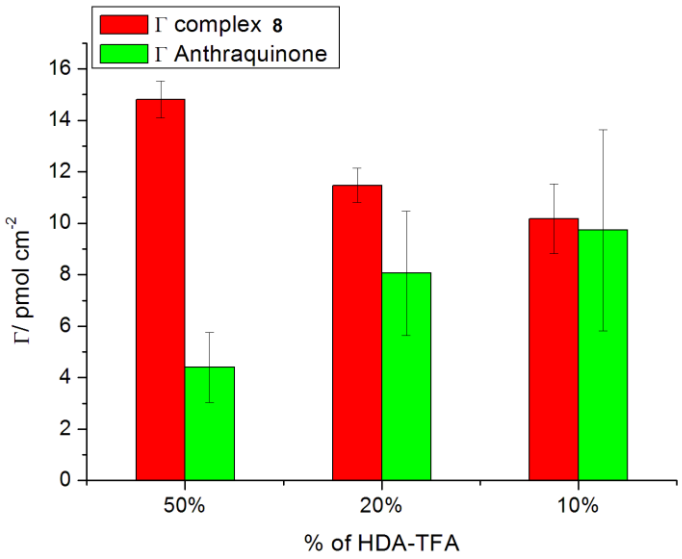

Figure 55. *Barplot for the variation of Γ of complex* ***8*** *and* ***AQ*** *according to the ratio of HDA-tfa linker in solution. The surface coverage of complex* ***8*** *was calculated by averaging the values obtained for three*

*replicates. The surface coverage of **AQ** was calculated by averaging the values obtained for two replicates and was corrected by the corresponding controls Γ, obtained by dipping amine modified electrodes in a neat 50 mM solution of **AQ** in DMF.*

Another important factor to consider when designing the system at the surface is that the maleimide moiety needs to be exposed from the underlying monolayer for the enzyme to be able to react with it without any hindrance. Figure **56** shows the thickness of the monolayer on the surface after the coupling of complex **8**: to overcome ~ 25 Å, EDA-Boc was substituted with HDA-Boc as the second linker**,** 8-amino-3,6-dioxaoctanoic acid (ADOA) was chosen as spacer and a maleimide with a 6 carbon chain (**66**) was used.[11]

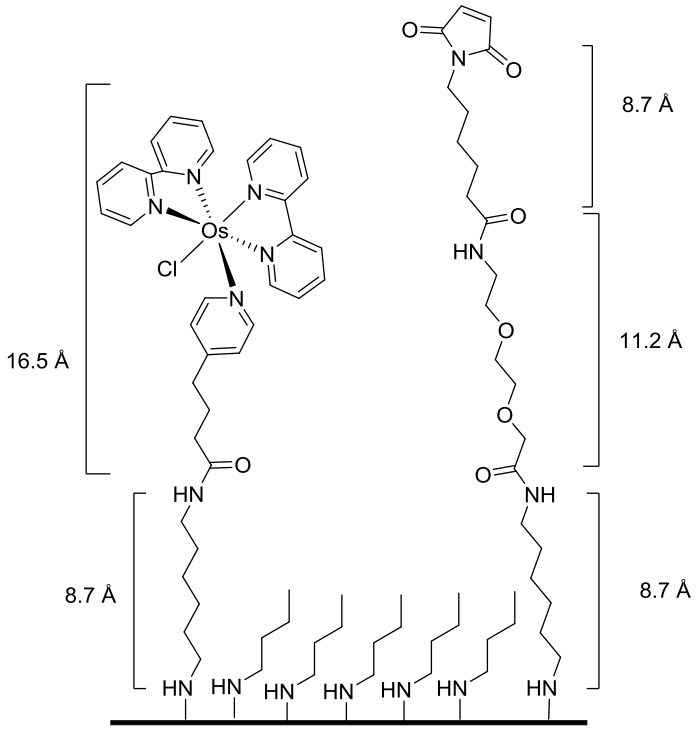

***Figure 56.** Representation of the mixed monolayer designed for the attachment of GcGDH after the coupling of complex **8**.*

4.4. Construction of a biosensor and test of the response

Three sets of electrodes were modified considering this design: the solution ratio of HDA-Boc was kept constant at 10% while the ratio of HDA-tfa was varied from 20% to 10% and 1%, the two linkers were diluted on the surface with 1-BA. After the removal of the tfa group, complex **8** was coupled to the surface and the surface coverage values calculated. Following the acylation step, the Boc group was removed and Boc-ADOA was attached to the surface. After deprotection of the spacer, 6-maleimidocaproic acid (**66**) was coupled to the surface and the mutated variant T343C of GcGDH, presenting an exposed cysteine residue was attached to the surface.

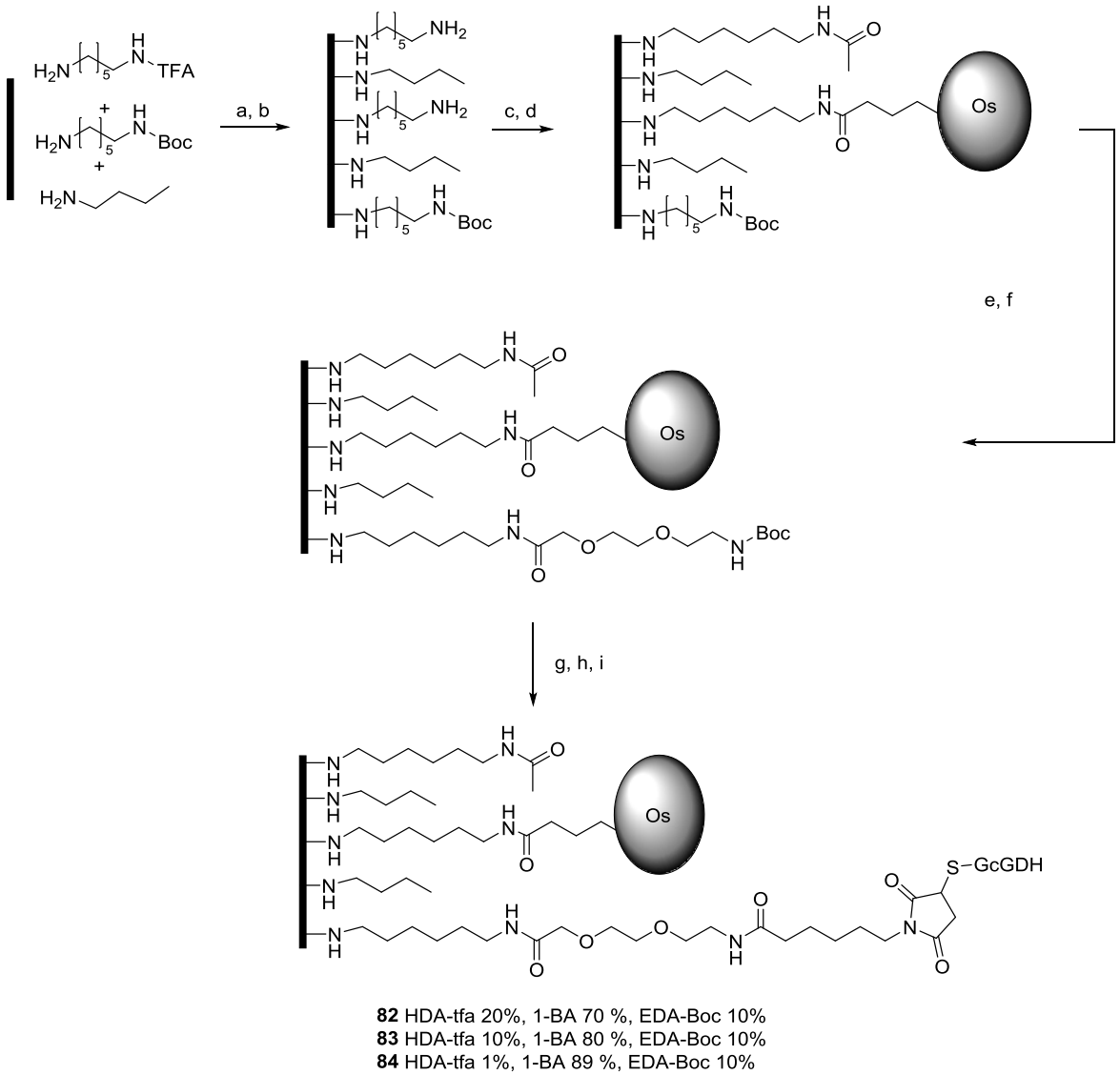

82 HDA-tfa 20%, 1-BA 70 %, EDA-Boc 10%
83 HDA-tfa 10%, 1-BA 80 %, EDA-Boc 10%
84 HDA-tfa 1%, 1-BA 89 %, EDA-Boc 10%

Scheme 37. *Synthetic steps for the creation of complex **8**/maleimide mixed monolayers Conditions: a) 20 mM solutions in CH_3CN with 0.1 M TBATFB, chronoamperometry 2 V, 180 s; b) 10% K_2CO_3 in MeOH/H_2O (7:3), r.t., 1 h; c) 10 mM complex **8**, 0.1 M EDC, 60 mM NHS in DMF, r.t., 16 h; d) 10 mM AcCl, DCM (dry), Et_3N,*

*DMAP(cat.), r.t., overnight; e) 4M HCl in dioxane, r.t., 1 h; f) 10 mM Boc-ADOA, 0.1 M EDC, 60 mM NHS in DMF, r.t., 16 h; g) 4M HCl in dioxane, r.t., 1 h; h) 10 mM **66**, 0.1 M EDC, 60 mM NHS in DMF, r.t., 16 h; i) GcGDH in 20 mM PBS pH 7, 0°C, overnight.*

The surface coverages calculated for complex **8** are shown in Figure **57**.

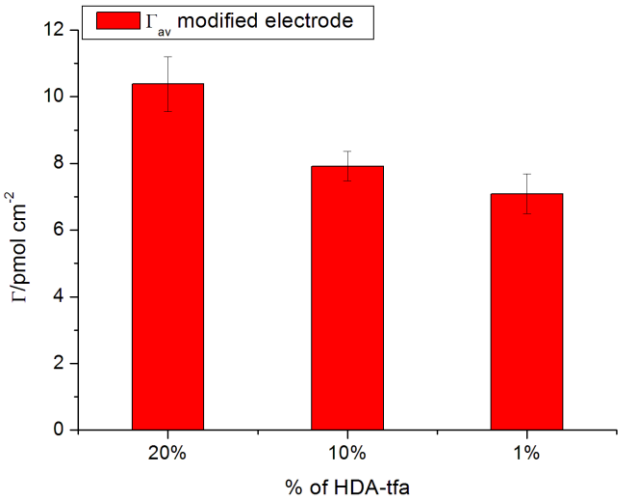

***Figure 57.** Barplot for the variation of Γ of complex **8** according to the ratio of HDA-tfa linker in solution. The surface coverage of complex **8** was calculated by averaging the values obtained for three replicates.*

It is interesting to note that once all the synthetic steps were performed and the enzyme was attached to the surface, the redox peaks of $Os^{2+/3+}$ seemed to decrease or disappear (Figure **58**): checking the electrodes by differential pulse voltammetry (DPV) confirmed that complex **8** was still present at the surface even though the current was strongly attenuated. Such behaviour was described in the past by Khor *et al.*, who exploited it for the design of a label-free electrochemical immuno-biosensor, and was explained by considering that the introduction of the proteic environment blocked the access of the electrolyte to the redox probe preventing the electron transfer.[12]

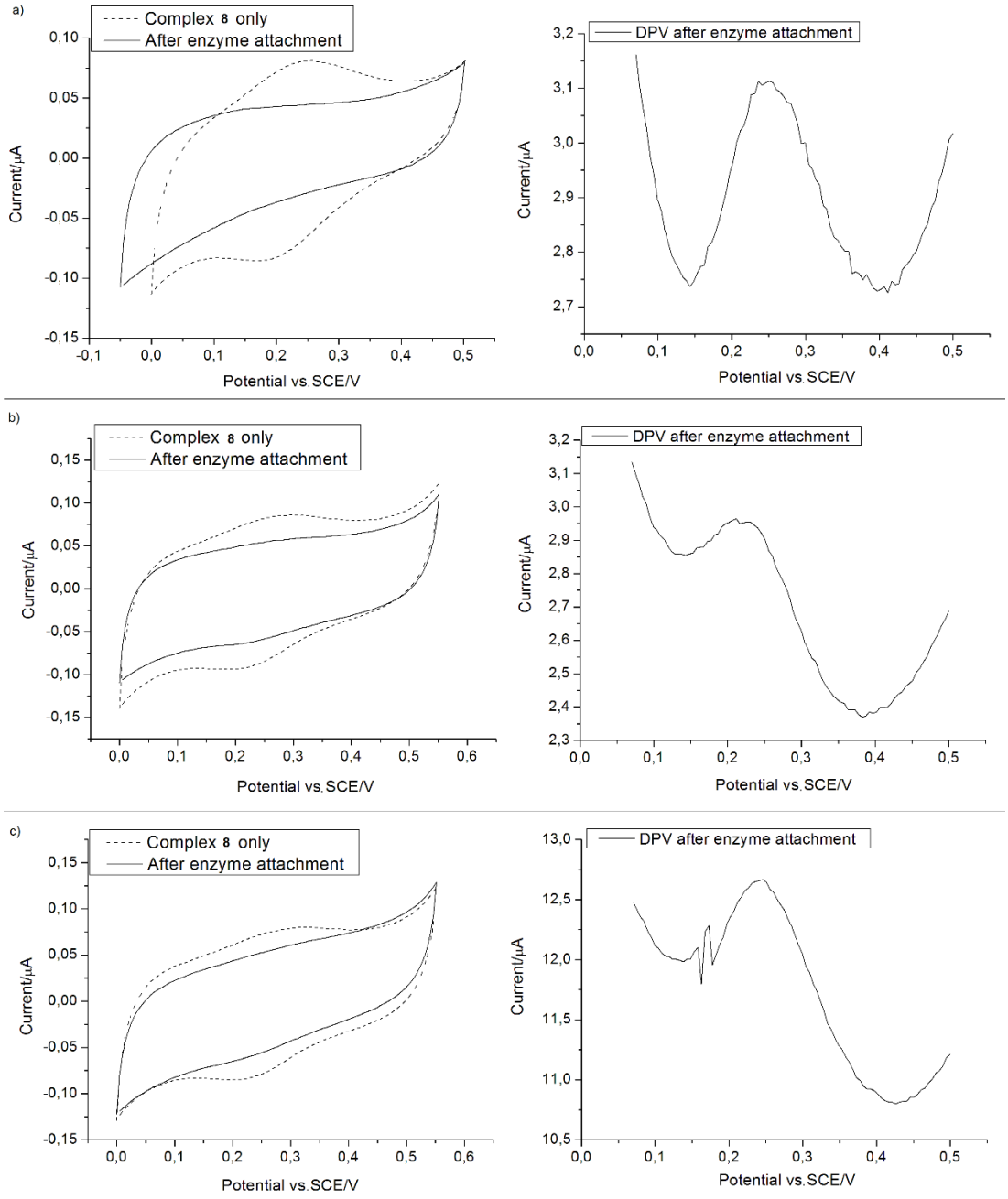

Figure 58 *Comparison of the CVs recorded in 50 mM citrate buffer solution pH 5.5 vs. SCE, electrode area 0.071 cm^2, at 50 mV s^{-1}scan rate for the surface modified with complex* ***8*** *only and after the enzyme attachment and corresponding DPV recorded at a scan rate of 10 mV s^{-1}, pulse amplitude 0.02 V and pulse time 0.002 s. a) conditions* ***82****; b) conditions* ***83****; c) conditions* ***84****.*

The mediated electron transfer between GcGDH and complex **8** at the surface was tested by recording the CVs at 5 mV s^{-1} for increasing D-(+)-glucose concentration in 50 mM citrate buffer solution pH 5.5. Analysing the results from a qualitative point of view, the systems with 20% (**82**) and 10% (**83**) of linker for the mediator on the surface (Figure **59a,b**) did not show a clear increase of oxidation current in relation to the concentration of glucose and the changes in the CVs were not clear

enough to confirm the catalysis. The system presenting 1% (**84**) of linker for complex **8** (figure **59c**) showed a response to the additions of glucose: not only the oxidation current increased, meaning that the catalytic process was occurring, but the osmium redox peak increased, suggesting that the electron transfer, "quenched" by the presence of the protein, had been restored by the enzyme transferring electrons to the mediator.

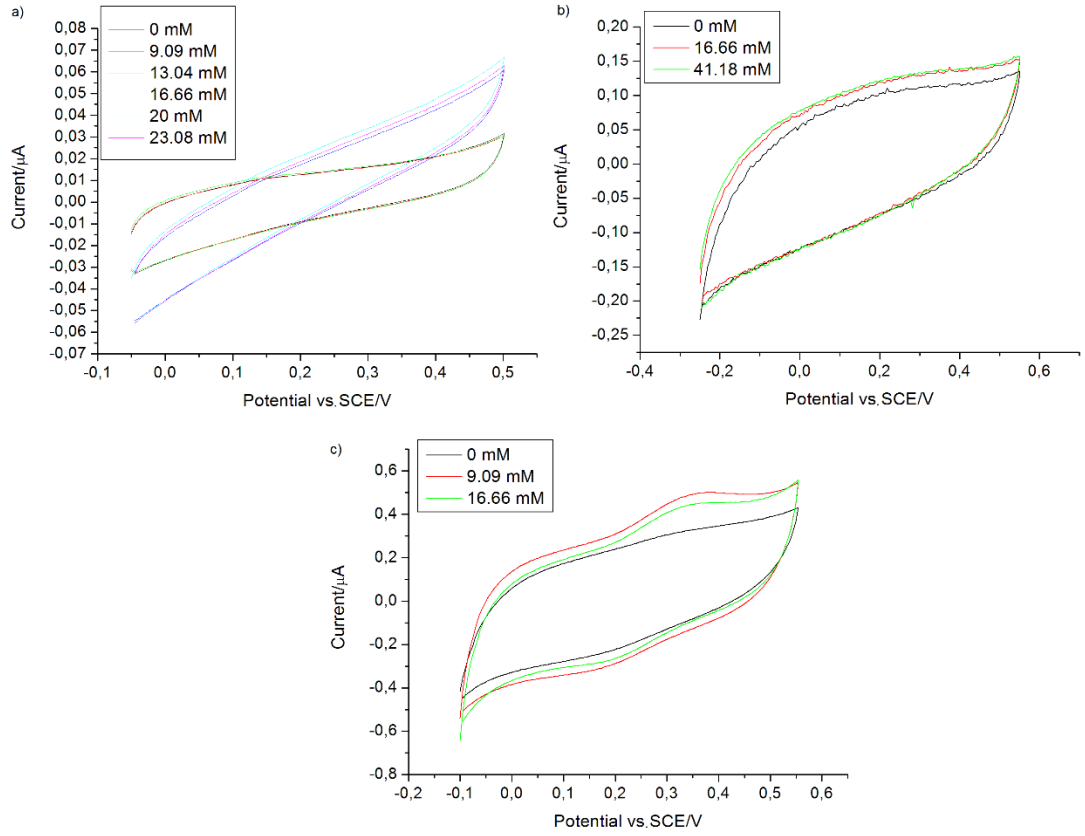

Figure 59. *CVs recorded at 5 mV s^{-1} in 50 mM citrate buffer solution pH 5.5 vs SCE with 0.1 M TEATFB, for increasing concentration of D-(+)-glucose; electrode area 0.071 cm^2. a) conditions **82**; b) conditions **83**; c) conditions **84**.*

In order to determine the cause of the lack of response for the electrodes modified according to conditions **82** and **83**, the same modified electrodes were tested adding 1.2 mM complex **8** to fresh buffer solution, this would have allowed verification of whether it depended on miscommunication between enzyme and mediator on the surface or on the enzyme not being covalently bound to the electrode. After gradually increasing the glucose concentration in solution, the response showed no clear behaviour that suggested the generation of a catalytic current for systems **82** and **83**, while system **84** presented a variation of current comparable with the results

obtained in Section **4.1.1**, where both enzyme and mediator were in solution. It was concluded that in **84** the distribution of the species on the surface was such to allow the enzyme to easily bind to the maleimide with no hindrance, which did not happen with **82** and **83**.

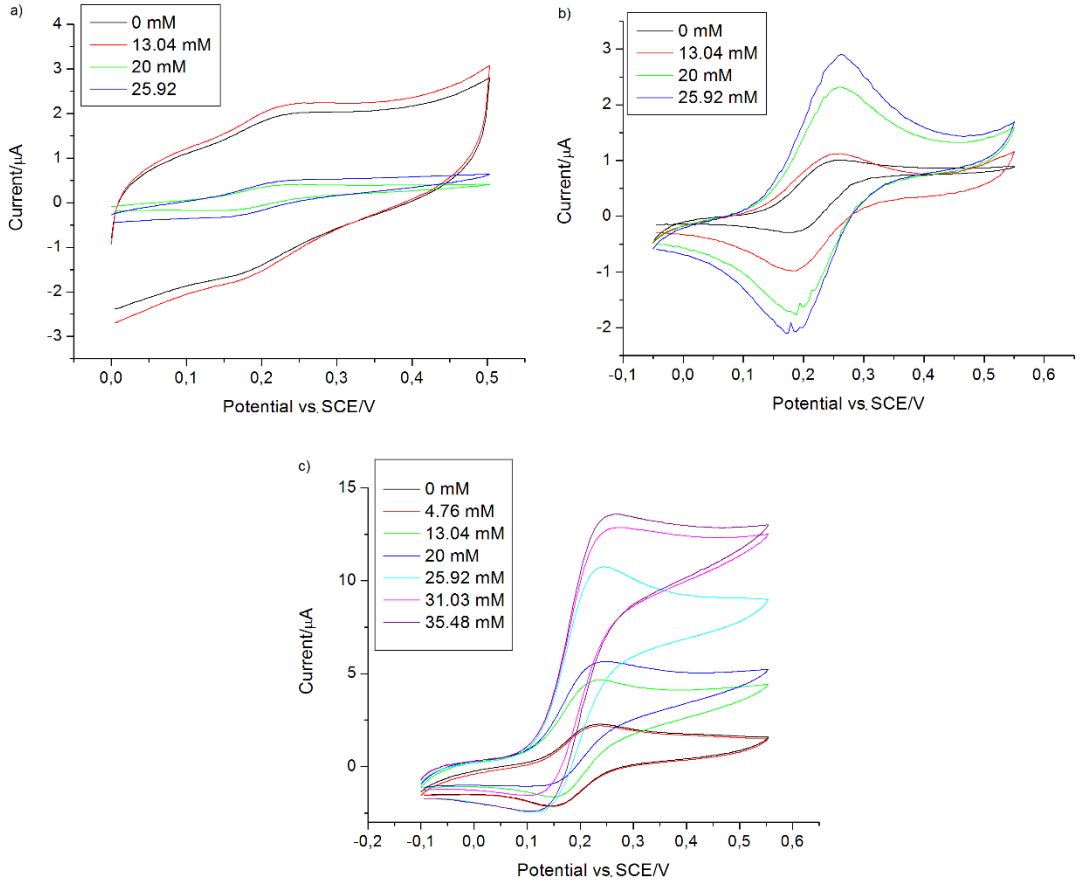

Figure 60. *CVs recorded in 50 mM citrate buffer solution pH 5.5 vs SCE with 0.1 M TEATFB and [complex **8**] = 1.2 mM, for increasing concentration of D-(+)-glucose at 5 mV s^{-1}, electrode area 0.071 cm^2. a) conditions **82**; b) conditions **83**; c) conditions **84.***

Figure **59c** shows that the mediated catalysis with both mediator and enzyme covalently bound to the surface is occurring, but the current generated is small I = 0.112 μA. Knowing the theoretical surface coverage for complex **8** (Γ_{Os} = 6.8 pmol cm^{-2}) it was possible to calculate the turnover frequency (k_{cat}) of the reactions enzyme/mediator using the relation:[4]

$$k_{\text{cat}} = \frac{I}{nFA\Gamma} \qquad \textbf{(23)}$$

The value obtained k_{cat} = 2.4 s^{-1} is very small compared to the value of k_{cat} = 358 s^{-1} calculated for the GcGDH/glucose reaction in the same system tested with the

mediator in solution considering Γ_{GDH} = 3.5 pmol cm^{-2} (Figure **60c**), which was consistent with literature values.[3] Such a result suggests that when GcGDH and complex **8** are both attached to the surface with a comparable surface coverage, the mediator struggles to keep up with the kinetics of the enzyme and the reaction between enzyme and mediator is the limiting step in the overall catalytic process. This could also be confirmed considering that in order to regenerate the oxidised form of the enzyme, two mediator molecules are required. Moreover, since controlling the precise orientation of the two components on the surface is difficult, the result could also suggest that not all the redox mediators at the surface presented the optimal orientation in relation to the active centre of the enzyme to conduct the mediation, meaning that the surface coverage of "active" redox mediator was lower than the one determined by integration of the redox peaks on the CV and consequently the real k_{cat} would have presented a higher value.

4.5. Conclusions

The methodology for the creation of mixed monolayers previously developed was applied for the creation of a modified GC surface presenting complex **8** as a redox mediator for the electrocatalytic oxidation of D-(+)-glucose by GcGDH, both covalently bound to amine linkers. First the fitness of the methodology for the formation of a mixed monolayer containing three different amines, EDA-Boc, HDA-tfa and 1-BA, was tested, followed by the optimisation of the maleimide chemistry required for the attachment of the engineered GcGDH to the surface through a cysteine moiety. The design of the final surface included HDA as a linker for complex **8**, EDA as linker for the maleimide derivative **66**, with the addition of ADOA as spacer. While the ratio of EDA linker was kept constant at 10%, three different HDA ratios were tested (20%, 10% and 1%) to verify the effect of different amounts of mediator on the overall catalytic process. The modified surfaces were tested by cyclic voltammetry in solutions with increasing D-(+)-glucose concentration and the generation of electrocatalytic current recorded. The systems with higher complex **8** amount, showed no response while the 1% HDA modified surface gave k_{cat} = 2.4 s^{-1}. The test of the same modified surfaces with the addition of mediator in the buffer solution revealed that no enzyme was present at the 20% and 10% HDA ratio electrodes, probably due to hindrance to the attachment; for the 1% HDA system k_{cat} = 358 s^{-1} was calculated, consistent with literature values. The experiment showed the importance of an accurate design of a modified surface in the creation of biosensing devices and how a small variation of the amount of the species at the surface can affect the response of the final system.

4.6. References

[1] Brady, D.; Jordaan, J. *Biotechnol. Lett.* **2009,** *31,* 1639-1650.

[2] Campas, M.; Prieto-Simon, B.; Marty, J.-L. *Semin. Cell. Dev. Biol.* **2009,** *20,* 3-9.

[3] a) Sygmund, C.; Staudigl, P.; Klausberger, M.; Pinotsis, N.; Djinovic-Carugo, K.; Gorton, L.; Haltrich, D.; Ludwig, R. *Microb. Cell. Fact.* **2011,** *10,* 106-114. b) Sygmund, C.; Klausberger, M.; Felice, A.K.; Ludwig, R. *Microbiology* **2011,** *157,* 3203-3212. c) Zafar, M.N.; Wang, X.; Sygmund, C.; Ludwig, R.; Leech, D.; Gorton, L. *Anal. Chem.* **2012,** *84,* 334-341.

[4] a) Albery, J.W.; Bartlett, P.; Driscoll, B.J.; Lennox, R.B. *J. Electroanal. Chem.* **1992,** *323,* 77-102. b) Batlett, P.N.; Toh, C.S.; Calvo, E.J.; Flexer, V. Modelling biosensor responses in Bioelectrochemistry; Ed. Bartlett, P.N.; Wiley, Chichester, 2008.

[5] a) Baldwin, A.D.; Kiick, K.L. *Bioconjugate Chem.* **2011,** *22,* 1946-1953; b) Sun, G.; Hovestadt, M.; Zhang, X.; Hinrichs, K.; Rosu, D.M.; Lauermann, I.; Zielke, C.; Vollmer, A.; Lochel, H.; Ay, B.; Holzhutter, H.-G.; Schade, U.; Esser, N.; Volkmerb, R.; Rappichc, J. *Surf. Interface Anal.* **2011,** *43,* 1203-1210.

[6] Fellet, M.S.; Bartels, J.L.; Bi, B.; Moeller, K.D. *J. Am. Chem. Soc.* **2012,** *134,* 16891-16898.

[7] Wright, E.J.; Sosna, M.; Bloodworth, S.; Kilburn, J.D.; Bartlett, P.N. *Chem. Eur. J.* **2014,** *20,* 5550-5554.

[8] De Figueiredo, R.M.; Oczipka, P.¸ Frohlich, R.; Christmann, M. *Synthesis* **2008,** *8,* 1316-1318.

[9] Numao, N.; Hemmi, H.; Naujokaitis, S.A.; Rabinovitz, M.; Beisler, J.A. *J. Med. Chem.* **1981,** *24,* 515-520.

[10] Gooding, J.J.; Ciampi, S. *Chem. Soc. Rev.* **2011,** *40,* 2704-2718.

[11] Guerrini, L.; Izquierdo-Lorenzo, I.; Rodriguez-Oliviero, R.; Sanchez-Gil, J.A.; Sanchez-Cortes, S.; Garcia-Ramos, J.V.; Domingo, C. *Plasmonics* **2010,** *5,* 273-286.

[12] Khor, S.M.; Liu, G.; Fairman, C.; Iyengar, S.G.; Gooding, J.J. *Biosens. Bioelectron.* **2011**, *26,* 2038-2044.

5. Further approaches to the control of the organisation of species at GC surfaces

5.1. Spatial control over the attachment of the linkers

The results described in the previous chapter, involving the catalytic oxidation of glucose by GcGDH and mediated by an osmium bipyridyl complex when both species are covalently bound to the GC surface, suggested that, although the electron transfer between enzyme and mediator was occurring, the response was lower compared to the experiment where both species are in solution. One reason for such behaviour could be the orientation of mediator relative to the active site of the enzyme: the distribution of the diamine linkers during the grafting process and the coupling of the species occurs randomly, making it difficult to control the position of the components at the molecular level. An improvement over the methodology developed in the previous chapters would be grafting the two different linkers at a fixed distance. A possible way of achieving this is to create a spacing unit with different cleavage properties at its extremities, so that, once the linkers are attached to the electrode surface, they could be sequentially cleaved and modified (Scheme **38**).

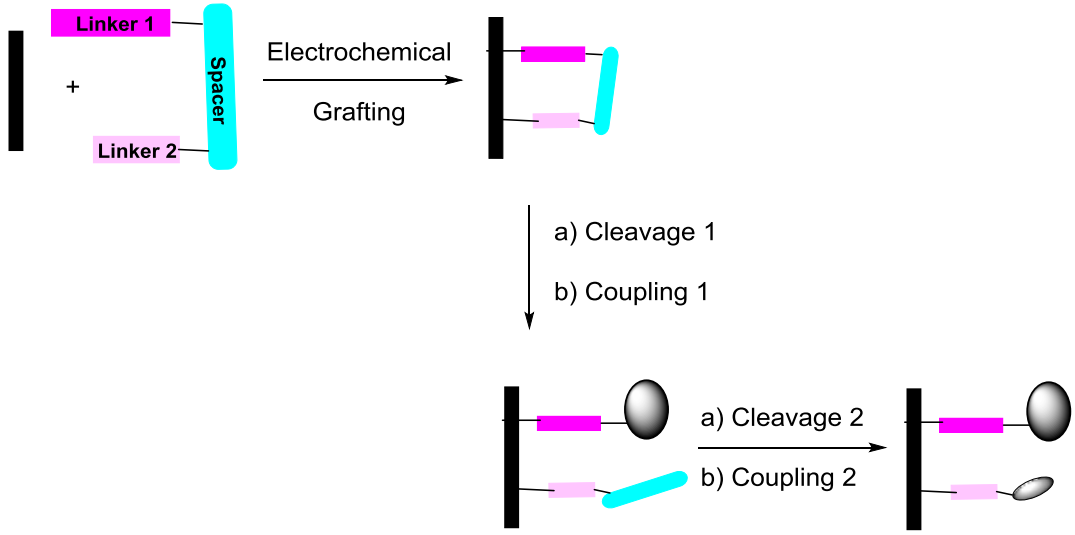

Scheme 38. *General surface modification methodology with control over the distance between two linkers.*

The work regarding this part of the project involved only the design and optimisation of the synthetic steps for a model spacing unit, leaving the testing and application of the synthesised molecule for future development.

5.2. Design of the spacing unit

When designing such a spacing unit, three characteristics have to be considered: it should be rigid enough to maintain the linkers at a fixed distance, its length should be tuneable according to the system that needs to be created at the surface and each linker-spacer bond should be cleaved selectively. Rigidity of the spacer can be ensured by using aromatic rings and double bonds, while the length can be varied including easily repeatable units within the structure. The resins used for solid phase synthesis are useful models for creating a spacer which requires selective conditions for the bonds at its ends. The general concepts of solid phase synthesis have been described in section **1.4**: it was explained that the starting material is anchored to a solid support, insoluble in the reaction solvent, and the product can be isolated by cleaving its bond to the support, usually in mild conditions. The solid supports are commonly called resins: they are composed of a polymeric matrix functionalised with side groups that can be reversibly bound to the reactants. Tens of resins characterised by very different cleavage conditions are currently used in solid phase synthesis.[1] Figure **61** shows the resins chosen as a model for the main functionalities of the spacer: the number of oxygen substituents on the aromatic ring affects its electronic properties making it possible to cleave the amine-resin bond with 95% trifluoroacetic acid (TFA) for the Wang resin and 1% TFA for the 4-(4-hydroxymethyl-3-methoxyphenoxy)butyryl (HMPB) resin.

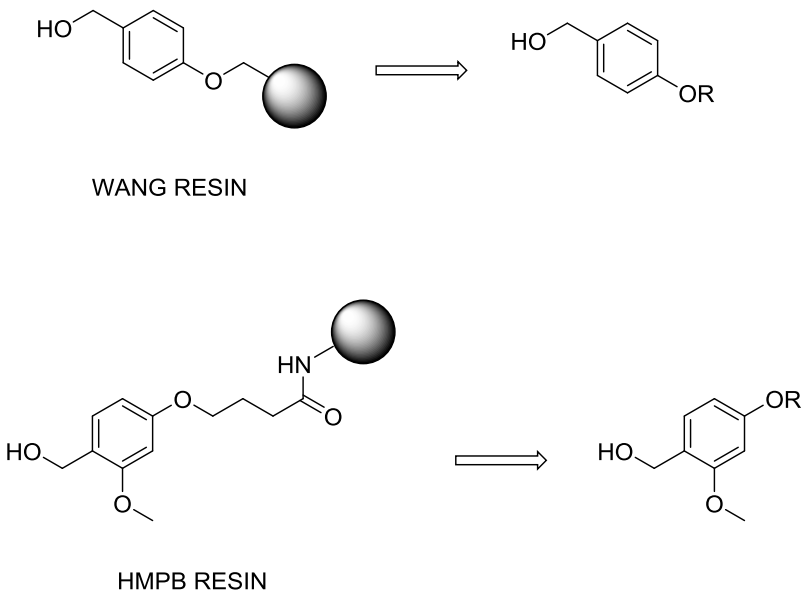

***Figure 61**. SPS resins chosen as models for the main synthons of the spacing unit.*

Figure **62** shows the general structure designed for the spacing unit: the two main components are connected through chains of tuneable length, which could also contain double bonds to increase the rigidity of the system, and the connecting point should be represented by a stable functional group unlikely to bend.

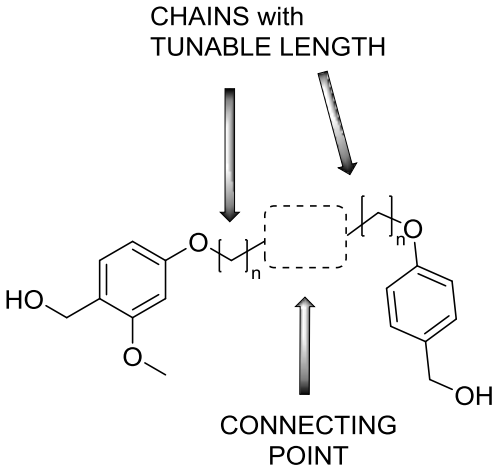

***Figure 62**. Final design for the spacing unit.*

5.3. Synthesis of the spacing unit

It was decided to use the 1,2,3-triazole group as a connecting point for the two main synthons. 1,2,3-triazoles are aromatic heterocycles that can be easily obtained by copper (I) catalysed Huisgen reaction between an alkyne and a azide in very mild conditions.[2] Scheme **39** shows the disconnections followed for the synthesis of compound **92**.

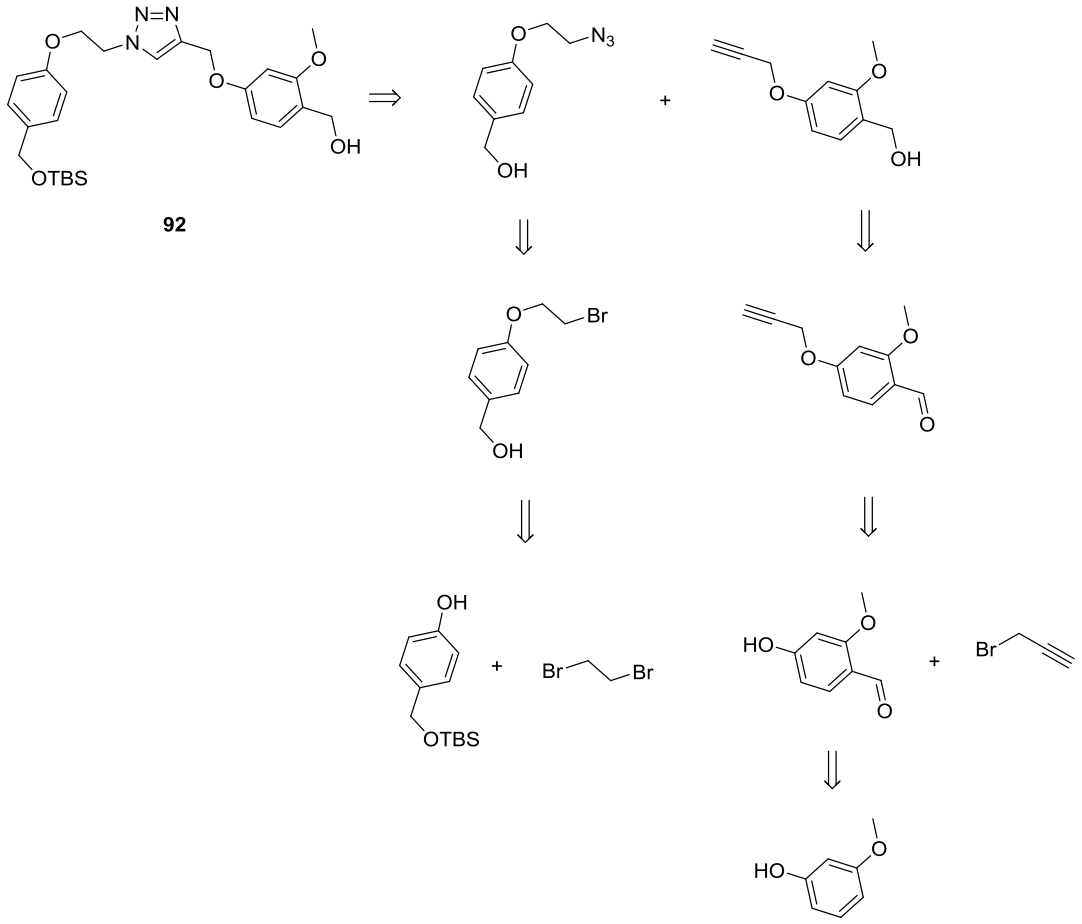

***Scheme 39**. Disconnections for the synthesis of spacing unit **92**.*

Compound **85** was obtained following the procedure described by Sheppard for the formylation of the commercially available 3-methoxy phenol.[3] The procedure consisted in the Vilsmeier-Haack reaction: phosphorus oxychloride ($POCl_3$) reacted with DMF to generate the electrophile that reacted with 3-methoxyphenol in position 4. The addition of water caused the hydrolysis of the intermediate. **85** was obtained in 19% yield (*Lit.*[3] 20%) as a white solid.

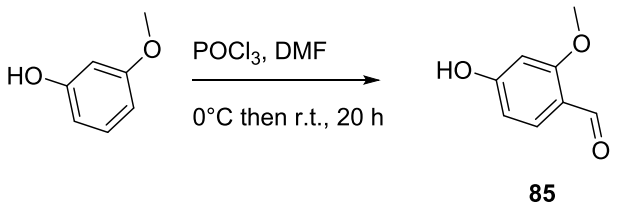

85

Scheme 40. *Synthesis of compound **85**.*

Table **1** shows the conditions tested for the reduction of compound **85** with sodium boron hydride ($NaBH_4$): in all cases the expected product was not obtained. The LC-MS analysis of the compound isolated presented a peak at m/z 162 corresponding to the protonated molecular ion of compound **86**: this intermediate should hydrolyse during the work-up in acidic conditions, but remained stable even after chromatographic purification, probably due to the electronic delocalisation of the charges.

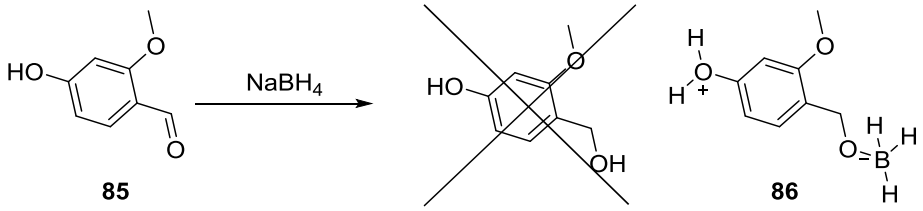

85 **86**

Conditions	Solvent	T(°C)	Reaction time	Notes
1[3]	NaOH(1M)/MeOH/H_2O	r.t.	1.5 hours	
2[4]	EtOH	0°C then r.t.	30 min	
3[4]	EtOH	0°C then r.t.	overnight	
4[5]	none	r.t.	10 min	p-toluensulfonic acid added

Table 1. *Conditions tested for the reduction of compound **85**.*

A different approach was tested by first alkylating the hydroxy group in the para position to the aldehyde, followed by the reduction. **85** was reacted with the commercially available 3-bromopropyne in an Sn2 reaction following an adapted literature procedure[6] to obtain **87** as a white solid in 98% yield.

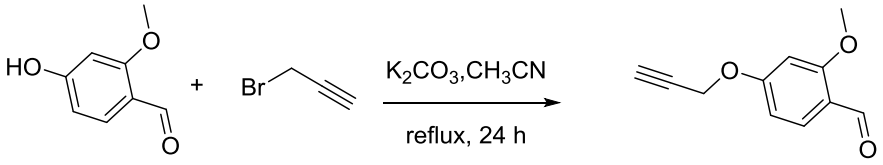

85 **87**

Scheme 41. *Synthesis of compound **87.***

The reduction of **87** was then achieved with $NaBH_4$ in ethanol to obtain **88** as a white solid in 43% yield.

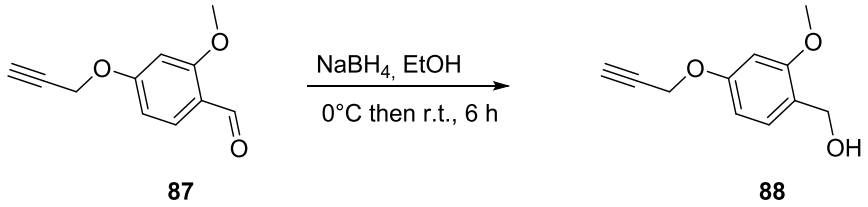

87 **88**

Scheme 42. *Synthesis of compound **88**.*

The second component of the spacing unit was obtained starting from 4-(hydroxymethyl)phenol. First, the more reactive hydroxymethyl group was protected with tert-butyldimethylsilyl chloride (TBSCl) in presence of imidazole (Im) as catalyst to obtain **89** as a yellow oil in 98% yield (*Lit.*[6] 95%).

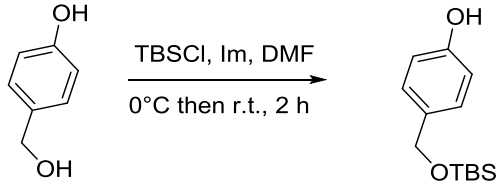

89

Scheme 43. *Synthesis of compound **89**.*

The alkylation of **89** with 1,2-dibromoethane was achieved using adapted conditions previously described for compound **85**: the reaction was run in excess of dibromide in order to limit the formation of the di-substituted product. Product **90** was isolated as a colourless oil in 28% yield.

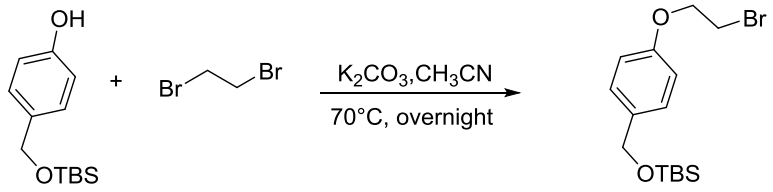

89 **90**

Scheme 44. *Synthesis of compound **90**.*

The bromide group present on **90** was converted to azide following a literature procedure which involved the heating of the starting material in DMF in the presence of sodium azide.[6] The product **91** was a colourless oil obtained in 80% yield.

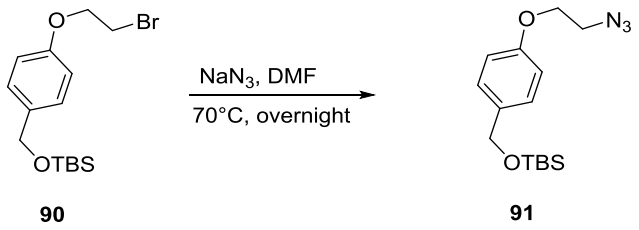

90 **91**

Scheme 45. *Synthesis of compound **91**.*

The Huisgen reaction is a 1,3-dipolar cycloaddition and the copper (I) catalysed variation is considered a click reaction because of the mild conditions, high yields and ease of preparation.[2,7] Alkyne derivative **88** was reacted with azide **91** in presence of copper iodide (CuI) and triethylamine (Et_3N) to obtain the final model spacing unit **92** in 77% yield as an orange oil.

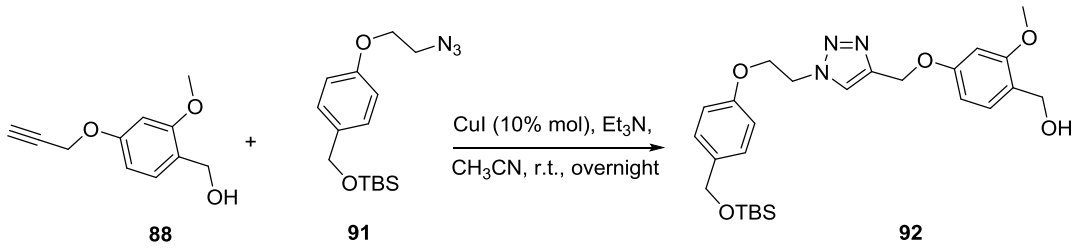

88 **91** **92**

Scheme 46. *Synthesis of compound **92**.*

The TBS protecting group was maintained on **92** in order to sequentially introduce different alkyl diamine groups at the ends of the spacing unit according to the amine mixed monolayer planned to be created at the GC surface. The synthetic procedure optimised for this model spacing unit could be applied to obtain a library of spacing units of variable length to be used for different enzyme/mediator combinations.

5.4. Future work

The future development of this project will involve experiments for the optimisation in solution of the chemistry that will be applied at the electrode surface followed by testing of the system at the surfaces.

5.4.1. Introduction of the linkers at the spacing unit ends and cleavage conditions tests

The linkers need to be attached to the hydroxymethyl groups at the ends of the spacing unit in a form that will allow to obtain free primary amines at the electrode surface after cleavage. One of the possible ways to achieve this is through the use of isocyanates: a test reaction was run (Scheme **47**) adapting a literature procedure[8] by adding dimethylamino pyridine (DMAP) as a catalyst. Compound **94** was isolated in 42% yield, although the conditions could be further improved.

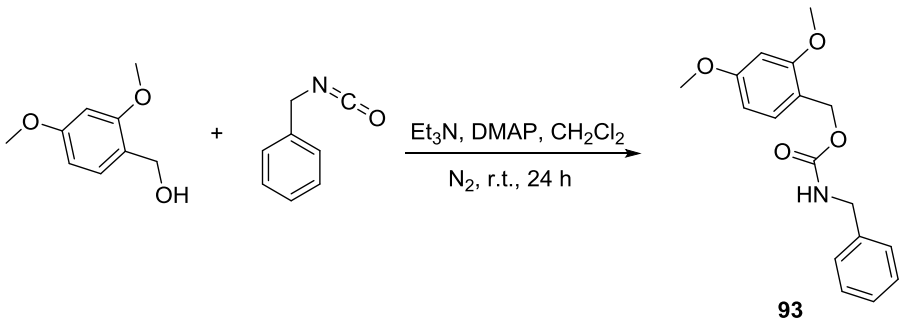

***Scheme 47**. Test reaction for the attachment of an isocyanate to **93**.*

Once the reaction conditions will be improved for both model molecules, the products will be used to test and optimise the cleavage conditions by treatment with TFA (Scheme **48**).

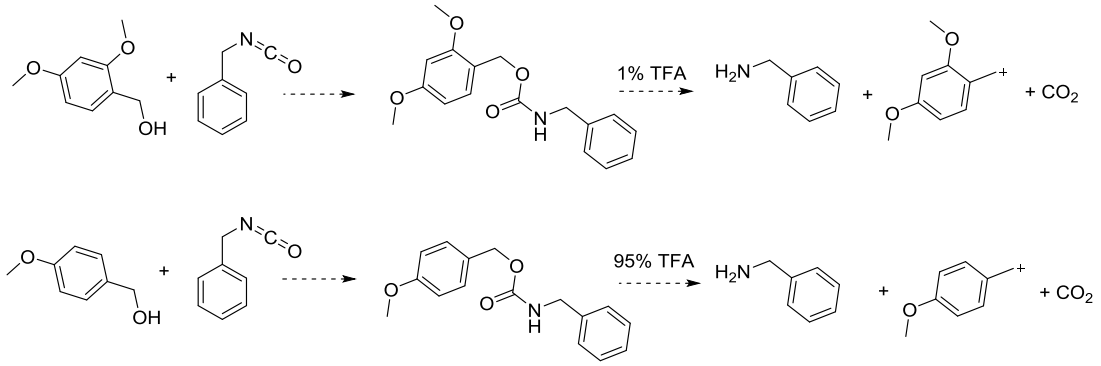

***Scheme 48**. Test reactions.*

The optimised conditions will then be applied to compound **92**.

5.4.2. Testing of the effectiveness of the spacing unit

The design and synthesis of a suitable spacing unit for a mediator/enzyme system will also mean the testing of the behaviour of the spacing unit at the electrode surface, there the main issues will be:

- The control over the linker grafting process: will the linkers be grafted at the right distance?
- The overlap between molecules upon grafting.

In order to investigate these points, techniques are necessary that allow the study of surfaces at a molecular level.

Single molecule fluorescence resonance energy transfer (smFRET) is a technique that exploits the ability of two fluorescent molecules, donor and acceptor, to transfer energy with an efficiency proportional to their distance, with a maximum at a precise value defined Förster distance. It is a technique commonly used in biophysics to study protein folding and configuration, but that could be applied to any system where donor and acceptor are located at a distance within 2 nm and 8 nm.[9] If a suitable donor acceptor couple is sequentially attached to the linkers at the electrode surface after the cleavage of the spacing unit, it would be possible to verify the distribution of the linkers on the surface.

5.5. Conclusions

A model spacing unit to potentially control the grafting distance of two linkers was designed and synthesised. Such a molecule, inspired by the support resins used in solid phase synthesis, was characterised by asymmetrical cleavage properties at its ends, in order to allow sequential modification of an electrode surface for the creation of spatially controlled mixed monolayers. Future work will require the optimisation of the linker attachment to the spacing unit and cleavage conditions. Moreover the performance of the spacing unit at surfaces will need to be tested using microscopy techniques such as smFRET.

5.6. References

[1] a) Blackburn, C. *Biopolymers* **1998,** *47*, 311-351. b) Drewry, D.H.; Coe, D.M.; Poon, S. *Med. Res. Rew.* **1999,** *19*, 97-148.

[2] Bock, V.D.; Hiemstra, H.; van Maarseveen, J.H. *Eur. J. Org. Chem.* **2006,** 51-68.

[3] Sheppard, R.C.; Williams, B.J. *Int. J. Peptide Protein Res.* **1982,** *20*, 451-454.

[4] Parihar, S.; Kumar, A.; Chaturvedi, A.K.; Sachan, N.K.; Luqman, S.; Changkija, B.; Manohar, M.; Prakash, O.; Chanda, D.; Khan, F.; Chanotiya, C.S.; Shanker, K,; Dwivedi, A.; Konwar, R.; Negi, A.S. J. Steroid Biochem. Mol. Biol. 2013, 137, 332-344.

[5] Cho, B.T.; Kang, S.K.; Kim, M.S.; Ryu, S.R.; An, D.K. *Tetrahedron* **2006,** 62, 8164-8168.

[6] Smith, J.M; Vitali, F.; Archer, S.A.; Fasan, R. *Angew. Chem.* **2011,** *50*, 5075-5080.

[7] Kolb, H.C.; Sharpless, K.B. *Drug Discov. Today* **2003,** *8*, 1128-1137.

[8] Castaneda, L.; Maurani, A.; Schumacher, F.F.; Miranda, E.; Chudasama, V.; Chester, K.A.; Baker, J.R.; Smith, M.E.B.; Caddick, S. *Chem. Commun.* **2013,** *49*, 8187-8189.

[9] Roy, R.; Hohng, S.; Ha, T. *Nature Methods* **2008,** *5*, 507-516.

6. Experimental

6.1. Synthesis in solution

6.1.1. General

All the chemicals were obtained from Sigma-Aldrich and were all used without further purification. Ethylene glycol was distilled and stored over molecular sieves (0.5 nm), under N_2. Dichloromethane (DCM) and dimethylformamide (DMF) were distilled using a MBraun MB SPS-800 solvent purification system. Flash chromatography columns were performed on silica gel (VWR Prolabo) particle size 40 μm - 63 μm, pH = 6.4. Thin layer chromatography (TLC) was performed on silica pre-coated aluminium plates (Merck Silica gel F_{254}) and the spots were visualised with UV light or ninhydrin stain. ^{1}H NMR and ^{13}C NMR were obtained on a Bruker AVIII 400 Spectrometer; the chemical shifts (δ) are reported in ppm and coupling constants (J) in Hertz (Hz) are rounded up to the .5 or .0 value. Abbreviations for signals: s = singlet, d = doublet, t = triplet, q = quadruplet, m = multiplet, b = broad. All ^{13}C NMR chemical shifts are reported to one decimal place, except when, in order to discriminate, the second decimal figure is reported in brackets. UV-vis spectra were recorded on a Perkin Helmer Lambda35 spectrometer. LC-MS spectra were recorded on a Bruker Daltonics Esquire3000 plus. X-ray diffraction analyses were performed with a Kappa Apex II Duo diffractometer with dual Cu and Mo sources and Apex II CCD area detector. High-Res Mass spectra were recorded by the EPSRC UK National Mass Spectrometry Facility at Swansea University.

6.1.2. Cis-bis(2,2'-bipyridyl) osmium (II) chloride (1)[1]

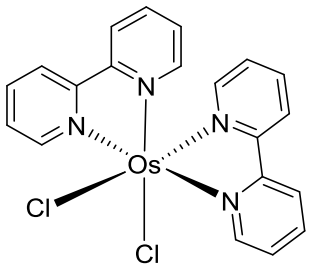

Ammonium hexachloroosmate(IV) ($(NH_4)_2OsCl_6$) (0.5 g, 1.14 mmol) and 2-2'-bipyridyl (0.36 g, 2.30 mmol) were mixed with ethylene glycol (15 mL) and purged for 10 minutes with nitrogen (N_2). The mixture was refluxed for 1 hour, then allowed to cool at room temperature, before immersion in an ice-bath. Sodium dithionite ($Na_2S_2O_4$) (0.69 g, 3.98 mmol) was dissolved in 25 mL of deionised water (H_2O) and added drop wise to the stirred reaction mixture. The mixture was stored at 0°C overnight to allow the precipitation of the product. The solid was filtered and washed with 250 mL of H_2O and 100 mL of diethyl ether (EtOEt). The product was a black-purple powder obtained in 86 % yield. **UV-vis:** λ_{max} (CH_3CN)/nm 381 (ε/dm^{3}mol^{-1}cm^{-1} 11976), 462 (ε/dm^{3}mol^{-1}cm^{-1} 10940), 554 (ε/dm^{3}mol^{-1}cm^{-1} 12662). **IR:** ν_{max}/cm^{-1} 3041 (w), 1464 (m), 1412 (m), 1452 (m), 1249 (m), 1011 (m), 756 (s), 715 (m), 646 (m). **^{1}H NMR** (400 MHz, DMSO-d_6): δ = 9.64 (2 H, d, *J* = 5.5), 8.57 (2 H, d, *J* = 7.5), 8.37 (2 H, d, *J* = 7.5), 7.60 (2 H, t with fine splitting, *J* = 7.5), 7.54 (2 H, t with fine splitting, *J* = 5.5), 7.27 (4 H, m), 6.80 (2 H, t with fine splitting, *J* = 5.5). It was not possible to obtain the **^{13}C NMR** of the complex due to its low solubility. **LR-MS ES+** m/z 574.0 $[M+H]^+$ (100%). **XRD** Crystals of the complex were obtained by recrystallization from DCM. See appendix II for full structure report.

6.1.3. 4-(4-pyridil)butyric acid (2)[2]

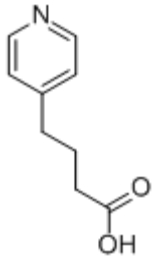

Sodium hydride (60% dispersion in mineral oil) (0.5 g, 22 mmol) was added portion-wise to dry ethanol (EtOH) (35 mL) under stirring. The solution was allowed to return to room temperature and diethylmalonate (7.1 mL, 47 mmol) was added. The mixture was stirred at 80°C for 1 hour, then cooled to room temperature. 4-vinylpyridine (2.2 mL, 20 mmol) was added and the solution was stirred at reflux for 3 hours. EtOH was removed, the oily residue dissolved with 20% hydrochloric acid (HCl) (50 mL) and the solution refluxed overnight. The aqueous phase was extracted with ethyl acetate (AcOEt) (3 x 30 mL) and the H_2O removed. The solid residue was dissolved with the minimum volume of hot methanol (MeOH), any insoluble salt was filtered and AcOEt was added to the filtrate to precipitate the product. The solid was filtered to obtain the product as a white solid in 60 % yield. **^{1}H NMR** (400 MHz, $CDCl_3$): δ = 10.26 (1 H, bs), 8.51 (2 H, d, *J* = 6), 7.25 (2 H, d, *J* = 6), 2.75 (2 H, t, *J* = 7.5), 2.40 (2 H, t, *J* = 7.3), 2.01 (2 H, m).

6.1.4. Methyl 4-(pyridin-4-yl)butanoate (3)[3]

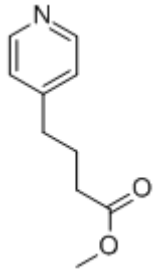

Compound **2** (0.4 g, 2.3 mmol) was dissolved in MeOH (15 mL) and sulphuric acid (0.1 mL, 2.5 mmol) in MeOH (5 mL) was added. The mixture was stirred at reflux for 3 hours. The solvent was removed and the oily residue dissolved with H_2O (30 mL). The pH of the solution was adjusted to 9 by addition of a 1 M sodium hydroxide (NaOH) and the aqueous phase extracted with AcOEt (3 x 25 mL). The organic phase was dried over magnesium sulphate ($MgSO_4$) and the solvent evaporated. The product was purified by flash chromatography over silica (DCM:

MeOH = 95:5), to obtain a colourless oil in 47 % yield. **^{1}H NMR** (400 MHz, $CDCl_3$): δ = 8.47 (2 H, d, *J* = 7.5), 7.08 (2 H, d, *J* = 7.5), 3.64 (3 H, s), 2.63 (2 H, t, *J* = 7.6), 2.32 (2 H, t, *J* = 7.3,), 1.95 (2 H, m).

6.1.5. Synthesis of 2-(1H-imidazol-2-yl)pyridine (4)[4]

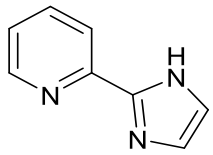

Pyridine-2-carboxyaldehyde (3.6 mL, 38 mmol) was dissolved in EtOH (5 mL) and the solution cooled down to 0°C. Glyoxal (aq. solution 40%) (5.4 mL, 47 mmol) was mixed with EtOH (4 mL) and cooled down to 0°C. The two solutions were mixed and a cold solution of ammonium hydroxide (12.8 mL) was quickly added. The solution was stirred at 0°C until it turned brown. The reaction mixture was allowed to reach room temperature and stirred for 1 hour. The solvent volume was reduced and the solution left was extracted with EtOEt (30 mL x 6). The organic phase was dried with $MgSO_4$ and the solvent evaporated to obtain a yellow oil. The product was purified by flash chromatography (eluents from DCM:MeOH = 99:1 to DCM:MeOH = 9:1). The product was a yellow solid obtained in 21 % yield. **^{1}H NMR** (400 MHz, $CDCl_3$) δ = 10.76 (1 H, bs), 8.55 (1 H, dq, J = 1.0, 5.0), 8.21 (1 H, td, J = 1.0, 8.0), 7.81 (1 H, td, J = 1.5, 8.0), 7.27 (1 H, ddd (partly obscured), J = 1.0, 5.0, 8.0), 7.18 (2 H, bs).

6.1.6. Synthesis of tert-butyl 2-(2-(pyridin-2-yl)-1H-imidazol-1-yl)acetate (5)[5]

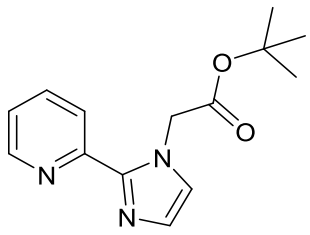

Compound **4** (0.4 g, 2.7 mmol) was dissolved in dry THF (5 mL) and the solution purged with N_2 for 10 minutes. The solution was cooled to –78°C and *n*-BuLi (2.5 M in hexane) (1.21 mL, 3 mmol) was added dropwise. The reaction mixture was stirred at –78°C for 3 hours. *tert*-butyl bromoacetate (0.44 mL, 3 mmol) was dissolved in dry THF (5 mL), the solution purged with N_2 for 5 minutes and added to the reaction mixture dropwise. After 15 minutes the solution was allowed to reach room

temperature and stirred overnight. The solvent was removed by evaporation and the crude left dissolved with H_2O (20 mL) and extracted with DCM (20 mL x 3). The organic phase was dried over $MgSO_4$ and the solvent evaporated. The product was purified by flash chromatography (eluent: DCM:MeOH = 95: 5). The product was a yellow oil obtained in 75 % yield. **^{1}H NMR** (400 MHz, $CDCl_3$) δ = 8.52 (1 H, bd, J = 5.0), 8.26 (1 H, dt, J = 8.0, 1.0), 7.77 (1 H, td, J = 8.0, 1.5), 7.22 (1 H, m), 7.19 (1 H, d, J = 1.0), 7.00 (1 H, d, J = 1.0), 5.22 (2 H, s), 1.42 (9H, s).

6.1.7. General procedure for the synthesis of osmium complexes[1]

Compound **1** (0.1 g, 0.17 mmol) and ligand (1.1 eq, 0.19 mmol) were mixed with ethylene glycol (5 mL) and purged with N_2 for 10 minutes. The mixture was heated at 100°C for 2 hours and then allowed to cool to room temperature. Ammonium hexafluorophosphate (NH_4PF_6) (0.1 g, 0.61 mmol) was dissolved in H_2O (10 mL) and added to the reaction mixture for the exchange of the anion. The solution was stirred at 0°C for 2 hours to allow the precipitation of the solid, which was filtered and washed with H_2O and EtOEt.

*6.1.7.1. bis-(2,2'-bipyridyl) (Methyl 4-(pyridin-4-yl)butanoate) chloride osmium (II) hexafluorophosphate (**6**)*

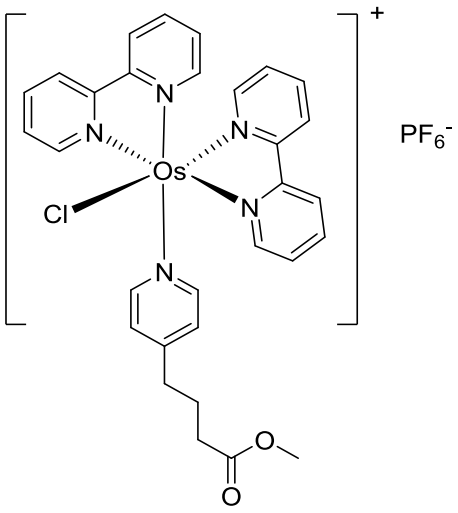

The product was a red-black solid obtained in 80 % yield. **m.p.** 152-158°C (from DCM). **UV-vis:** λ_{max} (CH_3CN)/nm 360 (ε/$dm^3mol^{-1}cm^{-1}$14563), 429 (ε/$dm^3mol^{-1}cm^{-1}$ 13140), 500 (ε/$dm^3mol^{-1}cm^{-1}$ 13057). **IR:** ν_{max}/cm^{-1} 3073 (w), 2924 (w), 1727 (m), 1458 (m), 1418 (m), 1255 (m), 1062 (m), 831 (s), 758 (s), 723 (m), 658 (m). **^{1}H NMR** (400 MHz, DMSO-d_6) δ = 9.63 (1 H, bd, *J* = 5.5), 8.74 (1 H, bd, *J* = 8.0), 8.60

(2 H, bd, *J* = 8.0), 8.48 (1 H, bd, *J* = 8.0), 8.30 (3 H, bd, *J* = 5.5), 7.84-7.73 (3 H, m), 7.71 (1 H, bd, *J* = 5.5), 7.64 (1 H, t with fine splitting), 7.59 (1 H, t with fine splitting), 7.53 (1 H, t with fine splitting), 7.37 (1 H, bd, *J* = 5.5), 7.17 (2 H, bd, *J* = 5.5), 7.10 (2 H, m), 3.52 (3H, s), 2.54 (2H, t, *J* = 7.5), 2.30 (2H, t, *J* = 7.3), 1.78 (2H, m). **^{13}C NMR** (400 MHz, DMSO-d_6): δ = 172.8, 162.5, 160.8, 159.6, 151.9, 151.7, 150.6, 135.9, 135.0, 133.7, 135.5, 127.9, 127.5, 126.9, 125.8, 124.2, 123.6, 123.2, 123.1, 33.1, 32.6, 24.1. **LR-MS ES+** m/z**:** 718.0 $[M\text{-}PF_6]^+$ (100%). **HR-MS** m/z: $[M\text{-}PF_6]^+$ calculated for $C_{30}H_{29}ClN_5O_2Os$: 718.1609, observed: 718.1594.

6.1.7.2. bis-(2,2'-bipyridyl) (tert-butyl 2-(2-(pyridin-2-yl)-1H-imidazol-1-yl)acetate) osmium (II) dihexafluorophosphate (7)

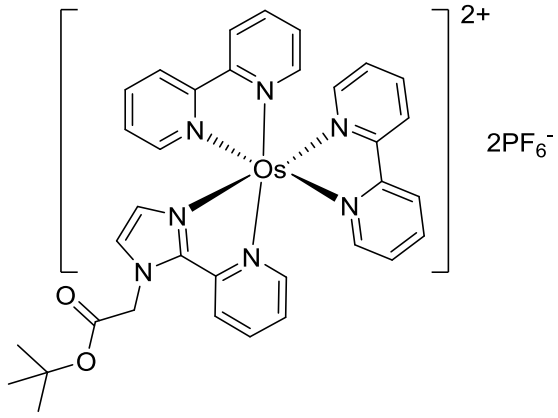

The product was a green solid obtained in 49 % yield. **m.p.** 198-203°C (from EtOEt). **UV-vis:** λ_{max} (CH_3CN)/nm 403 (ε/$dm^3mol^{-1}cm^{-1}$15640), 435 (ε/$dm^3mol^{-1}cm^{-1}$ 18800), 486 (ε/$dm^3mol^{-1}cm^{-1}$ 16160). **IR:** ν_{max}/cm^{-1} 1729 (m), 1459 (m), 1419 (m), 1017 (m), 832 (s), 759 (s), 724 (m), 658 (m).). **^{1}H NMR** (400 MHz, DMSO-d_6) δ = 8.79-8.75 (4 H, m), 8.11 (1 H, bd), 8.00-7.86 (5 H, m), 7.73-7.60 (6 H, m), 7.50-7.28 (5 H, m), 6.52 (1 H, bs), 5.63 (2 H, s), 1.38 (9 H, s). It was not possible to obtain the **^{13}C NMR** of the complex due to its low solubility. **LR-MS ES+** m/z**:** 908 $[M\text{-}PF_6]^+$ (20%), 382 $[M\text{-}2PF_6]^{2+}$ (30%).

6.1.7.3. bis-(2,2'-bipyridyl) (pyridine) chloride osmium(II) hexafluorophosphate ***(16)***

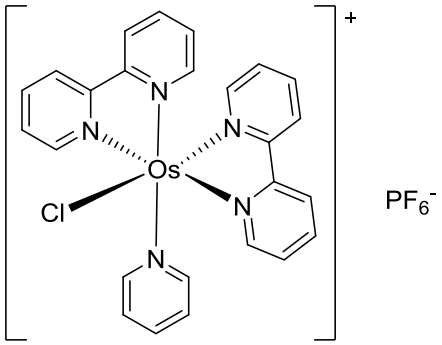

The product was a black red solid obtained in 43% yield. **UV-vis:** λ_{max} (CH_3CN)/nm 356 (ε/$dm^3mol^{-1}cm^{-1}$ 20256), 429 (ε/$dm^3mol^{-1}cm^{-1}$ 17401), 488 (ε/$dm^3mol^{-1}cm^{-1}$ 17864). **IR:** ν_{max}/cm^{-1} 3070 (w), 1474 (m), 1457 (m), 1418 (m), 1255 (m), 1010 (m), 825 (s), 756 (s), 723 (m), 698 (m), 657 (m). **^{1}H NMR** (400 MHz, DMSO-d_6) δ = 9.63 (1 H, bd, J = 5.5), 8.75 (1 H, bd, J = 8.0), 8.61 (2 H, bd, J = 8.0), 8.49 (1 H, bd, J = 8.0), 8.46 (2 H, bs), 8.30 (1 H, d, J = 5.5), 7.85-7.74 (4 H, m), 7.72 (1 H, bd, J = 5.5,), 7.65 (1 H, t with fine splitting), 7.60 (1 H, t with fine splitting), 7.54 (1 H, t), 7.39 (1 H, bd, J = 5.5), 7.31 (2 H, t with fine splitting), 7.15-7.09 (2 H, m). **^{13}C NMR** (600 MHz, DMSO-d_6): δ = 163.0, 161.2, 160.9, 160.1, 158.9, 152.6, 152.5, 152.4, 151.2(7), 151.2(1), 150.5, 137.3, 136.5, 135.7, 135.5, 134.4, 128.4, 128.0, 127.5, 126.9, 126.4, 124.7, 124.1, 123.8, 123.6. **LR-MS ES+** m/z 618.1 $[M\text{-}PF_6]^+$ (81%)

*6.1.7.3. bis-(2,2'-bipyridyl) ((3-oxo-3-((pyridin-4-ylmethyl)amino)propyl) ethanethioate) chloride osmium(II) hexafluorophosphate (**75**)*

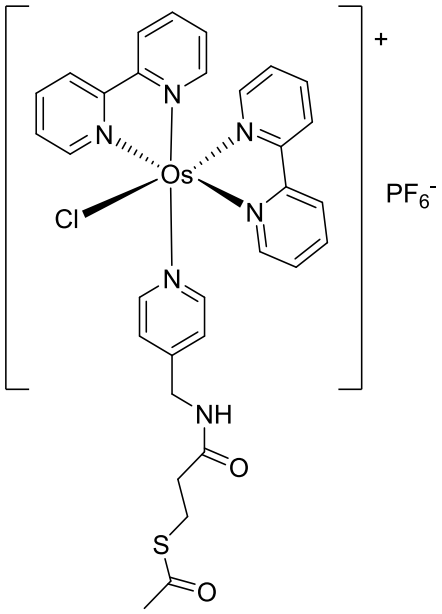

The product was a red-black solid obtained in 64 % yield. **m.p.** 168-172°C (from DCM). **UV-vis:** λ_{max} (CH_3CN)/nm 356 (ε/$dm^3mol^{-1}cm^{-1}$13400), 427 (ε/$dm^3mol^{-1}cm^{-1}$ 11820), 471 (ε/$dm^3mol^{-1}cm^{-1}$ 11240). **IR:** ν_{max}/cm^{-1} 2962 (w), 1669 (w), 1459 (m), 1418 (m), 1258 (m), 1095 (m), 1016 (s), 829 (s), 797 (s), 758 (s), 724 (m), 658 (m). **^{1}H NMR** (400 MHz, DMSO-d_6) δ = 9.61 (1 H, bd, *J* = 5.5), 8.75 (1 H, d, *J* = 8.0), 8.60 (2 H, d, *J* = 8.0), 8.48 (1 H, d, *J* = 8.0), 8.43 (1 H, d, *J* = 7.5), 8.35 (1 H, bs), 8.25 (1 H, bd), 7.85-7.79 (2 H, m), 7.75 (1 H, t, *J* = 5.5), 7.69 (1 H, bd, *J* = 5.5), 7.64 (1 H, t, *J* = 7.5), 7.59 (1 H, t, *J* = 5.5), 7.53 (1 H, t, *J* = 5.5), 7.35 (1 H, bd), 7.16-7.11 (4H, m), 4.21 (2H, d, *J* = 4.0), 3.00 (2H, t, *J* = 7.0), 2.45 (2H, t, *J* = 7.0), 2.29 (3H, s). **^{13}C NMR** (400 MHz, DMSO-d_6): δ = 192.7, 177.7, 171.0, 155.07, 151.26, 150.2, 136.5, 124.4, 124.1, 123.8, 35.2, 34.5, 31.0, 24.8. **LR-MS ES+** m/z**:** 777.1 $[M-PF_6]^+$ (100%). **HR-MS** m/z: $[M-PF_6]^+$ calculated for $C_{31}H_{30}ClN_6O_2OsS$: 777.1446, observed: 777.1421.

6.1.8. bis-(2,2'-bipyridyl) (2-(2-(pyridin-2-yl)-1H-imidazol-1-yl)acetic acid) osmium (II) dihexafluorophosphate (9)

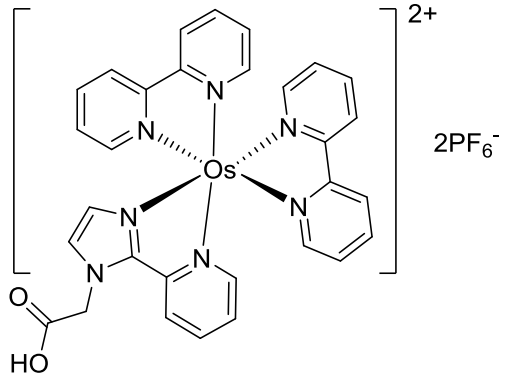

Compound **7** (0.1 g, 0.09 mmol) was dissolved in a 20% solution of TFA in dry DCM (5 mL) and stirred at room temperature overnight. The unreacted TFA was removed by azeotropic distillation with toluene until a solid residue was obtained. The crude was dissolved in H_2O and an excess of NH_4PF_6 (aq) (0.2 g, 1.2 mmol) was added to precipitate the product. The solution was stirred at 0°C for 2 hours and the precipitate was filtered and washed with H_2O and EtOEt. The product was a green solid obtained in 95% yield. **m.p.** 270-274°C. **UV-vis:** λ_{max} (CH_3CN)/nm 403 (ε/dm^{3}mol^{-1}cm^{-1}15580), 433 (ε/dm^{3}mol^{-1}cm^{-1} 12760), 487 (ε/dm^{3}mol^{-1}cm^{-1} 11000). **IR:** ν_{max}/cm^{-1} 1605 (m), 1464 (m), 1449 (m), 1421 (m), 1251 (w), 1160 (w), 830 (s), 761 (s). **^{1}H NMR** (400 MHz, DMSO-d_6) δ = 11.5 (1H, bs), 8.78 (4 H, m), 8.04 (1 H, d, *J* = 7.5), 7.92-7.85 (5 H, m), 7.72-7.66 (5 H, m), 7.59 (1 H, d, *J* = 5.5), 7.45 (2 H, t, *J* = 5.5), 7.41-7.36 (2 H, m), 7.27 (2 H, t, *J* = 5.5), 6.45 (1H, s), 5.27 (2H, d, *J* = 8). It was not possible to obtain the **^{13}C NMR** of the complex due to its low solubility. **LR-MS ES+** m/z**:** 353 $[M-2PF_6]^{2+}$ (50%).

6.1.9. bis-(2,2'-bipyridyl) (4-(pyridin-4-yl)butanoic acid) chloride osmium (II) hexafluorophosphate (8)

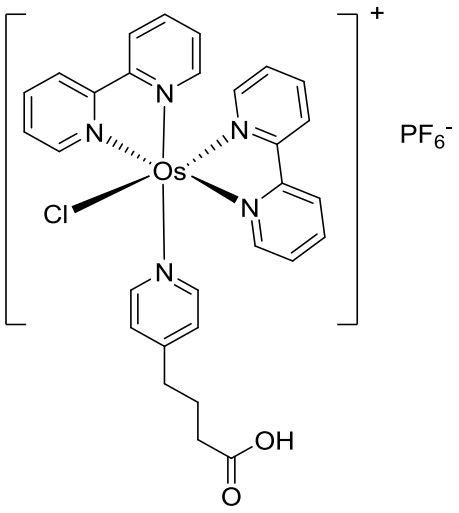

Compound **6** (0.1 g, 0.1 mmol) was dissolved in a 2 M solution of potassium hydroxide (1 g, 20 mmol) in MeOH/H_2O (1:1) (10 mL) and the mixture was refluxed for 3 hours. The organic solvent was removed and H_2O was added. The aqueous phase was extracted with DCM (3 x 15 mL) in order to remove any starting material left. The pH of the aqueous phase was adjusted to 2 by addition of 1 M HCl and the resulting solution extracted with DCM (3 x 30 mL). The organic phase was dried over $MgSO_4$ and the solvent removed to obtain the product as a red-black solid in 83% yield. **m.p.** 172-175°C (from DCM/ MeOH) **UV-vis:** λ_{max} (CH_3CN)/nm 359 (ε/$dm^3mol^{-1}cm^{-1}$14876), 430 (ε/$dm^3mol^{-1}cm^{-1}$ 13417), 505 (ε/$dm^3mol^{-1}cm^{-1}$ 13325). **IR:** ν_{max}/cm^{-1} 3069 (w), 1720 (m), 1499 (m), 1476 (m), 1319 (m), 1017 (m), 828 (s), 761 (s), 723 (m), 658 (m). **^{1}H NMR** (400 MHz, DMSO-d_6) δ = 12.04 (1H, bs), 9.62 (1 H, bd, *J* = 5.5), 8.74 (1 H, bd, *J* = 8.0), 8.60 (2 H, bd, *J* = 8.0), 8.48 (1 H, bd, *J* = 8.0), 8.29 (3 H, bd, *J* = 5.5), 7.84-7.73 (3 H, m), 7.70 (1 H, bd, *J* = 5.5), 7.64 (1 H, t with fine splitting,), 7.59 (1 H, t with fine splitting), 7.52 (1 H, t with fine splitting), 7.36 (1 H, bd, *J* = 5.5,), 7.17 (2 H, bd, *J* = 5.5), 7.10 (2 H, m), 2.54 (2H, t, *J* = 7.5), 2.20 (2H, t, *J* = 7.5), 1.74 (2H, m). **^{13}C NMR** (400 MHz, DMSO-d_6): δ = 173.9, 162.5, 160.8, 159.6, 151.9, 151.7, 150.6, 135.9, 135.0, 133.7, 135.5, 127.9, 127.5, 126.9, 125.8, 124.2, 123.6, 123.2, 123.1, 33.1, 30.6, 24.3. **LR-MS ES+** m/z**:** 704.1 $[M\text{-}PF_6]^+$ (100%). **HR-MS** m/z: $[M\text{-}PF_6]^+$ calculated for $C_{29}H_{27}ClN_5O_2Os$: 704.1461, observed: 704.1442. **XRD** Crystals of the complex were obtained by recrystallization from DCM/MeOH. See appendix II for full structure report.

6.1.10. General procedure for the mono protection of diamines with trifluoroacetamide group[6]

α,ω-diamine (4 mmol) was dissolved in MeOH (20 mL) and the solution was cooled at -70°C. Ethyltrifluoroacetate (0.8 mmol) was dissolved in MeOH (10 mL) and added drop-wise to the amine solution. The mixture was stirred for 2 hours, then allowed to reach 0°C and stirred for 1 hour. The solvent was evaporated to obtain and the residue dissolved with H_2O (30 mL). The product was extracted with AcOEt (3 x 25 mL), the organic phase was dried with $MgSO_4$ and the solvent removed.

*6.1.10.1. N-(6-aminoethyl)-2,2,2-trifluoroacetamide (**30**)*

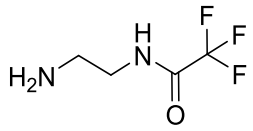

The product was a yellow oil obtained in 16 % yield. **^{1}H NMR** (400 MHz, MeOD-d_4): δ = 3.35 (2 H, t, *J* = 6.5), 2.79 (2 H, t, *J* = 6.5).

*6.1.10.2. N-(6-aminohexyl)-2,2,2-trifluoroacetamide (**33**)*

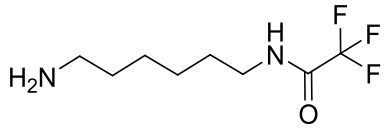

The product was a white solid obtained in 62 % yield. **^{1}H NMR** (400 MHz, MeOD-d_4): δ = 3.28 (2 H, t, *J* = 7.0), 2.66 (2 H, t, *J* = 7.0), 1.58 (2 H, m), 1.50 (2 H, m), 1.37 (4 H, m).

6.1.11. General procedure for the synthesis of maleimide derivatives[7]

Maleic anhydride (1.3 g, 10 mmol) was dissolved in acetic acid (10 mL) and the amino acid (10 mmol) was added. The mixture was refluxed for 90 minutes, followed by the removal of the solvent. The crude oil obtained was dissolved in H_2O (15 mL) and the product was extracted with AcOEt (15 mL x 3). The organic phase was dried over $MgSO_4$ and the solvent evaporated.

*6.1.11.1. 3-(2,5-dioxo-2,5-dihydro-1H-pyrrol-1-yl)propanoic acid (**65**)*

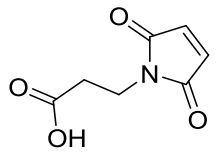

The product was further purified by column chromatography over silica (eluents: AcOEt) to obtain a white solid in 25% yield. **^{1}H NMR** (400 MHz, $CDCl_3$): δ = 6.72 (2 H, s), 3.84 (2 H, t, *J* = 7), 2.71 (2 H, t, *J* = 7).

*6.1.11.2. 6-(2,5-dioxo-2,5-dihydro-1H-pyrrol-1-yl)hexanoic acid (**66**)*

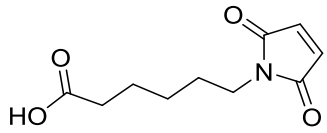

The product was further purified by column chromatography over silica (eluents: DCM:MeOH = 9.5:0.5) to obtain a white solid in 28% yield. **^{1}H NMR** (400 MHz, $CDCl_3$): δ = 6.69 (2 H, s), 3.51 (2 H, t, *J* = 7.0), 2.34 (2 H, t, *J* = 7.0), 1.63 (4 H, m), 1.34 (2 H, m).

6.1.12. 3-(2,5-dioxo-3-(phenylselanyl)-2,5-dihydro-1H-pyrrol-1-yl)propanoic acid (70)[8]

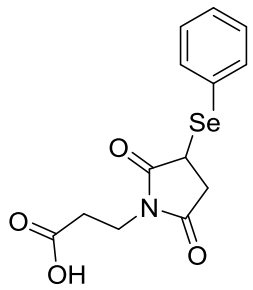

Compound **65** (0.18 g, 0.8 mmol) was dissolved with acetonitrile (CH_3CN) (1.5 mL) and phenylselenol (80 μl, 0.8 mmol) was added. After 5 minutes stirring at room

temperature, a white precipitate formed. The mixture was left stirring for further 2.5 hours, then the precipitate was filtered, washed with cold CH_3CN and vacuum dried. The product was a white solid obtained in 40% yield. **^{1}H NMR** (400 MHz, $CDCl_3$): δ = 7.62 (2 H, dd. *J* = 7.0, 2.0), 7.42 (1 H, td, *J* = 7.0, 2.0), 7.34 (2 H, dd, *J* = 7.0, 2.0), 4.07 (1 H, dd, *J* = 9.0, 3.0), 3.65 (2 H, t, *J* = 7.0), 3.22 (1 H, dd, *J* = 19.0, 9.0), 2.81 (3 H, dd, *J* = 19.0, 3.0), 2.46 (2 H, t, *J* = 7.0).

6.1.13. 3-(acetylthio)propanoic acid (73)[9]

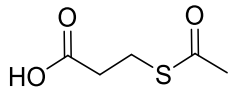

3-mercaptopropionic acid (0.5 mL, 5.7 mmol) was mixed with DCM (2 mL) and the solution was cooled at 0°C. Acetyl chloride (1.5 mL, 21 mmol) and acetic acid (1.5 mL, 26 mmol) were mixed with DCM (3 mL) and added dropwise to the 3-mercaptopropionic acid solution. The mixture was left stirring at room temperature for 48 hours. The solvent and the excess of acetic acid and acetyl chloride were removed to obtain the product as a white solid in 91% yield**^{1}H NMR** (400 MHz, $CDCl_3$): δ = 11.37 (1 H, bs), 3.10 (2 H, t, *J* = 7.0), 2.69 (2 H, t, *J* = 7.0), 2.33 (3 H, s).

6.1.14. (3-oxo-3-((pyridin-4-ylmethyl)amino)propyl) ethanethioate (74)

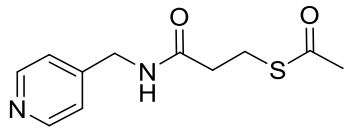

Compound **73** (0.5 g, 3.4 mmol) was dissolved in DMF (10 mL) and EDC.HCl (1.65 g, 8 mmol) was added with triethylamine (2.73 mL, 19 mmol) followed by HOBt (1.36 g, 10 mmol). 4-(aminomethyl)pyridine (0.512 mL, 5.5 mmol) was added and the solution was left stirring overnight at room temperature. The solvent was evaporated and the oily residue dissolved with H_2O (20 mL) and the crude product was extracted with DCM (20 mL x 3). The organic layer was dried over $MgSO_4$ and the solvent removed. The product was purified by column chromatography over silica (eluents: DCM:MeOH = 9:1) to obtain a white solid in 27% yield. **m.p.** 79-83°C. **IR:** ν_{max}/cm^{-1} 3015 (w), 2926 (w), 1675 (s), 1402 (m), 1336 (w), 1265 (m), 1201 (m), 1134 (m), 1057 (w), 957 (m), 908 (m), 623 (m). **^{1}H NMR** (400 MHz, $CDCl_3$) δ = 8.54 (2 H, d, *J* = 6.0), 7.18 (2 H, d, *J* = 6.0), 6.30 (1 H, bs), 4.45 (2 H, d,

J = 6.0), 3.17 (2 H, t, *J* = 7.0), 2.57 (2 H, t, *J* = 7.0), 2.32 (3 H, s). **^{13}C NMR** (400 MHz, $CDCl_3$): δ = 196.1, 170.9, 150.0, 147.2, 122.3, 42.4, 36.2, 30.6, 24.9 **LR-MS ES+** m/z**:** 239 $[M+H]^+$ (100%). **HR-MS** m/z: $[M+H]^+$ calculated for $C_{11}H_{15}N_2O_2S$: 239.0849, observed: 239.0847.

6.1.15. bis-(2,2'-bipyridyl) (3-mercapto-N-(pyridin-4-ylmethyl)propanamide) chloride osmium (II) hexafluorophosphate (76)[10]

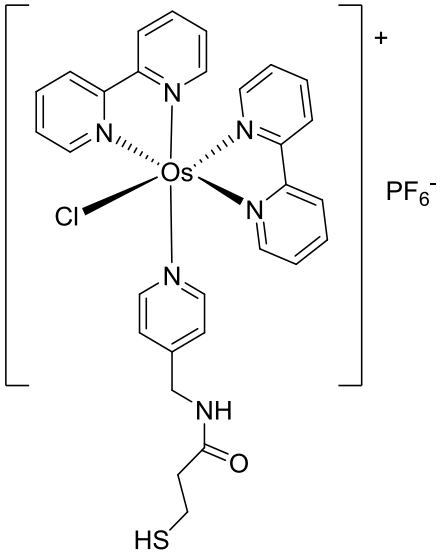

Compound **75** (0.1 g, 0.1 mmol) was dissolved in a 10 mL solution of NaOH (0.1 g, 2.45 mmol) in MeOH. The mixture was stirred at room temperature for 2 hours under N_2 atmosphere. 5% HCl (10 mL) was added and the mixture was left stirring for 1 hour. Brine (10 mL) was added and the product was extracted with DCM (20 mL x 3). The organic phase was dried over $MgSO_4$ and the solvent removed to obtain the product as a dark red solid in 53% yield. **m.p.** 135-140°C (from DCM) **UV-vis:** λ_{max} (CH_3CN)/nm 355 (ε/$dm^3mol^{-1}cm^{-1}$11120), 427 (ε/$dm^3mol^{-1}cm^{-1}$ 9760), 476 (ε/$dm^3mol^{-1}cm^{-1}$ 9540). **IR:** ν_{max}/cm^{-1} 3643 (w), 3430 (w), 2923 (w), 1667 (m), 1459 (m), 1419 (m), 1257 (m), 1018 (m), 831 (s), 761 (m), 724 (m), 658 (m). **^{1}H NMR** (400 MHz, DMSO-d_6) δ = 9.62 (1 H, bd, *J* = 5.5), 8.75 (1 H, d, *J* = 8.0), 8.62-8.60 (2 H, m), 8.52-8.46 (2 H, m), 8.36 (1 H, bs), 8.28 (1 H, d), 7.84-7.70 (4 H, m), 7.65 (1 H, t, *J* = 7.5), 7.58 (1 H, t, *J* = 5.5), 7.52 (1 H, t, *J* = 5.5), 7.38 (1 H, bd), 7.16-7.08 (4H, m), 4.21 (2H, d, *J* = 4.0), 2.88 (2H, t, *J* = 7.0), 2.54 (2H, t, *J* = 7.0), 2.29 (1H, s). **^{13}C NMR** (400 MHz, DMSO-d_6): δ = 170.5, 155.07, 151.26, 150.2, 136.5, 124.4, 124.1, 123.8, 34.7, 33.5. **LR-MS ES+** m/z**:** 733.0 $[M-PF_6]^+$ (100%).

HR-MS m/z: $[M\text{-}PF_6]^+$ calculated for $C_{29}H_{28}ClN_6OOsS$: 733.1331, observed: 733.1344.

6.1.16. 4-hydroxy-2-methoxybenzaldehyde (85)[11]

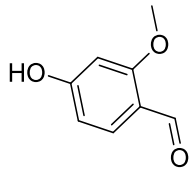

3-methoxyphenol (2.9 mL, 26 mmol) was mixed with $POCl_3$ (4.1 mL, 44 mmol) at 0°C and DMF (3.3 mL, 42 mmol) was added dropwise. The reaction was allowed to reach room temperature and left stirring for 20 hours. The mixture was poured over crushed ice (100 mL) and stirred until complete dissolution of the ice and separation of an oily phase at the bottom of the flask. The aqueous phase was extracted with EtOEt (40 mL x 3), then 0.1 M NaOH was added until pH 5. The aqueous layer was extracted with AcOEt (30 mL x 3), the organic layer was dried over $MgSO_4$ and the solvent evaporated. The solid obtained was triturated with boiling petroleum ether (20 mL), filtered and washed with hot petroleum ether. The product was a white solid obtained in 39% yield. **^{1}H NMR** (400 MHz, $CDCl_3$): δ = 10.28 (1 H, s), 7.77 (1 H, d, *J* = 9.0), 6.48 (1 H, dd, *J* = 9.0, 1.5), 6.45 (1 H, d, *J* = 1.5), 3.91 (3 H, s).

6.1.17. 2-methoxy-4-(prop-2-yn-1-yloxy)benzaldehyde (87)[12]

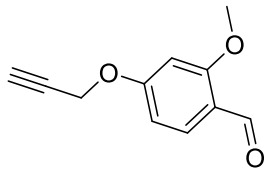

Compound **85** (1.5 g, 10 mmol) was dissolved in CH_3CN (40 mL) and potassium carbonate (K_2CO_3) (1.5 g, 15 mmol) was added. The mixture was stirred at 70°C under N_2 atmosphere for 30 minutes, then allowed to cool down to room temperature and propargyl bromide (1.35 mL, 15 mmol) was added. The reaction was left stirring at 70°C overnight. The solvent was removed, the solid residue was dissolved with H_2O (20 mL) and 10% HCl was added to quench the residual base. The aqueous phase was extracted with AcOEt (20 mL x 3); the organic phase was dried over $MgSO_4$ and the solvent removed. The product was purified by column chromatography over silica (eluent: AcOEt) to obtain an orange solid in 93% yield. **m.p.** 134-140°C (from EtOEt). **IR:** ν_{max}/cm^{-1} 3132 (m), 3019 (m), 1613 (m), 1590

(m), 1556 (s), 1502 (m), 1446 (m), 1312 (w), 1249 (m), 1203 (m), 1191 (m), 1156 (m), 1125 (m), 1027 (m), 836 (m), 784 (w), 666 (m), 647 (m). **^{1}H NMR** (400 MHz, $CDCl_3$) δ = 10.31 (1 H, s), 7.83 (1 H, d, *J* = 9.0), 6.63 (1 H, dd, *J* = 9.0, 1.5), 6.55 (1 H, d, *J* = 1.5), 4.76 (2 H, s), 3.91 (3 H, s), 2.58 (1 H, s). **^{13}C NMR** (400 MHz, $CDCl_3$): δ = 191.2, 158.5, 129.5, 122.6, 104.9, 78.4, 75.5, 61.5, 55.3. **LR-MS ES+** m/z**:** 190 $[M]^+$ (100%).

6.1.18. (2-methoxy-4-(prop-2-yn-1-yloxy)phenyl)methanol (88)[11]

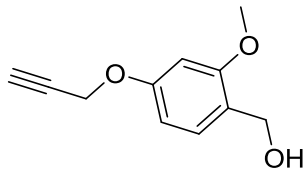

Compound **87** (0.52 g, 2.7 mmol) was dissolved in MeOH/H_2O (1:1) (10 mL) and the solution was cooled to 0°C. Sodium boron hydride (0.1 g, 2.7 mmol) was dissolved in 1 M NaOH (2 mL) and added dropwise to the starting material solution. The reaction was stirred at room temperature for 3 hours. The reaction was quenched by adding 10% HCl at 0°C until the formation of gas stopped. The aqueous phase was extracted with AcOEt (15 mL x 3); the organic phase was dried over $MgSO_4$ and the solvent removed. The product was purified by column chromatography over silica (eluent: Hexane:AcOEt = 6:4) to obtain an white solid in 43% yield. **m.p.** 57-60°C (from EtOEt). **IR:** ν_{max}/cm^{-1} 3285 (bw), 3235 (m), 2972-2851 (w), 1613 (m), 1590 (m), 1502 (m), 1446 (m), 1312 (w), 1249 (m), 1203 (m), 1191 (m), 1156 (m), 1125 (m), 1027 (s), 831 (m), 791 (w), 689 (m), 671 (m). **^{1}H NMR** (400 MHz, $CDCl_3$): δ = 7.19 (1 H, d, *J* = 9), 6.54 (2 H, m), 4.70 (2 H, s), 4.63 (2 H, s), 3.85 (3 H, s), 2.54 (1 H, s). **^{13}C NMR** (400 MHz, $CDCl_3$): δ = 158.5, 129.5, 122.6, 104.9, 99.51, 78.4, 75.5, 61.5, 55.3. **LR-MS ES+** m/z: 191 $[M-1]^+$ (20%), 175 $[M-H_2O+H]^+$ (100%).

6.1.19. 4-(((tert-butyldimethylsilyl)oxy)methyl)phenol (89)[12]

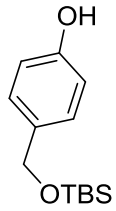

4-hydroxyphenol (1 g, 8 mmol) was dissolved in DMF (15 mL) and imidazole (0.6 g, 10 mmol) was added. The mixture was cooled to 0°C and t-butyldimethylsilyl chloride (1.45 g, 10 mmol) was added. The reaction was allowed to reach room temperature and stirred for 2 hours. The solvent was removed, the oily residue was dissolved with H_2O (20 mL) and the aqueous phase was extracted with AcOEt (20 mL x 3); the organic phase was dried over $MgSO_4$ and the solvent removed. The product was purified by column chromatography over silica (eluent: Hexane:AcOEt = 8:2) to obtain a colourless oil in 76% yield. **^{1}H NMR** (400 MHz, $CDCl_3$): δ = 7.20 (2 H, d, *J* = 9.0), 6.79 (2 H, d, *J* = 9), 4.67 (2 H, s), 0.94 (9 H, s), 0.10 (6 H, s).

6.1.20. ((4-(2-bromoethoxy)benzyl)oxy)(tert-butyl)dimethylsilane (90)[12]

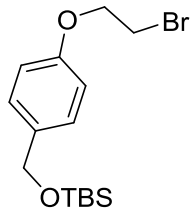

Compound **90** (2 g, 8.4 mmol) was dissolved in CH_3CN (40 mL) and potassium carbonate (K_2CO_3) (1.2 g, 12 mmol) was added. The mixture was stirred at 70°C for 30 minutes and 1,2-dibromoethane (2.16 mL, 25 mmol) was added. The reaction was left stirring at 70°C for 3 days. The solvent was removed, the solid residue was dissolved with H_2O (20 mL) and 10% HCl was added to quench the residual base. The aqueous phase was extracted with AcOEt (20 mL x 3); the organic phase was dried over $MgSO_4$ and the solvent removed. The product was purified by column chromatography over silica (eluent: Hexane:AcOEt = 8.5:1.5) to obtain a colourless oil in 20% yield. **IR:** ν_{max}/cm^{-1} 2951 (w), 2927 (w), 2855 (w), 1610 (w), 1508 (m), 1473 (w), 1377 (w), 1248 (s), 1218 (s), 1170 (w), 1089 (m), 1063 (s), 835 (s), 773 (s).**^{1}H NMR** (400 MHz, $CDCl_3$) δ = 7.16 (2 H, d, *J* = 9.0), 6.79 (2 H, d, *J* = 9.0), 4.59 (2 H, s), 4.19 (2 H, t, *J* = 5.0), 3.54 (2 H, t, *J* = 5.0), 0.85 (9 H, s), 0.00 (6 H, s).

^{13}C NMR (400 MHz, $CDCl_3$): δ = 157.1, 134.5, 127.6, 114.6, 67.9, 64.6, 29.1, 25.9, 18.4, -5.2. **LR-MS ES+** m/z**:** 346 $[M]^+$ (20%), 371 $[M+ Na]^+$ (100%).

6.1.21. ((4-(2-azidoethoxy)benzyl)oxy)(tert-butyl)dimethylsilane (91)[12]

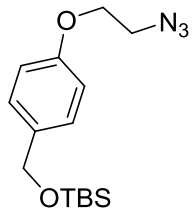

Compound **91** (0.7 g, 2 mmol) was dissolved in DMF (15 mL) and sodium azide (0.4 g, 6 mmol) was added. The mixture was stirred at 70°C overnight. The solvent was removed, the oily residue was dissolved with H_2O (30 mL) and the aqueous phase was extracted with AcOEt (40 mL x 3); the organic phase was dried over $MgSO_4$ and the solvent removed. The product was purified by column chromatography over silica (eluent: Hexane:AcOEt = 8:2) to obtain a colourless oil in 80% **IR:** ν_{max}/cm^{-1} 2953 (w), 2929 (w), 2856 (w), 2108 (m). 1612 (w), 1510 (m), 1462 (w), 1240 (s), 1170 (w), 1083 (m), 1063 (m), 922 (w), 834 (s), 775 (m).**^{1}H NMR** (400 MHz, $CDCl_3$) δ = 7.23 (2 H, d, *J* = 9.0), 6.87 (2 H, d, *J* = 9.0), 4.66 (2 H, s), 4.13 (2 H, t, *J* = 5.0), 3.57 (2 H, t, *J* = 5.0), 0.92 (9 H, s), 0.07 (6 H, s) **^{13}C NMR** (400 MHz, $CDCl_3$): δ = 157.2, 134.3, 127.5, 114.3, 67.0, 64.6, 50.1, 25.9, 18.4, -5.2. **LR-MS ES+** m/z**:** 307 $[M]^+$ (10%), 330 $[M+Na]^+$ (80%).

6.1.22. (4-((1-(2-(4-(((tert-butyldimethylsilyl)oxy)methyl)phenoxy)ethyl)-1H-1,2,3-triazol-4-yl)methoxy)-2-methoxyphenyl)methanol (92)

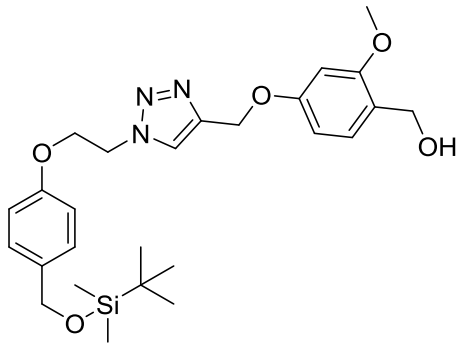

Compound **88** (0.1 g, 0.5 mmol) and **91** (0.16 g, 0.5 mmol) were dissolved in CH_3CN (3 mL) and copper (I) iodide (0.001 g, 0.05 mmol), triethylamine (7.2 μl, 0.05 mmol) was added. The mixture was stirred at room temperature overnight. The solvent was removed, the oily residue was dissolved with brine (15 mL) and the

aqueous phase was extracted with DCM (15 mL x 3); the organic phase was dried over $MgSO_4$ and the solvent removed. The product was purified by column chromatography over silica (eluent: Hexane:AcOEt = 1:9) to obtain an orange oil in 77% yield. **IR:** ν_{max}/cm^{-1} 2953 (w), 2929 (w), 2855 (w), 1611 (m), 1588 (m), 1508 (m), 1462 (m), 1242 (m), 1196 (m), 1158 (m), 1043 (m), 908 (s), 776 (m).**^{1}H NMR** (400 MHz, $CDCl_3$) δ = 7.83 (1 H, s), 7.24 (2 H, d, *J* = 9.0,), 7.16 (1 H, d, *J* = 8.0), 6.82 (2 H, d, *J* = 9.0), 6.55 (2 H, m), 5.22 (2 H, s), 4.76 (2 H, t, *J* = 5.0), 4.67 (2 H, s), 4.61 (2 H, s), 4.36 (2 H, t, J = 5.0), 3.82 (3 H, s), 0.93 (9 H, s), 0.09 (6 H, s). **^{13}C NMR** (400 MHz, $CDCl_3$): δ = 159.2, 158.5, 156.7, 134.8, 129.6, 127.5, 123.8, 122.2, 114.3, 104.9, 99.3, 66.3, 64.8, 62.0, 61.5, 55.3, 49.83, 25.9, 18.3, -5.2. **LR-MS ES+** m/z**:** 482 $[M-H_2O+H]^+$ (100%). **HR-MS** m/z: $[M+NH_4]^+$ calculated for $C_{26}H_{41}N_4O_5Si$: 517.2841, observed: 517.2827.

6.2. Electrochemical experiments and solid phase synthesis

6.2.1. General

All the non synthesised chemicals were obtained from Sigma-Aldrich and were all used without further purification. DCM and DMF were distilled using a MBraun MB SPS-800 solvent purification system. Milli-Q H_2O was purified using an Elga Purelab Ultra purification system. GcGDH was supplied by the University of Natural Resources and Life Sciences, Vienna, Austria. The mutated variant GDH T343C was supplied in 50 mM pH 5.5 citrate buffer at a concentration of 3.5 mg/mL (Bradford assay) and activity (DCIP assay, pH 5.5, 30°C) = 2200 U/mL. Electrochemical experiments for single electrodes were recorded on an Autolab PGSTAT30 Potentiostat/Galvanostat and data were analysed with Origin 7.0 software. Electrochemical experiments were performed using a three electrodes electrochemical system: the counter electrode was a 1 cm^2 platinum gauze, the reference electrode was a homemade saturated calomel electrode (SCE) or silver/silver chloride (Ag/AgCl) electrode. The working electrode was a 3 mm diameter (geometrical area of 0.071 cm^2) glassy carbon disc (HTW, Hochtemperatur-Werkstoffe GmbH, Germany) sealed in a glassy tube and wired up with copper wire by using melted indium. Prior to modification, the working GC electrodes were dry polished on silicon carbide coated abrasive paper grade P800, followed by silicon carbide coated abrasive paper grade P1200 and Aluminium Oxide Fibre Optic Lapping Film (3M) grade 5 μm. The electrodes were rinsed with Milli-Q. The electrodes were then polished successively with Buehler alumina (grade 1 μm and 0.3 μm) slurries with Milli-Q H_2O on Buehler polishing pads, rinsed with Milli-Q H_2O between each step and stored in HPLC grade CH_3CN. Unless otherwise stated, the electrochemical characterisation of the modified electrodes was performed in 0.1 M phosphate buffer pH 7, except for electrodes modified with GcGDH which were characterised in 50 mM citrate buffer pH 5.5 with 0.1 M TEATFB added as supporting electrolyte.

6.2.2. General procedure for electrochemical attachment of mixtures of amines at GC electrodes[13]

The attachment of mixtures of amine linkers was carried out in a 20 mM solution of the two components in CH_3CN (5 mL) and TBATFB (0.1 M, 0.165 g), varying the amount of each according to their fraction, by chronoamperometry, holding the

potential at 2.1 V vs. Ag/AgCl for 3 minutes. The electrode was rinsed with distilled H_2O (5 mL) and CH_3CN (5 mL) and dried with air for 10 seconds.

6.2.3. General procedure for the Boc-deprotection of modified GC electrodes[13]

The electrode was suspended in a 4 M solution of HCl (10 mL) in 1,4-dioxane for 1 hour at room temperature. The deprotected electrode was then rinsed with deionised H_2O (5 mL), CH_3CN (5 mL) and dried in air for 10 seconds.

6.2.4. General procedure for the tfa-deprotection of modified GC electrodes[14]

The electrode was suspended in a 10% solution of K_2CO_3 (10 mL) in MeOH/H_2O (7:3) for 6 hours at room temperature. The deprotected electrode was then rinsed with deionised H_2O (5 mL), CH_3CN (5 mL) and dried in air for 10 seconds.

6.2.5. Coupling of complex 8 to the amine modified GC electrodes

A 3 mL solution containing complex **8** (10 mM) (0.025 g, 0.03 mmol), EDC (0.054 mL, 0.3 mmol) and NHS (0.007 g, 0.2 mmol) in dry DMF was stirred for 1 hour at room temperature. The electrode was dipped in the solution for 16 hours at room temperature. The electrode was rinsed with deionised H_2O (5 mL), CH_3CN (5 mL) and left to dry in air for 5 minutes. After a first check by cyclic voltammetry, the electrode was left in stirring CH_3CN for 24 hours and checked by cyclic voltammentry.

6.2.6. Coupling of anthraquinone-2-carboxylic acid at amine modified GC electrodes

A 3 mL solution containing anthraquinone-2-carboxylic acid (0.012 g, 0.05 mmol), EDC (0.088 mL, 0.5 mmol) and NHS (0.034 g, 0.3 mmol) in dry DMF was stirred for 1 hour at room temperature. The electrode was dipped in the solution for 16 hours at room temperature. The electrode was rinsed with deionised H_2O (5 mL), CH_3CN (5 mL) and left to dry in air for 5 minutes. After a first check by cyclic voltammetry, the electrode was left in stirring CH_3CN for 45 hours and checked by cyclic voltammetry.

6.2.7. General procedure for the capping of the residual free amines on the modified GC electrodes

The electrode was dipped in a 10 mM solution of AcCl (0.004 mL; 0.05 mmol) in dry DCM (5 mL) with Et_3N (0.008 mL; 0.055 mmol) and DMAP (0.6 mg; 0.005

mmol), under N_2 and left stirring overnight at room temperature. The electrodes were rinsed with HPLC grade CH_3CN and dried with air for 30 seconds.

6.2.8. Coupling of Boc-8-amino-3,6-dioxaoctanoic acid at amine modified GC electrodes

A 3 mL solution containing Boc-8-amino-3,6-dioxaoctanoic acid (dicyclohexylammonium) salt (10 mM) (0.013 g, 0.03 mmol), EDC (0.054 mL, 0.3 mmol) and NHS (0.007 g, 0.2 mmol) in dry DMF was stirred for 1 hour at room temperature. The electrode was dipped in the solution for 16 hours at room temperature The electrode was rinsed with deionised H_2O (5 mL), CH_3CN (5 mL) and left to dry in air for 5 minutes. The electrode was left in stirring CH_3CN overnight and checked by cyclic voltammentry.

6.2.9. Coupling of maleimide derivatives 66, 67 and 71 at amine modified GC electrodes

A 3 mL solution containing the maleimide derivative (10 mM) (0.03 mmol), EDC (0.054 mL, 0.3 mmol) and NHS (0.007 g, 0.2 mmol) in dry DMF was stirred for 1 hour at room temperature. The electrode was dipped in the solution for 16 hours at room temperature. The electrode was rinsed with deionised H_2O (5 mL), CH_3CN (5 mL) and left to dry in air for 5 minutes. The electrode was left in stirring CH_3CN overnight and checked by cyclic voltammentry.

6.2.10. General procedure for the phenylselenyl group removal[8]

The electrode was dipped in a 5 mL solution of 10 mM m-CPBA (0.006 g, 0.05 mmol) in CH_3CN for 1 hour at 0°C. The solution was then left to reach room temperature and left for 1 hour stirring. The electrode was washed in CH_3CN for 2 hours.

6.2.11. Attachment of complex 77 to maleimide modified electrodes[15]

Complex **77** (0.026 g, 0.03 mmol) was dissolved in MeOH (3 mL) and triethylamine (40 μl, 0.7 μmol) was added. The electrode was dipped in the solution and left stirring at room temperature overnight. The electrode was washed in CH_3CN overnight and checked by cyclic voltammetry.

6.2.12. GcGDH T343C attachment to maleimide modified electrodes

The GcGDH T343C buffer was exchanged from 50 mM citrate buffer pH 5.5 to 20 mM phosphate buffer pH 7 using mini dialysis wells (Fisher Scientific) with 10 KDa cut off. 50 μL fractions of the enzyme were transferred to each dialysis well and stirred in 20 mM phosphate buffer pH 7 (200 mL) for 10 minutes. The buffer was replaced with fresh one (200 mL) and the dialysis wells were left stirring for further 20 minutes. The dialysis units were then transferred to fresh buffer (500 mL) and left at 4°C for 1.5 hours. 20 μL of enzyme containing phosphate buffer was drop casted on the modified electrode surface, the electrode was sealed in a pipette tip and stored at 4°C overnight. The electrode was rinsed with 50 mM citrate buffer pH 5.5 and stored in such buffer in between experiments.

6.3. References

[1] Kober, E.M.; Caspar, J.V.; Sullivan, B.P.; Meyer, T.J. *Inor. Chem.* **1988,** *25,* 4587-4598.

[2] Menghin, S.; Pertz, H.H.; Kramer, K.; Seifert, R.; Schunack, W.; Elz, S. *J. Med. Chem.*, **2003,** *46,* 5458-5464.

[3] Aotsuka, T.; Kumazawa, K.; Wagatsuma, N.; Ishitani, K. **Patent EP1236725**, **2004**.

[4]] a) Yue, S.-M.; Xu, H.-B.; Ma, J.-F.; Su, Z.-M.; Kan, Y.-H.; Zhang, H.-J. *Polyhedron* **2006**, *25,* 635–644. b) Saha, D.; Das, S.; Maity, D.; Baitalik, S.; *Indian J. Chem.* **2011**, *50A,* 1418-1428.

[5] Pinczewska, A.; Sosna, M.; Bloodworth, S.; Kilburn, J.D.; Bartlett, P.N. *J. Am. Chem. Soc*. **2012,** *134,* 18022-18033.

[6] Ling, X.; Samuel, E.L.; Patchell, D.L.; Masson, E. *Org. Lett.* **2010,** *12,* 2730-2733.

[7] De Figueiredo, R.M.; Oczipka, P., Frohlich, R.; Christmann, M. *Synthesis* **2008,** *8,* 1316-1318.

[8] Numao, N.; Hemmi, H.; Naujokaitis, S.A.; Rabinovitz, M.; Beisler, J.A. *J. Med. Chem.* **1981,** *24,* 515-520.

[9] Larsson, R.; Pei, Z.; Ramstrom, O. *Angew. Chem.* **2004,** *28,* 3716-3718.

[10] Clegg, R.S.; Hutchinson, J.E. *J. Am. Chem. Soc.* **1999,** *121,* 5319-5327.

[11] Sheppard, R.C.; Williams, B.J. *Int. J. Peptide Protein Res.* **1982,** *20,* 451-454.

[12] Smith, J.M; Vitali, F.; Archer, S.A.; Fasan, R. *Angew. Chem.* **2011,** *50,* 5075-5080.

[13] Chretien, J.-M.; Ghanem, M.A.; Bartlett, P.N.; Kilburn, J.D. *Chem. Eur. J.* **2008,** *14,* 2548-2556.

[14] Boger, D.L.; Yohannes, D. *J. Org. Chem.*, **1989,** *54,* 2498.

[15] Baldwin, A.D.; Kiick, K.L. *Bioconjugate Chem.* **2011,** *22,* 1946-1953.

Appendix I: Tables of the surface coverage data

Chapter 3

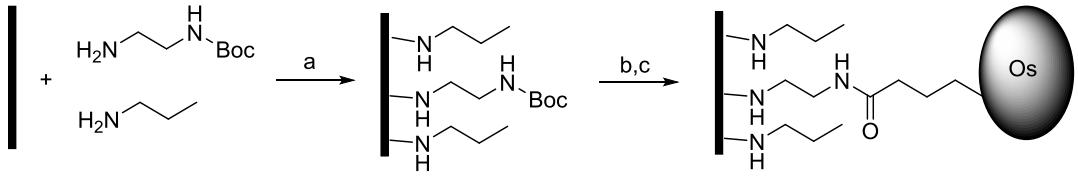

22 100% EDA-Boc
23 10% EDA-Boc
24 1% EDA-Boc
25 0.1% EDA-Boc

Modification	Average Γ (pmol cm^{-2})	Error (pmol cm^{-2})	Control Γ (pmol cm^{-2})
22	21.1	7.45	-
23	9.21	0.09	-
24	17.7	11.4	-
25	12.5	6.45	18.2

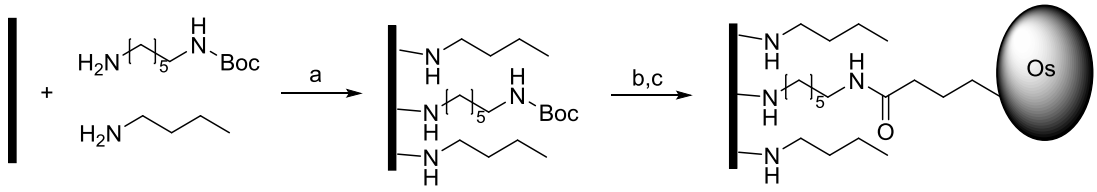

26 100%HDA-Boc
27 10% HDA-Boc
28 1% HDA-Boc
29 0.1% HDA-Boc

Modification	Average Γ (pmol cm^{-2})	Error (pmol cm^{-2})	Control Γ (pmol cm^{-2})
26	13.9	0.25	-
27	8.18	0.53	-
28	6.31	1.55	-
29	4.73	2.85	-

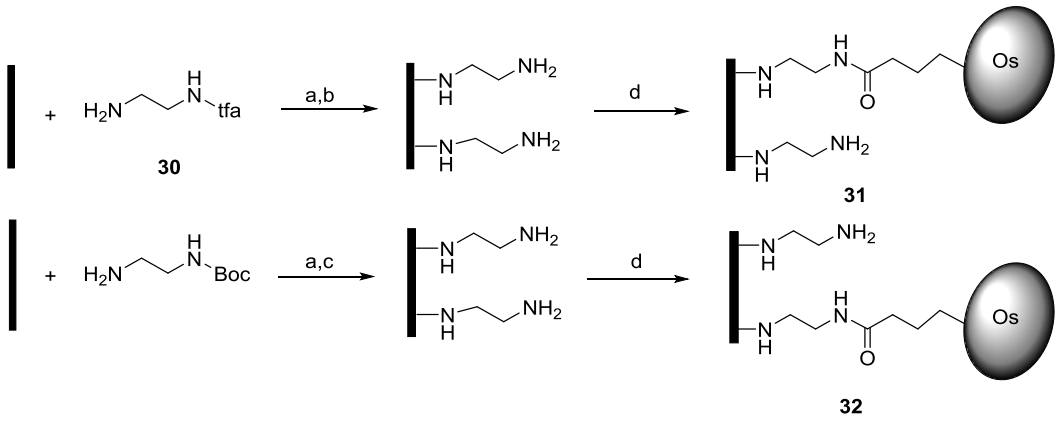

Modification	Average Γ (pmol cm^{-2})	Error (pmol cm^{-2})	Control Γ (pmol cm^{-2})
31	22.4	2.57	7.27
32	30.4	7.35	22.1

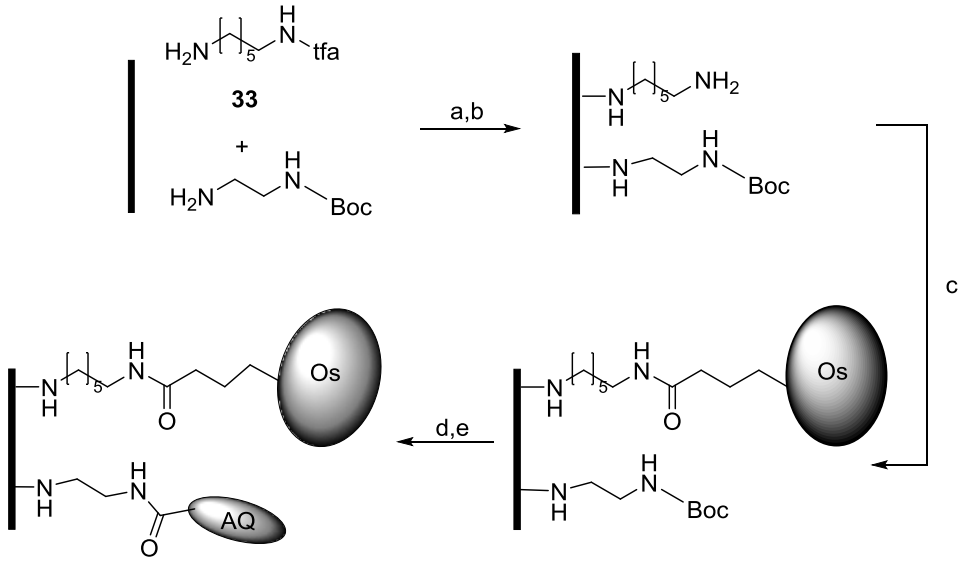

38 100%HDA-tfa
39 50% HDA-tfa
40 10% HDA-tfa
41 1% HDA-tfa

34 100%HDA-tfa
35 50% HDA-tfa
36 10% HDA-tfa
37 1% HDA-tfa

Modification	Average Γ (pmol cm^{-2})	Error (pmol cm^{-2})	Control Γ (pmol cm^{-2})
34	64.1	5.31	20.5
35	33.6	5.10	10.6
36	18.2	0.52	8.02
37	9.99	3.45	4.20

Modification	Average Γ (pmol cm^{-2})	Error (pmol cm^{-2})	Control Γ (pmol cm^{-2})
38	97.8	0.72	39.9
39	146.3	32.9	55.4
40	140.9	2.31	21.5
41	166.9	16.9	25.5

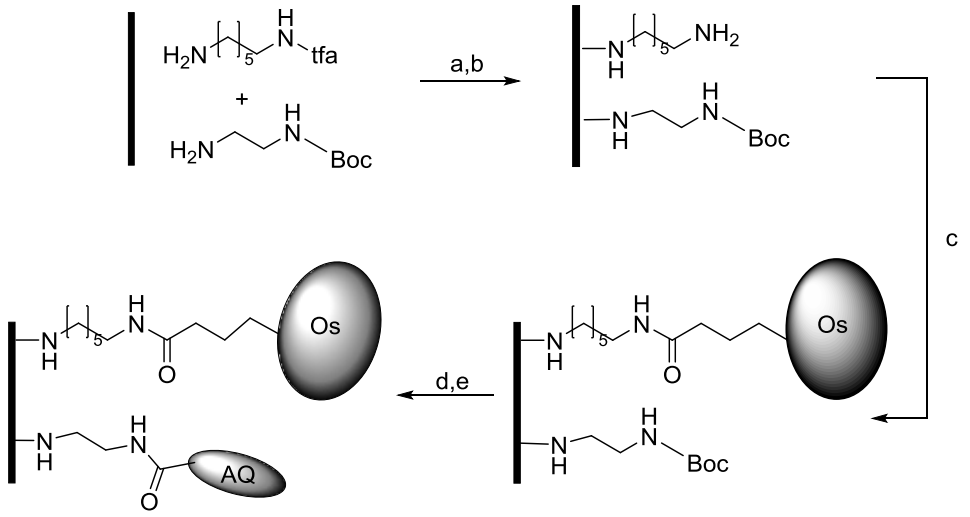

45 100%HDA-tfa
46 10% HDA-tfa
47 1% HDA-tfa

42 100%HDA-tfa
43 10% HDA-tfa
44 1% HDA-tfa

Modification	Average Γ (pmol cm^{-2})	Error (pmol cm^{-2})	Control Γ (pmol cm^{-2})
42	19.1	1.33	-
43	14.8	3.58	-
44	8.81	0.27	-
45	74.7	2.76	51.4
46	91.0	25.1	57.8
47	97.9	3.82	57.7

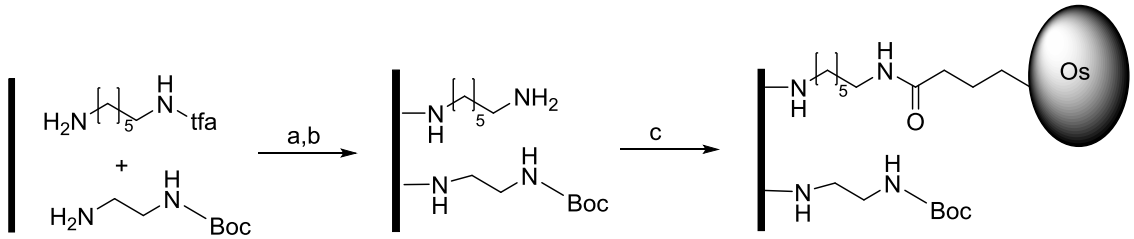

48 0.1% HDA-tfa
49 0.01% HDA-tfa

Modification	Average Γ (pmol cm^{-2})	Error (pmol cm^{-2})	Control Γ (pmol cm^{-2})
48	4.96	1.13	-
49	5.35	1.30	-

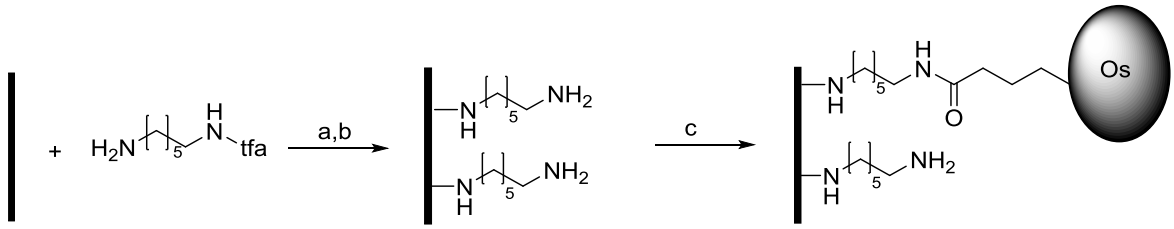

51 30 min
52 1 h
53 3 h
54 6 h

Modification	Average Γ (pmol cm^{-2})	Error (pmol cm^{-2})	Control Γ (pmol cm^{-2})
51	9.63	0.27	-
52	18.4	0.59	-
53	17.2	7.13	-
54	19.1	1.33	-

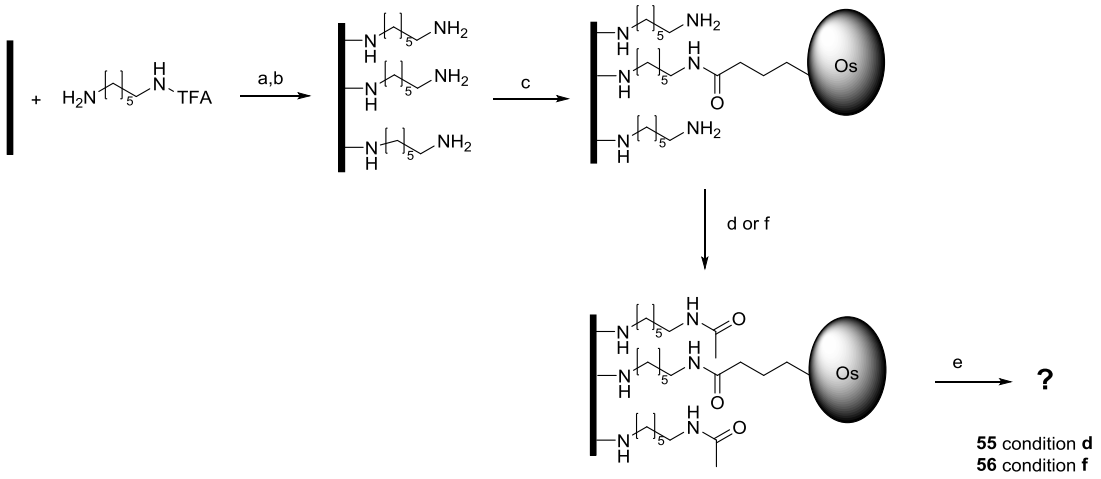

Modification	Average Γ (pmol cm^{-2})	Error (pmol cm^{-2})	Control Γ (pmol cm^{-2})
55	6.10	2.34	1.87
56	4.34	0.21	2.44

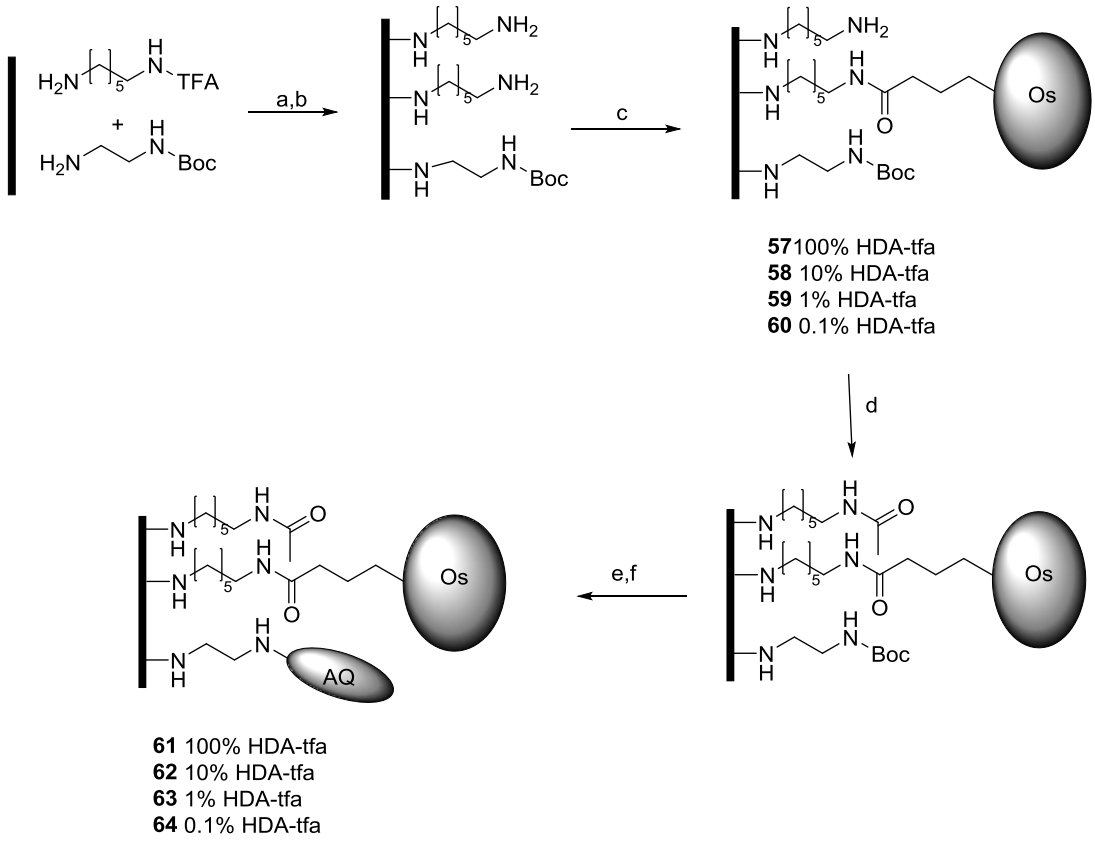

57 100% HDA-tfa
58 10% HDA-tfa
59 1% HDA-tfa
60 0.1% HDA-tfa

61 100% HDA-tfa
62 10% HDA-tfa
63 1% HDA-tfa
64 0.1% HDA-tfa

Modification	Average Γ (pmol cm^{-2})	Error (pmol cm^{-2})
57	18.1	2.51
58	13.7	0.74
59	8.39	1.20
60	3.27	0.96
61	6.38	1.58
62	16.9	0.83
63	32.8	4.58
64	36.1	14.9

Chapter 4

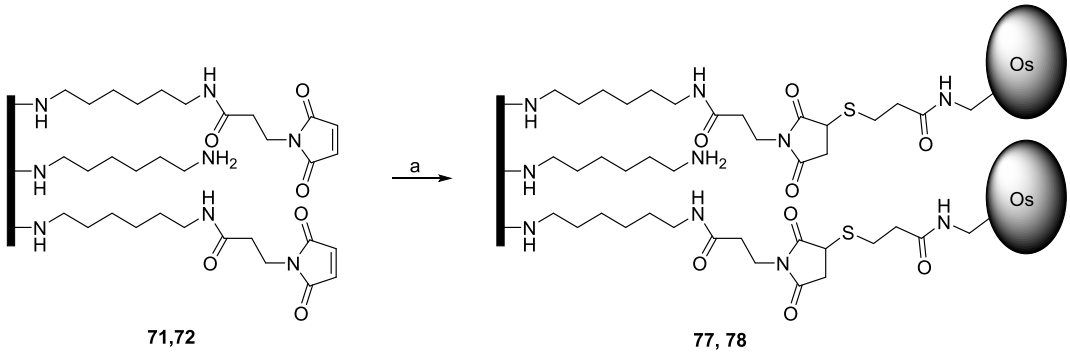

71,72 77, 78

Modification	Average Γ (pmol cm^{-2})	Error (pmol cm^{-2})
77	20.5	7.72
78	16.2	5.4

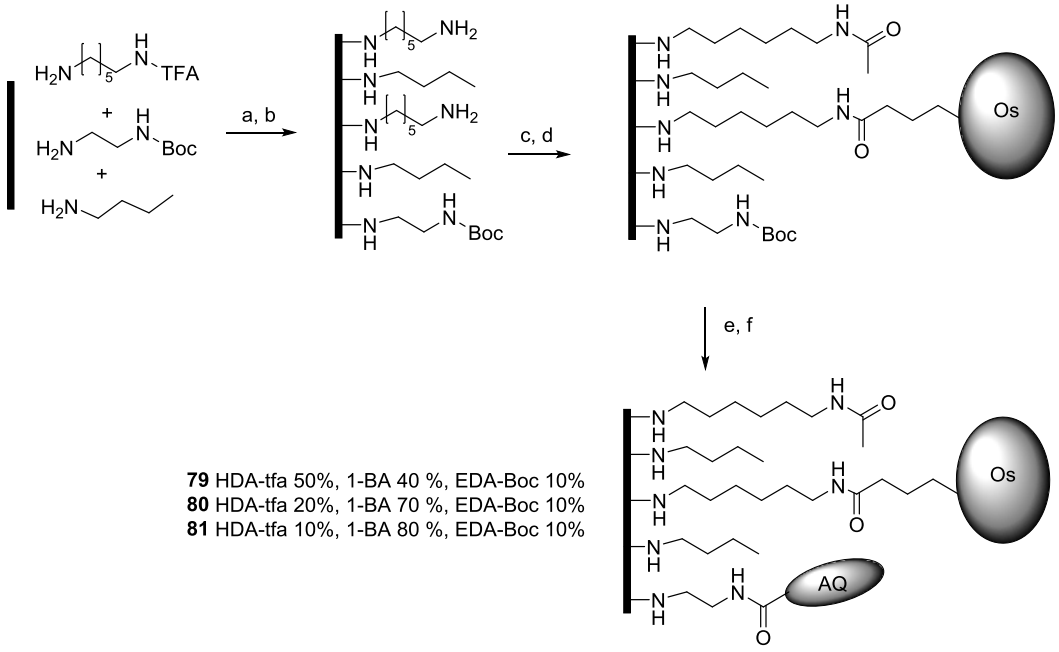

79 HDA-tfa 50%, 1-BA 40 %, EDA-Boc 10%
80 HDA-tfa 20%, 1-BA 70 %, EDA-Boc 10%
81 HDA-tfa 10%, 1-BA 80 %, EDA-Boc 10%

Modification	Γ_{Os} (pmol cm^{-2})	Err (pmol cm^{-2})	Γ_{AQ} (pmol cm^{-2})	Err (pmol cm^{-2})
79	14.8	0.72	4.40	1.36
80	11.5	0.66	8.06	2.41
81	10.2	1.35	9.73	3.91

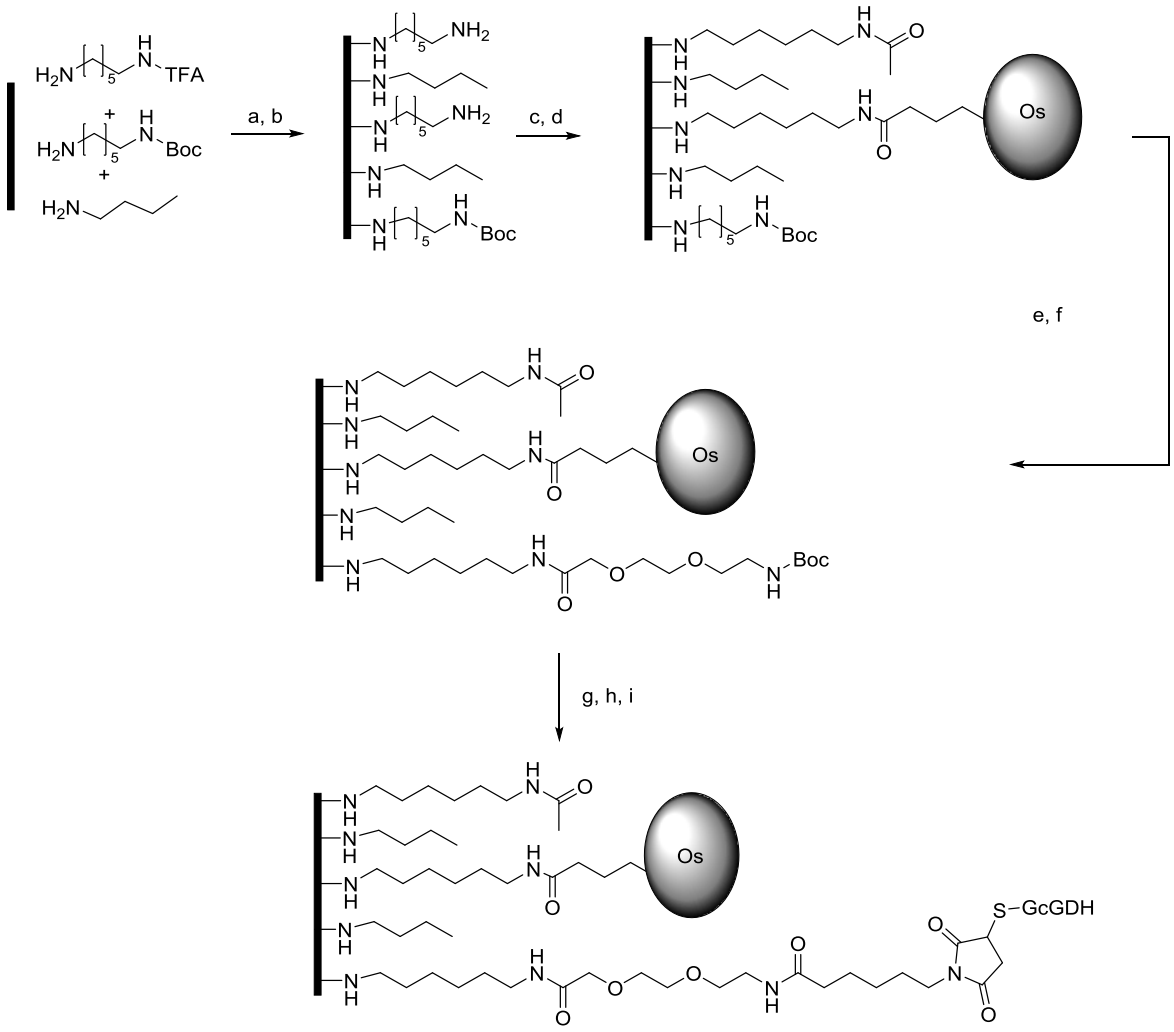

82 HDA-tfa 20%, 1-BA 70 %, EDA-Boc 10%
83 HDA-tfa 10%, 1-BA 80 %, EDA-Boc 10%
84 HDA-tfa 1%, 1-BA 89 %, EDA-Boc 10%

Modification	Average Γ (pmol cm^{-2})	Error (pmol cm^{-2})
82	10.4	0.82
83	7.91	0.44
84	7.08	0.60

Appendix II: ^{1}H-NMR spectra of the synthesised complexes

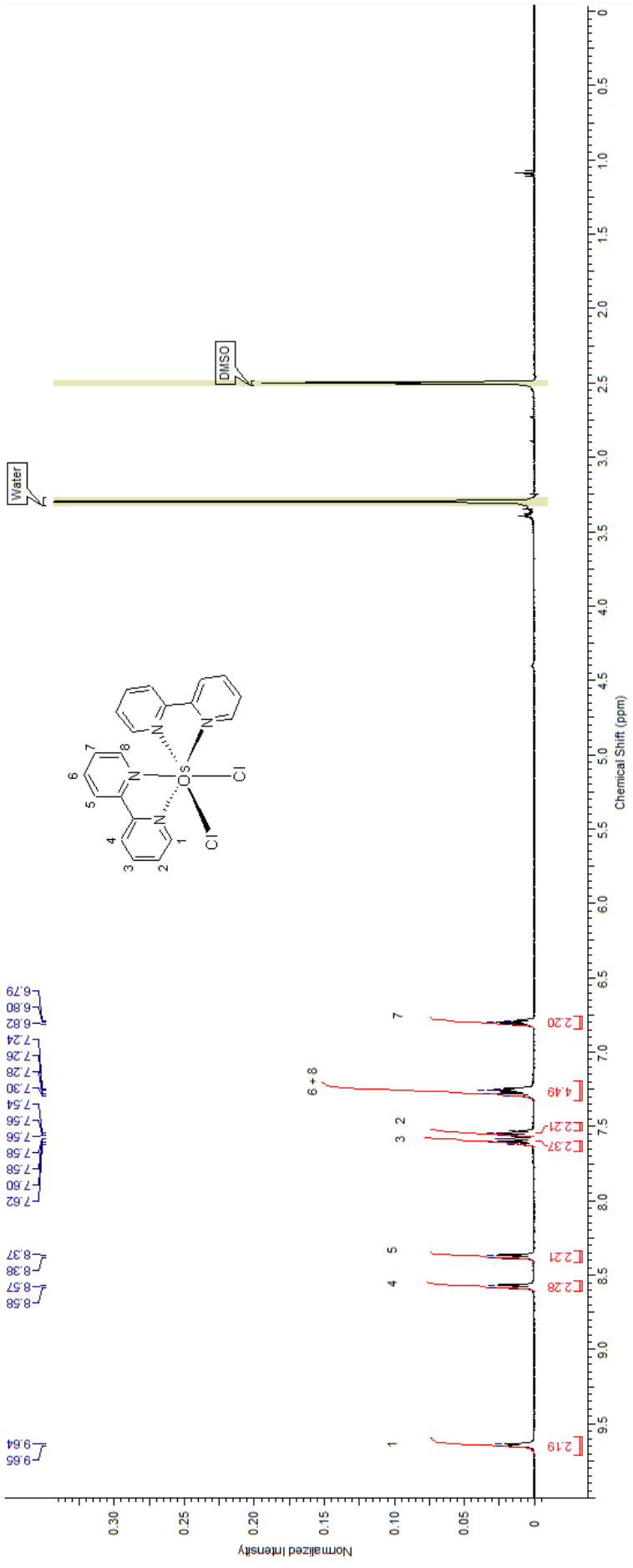
Water
DMSO
Os
Cl
Cl
N
N
N
N
Normalized Intensity
Chemical Shift (ppm)
9.65
9.64
8.58
8.57
8.38
8.37
7.82
7.60
7.58
7.58
7.56
7.56
7.54
7.30
7.28
7.26
7.24
6.82
6.80
6.79
2.19
2.28
2.21
2.37
2.21
4.49
2.20

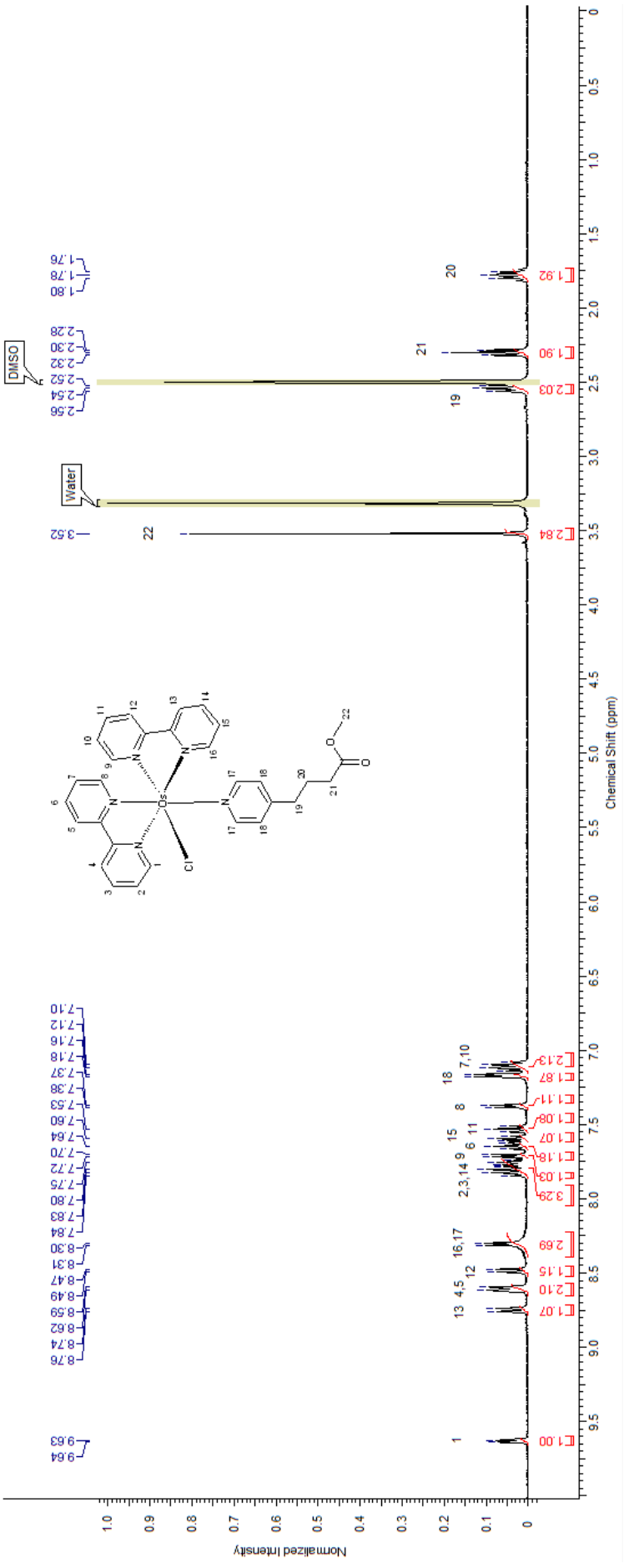
Normalized Intensity
Chemical Shift (ppm)
DMSO
Water
Os
N
Cl
O

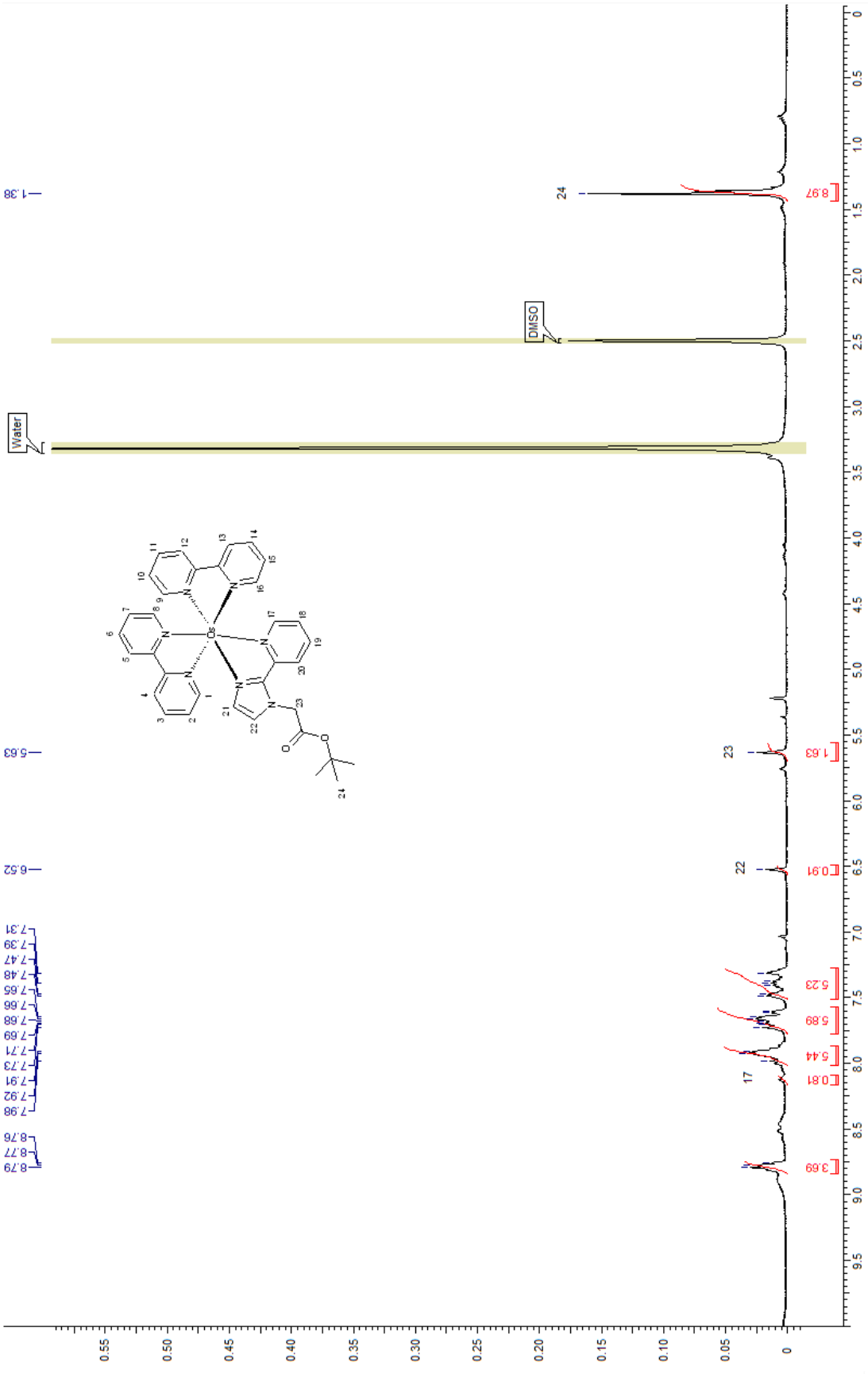
Water
DMSO
24
23
22
17
1.38
5.63
6.52
7.31
7.39
7.47
7.48
7.65
7.66
7.68
7.69
7.71
7.73
7.91
7.92
7.98
8.76
8.77
8.79
8.97
1.63
0.91
5.23
5.89
5.44
0.81
3.69

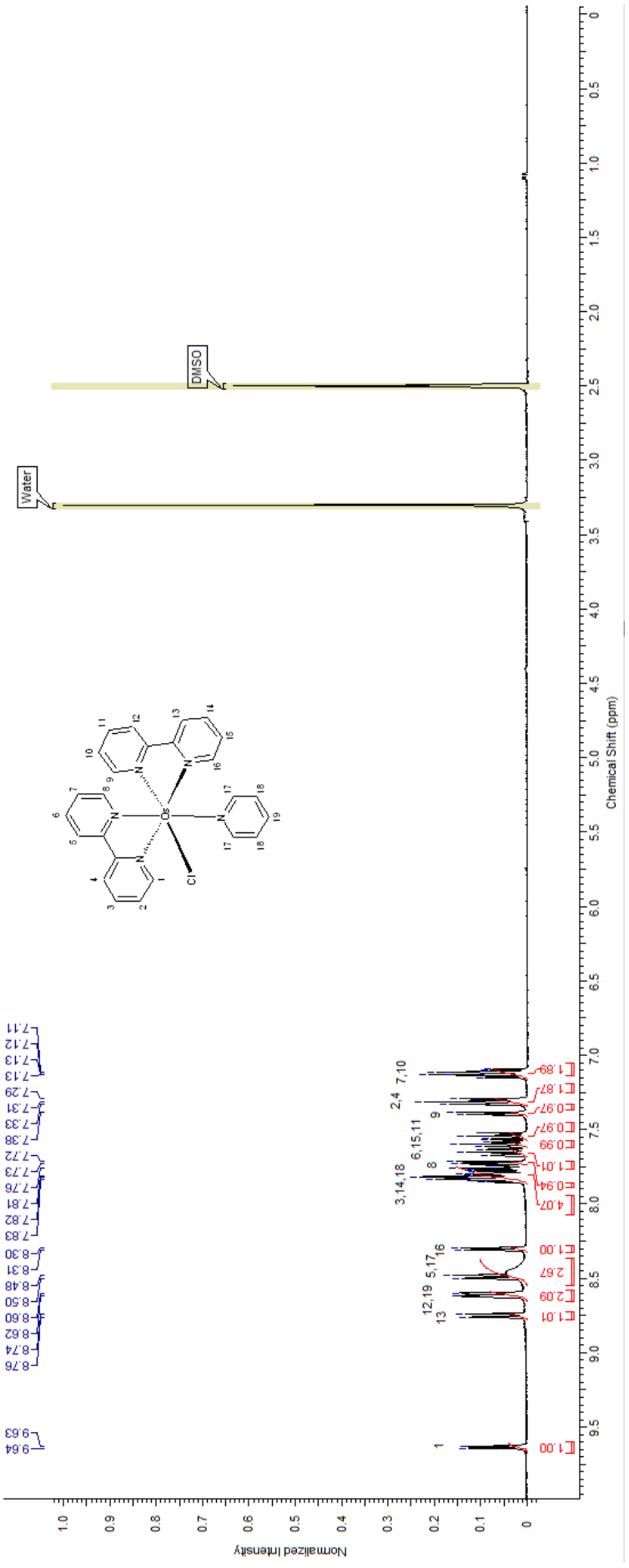
Water
DMSO
Os
Cl
Chemical Shift (ppm)
Normalized Intensity

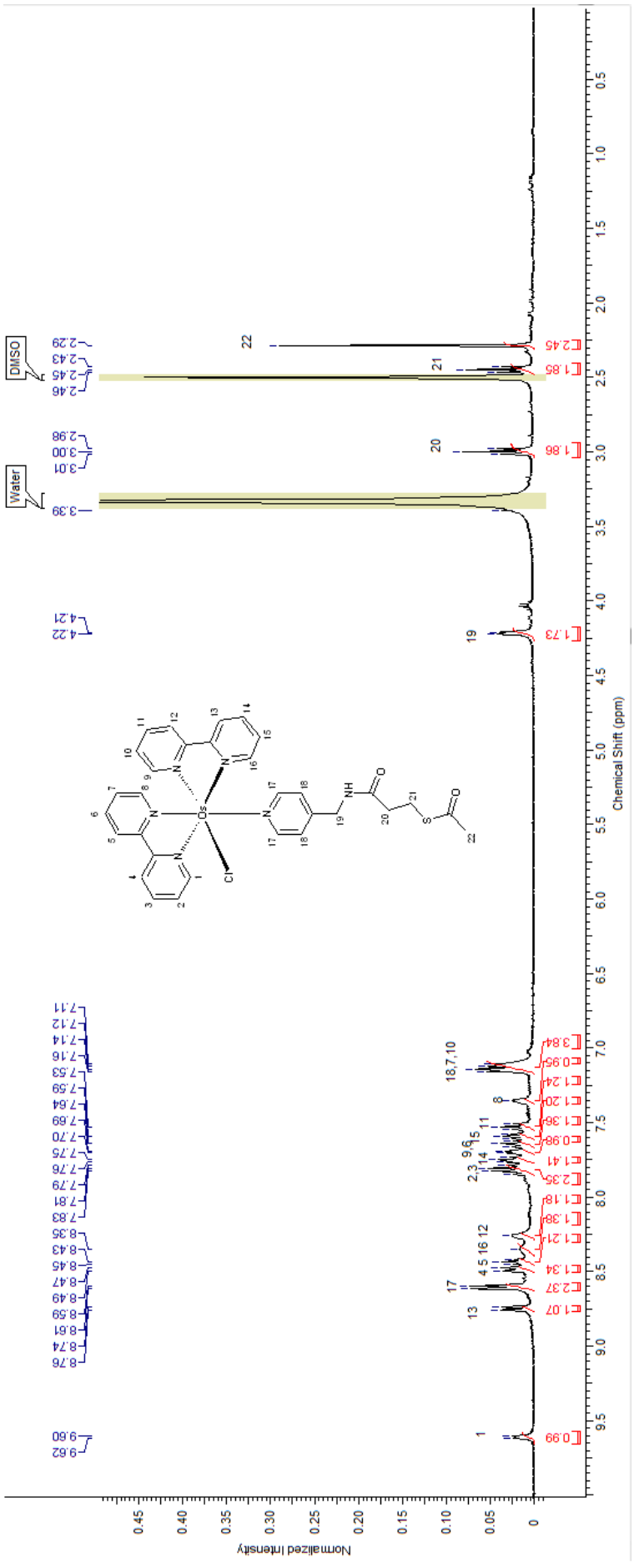
Chemical Shift (ppm)
Normalized Intensity
DMSO
Water
Os
Cl
NH
S

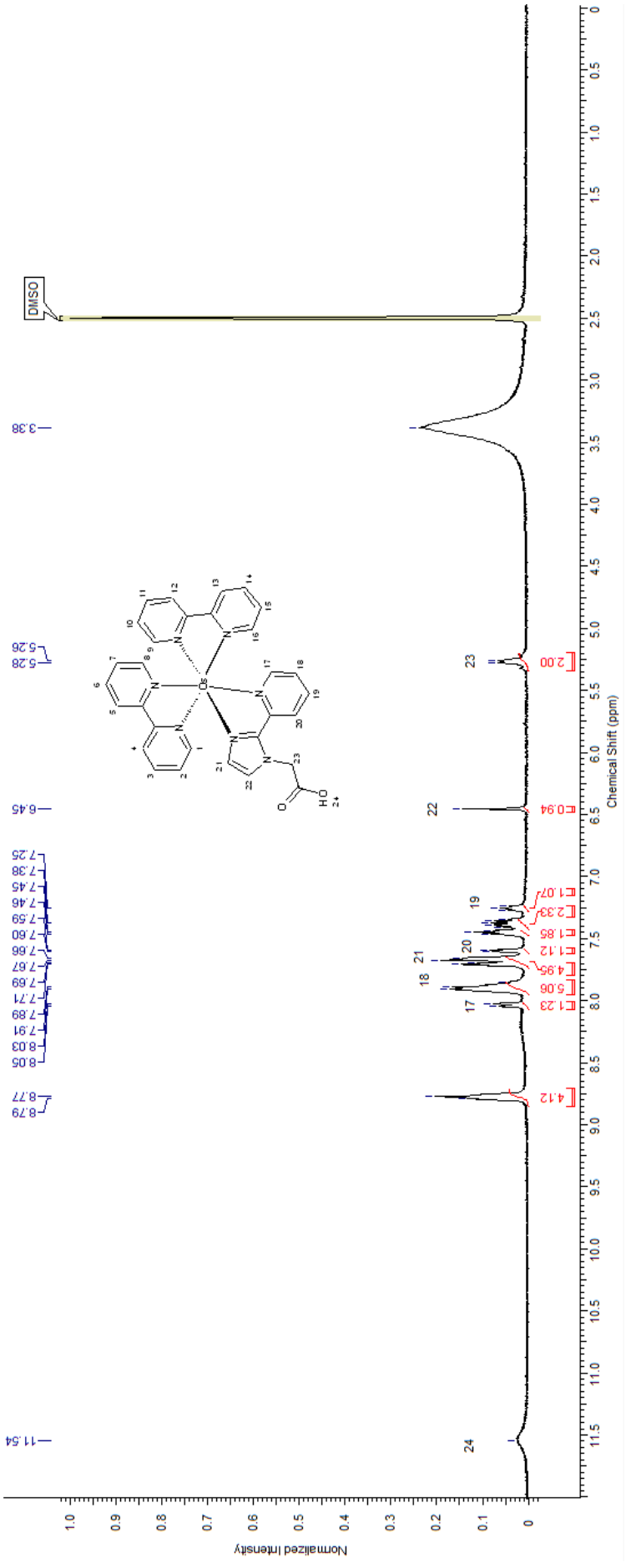
DMSO
3.38
5.26
5.28
6.45
7.25
7.38
7.45
7.46
7.59
7.60
7.66
7.67
7.69
7.71
7.89
7.91
8.03
8.05
8.77
8.79
11.54
2.00
0.94
1.07
2.33
1.85
1.12
4.95
5.06
1.23
4.12
Os
Chemical Shift (ppm)
Normalized Intensity

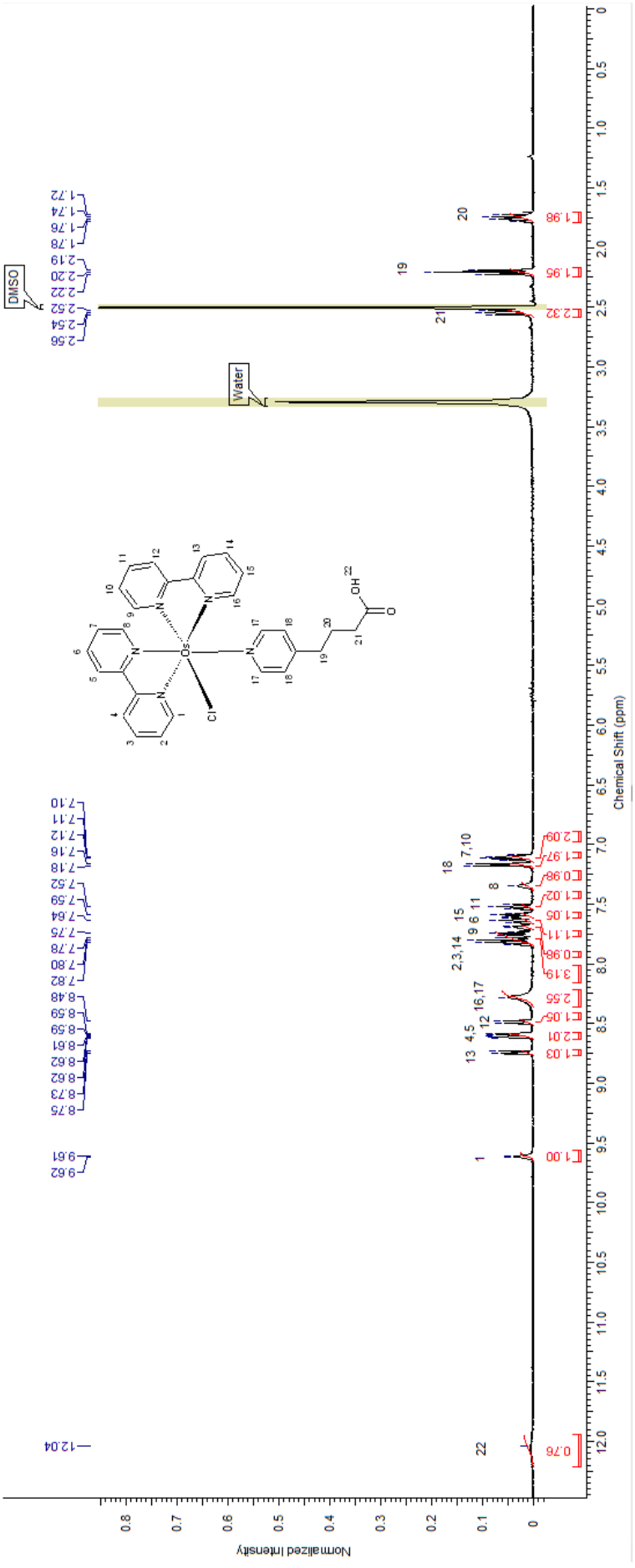
Normalized Intensity
Chemical Shift (ppm)
DMSO
Water
Os
Cl
OH
O
N

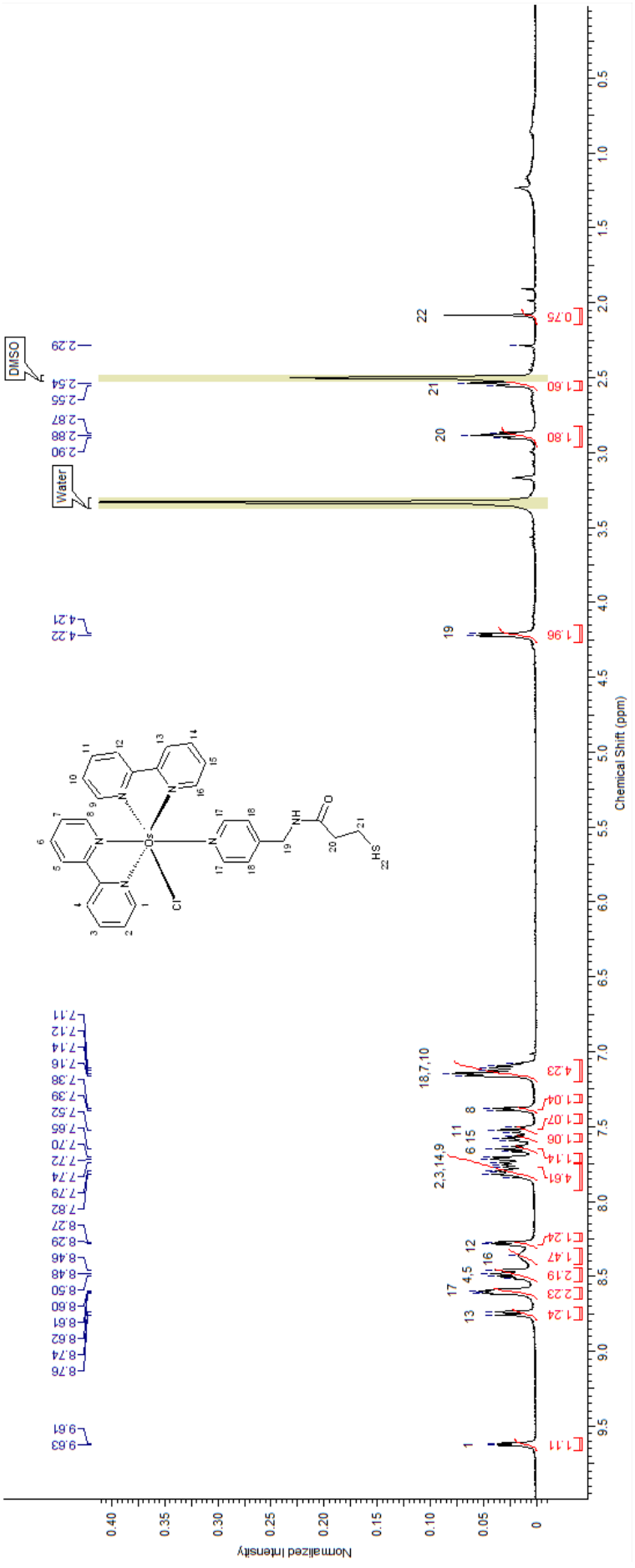
Normalized Intensity
Chemical Shift (ppm)
DMSO
Water
Os
Cl
NH
HS
O
N

Appendix III: crystal structure reports

Crystal structure report for complex (1)

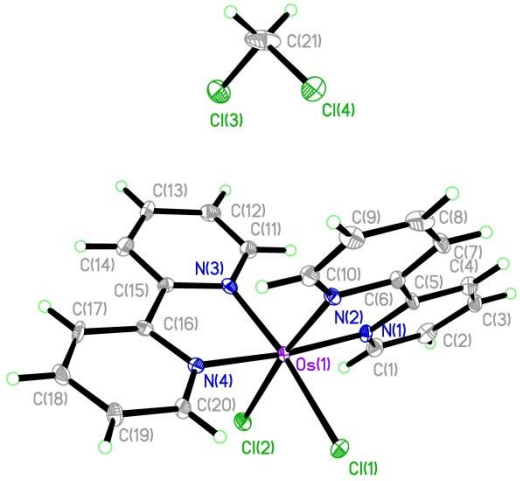

A metallic dark black block-like specimen of $C_{21}H_{18}Cl_4N_4Os$, approximate dimensions 0.100 mm x 0.120 mm x 0.150 mm, was used for the X-ray crystallographic analysis. The X-ray intensity data were measured.

Table 1: Data collection details for complex (1).

Axis	dx/mm	2θ/°	ω/°	φ/°	χ/°	Width/°	Frames	Time/s	Wavelength/Å	Voltage/kV	Current/mA	Temperature/K
Phi	38.037	36.00	49.98	-17.59	-39.60	0.50	739	10.00	0.71073	50	30.0	99.99
Phi	38.037	36.00	137.05	-42.82	-78.00	0.50	739	10.00	0.71073	50	30.0	99.99
Omega	38.037	38.00	-32.47	-166.66	96.92	0.50	120	10.00	0.71073	50	30.0	99.99

A total of 1598 frames were collected. The total exposure time was 4.44 hours. The frames were integrated with the Bruker SAINT software package using a narrow-frame algorithm. The integration of the data using a monoclinic unit cell yielded a total of 14305 reflections to a maximum θ angle of 30.58° (0.70 Å resolution), of which 6085 were independent (average redundancy2.351, completeness = 99.4%, R_{int} = 1.11%, R_{sig} = 1.42%) and 5929 (97.44%) were greater than $2\sigma(F^2)$. The final cell constants of a = 15.4660(3) Å, b = 10.9919(2) Å, c = 13.7706(3) Å, β =112.9060(10)°, volume = 2156.41(7) $Å^3$, are based upon the refinement of the XYZ-centroids of 9936 reflections above 20 σ(I) with 5.007° < 2θ < 61.16°. Data were corrected for absorption effects using the multi-scan method (SADABS). The ratio of minimum to maximum apparent transmission was 0.839. The calculated minimum and maximum transmission coefficients (based on crystal size) are 0.4457 and 0.5659.

The structure was solved and refined using the Bruker SHELXTL Software Package, using the space group C 1 c 1, with Z = 4 for the formula unit, $C_{21}H_{18}Cl_4N_4Os$. The final anisotropic full-matrix least-squares refinement on F^2 with 271 variables converged at R1 = 1.07%, for the observed data and wR2 = 2.59% for all data. The goodness-of-fit was 1.166. The largest peak in the final difference electron density synthesis was 0.523 $e^-/Å^3$ and the largest hole was -0.583 $e^-/Å^3$ with an RMS deviation of 0.063 $e^-/Å^3$. On the basis of the final model, the calculated density was2.028 g/cm^3 and F(000), 1264 e^-.

Table 2. Sample and crystal data for Complex (1).

Identification code	JG_1025	
Chemical formula	$C_{21}H_{18}Cl_4N_4Os$	
Formula weight	658.39	
Temperature	100(2) K	
Wavelength	0.71073 Å	
Crystal size	0.100 x 0.120 x 0.150 mm	
Crystal habit	metallic dark black block	
Crystal system	monoclinic	
Space group	C 1 c 1	
Unit cell dimensions	a = 15.4660(3) Å	α = 90°
	b = 10.9919(2) Å	β = 112.9060(10)°
	c = 13.7706(3) Å	γ = 90°
Volume	2156.41(7) $Å^3$	
Z	4	
Density (calculated)	2.028 Mg/cm^3	
Absorption coefficient	6.426 mm^{-1}	
F(000)	1264	

Table 3. Data collection and structure refinement for Complex (1).

Theta range for data collection	2.34 to 30.58°
Index ranges	-21<=h<=22, -15<=k<=15, -19<=l<=17
Reflections collected	14305
Independent reflections	6085 [R(int) = 0.0111]
Coverage of independent reflections	99.4%
Absorption correction	multi-scan
Max. and min. transmission	0.5659 and 0.4457
Structure solution	direct methods

technique		
Structure solution program	SHELXS-97 (Sheldrick, 2008)	
Refinement method	Full-matrix least-squares on F^2	
Refinement program	SHELXL-97 (Sheldrick, 2008)	
Function minimized	$\Sigma\ w(F_o^2 - F_c^2)^2$	
Data / restraints / parameters	6085 / 2 / 271	
Goodness-of-fit on F^2	1.166	
Δ/σ_{max}	0.048	
Final R indices	5929 data; $I>2\sigma(I)$	R1 = 0.0107, wR2 = 0.0257
	all data	R1 = 0.0113, wR2 = 0.0259
Weighting scheme	$w=1/[\sigma^2(F_o^2)+(0.0101P)^2+1.1931P]$ where $P=(F_o^2+2F_c^2)/3$	
Absolute structure parameter	0.3(0)	
Largest diff. peak and hole	0.523 and -0.583 eÅ^{-3}	
R.M.S. deviation from mean	0.063 eÅ^{-3}	

Table 4. Atomic coordinates and equivalent isotropic atomic displacement parameters (Å^2) for Complex (1).

U(eq) is defined as one third of the trace of the orthogonalized U_{ij} tensor.

	x/a	**y/b**	**z/c**	**U(eq)**
C1	0.3513(3)	0.9925(4)	0.0269(3)	0.0164(8)
C2	0.2639(3)	0.9820(4)	-0.0518(3)	0.0176(8)
C3	0.1937(3)	0.9170(4)	-0.0339(3)	0.0157(8)
C4	0.2158(3)	0.8633(4)	0.0644(3)	0.0129(7)
C5	0.3064(2)	0.8757(3)	0.1419(3)	0.0122(7)
C6	0.3374(3)	0.8152(4)	0.2429(3)	0.0129(7)
C7	0.2811(3)	0.7446(4)	0.2774(3)	0.0150(7)
C8	0.3204(3)	0.6893(4)	0.3770(3)	0.0191(8)
C9	0.4131(3)	0.7057(4)	0.4372(3)	0.0175(8)
C10	0.4672(3)	0.7763(4)	0.3993(3)	0.0149(7)
C11	0.5343(3)	0.7766(4)	0.0978(3)	0.0143(7)
C12	0.5878(3)	0.7061(4)	0.0603(3)	0.0179(8)
C13	0.6843(3)	0.6892(4)	0.1228(3)	0.0185(8)
C14	0.7201(3)	0.7451(4)	0.2188(3)	0.0175(8)
C15	0.6626(3)	0.8159(3)	0.2534(3)	0.0106(7)

	x/a	y/b	z/c	U(eq)
C16	0.6961(3)	0.8758(3)	0.3568(3)	0.0110(7)
C17	0.7864(2)	0.8645(4)	0.4352(3)	0.0163(8)
C18	0.8079(3)	0.9180(4)	0.5314(3)	0.0154(8)
C19	0.7383(3)	0.9823(4)	0.5498(3)	0.0157(8)
C20	0.6495(3)	0.9936(4)	0.4686(3)	0.0128(7)
C21	0.4986(6)	0.36670(16)	0.2479(6)	0.0318(5)
Cl1	0.43768(6)	0.10560(10)	0.32705(7)	0.01466(19)
Cl2	0.56432(6)	0.10546(10)	0.16993(7)	0.01459(19)
Cl3	0.56373(9)	0.45766(12)	0.19248(10)	0.0218(2)
Cl4	0.43816(8)	0.45844(12)	0.30416(10)	0.0212(2)
N1	0.3731(2)	0.9415(3)	0.1235(3)	0.0104(6)
N2	0.4316(2)	0.8323(3)	0.3036(3)	0.0110(6)
N3	0.5695(2)	0.8315(3)	0.1934(3)	0.0110(6)
N4	0.6273(2)	0.9418(3)	0.3729(3)	0.0117(6)
Os1	0.50090(3)	0.951326(4)	0.24846(3)	0.00871(2)

Table 5. Bond lengths (Å) for Complex (1).

C1-N1	1.359(5)	C1-C2	1.370(6)
C1-H1	0.95	C2-C3	1.400(7)
C2-H2	0.95	C3-C4	1.392(6)
C3-H3	0.95	C4-C5	1.399(5)
C4-H4	0.95	C5-N1	1.361(5)
C5-C6	1.445(6)	C6-C7	1.381(6)
C6-N2	1.382(5)	C7-C8	1.404(6)
C7-H7	0.95	C8-C9	1.360(6)
C8-H8	0.95	C9-C10	1.383(6)
C9-H9	0.95	C10-N2	1.362(5)
C10-H10	0.95	C11-N3	1.355(5)
C11-C12	1.373(6)	C11-H11	0.95
C12-C13	1.416(6)	C12-H12	0.95
C13-C14	1.364(6)	C13-H13	0.95
C14-C15	1.398(5)	C14-H14	0.95
C15-N3	1.364(5)	C15-C16	1.468(5)
C16-N4	1.374(5)	C16-C17	1.399(5)
C17-C18	1.366(6)	C17-H17	0.95
C18-C19	1.390(6)	C18-H18	0.95
C19-C20	1.399(5)	C19-H19	0.95
C20-N4	1.352(5)	C20-H20	0.95
C21-Cl4	1.748(6)	C21-Cl3	1.787(6)
C21-H21A	0.99	C21-H21B	0.99

Cl1-Os1	2.4138(11)	Cl2-Os1	2.4140(11)
N1-Os1	2.057(3)	N2-Os1	2.017(3)
N3-Os1	2.015(4)	N4-Os1	2.040(3)

Table 6. Bond angles (°) for Complex (1).

N1-C1-C2	122.2(4)	N1-C1-H1	118.9
C2-C1-H1	118.9	C1-C2-C3	119.9(4)
C1-C2-H2	120.1	C3-C2-H2	120.1
C4-C3-C2	118.3(4)	C4-C3-H3	120.9
C2-C3-H3	120.9	C3-C4-C5	119.6(4)
C3-C4-H4	120.2	C5-C4-H4	120.2
N1-C5-C4	121.1(4)	N1-C5-C6	115.6(3)
C4-C5-C6	123.2(4)	C7-C6-N2	121.7(4)
C7-C6-C5	124.9(3)	N2-C6-C5	113.4(4)
C6-C7-C8	119.2(4)	C6-C7-H7	120.4
C8-C7-H7	120.4	C9-C8-C7	119.4(4)
C9-C8-H8	120.3	C7-C8-H8	120.3
C8-C9-C10	119.5(4)	C8-C9-H9	120.2
C10-C9-H9	120.2	N2-C10-C9	122.9(4)
N2-C10-H10	118.6	C9-C10-H10	118.6
N3-C11-C12	122.9(4)	N3-C11-H11	118.6
C12-C11-H11	118.6	C11-C12-C13	119.6(4)
C11-C12-H12	120.2	C13-C12-H12	120.2
C14-C13-C12	117.6(4)	C14-C13-H13	121.2
C12-C13-H13	121.2	C13-C14-C15	120.6(4)
C13-C14-H14	119.7	C15-C14-H14	119.7
N3-C15-C14	121.7(4)	N3-C15-C16	114.9(3)
C14-C15-C16	123.4(4)	N4-C16-C17	121.7(4)
N4-C16-C15	112.9(3)	C17-C16-C15	125.3(4)
C18-C17-C16	120.2(4)	C18-C17-H17	119.9
C16-C17-H17	119.9	C17-C18-C19	118.8(4)
C17-C18-H18	120.6	C19-C18-H18	120.6
C18-C19-C20	119.2(4)	C18-C19-H19	120.4
C20-C19-H19	120.4	N4-C20-C19	122.7(4)
N4-C20-H20	118.6	C19-C20-H20	118.6
Cl4-C21-Cl3	110.73(9)	Cl4-C21-H21A	109.5
Cl3-C21-H21A	109.5	Cl4-C21-H21B	109.5
Cl3-C21-H21B	109.5	H21A-C21-H21B	108.1
C1-N1-C5	118.9(3)	C1-N1-Os1	126.0(3)
C5-N1-Os1	115.1(3)	C10-N2-C6	117.2(4)

C10-N2-Os1	125.7(3)	C6-N2-Os1	116.7(3)
C11-N3-C15	117.6(4)	C11-N3-Os1	125.8(3)
C15-N3-Os1	116.1(3)	C20-N4-C16	117.4(3)
C20-N4-Os1	126.5(3)	C16-N4-Os1	116.2(3)
N3-Os1-N2	98.76(5)	N3-Os1-N4	79.02(14)
N2-Os1-N4	97.24(13)	N3-Os1-N1	97.25(13)
N2-Os1-N1	78.61(14)	N4-Os1-N1	174.02(4)
N3-Os1-Cl1	172.85(9)	N2-Os1-Cl1	85.39(11)
N4-Os1-Cl1	94.74(10)	N1-Os1-Cl1	89.25(10)
N3-Os1-Cl2	85.69(10)	N2-Os1-Cl2	172.62(9)
N4-Os1-Cl2	89.36(10)	N1-Os1-Cl2	95.05(10)
Cl1-Os1-Cl2	90.798(11)		

Table 7. Torsion angles (°) for Complex (1).

N1-C1-C2-C3	0.0(7)	C1-C2-C3-C4	-0.7(7)
C2-C3-C4-C5	0.1(6)	C3-C4-C5-N1	1.3(6)
C3-C4-C5-C6	-175.0(4)	N1-C5-C6-C7	179.7(4)
C4-C5-C6-C7	-3.9(7)	N1-C5-C6-N2	-1.5(5)
C4-C5-C6-N2	174.9(4)	N2-C6-C7-C8	0.4(6)
C5-C6-C7-C8	179.1(4)	C6-C7-C8-C9	-0.5(7)
C7-C8-C9-C10	0.0(7)	C8-C9-C10-N2	0.6(7)
N3-C11-C12-C13	-0.2(6)	C11-C12-C13-C14	-0.3(6)
C12-C13-C14-C15	0.3(7)	C13-C14-C15-N3	0.1(6)
C13-C14-C15-C16	178.3(4)	N3-C15-C16-N4	-2.5(5)
C14-C15-C16-N4	179.2(4)	N3-C15-C16-C17	174.4(4)
C14-C15-C16-C17	-3.9(6)	N4-C16-C17-C18	1.1(6)
C15-C16-C17-C18	-175.5(4)	C16-C17-C18-C19	0.6(6)
C17-C18-C19-C20	-2.0(7)	C18-C19-C20-N4	1.7(7)
C2-C1-N1-C5	1.4(6)	C2-C1-N1-Os1	-179.6(3)
C4-C5-N1-C1	-2.0(6)	C6-C5-N1-C1	174.5(4)
C4-C5-N1-Os1	178.8(3)	C6-C5-N1-Os1	-4.6(4)
C9-C10-N2-C6	-0.7(6)	C9-C10-N2-Os1	172.9(3)
C7-C6-N2-C10	0.2(6)	C5-C6-N2-C10	-178.7(4)
C7-C6-N2-Os1	-174.0(3)	C5-C6-N2-Os1	7.2(5)
C12-C11-N3-C15	0.6(6)	C12-C11-N3-Os1	172.6(3)
C14-C15-N3-C11	-0.6(6)	C16-C15-N3-C11	-178.9(3)
C14-C15-N3-Os1	-173.4(3)	C16-C15-N3-Os1	8.3(5)
C19-C20-N4-C16	0.0(6)	C19-C20-N4-Os1	180.0(3)
C17-C16-N4-C20	-1.4(6)	C15-C16-N4-C20	175.6(4)
C17-C16-N4-Os1	178.6(3)	C15-C16-N4-Os1	-4.4(4)

C11-N3-Os1-N2	84.0(4)	C15-N3-Os1-N2	-103.9(3)
C11-N3-Os1-N4	179.7(4)	C15-N3-Os1-N4	-8.2(3)
C11-N3-Os1-N1	4.5(4)	C15-N3-Os1-N1	176.5(3)
C11-N3-Os1-Cl1	-150.8(6)	C15-N3-Os1-Cl1	21.2(10)
C11-N3-Os1-Cl2	-90.1(3)	C15-N3-Os1-Cl2	82.0(3)
C10-N2-Os1-N3	83.3(4)	C6-N2-Os1-N3	-103.1(3)
C10-N2-Os1-N4	3.4(4)	C6-N2-Os1-N4	176.9(3)
C10-N2-Os1-N1	179.0(4)	C6-N2-Os1-N1	-7.4(3)
C10-N2-Os1-Cl1	-90.8(3)	C6-N2-Os1-Cl1	82.7(3)
C10-N2-Os1-Cl2	-150.0(6)	C6-N2-Os1-Cl2	23.6(10)
C20-N4-Os1-N3	-173.2(4)	C16-N4-Os1-N3	6.8(3)
C20-N4-Os1-N2	-75.6(4)	C16-N4-Os1-N2	104.4(3)
C20-N4-Os1-N1	-121.4(18)	C16-N4-Os1-N1	59.(2)
C20-N4-Os1-Cl1	10.3(3)	C16-N4-Os1-Cl1	-169.7(3)
C20-N4-Os1-Cl2	101.1(3)	C16-N4-Os1-Cl2	-78.9(3)
C1-N1-Os1-N3	-75.1(3)	C5-N1-Os1-N3	104.0(3)
C1-N1-Os1-N2	-172.6(4)	C5-N1-Os1-N2	6.5(3)
C1-N1-Os1-N4	-126.2(18)	C5-N1-Os1-N4	53.(2)
C1-N1-Os1-Cl1	101.9(3)	C5-N1-Os1-Cl1	-79.0(3)
C1-N1-Os1-Cl2	11.2(3)	C5-N1-Os1-Cl2	-169.7(3)

Table 8. Anisotropic atomic displacement parameters (Å^2) for Complex (1).

The anisotropic atomic displacement factor exponent takes the form: $-2\pi^2[h^2 a^{*2} U_{11} + ... + 2 h k a^* b^* U_{12}]$

	U_{11}	U_{22}	U_{33}	U_{23}	U_{13}	U_{12}
C1	0.0163(18)	0.0160(18)	0.020(2)	0.0024(15)	0.0111(15)	0.0013(14)
C2	0.022(2)	0.020(2)	0.0112(19)	0.0045(15)	0.0066(15)	0.0054(16)
C3	0.0099(16)	0.0178(18)	0.0159(19)	-0.0042(15)	0.0013(14)	0.0005(14)
C4	0.0134(15)	0.0146(16)	0.0101(14)	0.0041(12)	0.0040(12)	0.0013(13)
C5	0.0078(14)	0.0135(18)	0.0139(16)	-0.0030(13)	0.0027(13)	-0.0019(12)
C6	0.0086(14)	0.0137(16)	0.0135(17)	-0.0021(13)	0.0013(13)	-0.0006(12)
C7	0.0118(15)	0.0157(18)	0.0179(18)	0.0020(15)	0.0061(13)	-0.0032(14)
C8	0.033(2)	0.0134(17)	0.0179(18)	0.0054(13)	0.0172(16)	-0.0024(15)
C9	0.0231(19)	0.0171(19)	0.0140(19)	0.0048(14)	0.0090(15)	-0.0018(15)
C10	0.0142(17)	0.0155(17)	0.0123(18)	0.0022(14)	0.0021(14)	0.0008(14)
C11	0.0145(17)	0.0151(17)	0.0124(18)	-0.0014(14)	0.0045(14)	-0.0006(14)
C12	0.0222(19)	0.0157(19)	0.0133(18)	-0.0022(14)	0.0044(15)	-0.0014(15)
C13	0.0112(15)	0.0188(18)	0.025(2)	-0.0005(15)	0.0060(13)	0.0047(13)
C14	0.0152(17)	0.0169(19)	0.020(2)	0.0011(16)	0.0069(15)	0.0034(15)

	U_{11}	U_{22}	U_{33}	U_{23}	U_{13}	U_{12}
C15	0.0127(15)	0.0102(15)	0.0110(16)	-0.0005(12)	0.0067(13)	0.0006(12)
C16	0.0127(15)	0.0106(17)	0.0101(15)	-0.0010(12)	0.0048(13)	-0.0016(12)
C17	0.0073(14)	0.0163(17)	0.0233(18)	0.0093(14)	0.0036(13)	0.0039(13)
C18	0.0126(17)	0.0164(18)	0.0117(18)	0.0005(14)	-0.0012(14)	-0.0022(14)
C19	0.0106(17)	0.020(2)	0.0114(19)	0.0005(14)	-0.0009(14)	0.0004(14)
C20	0.0099(16)	0.0184(18)	0.0060(16)	-0.0025(13)	-0.0011(12)	0.0014(13)
C21	0.0554(13)	0.0177(7)	0.0387(10)	-0.004(3)	0.0361(10)	-0.007(3)
Cl1	0.0137(4)	0.0142(4)	0.0171(5)	-0.0009(4)	0.0072(4)	0.0028(3)
Cl2	0.0133(4)	0.0147(4)	0.0170(5)	0.0006(4)	0.0072(4)	-0.0025(3)
Cl3	0.0228(6)	0.0241(6)	0.0196(6)	0.0003(4)	0.0093(5)	-0.0039(4)
Cl4	0.0231(6)	0.0232(6)	0.0187(6)	0.0004(4)	0.0096(5)	0.0024(4)
N1	0.0076(13)	0.0145(15)	0.0085(15)	-0.0016(11)	0.0024(11)	0.0010(10)
N2	0.0112(14)	0.0117(16)	0.0110(15)	-0.0002(12)	0.0052(12)	-0.0023(11)
N3	0.0110(14)	0.0109(16)	0.0107(15)	0.0008(11)	0.0036(11)	-0.0028(11)
N4	0.0108(14)	0.0100(15)	0.0145(17)	-0.0013(11)	0.0053(12)	-0.0009(10)
Os1	0.00658(2)	0.01022(2)	0.00890(3)	-0.00003(10)	0.00254(2)	-0.00011(10)

Table 9. Hydrogen atomic coordinates and isotropic atomic displacement parameters ($Å^2$) for Complex (1).

	x/a	y/b	z/c	U(eq)
H1	-0.6017	0.0369	-0.9864	0.02
H2	-0.7490	0.0188	-1.1184	0.021
H3	-0.8675	-0.0903	-1.0875	0.019
H4	-0.8304	-0.1815	-0.9212	0.015
H7	-0.7834	-0.2664	-0.7658	0.018
H8	-0.7175	-0.3590	-0.5979	0.023
H9	-0.5595	-0.3312	-0.4953	0.021
H10	-0.4681	-0.2138	-0.5580	0.018
H11	-0.5304	-0.2127	-0.9452	0.017
H12	-0.4397	-0.3310	-1.0071	0.021
H13	-0.2772	-0.3595	-0.9012	0.022
H14	-0.2153	-0.2641	-0.7375	0.021
H17	-0.1671	-0.1804	-0.5784	0.02
H18	-0.1308	-0.0886	-0.4152	0.018
H19	-0.2490	0.0181	-0.3833	0.019
H20	-0.3970	0.0395	-0.5187	0.015
H21A	-0.5467	-0.6846	-0.8079	0.038

	x/a	y/b	z/c	U(eq)
H21B	-0.4580	-0.6877	-0.6976	0.038

Crystal structure report for complex (8)

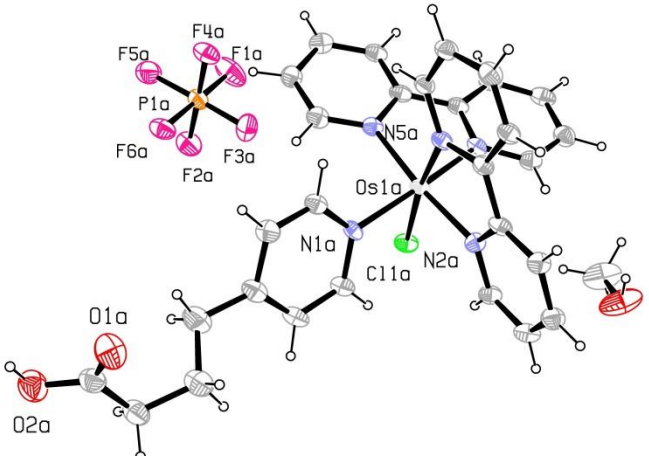

A specimen of $C_{30}H_{31}ClF_6N_5O_3OsP$, approximate dimensions 0.100 mm x 0.200 mm x 0.250 mm, was used for the X-ray crystallographic analysis. The X-ray intensity data were measured.

The total exposure time was 6.51 hours. The frames were integrated with the Bruker SAINT software package using a narrow-frame algorithm. The integration of the data using a triclinic unit cell yielded a total of 78596 reflections to a maximum θ angle of 35.00° (0.62 Å resolution), of which 26782 were independent (average redundancy 2.935, completeness = 97.8%, R_{int} = 2.61%, R_{sig} = 3.65%) and 21302 (79.54%) were greater than $2\sigma(F^2)$. The final cell constants of a = 15.7451(12) Å, b = 15.8246(12) Å, c = 15.9254(13) Å, α = 61.368(2)°, β = 80.962(2)°, γ =63.532(2)°, volume = 3109.6(4) $Å^3$, are based upon the refinement of the XYZ-centroids of 9804 reflections above 20 σ(I) with 5.049° < 2θ < 69.81°. Data were corrected for absorption effects using the multi-scan method (SADABS). The ratio of minimum to maximum apparent transmission was 0.851. The calculated minimum and maximum transmission coefficients (based on crystal size) are 0.4076 and 0.6688.

The structure was solved and refined using the Bruker SHELXTL Software Package, using the space group P -1, with Z = 4 for the formula unit, $C_{30}H_{31}ClF_6N_5O_3OsP$. The final anisotropic full-matrix least-squares refinement on F^2 with 853 variables converged at R1 = 2.83%, for the observed data and wR2 = 6.52% for all data. The goodness-of-fit was 1.010. The largest peak in the final difference electron density synthesis was 2.889 $e^-/Å^3$ and the largest hole was -1.388 $e^-/Å^3$ with an RMS deviation of 0.143 $e^-/Å^3$. On the basis

of the final model, the calculated density was 1.880 g/cm^3 and F(000), 1728 e$^-$.

Table 1. Sample and crystal data for complex (8).

Identification code	JG_3031	
Chemical formula	$C_{30}H_{31}ClF_6N_5O_3OsP$	
Formula weight	880.22	
Temperature	100(2) K	
Wavelength	0.71073 Å	
Crystal size	0.100 x 0.200 x 0.250 mm	
Crystal system	triclinic	
Space group	P -1	
Unit cell dimensions	a = 15.7451(12) Å	α = 61.368(2)°
	b = 15.8246(12) Å	β = 80.962(2)°
	c = 15.9254(13) Å	γ = 63.532(2)°
Volume	3109.6(4) Å^3	
Z	4	
Density (calculated)	1.880 g/cm^3	
Absorption coefficient	4.316 mm^{-1}	
F(000)	1728	

Table 2. Data collection and structure refinement for complex (8).

Theta range for data collection	1.45 to 35.00°
Index ranges	-25<=h<=25, -25<=k<=25, -25<=l<=25
Reflections collected	78596
Independent reflections	26782 [R(int) = 0.0261]
Coverage of independent reflections	97.8%
Absorption correction	multi-scan
Max. and min. transmission	0.6688 and 0.4076
Structure solution technique	direct methods
Structure solution program	SHELXS-97 (Sheldrick, 2008)
Refinement method	Full-matrix least-squares on F^2
Refinement program	SHELXL-2013 (Sheldrick, 2013)
Function minimized	$\Sigma\, w(F_o^2 - F_c^2)^2$
Data / restraints / parameters	26782 / 0 / 853
Goodness-of-fit on F^2	1.010

Δ/σ_{max}	0.003	
Final R indices	21302 data; I>2σ(I)	R1 = 0.0283, wR2 = 0.0604
	all data	R1 = 0.0438, wR2 = 0.0652
Weighting scheme	w=1/[$\sigma^2(F_o^2)$+(0.0277P)^2+2.9010P] where P=(F_o^2+2F_c^2)/3	
Absolute structure parameter	0.0(0)	
Largest diff. peak and hole	2.889 and -1.388 eÅ^{-3}	
R.M.S. deviation from mean	0.143 eÅ^{-3}	

Table 3. Atomic coordinates and equivalent isotropic atomic displacement parameters (Å^2) for complex (8).

U(eq) is defined as one third of the trace of the orthogonalized U_{ij} tensor.

	x/a	y/b	z/c	U(eq)
C30B	0.9132(2)	0.6936(2)	0.0313(3)	0.0364(7)
O3B	0.96760(18)	0.59146(17)	0.0385(2)	0.0508(7)
C30A	0.0128(3)	0.8986(4)	0.3983(3)	0.0610(12)
C1A	0.24578(15)	0.04151(17)	0.55080(16)	0.0142(4)
C2A	0.24854(15)	0.94615(17)	0.56780(16)	0.0152(4)
C3A	0.24398(16)	0.87218(17)	0.66073(17)	0.0157(4)
C4A	0.23501(16)	0.90131(17)	0.73330(16)	0.0157(4)
C5A	0.23154(15)	0.99857(17)	0.71109(16)	0.0147(4)
C6A	0.24755(18)	0.76776(19)	0.68059(17)	0.0193(4)
C7A	0.18016(18)	0.73317(18)	0.75453(18)	0.0200(4)
C8A	0.1806(2)	0.6330(2)	0.76447(19)	0.0229(5)
C9A	0.12172(17)	0.59009(18)	0.84229(18)	0.0193(4)
C10A	0.27810(18)	0.36534(19)	0.62823(17)	0.0199(4)
C11A	0.2675(2)	0.4638(2)	0.61200(19)	0.0245(5)
C12A	0.2053(2)	0.5556(2)	0.53661(19)	0.0249(5)
C13A	0.15440(18)	0.54599(18)	0.48113(17)	0.0202(5)
C14A	0.16615(16)	0.44496(17)	0.50188(16)	0.0158(4)
C15A	0.11196(15)	0.42559(17)	0.45182(16)	0.0149(4)
C16A	0.04568(16)	0.50578(18)	0.37419(17)	0.0196(4)
C17A	0.99750(17)	0.47986(19)	0.33154(18)	0.0220(5)
C18A	0.01631(17)	0.3731(2)	0.36842(18)	0.0207(5)
C19A	0.08190(15)	0.29700(18)	0.44647(17)	0.0175(4)
C20A	0.35267(16)	0.07763(18)	0.79052(16)	0.0167(4)
C21A	0.43239(17)	0.00116(19)	0.85259(17)	0.0183(4)

	x/a	y/b	z/c	U(eq)
C22A	0.51844(17)	0.95860(19)	0.81569(18)	0.0202(4)
C23A	0.52124(16)	0.99488(18)	0.71762(17)	0.0176(4)
C24A	0.43841(14)	0.07223(16)	0.65815(15)	0.0123(4)
C25A	0.43352(14)	0.12008(17)	0.55303(16)	0.0127(4)
C26A	0.51208(15)	0.09851(19)	0.49947(17)	0.0168(4)
C27A	0.50093(16)	0.1502(2)	0.40048(17)	0.0191(4)
C28A	0.40990(16)	0.22380(19)	0.35621(17)	0.0183(4)
C29A	0.33442(16)	0.24303(18)	0.41190(16)	0.0162(4)
C1B	0.44034(15)	0.58063(18)	0.21173(17)	0.0160(4)
C2B	0.50616(17)	0.51370(19)	0.29028(19)	0.0208(5)
C3B	0.48129(18)	0.45283(19)	0.37966(18)	0.0220(5)
C4B	0.38932(18)	0.46018(19)	0.38250(18)	0.0218(5)
C5B	0.32705(17)	0.52847(19)	0.30120(17)	0.0185(4)
C6B	0.5481(2)	0.3895(2)	0.4691(2)	0.0349(7)
C7B	0.56619(19)	0.2744(2)	0.52899(19)	0.0247(5)
C8B	0.62609(19)	0.2225(2)	0.62169(19)	0.0261(5)
C9B	0.72460(19)	0.2188(2)	0.60342(19)	0.0238(5)
C10B	0.39244(15)	0.73013(18)	0.94863(16)	0.0148(4)
C11B	0.44932(16)	0.71283(19)	0.87812(17)	0.0178(4)
C12B	0.45808(17)	0.6313(2)	0.85970(17)	0.0197(4)
C13B	0.40934(16)	0.57009(19)	0.91437(16)	0.0169(4)
C14B	0.35331(14)	0.59034(17)	0.98517(15)	0.0126(4)
C15B	0.29872(14)	0.53114(16)	0.04547(15)	0.0127(4)
C16B	0.30274(16)	0.44098(18)	0.04610(17)	0.0175(4)
C17B	0.24628(17)	0.39232(19)	0.10466(18)	0.0197(4)
C18B	0.18567(17)	0.43588(18)	0.16120(18)	0.0196(4)
C19B	0.18461(15)	0.52497(18)	0.15841(17)	0.0159(4)
C20B	0.31570(16)	0.84358(18)	0.12386(16)	0.0163(4)
C21B	0.31729(18)	0.93804(19)	0.10348(18)	0.0197(4)
C22B	0.25393(18)	0.03345(19)	0.03209(18)	0.0210(5)
C23B	0.19014(17)	0.02988(18)	0.98432(18)	0.0193(4)
C24B	0.19184(15)	0.93213(17)	0.00746(16)	0.0139(4)
C25B	0.12757(15)	0.92066(17)	0.96064(15)	0.0140(4)
C26B	0.05186(16)	0.00606(18)	0.89427(17)	0.0190(4)
C27B	0.99470(16)	0.98618(19)	0.85557(17)	0.0203(5)
C28B	0.01493(17)	0.8811(2)	0.88214(18)	0.0207(5)
C29B	0.09003(16)	0.79941(18)	0.94905(17)	0.0164(4)
Cl1A	0.11610(4)	0.22394(4)	0.70984(4)	0.01980(11)
Cl1B	0.12528(4)	0.72785(4)	0.20528(4)	0.01610(9)
F1A	0.32834(11)	0.25833(13)	0.98973(11)	0.0267(3)

	x/a	y/b	z/c	U(eq)
F2A	0.43288(12)	0.13174(12)	0.94892(12)	0.0297(4)
F3A	0.45059(11)	0.26037(14)	0.80799(11)	0.0300(4)
F4A	0.30338(11)	0.26740(14)	0.84846(12)	0.0297(4)
F5A	0.47503(12)	0.25024(14)	0.95019(12)	0.0301(4)
F6A	0.34699(13)	0.38638(13)	0.84948(13)	0.0352(4)
F1B	0.85087(15)	0.94028(19)	0.74104(16)	0.0488(5)
F2B	0.90252(15)	0.76366(17)	0.79031(15)	0.0581(7)
F3B	0.73090(11)	0.97696(13)	0.64969(11)	0.0286(3)
F4B	0.78211(17)	0.80257(16)	0.69726(14)	0.0469(5)
F5B	0.75106(13)	0.86113(15)	0.80805(12)	0.0351(4)
F6B	0.88267(12)	0.87956(16)	0.63163(13)	0.0392(4)
N1A	0.23688(12)	0.06963(14)	0.62082(13)	0.0127(3)
N2A	0.22884(13)	0.35488(14)	0.57428(13)	0.0144(3)
N3A	0.13097(13)	0.32057(14)	0.48780(13)	0.0137(3)
N4A	0.35353(12)	0.11233(14)	0.69457(13)	0.0123(3)
N5A	0.34439(12)	0.19241(14)	0.50946(13)	0.0116(3)
N1B	0.35026(13)	0.59084(14)	0.21560(13)	0.0129(3)
N2B	0.34344(12)	0.67188(14)	0.00209(13)	0.0118(3)
N3B	0.24062(12)	0.57289(14)	0.10282(13)	0.0126(3)
N4B	0.25513(13)	0.83831(14)	0.07652(13)	0.0130(3)
N5B	0.14561(12)	0.81762(14)	0.98877(13)	0.0128(3)
O3A	0.05511(15)	0.80978(17)	0.37222(16)	0.0330(5)
O1A	0.10277(13)	0.60807(15)	0.91061(14)	0.0232(4)
O2A	0.09515(15)	0.52922(16)	0.82870(14)	0.0285(4)
O1B	0.76556(15)	0.21544(19)	0.53315(15)	0.0351(5)
O2B	0.76269(14)	0.21851(18)	0.67228(15)	0.0304(4)
Os1A	0.23713(2)	0.21260(2)	0.59669(2)	0.01097(2)
Os1B	0.24872(2)	0.70147(2)	0.09757(2)	0.01016(2)
P1A	0.38910(4)	0.25842(5)	0.89924(4)	0.01596(11)
P1B	0.81741(5)	0.87012(5)	0.72072(5)	0.02085(12)

Table 4. Bond lengths (Å) for complex (8).

C30B-O3B	1.406(3)	C30B-H57	0.98
C30B-H59	0.98	C30B-H62	0.98
O3B-H3B	0.84	C30A-O3A	1.493(5)
C30A-H30A	0.98	C30A-H30B	0.98
C30A-H30C	0.98	C1A-N1A	1.354(3)
C1A-C2A	1.381(3)	C1A-H1A	0.95
C2A-C3A	1.395(3)	C2A-H2A	0.95
C3A-C4A	1.403(3)	C3A-C6A	1.502(3)

C4A-C5A	1.381(3)	C4A-H4A	0.95
C5A-N1A	1.355(3)	C5A-H5A	0.95
C6A-C7A	1.523(3)	C6A-H6A	0.99
C6A-H6B	0.99	C7A-C8A	1.513(3)
C7A-H7B	0.99	C7A-H7A	0.99
C8A-C9A	1.500(4)	C8A-H8A	0.99
C8A-H8B	0.99	C9A-O1A	1.214(3)
C9A-O2A	1.318(3)	C10A-N2A	1.352(3)
C10A-C11A	1.385(3)	C10A-H10A	0.95
C11A-C12A	1.393(4)	C11A-H11A	0.95
C12A-C13A	1.381(4)	C12A-H12A	0.95
C13A-C14A	1.396(3)	C13A-H13A	0.95
C14A-N2A	1.365(3)	C14A-C15A	1.462(3)
C15A-N3A	1.370(3)	C15A-C16A	1.396(3)
C16A-C17A	1.383(4)	C16A-H16A	0.95
C17A-C18A	1.395(4)	C17A-H17A	0.95
C18A-C19A	1.386(3)	C18A-H18A	0.95
C19A-N3A	1.349(3)	C19A-H19A	0.95
C20A-N4A	1.354(3)	C20A-C21A	1.381(3)
C20A-H20A	0.95	C21A-C22A	1.397(3)
C21A-H21A	0.95	C22A-C23A	1.383(3)
C22A-H22A	0.95	C23A-C24A	1.396(3)
C23A-H23A	0.95	C24A-N4A	1.371(3)
C24A-C25A	1.468(3)	C25A-N5A	1.369(3)
C25A-C26A	1.395(3)	C26A-C27A	1.381(3)
C26A-H26A	0.95	C27A-C28A	1.397(3)
C27A-H27A	0.95	C28A-C29A	1.377(3)
C28A-H28A	0.95	C29A-N5A	1.361(3)
C29A-H29A	0.95	C1B-N1B	1.349(3)
C1B-C2B	1.385(3)	C1B-H1B	0.95
C2B-C3B	1.398(4)	C2B-H2B	0.95
C3B-C4B	1.395(4)	C3B-C6B	1.517(4)
C4B-C5B	1.385(3)	C4B-H4B	0.95
C5B-N1B	1.357(3)	C5B-H5B	0.95
C6B-C7B	1.507(4)	C6B-H6C	0.99
C6B-H6D	0.99	C7B-C8B	1.526(4)
C7B-H7D	0.99	C7B-H7C	0.99
C8B-C9B	1.512(4)	C8B-H8D	0.99
C8B-H8C	0.99	C9B-O1B	1.213(3)
C9B-O2B	1.327(3)	C10B-N2B	1.358(3)
C10B-C11B	1.378(3)	C10B-H10B	0.95

C11B-C12B	1.400(3)	C11B-H11B	0.95
C12B-C13B	1.389(3)	C12B-H12B	0.95
C13B-C14B	1.391(3)	C13B-H13B	0.95
C14B-N2B	1.379(3)	C14B-C15B	1.461(3)
C15B-N3B	1.373(3)	C15B-C16B	1.395(3)
C16B-C17B	1.384(3)	C16B-H16B	0.95
C17B-C18B	1.391(3)	C17B-H17B	0.95
C18B-C19B	1.382(3)	C18B-H18B	0.95
C19B-N3B	1.358(3)	C19B-H19B	0.95
C20B-N4B	1.357(3)	C20B-C21B	1.381(3)
C20B-H20B	0.95	C21B-C22B	1.391(3)
C21B-H21B	0.95	C22B-C23B	1.387(4)
C22B-H22B	0.95	C23B-C24B	1.396(3)
C23B-H23B	0.95	C24B-N4B	1.367(3)
C24B-C25B	1.464(3)	C25B-N5B	1.366(3)
C25B-C26B	1.398(3)	C26B-C27B	1.379(4)
C26B-H26B	0.95	C27B-C28B	1.394(4)
C27B-H27B	0.95	C28B-C29B	1.385(3)
C28B-H28B	0.95	C29B-N5B	1.350(3)
C29B-H29B	0.95	Cl1A-Os1A	2.4160(6)
Cl1B-Os1B	2.4104(5)	F1A-P1A	1.5994(16)
F2A-P1A	1.5935(16)	F3A-P1A	1.6099(16)
F4A-P1A	1.5993(16)	F5A-P1A	1.6106(16)
F6A-P1A	1.6120(17)	F1B-P1B	1.592(2)
F2B-P1B	1.5897(19)	F3B-P1B	1.6099(16)
F4B-P1B	1.6028(19)	F5B-P1B	1.5912(18)
F6B-P1B	1.6022(19)	N1A-Os1A	2.1073(18)
N2A-Os1A	2.0485(18)	N3A-Os1A	2.0607(18)
N4A-Os1A	2.0594(18)	N5A-Os1A	2.0226(18)
N1B-Os1B	2.1094(18)	N2B-Os1B	2.0255(18)
N3B-Os1B	2.0562(18)	N4B-Os1B	2.0736(18)
N5B-Os1B	2.0464(18)	O3A-H3A	0.84
O2A-H2A1	0.84	O2B-H2B1	0.84

Table 5. Bond angles (°) for complex (8).

O3B-C30B-H57	109.5	O3B-C30B-H59	109.5
H57-C30B-H59	109.5	O3B-C30B-H62	109.5
H57-C30B-H62	109.5	H59-C30B-H62	109.5
C30B-O3B-H3B	109.5	O3A-C30A-H30A	109.5
O3A-C30A-H30B	109.5	H30A-C30A-H30B	109.5
O3A-C30A-H30C	109.5	H30A-C30A-H30C	109.5
H30B-C30A-H30C	109.5	N1A-C1A-C2A	123.1(2)
N1A-C1A-H1A	118.5	C2A-C1A-H1A	118.5
C1A-C2A-C3A	120.4(2)	C1A-C2A-H2A	119.8
C3A-C2A-H2A	119.8	C2A-C3A-C4A	116.5(2)
C2A-C3A-C6A	121.1(2)	C4A-C3A-C6A	122.4(2)
C5A-C4A-C3A	120.1(2)	C5A-C4A-H4A	119.9
C3A-C4A-H4A	119.9	N1A-C5A-C4A	123.1(2)
N1A-C5A-H5A	118.4	C4A-C5A-H5A	118.4
C3A-C6A-C7A	113.92(19)	C3A-C6A-H6A	108.8
C7A-C6A-H6A	108.8	C3A-C6A-H6B	108.8
C7A-C6A-H6B	108.8	H6A-C6A-H6B	107.7
C8A-C7A-C6A	111.2(2)	C8A-C7A-H7B	109.4
C6A-C7A-H7B	109.4	C8A-C7A-H7A	109.4
C6A-C7A-H7A	109.4	H7B-C7A-H7A	108.0
C9A-C8A-C7A	113.5(2)	C9A-C8A-H8A	108.9
C7A-C8A-H8A	108.9	C9A-C8A-H8B	108.9
C7A-C8A-H8B	108.9	H8A-C8A-H8B	107.7
O1A-C9A-O2A	124.3(2)	O1A-C9A-C8A	123.4(2)
O2A-C9A-C8A	112.2(2)	N2A-C10A-C11A	122.3(2)
N2A-C10A-H10A	118.9	C11A-C10A-H10A	118.9
C10A-C11A-C12A	119.3(2)	C10A-C11A-H11A	120.4
C12A-C11A-H11A	120.4	C13A-C12A-C11A	119.0(2)
C13A-C12A-H12A	120.5	C11A-C12A-H12A	120.5
C12A-C13A-C14A	119.4(2)	C12A-C13A-H13A	120.3
C14A-C13A-H13A	120.3	N2A-C14A-C13A	121.5(2)
N2A-C14A-C15A	114.26(19)	C13A-C14A-C15A	124.2(2)
N3A-C15A-C16A	121.7(2)	N3A-C15A-C14A	114.31(19)
C16A-C15A-C14A	123.9(2)	C17A-C16A-C15A	119.9(2)
C17A-C16A-H16A	120.1	C15A-C16A-H16A	120.1

C16A-C17A-C18A	118.5(2)	C16A-C17A-H17A	120.8
C18A-C17A-H17A	120.8	C19A-C18A-C17A	119.1(2)
C19A-C18A-H18A	120.4	C17A-C18A-H18A	120.4
N3A-C19A-C18A	123.2(2)	N3A-C19A-H19A	118.4
C18A-C19A-H19A	118.4	N4A-C20A-C21A	122.7(2)
N4A-C20A-H20A	118.6	C21A-C20A-H20A	118.6
C20A-C21A-C22A	119.3(2)	C20A-C21A-H21A	120.4
C22A-C21A-H21A	120.4	C23A-C22A-C21A	118.8(2)
C23A-C22A-H22A	120.6	C21A-C22A-H22A	120.6
C22A-C23A-C24A	119.5(2)	C22A-C23A-H23A	120.2
C24A-C23A-H23A	120.2	N4A-C24A-C23A	121.7(2)
N4A-C24A-C25A	113.89(18)	C23A-C24A-C25A	124.44(19)
N5A-C25A-C26A	121.3(2)	N5A-C25A-C24A	114.41(18)
C26A-C25A-C24A	124.26(19)	C27A-C26A-C25A	120.1(2)
C27A-C26A-H26A	119.9	C25A-C26A-H26A	119.9
C26A-C27A-C28A	118.5(2)	C26A-C27A-H27A	120.8
C28A-C27A-H27A	120.8	C29A-C28A-C27A	119.4(2)
C29A-C28A-H28A	120.3	C27A-C28A-H28A	120.3
N5A-C29A-C28A	122.6(2)	N5A-C29A-H29A	118.7
C28A-C29A-H29A	118.7	N1B-C1B-C2B	123.2(2)
N1B-C1B-H1B	118.4	C2B-C1B-H1B	118.4
C1B-C2B-C3B	120.7(2)	C1B-C2B-H2B	119.6
C3B-C2B-H2B	119.6	C4B-C3B-C2B	115.9(2)
C4B-C3B-C6B	122.4(3)	C2B-C3B-C6B	121.6(2)
C5B-C4B-C3B	120.4(2)	C5B-C4B-H4B	119.8
C3B-C4B-H4B	119.8	N1B-C5B-C4B	123.4(2)
N1B-C5B-H5B	118.3	C4B-C5B-H5B	118.3
C7B-C6B-C3B	116.6(2)	C7B-C6B-H6C	108.2
C3B-C6B-H6C	108.2	C7B-C6B-H6D	108.2
C3B-C6B-H6D	108.2	H6C-C6B-H6D	107.3
C6B-C7B-C8B	111.6(2)	C6B-C7B-H7D	109.3
C8B-C7B-H7D	109.3	C6B-C7B-H7C	109.3
C8B-C7B-H7C	109.3	H7D-C7B-H7C	108.0
C9B-C8B-C7B	112.4(2)	C9B-C8B-H8D	109.1
C7B-C8B-H8D	109.1	C9B-C8B-H8C	109.1
C7B-C8B-H8C	109.1	H8D-C8B-H8C	107.9
O1B-C9B-O2B	122.9(3)	O1B-C9B-C8B	123.5(2)
O2B-C9B-C8B	113.5(2)	N2B-C10B-C11B	123.3(2)
N2B-C10B-H10B	118.3	C11B-C10B-H10B	118.3
C10B-C11B-C12B	119.2(2)	C10B-C11B-H11B	120.4
C12B-C11B-H11B	120.4	C13B-C12B-C11B	118.3(2)

C13B-C12B-H12B	120.8	C11B-C12B-H12B	120.8
C12B-C13B-C14B	120.3(2)	C12B-C13B-H13B	119.9
C14B-C13B-H13B	119.9	N2B-C14B-C13B	121.4(2)
N2B-C14B-C15B	114.41(18)	C13B-C14B-C15B	124.2(2)
N3B-C15B-C16B	121.6(2)	N3B-C15B-C14B	113.69(18)
C16B-C15B-C14B	124.66(19)	C17B-C16B-C15B	119.9(2)
C17B-C16B-H16B	120.1	C15B-C16B-H16B	120.1
C16B-C17B-C18B	118.6(2)	C16B-C17B-H17B	120.7
C18B-C17B-H17B	120.7	C19B-C18B-C17B	119.3(2)
C19B-C18B-H18B	120.3	C17B-C18B-H18B	120.3
N3B-C19B-C18B	123.1(2)	N3B-C19B-H19B	118.5
C18B-C19B-H19B	118.5	N4B-C20B-C21B	123.0(2)
N4B-C20B-H20B	118.5	C21B-C20B-H20B	118.5
C20B-C21B-C22B	119.7(2)	C20B-C21B-H21B	120.2
C22B-C21B-H21B	120.2	C23B-C22B-C21B	118.1(2)
C23B-C22B-H22B	120.9	C21B-C22B-H22B	120.9
C22B-C23B-C24B	119.9(2)	C22B-C23B-H23B	120.1
C24B-C23B-H23B	120.1	N4B-C24B-C23B	121.9(2)
N4B-C24B-C25B	114.40(19)	C23B-C24B-C25B	123.7(2)
N5B-C25B-C26B	121.3(2)	N5B-C25B-C24B	114.39(18)
C26B-C25B-C24B	124.3(2)	C27B-C26B-C25B	119.5(2)
C27B-C26B-H26B	120.3	C25B-C26B-H26B	120.3
C26B-C27B-C28B	119.1(2)	C26B-C27B-H27B	120.4
C28B-C27B-H27B	120.4	C29B-C28B-C27B	119.1(2)
C29B-C28B-H28B	120.5	C27B-C28B-H28B	120.5
N5B-C29B-C28B	122.5(2)	N5B-C29B-H29B	118.8
C28B-C29B-H29B	118.8	C1A-N1A-C5A	116.82(19)
C1A-N1A-Os1A	123.48(14)	C5A-N1A-Os1A	119.64(15)
C10A-N2A-C14A	118.44(19)	C10A-N2A-Os1A	124.57(15)
C14A-N2A-Os1A	116.94(15)	C19A-N3A-C15A	117.55(19)
C19A-N3A-Os1A	126.13(15)	C15A-N3A-Os1A	116.25(15)
C20A-N4A-C24A	117.94(18)	C20A-N4A-Os1A	126.39(15)
C24A-N4A-Os1A	115.51(14)	C29A-N5A-C25A	118.02(18)
C29A-N5A-Os1A	125.27(14)	C25A-N5A-Os1A	116.70(14)
C1B-N1B-C5B	116.25(19)	C1B-N1B-Os1B	122.34(16)
C5B-N1B-Os1B	121.37(15)	C10B-N2B-C14B	117.52(18)
C10B-N2B-Os1B	125.58(14)	C14B-N2B-Os1B	116.71(14)
C19B-N3B-C15B	117.42(18)	C19B-N3B-Os1B	126.21(14)
C15B-N3B-Os1B	116.36(14)	C20B-N4B-C24B	117.34(19)
C20B-N4B-Os1B	126.62(15)	C24B-N4B-Os1B	116.03(14)
C29B-N5B-C25B	118.49(19)	C29B-N5B-Os1B	124.39(15)

C25B-N5B-Os1B	116.90(15)	C30A-O3A-H3A	109.5
C9A-O2A-H2A1	109.5	C9B-O2B-H2B1	109.5
N5A-Os1A-N2A	93.34(7)	N5A-Os1A-N4A	78.76(7)
N2A-Os1A-N4A	98.43(7)	N5A-Os1A-N3A	95.54(7)
N2A-Os1A-N3A	78.06(8)	N4A-Os1A-N3A	173.20(7)
N5A-Os1A-N1A	89.59(7)	N2A-Os1A-N1A	176.58(7)
N4A-Os1A-N1A	83.86(7)	N3A-Os1A-N1A	99.91(7)
N5A-Os1A-Cl1A	175.83(5)	N2A-Os1A-Cl1A	89.19(5)
N4A-Os1A-Cl1A	97.60(5)	N3A-Os1A-Cl1A	88.22(5)
N1A-Os1A-Cl1A	87.99(5)	N2B-Os1B-N5B	90.77(7)
N2B-Os1B-N3B	78.60(7)	N5B-Os1B-N3B	97.29(7)
N2B-Os1B-N4B	97.40(7)	N5B-Os1B-N4B	78.06(7)
N3B-Os1B-N4B	173.90(7)	N2B-Os1B-N1B	93.21(7)
N5B-Os1B-N1B	174.83(7)	N3B-Os1B-N1B	86.75(7)
N4B-Os1B-N1B	98.13(7)	N2B-Os1B-Cl1B	172.65(5)
N5B-Os1B-Cl1B	86.37(5)	N3B-Os1B-Cl1B	95.03(5)
N4B-Os1B-Cl1B	88.64(5)	N1B-Os1B-Cl1B	90.06(5)
F2A-P1A-F4A	90.68(9)	F2A-P1A-F1A	90.22(9)
F4A-P1A-F1A	90.43(9)	F2A-P1A-F3A	90.65(9)
F4A-P1A-F3A	90.22(9)	F1A-P1A-F3A	178.90(10)
F2A-P1A-F5A	89.71(9)	F4A-P1A-F5A	179.60(10)
F1A-P1A-F5A	89.47(9)	F3A-P1A-F5A	89.87(9)
F2A-P1A-F6A	178.76(10)	F4A-P1A-F6A	90.51(10)
F1A-P1A-F6A	90.13(9)	F3A-P1A-F6A	88.99(10)
F5A-P1A-F6A	89.10(10)	F2B-P1B-F5B	90.15(11)
F2B-P1B-F1B	91.14(13)	F5B-P1B-F1B	90.65(11)
F2B-P1B-F6B	90.55(11)	F5B-P1B-F6B	178.94(10)
F1B-P1B-F6B	90.12(12)	F2B-P1B-F4B	90.46(13)
F5B-P1B-F4B	90.02(11)	F1B-P1B-F4B	178.27(12)
F6B-P1B-F4B	89.19(11)	F2B-P1B-F3B	179.16(13)
F5B-P1B-F3B	90.00(9)	F1B-P1B-F3B	89.69(11)
F6B-P1B-F3B	89.29(9)	F4B-P1B-F3B	88.71(11)

Table 6. Torsion angles (°) for complex (8).

N1A-C1A-C2A-C3A	-1.3(3)	C1A-C2A-C3A-C4A	1.0(3)
C1A-C2A-C3A-C6A	-179.6(2)	C2A-C3A-C4A-C5A	-0.3(3)
C6A-C3A-C4A-C5A	-179.6(2)	C3A-C4A-C5A-N1A	-0.3(3)
C2A-C3A-C6A-C7A	-140.1(2)	C4A-C3A-C6A-C7A	39.2(3)
C3A-C6A-C7A-C8A	174.8(2)	C6A-C7A-C8A-C9A	175.1(2)
C7A-C8A-C9A-O1A	-24.0(4)	C7A-C8A-C9A-O2A	157.4(2)

N2A-C10A-C11A-C12A	-1.1(4)	C10A-C11A-C12A-C13A	1.2(4)
C11A-C12A-C13A-C14A	0.2(4)	C12A-C13A-C14A-N2A	-1.8(3)
C12A-C13A-C14A-C15A	176.2(2)	N2A-C14A-C15A-N3A	1.9(3)
C13A-C14A-C15A-N3A	-176.2(2)	N2A-C14A-C15A-C16A	-178.4(2)
C13A-C14A-C15A-C16A	3.5(4)	N3A-C15A-C16A-C17A	-0.1(3)
C14A-C15A-C16A-C17A	-179.8(2)	C15A-C16A-C17A-C18A	0.5(4)
C16A-C17A-C18A-C19A	0.4(4)	C17A-C18A-C19A-N3A	-1.7(4)
N4A-C20A-C21A-C22A	1.3(4)	C20A-C21A-C22A-C23A	0.3(4)
C21A-C22A-C23A-C24A	-0.4(4)	C22A-C23A-C24A-N4A	-1.0(3)
C22A-C23A-C24A-C25A	177.2(2)	N4A-C24A-C25A-N5A	-3.2(3)
C23A-C24A-C25A-N5A	178.4(2)	N4A-C24A-C25A-C26A	174.6(2)
C23A-C24A-C25A-C26A	-3.8(3)	N5A-C25A-C26A-C27A	-0.2(3)
C24A-C25A-C26A-C27A	-177.8(2)	C25A-C26A-C27A-C28A	0.1(4)
C26A-C27A-C28A-C29A	0.2(4)	C27A-C28A-C29A-N5A	-0.5(4)
N1B-C1B-C2B-C3B	-0.6(4)	C1B-C2B-C3B-C4B	3.1(4)
C1B-C2B-C3B-C6B	-172.4(2)	C2B-C3B-C4B-C5B	-3.0(4)
C6B-C3B-C4B-C5B	172.5(2)	C3B-C4B-C5B-N1B	0.2(4)
C4B-C3B-C6B-C7B	55.0(4)	C2B-C3B-C6B-C7B	-129.7(3)
C3B-C6B-C7B-C8B	-174.2(3)	C6B-C7B-C8B-C9B	-63.7(3)
C7B-C8B-C9B-O1B	-27.8(4)	C7B-C8B-C9B-O2B	152.7(2)
N2B-C10B-C11B-C12B	-0.1(3)	C10B-C11B-C12B-C13B	-0.6(3)
C11B-C12B-C13B-C14B	0.2(3)	C12B-C13B-C14B-N2B	1.0(3)
C12B-C13B-C14B-C15B	179.3(2)	N2B-C14B-C15B-N3B	5.3(3)
C13B-C14B-C15B-N3B	-173.1(2)	N2B-C14B-C15B-C16B	-175.2(2)
C13B-C14B-C15B-C16B	6.3(3)	N3B-C15B-C16B-C17B	0.9(3)
C14B-C15B-C16B-C17B	-178.6(2)	C15B-C16B-C17B-C18B	0.6(4)
C16B-C17B-C18B-C19B	-1.0(4)	C17B-C18B-C19B-N3B	-0.2(4)
N4B-C20B-C21B-C22B	0.7(4)	C20B-C21B-C22B-C23B	0.7(4)
C21B-C22B-C23B-C24B	-1.0(4)	C22B-C23B-C24B-N4B	-0.1(3)
C22B-C23B-C24B-C25B	-179.8(2)	N4B-C24B-C25B-N5B	-4.4(3)
C23B-C24B-C25B-N5B	175.4(2)	N4B-C24B-C25B-C26B	174.1(2)
C23B-C24B-C25B-C26B	-6.2(3)	N5B-C25B-C26B-C27B	-0.6(3)
C24B-C25B-C26B-C27B	-179.0(2)	C25B-C26B-C27B-C28B	-1.3(4)
C26B-C27B-C28B-C29B	2.1(4)	C27B-C28B-C29B-N5B	-1.0(4)
C2A-C1A-N1A-C5A	0.7(3)	C2A-C1A-N1A-Os1A	177.90(16)
C4A-C5A-N1A-C1A	0.2(3)	C4A-C5A-N1A-Os1A	-177.20(17)
C11A-C10A-N2A-C14A	-0.5(4)	C11A-C10A-N2A-Os1A	-177.80(19)
C13A-C14A-N2A-C10A	1.9(3)	C15A-C14A-N2A-C10A	-176.2(2)
C13A-C14A-N2A-Os1A	179.46(17)	C15A-C14A-N2A-Os1A	1.3(2)
C18A-C19A-N3A-C15A	2.1(3)	C18A-C19A-N3A-Os1A	-174.86(18)
C16A-C15A-N3A-C19A	-1.1(3)	C14A-C15A-N3A-C19A	178.51(19)

C16A-C15A-N3A-Os1A	176.12(16)	C14A-C15A-N3A-Os1A	-4.2(2)
C21A-C20A-N4A-C24A	-2.6(3)	C21A-C20A-N4A-Os1A	172.59(17)
C23A-C24A-N4A-C20A	2.5(3)	C25A-C24A-N4A-C20A	-175.94(19)
C23A-C24A-N4A-Os1A	-173.26(17)	C25A-C24A-N4A-Os1A	8.3(2)
C28A-C29A-N5A-C25A	0.4(3)	C28A-C29A-N5A-Os1A	-178.15(18)
C26A-C25A-N5A-C29A	0.0(3)	C24A-C25A-N5A-C29A	177.83(19)
C26A-C25A-N5A-Os1A	178.62(16)	C24A-C25A-N5A-Os1A	-3.5(2)
C2B-C1B-N1B-C5B	-2.2(3)	C2B-C1B-N1B-Os1B	175.46(17)
C4B-C5B-N1B-C1B	2.4(3)	C4B-C5B-N1B-Os1B	-175.31(18)
C11B-C10B-N2B-C14B	1.2(3)	C11B-C10B-N2B-Os1B	-173.65(17)
C13B-C14B-N2B-C10B	-1.6(3)	C15B-C14B-N2B-C10B	179.86(18)
C13B-C14B-N2B-Os1B	173.70(16)	C15B-C14B-N2B-Os1B	-4.8(2)
C18B-C19B-N3B-C15B	1.7(3)	C18B-C19B-N3B-Os1B	-177.25(18)
C16B-C15B-N3B-C19B	-2.0(3)	C14B-C15B-N3B-C19B	177.50(19)
C16B-C15B-N3B-Os1B	177.04(17)	C14B-C15B-N3B-Os1B	-3.5(2)
C21B-C20B-N4B-C24B	-1.7(3)	C21B-C20B-N4B-Os1B	177.98(18)
C23B-C24B-N4B-C20B	1.4(3)	C25B-C24B-N4B-C20B	-178.90(19)
C23B-C24B-N4B-Os1B	-178.33(17)	C25B-C24B-N4B-Os1B	1.4(2)
C28B-C29B-N5B-C25B	-0.9(3)	C28B-C29B-N5B-Os1B	173.50(18)
C26B-C25B-N5B-C29B	1.8(3)	C24B-C25B-N5B-C29B	-179.77(19)
C26B-C25B-N5B-Os1B	-173.09(16)	C24B-C25B-N5B-Os1B	5.4(2)

Table 7. Anisotropic atomic displacement parameters (Å^2) for complex (8).

The anisotropic atomic displacement factor exponent takes the form: $-2\pi^2[h^2 a^{*2} U_{11} + ... + 2 h k a^* b^* U_{12}]$

	U_{11}	U_{22}	U_{33}	U_{23}	U_{13}	U_{12}
C30B	0.0348(15)	0.0210(12)	0.0448(18)	-0.0115(12)	0.0145(13)	-0.0127(11)
O3B	0.0451(14)	0.0233(10)	0.0742(19)	-0.0213(12)	0.0384(13)	-0.0192(10)
C30A	0.040(2)	0.071(3)	0.053(3)	-0.021(2)	0.0094(18)	-0.019(2)
C1A	0.0137(9)	0.0141(9)	0.0116(9)	-0.0041(7)	0.0008(7)	-0.0055(7)
C2A	0.0145(9)	0.0155(9)	0.0135(9)	-0.0057(8)	0.0018(7)	-0.0062(8)
C3A	0.0161(9)	0.0145(9)	0.0150(10)	-0.0059(8)	0.0013(8)	-0.0062(8)
C4A	0.0197(10)	0.0158(9)	0.0117(9)	-0.0045(8)	0.0022(8)	-0.0100(8)
C5A	0.0152(9)	0.0158(9)	0.0121(9)	-0.0051(8)	0.0017(7)	-0.0076(8)
C6A	0.0269(11)	0.0170(10)	0.0160(10)	-0.0076(8)	0.0042(9)	-0.0120(9)
C7A	0.0237(11)	0.0153(9)	0.0215(11)	-0.0080(9)	0.0049(9)	-0.0103(9)
C8A	0.0322(13)	0.0205(11)	0.0233(12)	-0.0121(10)	0.0072(10)	-0.0168(10)
C9A	0.0223(11)	0.0141(9)	0.0213(11)	-0.0066(8)	-0.0012(9)	-0.0087(8)
C10A	0.0296(12)	0.0169(10)	0.0143(10)	-0.0063(8)	0.0016(9)	-0.0119(9)

	U_{11}	U_{22}	U_{33}	U_{23}	U_{13}	U_{12}
C11A	0.0383(14)	0.0209(11)	0.0198(12)	-0.0101(10)	0.0026(10)	-0.0164(11)
C12A	0.0375(14)	0.0169(10)	0.0231(12)	-0.0109(9)	0.0086(11)	-0.0140(10)
C13A	0.0262(11)	0.0130(9)	0.0172(11)	-0.0059(8)	0.0058(9)	-0.0077(9)
C14A	0.0185(10)	0.0121(8)	0.0128(9)	-0.0053(7)	0.0058(8)	-0.0053(8)
C15A	0.0137(9)	0.0126(9)	0.0129(9)	-0.0050(7)	0.0039(7)	-0.0031(7)
C16A	0.0173(10)	0.0132(9)	0.0159(10)	-0.0022(8)	0.0028(8)	-0.0020(8)
C17A	0.0159(10)	0.0184(10)	0.0176(11)	-0.0029(9)	-0.0022(8)	-0.0010(8)
C18A	0.0164(10)	0.0215(11)	0.0185(11)	-0.0052(9)	-0.0035(8)	-0.0064(9)
C19A	0.0134(9)	0.0169(9)	0.0175(10)	-0.0058(8)	-0.0004(8)	-0.0047(8)
C20A	0.0203(10)	0.0164(9)	0.0137(10)	-0.0081(8)	0.0016(8)	-0.0070(8)
C21A	0.0223(11)	0.0188(10)	0.0131(10)	-0.0067(8)	-0.0004(8)	-0.0084(9)
C22A	0.0173(10)	0.0205(10)	0.0190(11)	-0.0078(9)	-0.0040(8)	-0.0048(8)
C23A	0.0133(9)	0.0185(10)	0.0169(10)	-0.0067(8)	-0.0003(8)	-0.0046(8)
C24A	0.0131(8)	0.0135(8)	0.0113(9)	-0.0059(7)	0.0014(7)	-0.0064(7)
C25A	0.0118(8)	0.0142(8)	0.0142(9)	-0.0071(7)	0.0019(7)	-0.0069(7)
C26A	0.0130(9)	0.0215(10)	0.0169(10)	-0.0097(9)	0.0037(8)	-0.0081(8)
C27A	0.0174(10)	0.0258(11)	0.0169(11)	-0.0116(9)	0.0074(8)	-0.0115(9)
C28A	0.0198(10)	0.0231(11)	0.0116(9)	-0.0068(8)	0.0051(8)	-0.0114(9)
C29A	0.0162(9)	0.0196(10)	0.0113(9)	-0.0058(8)	0.0023(7)	-0.0083(8)
C1B	0.0152(9)	0.0156(9)	0.0163(10)	-0.0074(8)	0.0012(8)	-0.0058(8)
C2B	0.0168(10)	0.0173(10)	0.0245(12)	-0.0068(9)	-0.0027(9)	-0.0062(8)
C3B	0.0245(11)	0.0143(9)	0.0197(11)	-0.0025(8)	-0.0076(9)	-0.0053(9)
C4B	0.0244(11)	0.0189(10)	0.0146(10)	-0.0031(8)	0.0008(9)	-0.0082(9)
C5B	0.0180(10)	0.0194(10)	0.0148(10)	-0.0053(8)	0.0025(8)	-0.0088(8)
C6B	0.0444(17)	0.0189(12)	0.0331(15)	-0.0027(11)	-0.0210(13)	-0.0097(12)
C7B	0.0265(12)	0.0209(11)	0.0222(12)	-0.0053(10)	-0.0043(10)	-0.0097(10)
C8B	0.0288(13)	0.0240(12)	0.0172(11)	-0.0021(9)	-0.0026(10)	-0.0115(10)
C9B	0.0281(12)	0.0179(10)	0.0206(12)	-0.0060(9)	-0.0041(10)	-0.0075(9)
C10B	0.0154(9)	0.0173(9)	0.0126(9)	-0.0070(8)	0.0026(7)	-0.0082(8)
C11B	0.0166(10)	0.0216(10)	0.0146(10)	-0.0077(8)	0.0043(8)	-0.0095(8)
C12B	0.0184(10)	0.0251(11)	0.0155(10)	-0.0116(9)	0.0057(8)	-0.0083(9)
C13B	0.0175(10)	0.0203(10)	0.0155(10)	-0.0114(8)	0.0036(8)	-0.0075(8)
C14B	0.0114(8)	0.0140(8)	0.0123(9)	-0.0068(7)	0.0005(7)	-0.0045(7)
C15B	0.0128(8)	0.0124(8)	0.0127(9)	-0.0065(7)	0.0014(7)	-0.0047(7)
C16B	0.0191(10)	0.0174(10)	0.0199(11)	-0.0121(9)	0.0036(8)	-0.0079(8)
C17B	0.0253(11)	0.0159(10)	0.0217(12)	-0.0094(9)	0.0024(9)	-0.0113(9)
C18B	0.0221(11)	0.0170(10)	0.0198(11)	-0.0071(9)	0.0057(9)	-0.0112(9)
C19B	0.0155(9)	0.0162(9)	0.0174(10)	-0.0086(8)	0.0069(8)	-0.0088(8)
C20B	0.0190(10)	0.0169(9)	0.0147(10)	-0.0087(8)	0.0002(8)	-0.0072(8)
C21B	0.0246(11)	0.0200(10)	0.0220(11)	-0.0127(9)	0.0018(9)	-0.0122(9)

	U_{11}	U_{22}	U_{33}	U_{23}	U_{13}	U_{12}
C22B	0.0261(11)	0.0161(10)	0.0235(12)	-0.0104(9)	0.0064(9)	-0.0111(9)
C23B	0.0230(11)	0.0123(9)	0.0207(11)	-0.0069(8)	0.0052(9)	-0.0080(8)
C24B	0.0143(9)	0.0123(8)	0.0134(9)	-0.0067(7)	0.0045(7)	-0.0048(7)
C25B	0.0144(9)	0.0127(8)	0.0113(9)	-0.0045(7)	0.0038(7)	-0.0050(7)
C26B	0.0188(10)	0.0143(9)	0.0155(10)	-0.0036(8)	0.0024(8)	-0.0043(8)
C27B	0.0155(10)	0.0191(10)	0.0167(11)	-0.0036(9)	-0.0006(8)	-0.0045(8)
C28B	0.0178(10)	0.0240(11)	0.0181(11)	-0.0074(9)	-0.0017(8)	-0.0087(9)
C29B	0.0170(9)	0.0173(9)	0.0155(10)	-0.0074(8)	-0.0002(8)	-0.0077(8)
Cl1A	0.0171(2)	0.0153(2)	0.0160(2)	-0.00483(19)	0.00664(19)	-0.00255(19)
Cl1B	0.0163(2)	0.0148(2)	0.0148(2)	-0.00763(18)	0.00594(18)	-0.00540(18)
F1A	0.0312(8)	0.0338(8)	0.0180(7)	-0.0149(7)	0.0070(6)	-0.0147(7)
F2A	0.0391(9)	0.0175(7)	0.0303(9)	-0.0111(7)	-0.0032(7)	-0.0083(7)
F3A	0.0275(8)	0.0414(10)	0.0207(8)	-0.0165(7)	0.0088(6)	-0.0142(7)
F4A	0.0247(8)	0.0460(10)	0.0219(8)	-0.0155(8)	-0.0014(6)	-0.0170(7)
F5A	0.0310(8)	0.0397(9)	0.0275(8)	-0.0138(8)	-0.0029(7)	-0.0218(8)
F6A	0.0455(10)	0.0166(7)	0.0308(9)	-0.0053(7)	0.0013(8)	-0.0090(7)
F1B	0.0569(13)	0.0686(14)	0.0477(12)	-0.0313(12)	-0.0003(10)	-0.0419(12)
F2B	0.0426(11)	0.0469(12)	0.0329(11)	-0.0062(9)	-0.0144(9)	0.0140(9)
F3B	0.0218(7)	0.0252(8)	0.0215(8)	-0.0019(6)	-0.0017(6)	-0.0052(6)
F4B	0.0821(15)	0.0396(11)	0.0352(11)	-0.0155(9)	0.0025(10)	-0.0402(11)
F5B	0.0359(9)	0.0404(10)	0.0188(8)	-0.0070(7)	0.0046(7)	-0.0162(8)
F6B	0.0253(8)	0.0520(12)	0.0295(9)	-0.0184(9)	0.0067(7)	-0.0099(8)
N1A	0.0103(7)	0.0111(7)	0.0130(8)	-0.0033(6)	0.0013(6)	-0.0042(6)
N2A	0.0182(8)	0.0120(7)	0.0112(8)	-0.0050(6)	0.0031(6)	-0.0059(7)
N3A	0.0120(7)	0.0117(7)	0.0119(8)	-0.0033(6)	0.0033(6)	-0.0037(6)
N4A	0.0128(7)	0.0116(7)	0.0121(8)	-0.0055(6)	0.0006(6)	-0.0049(6)
N5A	0.0112(7)	0.0138(7)	0.0111(8)	-0.0055(6)	0.0016(6)	-0.0069(6)
N1B	0.0130(7)	0.0135(8)	0.0133(8)	-0.0077(7)	0.0014(6)	-0.0051(6)
N2B	0.0120(7)	0.0125(7)	0.0095(7)	-0.0047(6)	0.0002(6)	-0.0044(6)
N3B	0.0117(7)	0.0129(7)	0.0126(8)	-0.0062(6)	0.0029(6)	-0.0051(6)
N4B	0.0159(8)	0.0136(8)	0.0109(8)	-0.0072(6)	0.0039(6)	-0.0067(6)
N5B	0.0123(7)	0.0131(7)	0.0116(8)	-0.0055(6)	0.0026(6)	-0.0051(6)
O3A	0.0310(10)	0.0315(11)	0.0314(11)	-0.0135(9)	0.0007(9)	-0.0100(9)
O1A	0.0271(9)	0.0248(9)	0.0239(9)	-0.0125(8)	0.0047(7)	-0.0155(7)
O2A	0.0449(12)	0.0282(10)	0.0252(10)	-0.0111(8)	0.0030(9)	-0.0273(9)
O1B	0.0306(11)	0.0486(13)	0.0279(11)	-0.0237(10)	0.0018(8)	-0.0117(10)
O2B	0.0293(10)	0.0426(12)	0.0240(10)	-0.0179(9)	0.0007(8)	-0.0161(9)
Os1A	0.01083(3)	0.00990(3)	0.00909(4)	-0.00323(3)	0.00200(3)	-0.00366(3)
Os1B	0.01133(3)	0.01019(3)	0.00896(4)	-0.00483(3)	0.00225(3)	-0.00463(3)

	U_{11}	U_{22}	U_{33}	U_{23}	U_{13}	U_{12}
P1A	0.0178(3)	0.0163(2)	0.0137(3)	-0.0066(2)	-0.0001(2)	-0.0072(2)
P1B	0.0200(3)	0.0213(3)	0.0168(3)	-0.0065(2)	-0.0034(2)	-0.0063(2)

Table 8. Hydrogen atomic coordinates and isotropic atomic displacement parameters ($Å^2$) for complex (8).

	x/a	y/b	z/c	U(eq)
H57	0.8569	0.6945	0.0680	0.055
H59	0.8931	0.7458	-0.0362	0.055
H62	0.9516	0.7117	0.0571	0.055
H3B	1.0140	0.5917	0.0043	0.076
H30A	0.0390	0.8733	0.4622	0.091
H30B	-0.0564	0.9233	0.3986	0.091
H30C	0.0279	0.9576	0.3512	0.091
H1A	0.2503	0.0896	0.4870	0.017
H2A	0.2536	-0.0692	0.5159	0.018
H4A	0.2313	-0.1460	0.7978	0.019
H5A	0.2251	0.0165	0.7615	0.018
H6A	0.3133	-0.2880	0.7035	0.023
H6B	0.2317	-0.2267	0.6198	0.023
H7B	0.1996	-0.2798	0.8174	0.024
H7A	0.1149	-0.2090	0.7349	0.024
H8A	0.1563	-0.3518	0.7027	0.027
H8B	0.2470	-0.4224	0.7780	0.027
H10A	0.3215	0.3030	0.6791	0.024
H11A	0.3024	0.4686	0.6518	0.029
H12A	0.1980	0.6238	0.5236	0.03
H13A	0.1117	0.6076	0.4293	0.024
H16A	0.0337	0.5780	0.3507	0.024
H17A	-0.0474	0.5336	0.2783	0.026
H18A	-0.0154	0.3528	0.3404	0.025
H19A	0.0928	0.2248	0.4721	0.021
H20A	0.2948	0.1071	0.8162	0.02
H21A	0.4287	-0.0222	0.9197	0.022
H22A	0.5740	-0.0943	0.8572	0.024
H23A	0.5791	-0.0326	0.6909	0.021
H26A	0.5734	0.0482	0.5311	0.02
H27A	0.5540	0.1359	0.3634	0.023

	x/a	y/b	z/c	U(eq)
H28A	0.4001	0.2603	0.2883	0.022
H29A	0.2729	0.2937	0.3810	0.019
H1B	0.4596	0.6213	0.1523	0.019
H2B	0.5689	0.5091	0.2833	0.025
H4B	0.3693	0.4181	0.4405	0.026
H5B	0.2649	0.5318	0.3056	0.022
H6C	0.6100	0.3925	0.4495	0.042
H6D	0.5219	0.4254	0.5101	0.042
H7D	0.5996	0.2353	0.4915	0.03
H7C	0.5046	0.2695	0.5447	0.03
H8D	0.5934	0.2630	0.6581	0.031
H8C	0.6317	0.1491	0.6615	0.031
H10B	0.3872	0.7856	-0.0395	0.018
H11B	0.4822	0.7557	-0.1576	0.021
H12B	0.4964	0.6182	-0.1889	0.024
H13B	0.4143	0.5142	-0.0967	0.02
H16B	0.3442	0.4130	0.0064	0.021
H17B	0.2488	0.3304	0.1062	0.024
H18B	0.1454	0.4047	0.2013	0.024
H19B	0.1427	0.5541	0.1972	0.019
H20B	0.3590	0.7793	0.1733	0.02
H21B	0.3614	0.9379	0.1380	0.024
H22B	0.2544	1.0992	0.0165	0.025
H23B	0.1454	1.0938	-0.0641	0.023
H26B	0.0399	1.0772	-0.1240	0.023
H27B	-0.0578	1.0434	-0.1886	0.024
H28B	-0.0223	0.8657	-0.1453	0.025
H29B	0.1029	0.7279	-0.0323	0.02
H3A	0.0125	0.8102	0.3460	0.05
H2A1	0.0713	-0.5022	0.8781	0.043
H2B1	0.8188	0.2111	0.6608	0.046

Table 9. Hydrogen bond distances (Å) and angles (°) for complex (8).

	Donor-H	Acceptor-H	Donor-Acceptor	Angle
C30B-H57···F4A	0.98	2.62	3.589(3)	170.0
C30B-H59···F2B	0.98	2.63	3.456(4)	142.5
O3B-H3B···O1A	0.84	1.88	2.715(3)	170.6
C1A-H1A···F4B	0.95	2.58	3.482(3)	157.8
C2A-H2A···F3B	0.95	2.36	3.089(3)	133.1
C5A-H5A···Cl1A	0.95	2.69	3.192(2)	113.7
C8A-H8B···F6A	0.99	2.44	3.296(3)	144.5
C10A-H10A···F4A	0.95	2.47	3.089(3)	122.4
C13A-H13A···O3A	0.95	2.60	3.313(3)	131.7
C16A-H16A···Cl1A	0.95	2.75	3.528(2)	140.0
C18A-H18A···O2A	0.95	2.54	3.160(3)	122.7
C20A-H20A···Cl1A	0.95	2.84	3.442(2)	122.3
C21A-H21A···F2A	0.95	2.59	3.267(3)	128.3
C23A-H23A···F3B	0.95	2.43	3.238(3)	142.9
C29A-H29A···N3A	0.95	2.59	3.151(3)	117.9
C1B-H1B···F5A	0.95	2.45	3.328(3)	153.2
C2B-H2B···F6A	0.95	2.58	3.327(3)	135.2
C5B-H5B···Cl1B	0.95	2.70	3.217(2)	115.0
C8B-H8C···F3B	0.99	2.55	3.298(3)	132.2
C10B-H10B···F5A	0.95	2.48	3.027(3)	116.6
C10B-H10B···N4B	0.95	2.68	3.227(3)	117.5
C18B-H18B···F4B	0.95	2.61	3.175(3)	118.1
C19B-H19B···Cl1B	0.95	2.70	3.338(2)	124.8
C26B-H26B···Cl1B	0.95	2.83	3.542(2)	132.1
C28B-H28B···F1B	0.95	2.38	3.201(3)	145.0
C29B-H29B···N3B	0.95	2.65	3.210(3)	118.3
C29B-H29B···O1A	0.95	2.47	3.283(3)	144.2
O3A-H3A···Cl1A	0.84	2.68	3.510(2)	169.4
O2A-H2A1···O3B	0.84	1.69	2.500(3)	161.6
O2B-H2B1···O3A	0.84	1.89	2.730(3)	175.1